1992

Studies on Photoaffinity Labeling and Mass Spectrometry of Bacteriorhodopsin

Charles John Beischel
Medical University of South Carolina

STUDIES ON
PHOTOAFFINITY LABELING AND MASS SPECTROMETRY
OF
BACTERIORHODOPSIN

by

Charles John Beischel

A dissertation submitted to the faculty of the Medical University of South Carolina in partial fulfillment of the requirements for the degree of Doctor of Philosophy in the College of Graduate Studies.

Department of Cell and Molecular Pharmacology and Experimental Therapeutics

1992

Approved by:

Daniel R. Knapp
Chairperson, Advisory Committee

Rosalie K. Crouch
Chairperson, Advisory Committee

CHARLES JOHN BEISCHEL. Studies on Photoaffinity Labeling and Mass Spectrometry of Bacteriorhodopsin. (Under the direction of ROSALIE K. CROUCH and DANIEL R. KNAPP.)

The objective of these studies was to further define the amino acids of bacteriorhodopsin in close proximity to the ring end of retinal by labeling them using a retinal analog modified to contain a photoactivatable group. The sites of labeling were to be identified using mass spectrometry and tandem mass spectrometry.

Eight potentially photoactivatable retinal analogs were characterized and thoroughly examined as bacteriorhodopsin analog pigments thus identifying those analogs that were most similar to the native retinal.

A versatile flash photolysis apparatus was compared to a continuous wave light source on the basis of total photon output and on efficiency of activation of a model photoactivatable compound. The flash apparatus activated the model compound four times more efficiently than the continuous wave source. The specially designed and constructed sample cell was efficient for photolysis studies.

Molecular modeling of the retinal analogs and bacteriorhodopsin allowed enhanced visualization of the structures and predictions of potentially labeled amino acids. The hypothesis is that a photoactivatable retinal analog would label the amino acids predicted by these studies. The previously published reports of labeling of bacteriorhodopsin were evaluated suggesting that only one** of the retinal analogs was in the retinal binding site.

Mass spectrometric analysis of cleavage fragments of bacteriorhodopsin identified 49% of the protein. Nine percent of the protein was sequenced by tandem mass spectrometry. An unusual protein cleavage site was identified and confirmed by tandem mass spectrometry. The identified peptides were the smallest of the predicted peptides from the cleavages. These initial studies indicated the utility of mass spectrometry in identification of labeled amino acids.

Analysis of the three available tritiated, photoactivatable retinal analogs that formed acceptable bacteriorhodopsin analog pigments by two different techniques showed no significant labeling of bacteriorhodopsin. Parallel positive control experiments estimated the limit of detection of labeling at <5%.

Several modifications are suggested that should increase the likelihood of success for photoaffinity labeling of bacteriorhodopsin with subsequent analysis by mass spectrometry.

Table of Contents

List of Figures

Abbreviations Used

ABS	absorbance
ATR	all-*trans* retinal
BO	bacterio-opsin, the apo-protein
BR	bacteriorhodopsin
BSA	bovine serum albumin
CID	collision induced dissociation
CNBr	cyanogen bromide
cpm	counts per minute
CW	continuous wave
DMSO	dimethylsulfoxide
DA	dark adapted
FAB	fast atom bombardment
FTIR	fourier transform infrared absorption spectroscopy
GC-MS	gas chromatography - mass spectrometry
GPCR	G-protein coupled receptor
HPLC	high pressure liquid chromatography
Ig	immunoglobulin
KFOX	potassium ferrioxalate
LA	light adapted
MALD	matrix assisted laser desorption
MS	mass spectrometry
MS/MS	tandem mass spectrometry
NBA	p-nitrobenzyl alcohol
NMR	nuclear magnetic resonance spectroscopy
OD	optical density unit
PM	purple membrane
PSB	protonated Schiff base

RPR-100	Rayonet Photochemical Reactor
RTBR	reduced tritiated bacteriorhodopsin
SBSM	synthetic basal salt media
SDS-PAGE	sodium dodecyl sulfate polyacrylamide gel electrophoresis
tBDMS	tert-butyldimethylsilyl
TFA	trifluoroacetic acid
TFABA	tetrafluoro-4-azidobenzaldehyde
TFCBA	4-cyclohexylaminotetrafluorobenzaldehyde
TF4N3	tetrafluoro-4-azidoretinal
TLC	thin layer chromatography
TMH	transmembrane helix(es)
UV-vis	ultra-violet-visible absorption spectrophotometry

Single letter amino acid codes

Name	3-letter code	Single letter code
Alanine	Ala	A
Arginine	Arg	R
Asparagine	Asn	N
Aspartic acid	Asp	D
Cysteine	Cys	C
Glutamine	Gln	Q
Glutamic acid	Glu	E
Glycine	Gly	G
Histidine	His	H
Isoleucine	Ile	I
Leucine	Leu	L
Lysine	Lys	K
Methionine	Met	M
Phenylalanine	Phe	F
Proline	Pro	P

Acknowledgements

I wish to thank the many people who aided in my graduate education; presented below are some of those who were most important. My mentors Rosalie Crouch and Dan Knapp generously supplied me with funds, space, equipment, direction and excellent people with whom to work. The other members of my advisory committee - Perry Halushka, Wes Corson, Don Menick and Kevin Schey - helped to teach me the value of genuine enthusiasm for biomedical research.

The Departments of Pharmacology and Ophthalmology and their chairmen, Tom Gaffney, Harry Margolius and David Apple, provided excellent facilities and opportunities during these studies.

I wish to thank my collaborators from outside MUSC: Valeria Balogh-Nair from the City College of New York for the synthesis of two retinal analogs and entrusting them to me for analysis; Steve Martin, of MIT and Genetics Institute, who taught me many techniques and generously let me join him for three months in Cambridge; Klaus Biemann who allowed me to work in his lab and made me a visiting scientist at MIT; and Rajni Govindjee and Tom Ebrey at the University of Illinois who enthusiastically performed the kinetic studies on many sets of BR analog pigments.

I wish to thank my many collaborators and friends at MUSC who have taught me a great deal of chemistry and many important lessons about life: Venkat Mani who made many retinal analogs and made me laugh; John Oatis who taught me chemistry usually in the hall on the back of a paper towel; Bernice Katz who struggled and persevered in making the toughest retinal analog; James Chapman who taught me chemistry, made me laugh, patiently named all of the retinal analogs *and* edited the entire dissertation; Starr Hazard who taught me many important things by example and how to use the molecular modeling package; and Heather Callahan who taught me to do everything three times - if possible.

The summer students for whom I had major responsibility patiently taught me how to teach and to lead and also did tons of work: Beth Cohen-Jonsson who initiated the studies on model photolysis which were finished by Stacie Moore, and Kevin Gray who wrestled with SYBYL over two summers to make it do what we wanted it to do.

Then, there is Patrice Goletz who taught me most every technique I learned and did so with patience and grace. She deserves much of the credit for the completion of this dissertation.

Teresa Thompson has kept the rest of my life fun, taught me how to make a decent slide and shown me what a joy it is to love a beautiful woman.

This dissertation is dedicated to my parents. They have generously supported me in every way for 23 years (so far) of formal education. Thank you, Mom and Dad.

Chapter 1

General Introduction

The objective of this research was to define which amino acids of bacteriorhodopsin (BR) are in close proximity to the ring portion of retinal. The methods used involve the design and synthesis of photoactivatable analogs of retinal, incorporation of the modified ligand into the apoprotein, characterization of the resulting analog pigments, photoactivation, and identification of labeled sites in the protein. A molecular model of BR was manipulated to predict the amino acids that are likely to be labeled by different retinal analogs and to evaluate already published labeling experiments.

First, it is necessary to introduce the structure of BR, why it is relevant to pharmacology, how photoaffinity labeling experiments may further define its structure, and how mass spectrometry may be useful in identifying the labeled sites. Next, the subjects of photoactivation, molecular modeling, and identification of the amount of labeling using radiolabeled photoactivatable reagent are briefly introduced. After this introduction, the objective, hypothesis and specific aims of this work are explicitly stated. The experimental investigation of the specific aims forms the body of the dissertation. Finally, in Chapter 7, the experimental results are summarized and suggestions are made for future work.

Structure of Bacteriorhodopsin. The present understanding of BR has been gained through the exploitation of numerous biochemical and biophysical techniques. The more important aspects are briefly described here. BR is a 26 kilodalton integral membrane protein from the archaebacterium *Halobacterium halobium.* The protein functions as a light driven proton pump. The ecological niche for this bacterium is in environments of extremely high salt concentration (4 M in NaCl, 25% by weight, ~25 times that of seawater) such as the salt flats outside of San Francisco, CA and fish curing barrels [Stoeckenius *et al.*, 1979]. In conditions that disfavor aerobic metabolism, such as low oxygen or lack of a reduced carbon source, BR provides the proton gradient necessary for the synthesis of ATP. The protein binds retinal (Vitamin A aldehyde, fig. 1.1) in a molar ratio of 1:1. This association of the retinal with the

protein shifts the absorbance spectrum of the retinal from 380 nm (free in ethanol) to 570 nm (bound in BR) giving the protein its characteristic purple color. The purple color and the fact that when BR is isolated from the bacterium it exists in small patches of membrane have given it the name of purple membrane. There are three other homologous proteins in *Halobacterium halobium*, they are a light-driven chloride pump (halorhodopsin) and two phototactic pigments (sensory rhodopsin I and II). These three proteins also bind retinal and are used by the bacterium to pump out excess chloride and to sense sources of useful light. Thus, these 'primitive' archaebacteria have developed a system that allows them to survive in very harsh conditions by harvesting sunlight when there is no food and no oxygen [Stoeckenius *et al.*, 1979].

The primary structure of BR has been determined by direct protein sequencing [Ovchinnikov *et al.*, 1979; Khorana *et al.*, 1979] and by DNA sequencing [Dunn *et al.*, 1981]. A relatively low resolution (7 angstrom) three dimensional model of BR which was based on electron diffraction data of a naturally occurring two dimensional crystal form of BR was published in 1975 [Henderson & Unwin, 1975]. This resolution gave information on only the relatively large alpha helices, but the seven transmembrane helical (TMH) motif was unmistakable. Analysis of the sequence for areas that would likely form transmembrane helices yielded seven such sequences of between twenty and twenty-five amino acids (fig. 1.2). The connectivities of the seven transmembrane helices were proposed and were eventually shown to be correct [Engelman *et al.*, 1980; Henderson *et al.*, 1990]. The retinal was shown to be linked by a protonated Schiff base to Lys216 [Bayley *et al.*, 1981]. Neutron diffraction and linear dichroism studies have established the position of the retinal to be in the barrel made by the seven transmembrane helices and angled toward the cytoplasmic surface at about 20 degrees with the Schiff base linkage deep within the protein and the ring end closer to the cytoplasmic surface [Heyn *et al.*, 1988] (see fig. 1.3).

As reviewed by Khorana (1988), several labs have investigated the function of BR and the tuning of the absorbance spectrum using mutants of the BR protein made with

molecular biological techniques. The mutants have been divided into three classes - those that seem to have no effect on absorbance or proton pumping function, those that perturb the absorbance spectrum, and those that influence the proton pumping. These last two classes are not mutually exclusive. It is believed that those in the second group must line the retinal binding pocket to be able to influence the absorbance spectrum of retinal and that those in the third group are directly involved in the proton pumping mechanism. The amino acids placed in these sets by BR mutation experiments correspond well with the placement of the amino acids in the two different groups by Henderson *et al.* (1990) (see fig. 1.4 & 1.5).

Upon the absorbance of a photon of light, BR photocycles through several spectrophotometrically discernible intermediate stages designated K through O which lead to proton pumping (fig. 1.6). The numbers associated with these different stages are the absorbance maxima of the intermediates in nanometers. Detailed spectroscopic studies have shown that the retinal cycles through changes in its conformation and protonation state. In the < 10 psec transition from the BR-570 state to the K-625 intermediate the retinal undergoes an isomerization from all-*trans* to 13-*cis*, but remains protonated. During the ~2 μsec transition from K-625 to L-550 the proton of the protonated Schiff base is believed to be being shifted to Asp85. Then after the ~ 40 μsec transition to the M intermediate, the Schiff base is unprotonated and the protein is believed to be shifting protons up from the inside of the membrane to reprotonate the Schiff base. The decay from M-412 to O-640 involves the reprotonation of the Schiff base and takes about 5 msec. This relatively slow decay makes it possible to take UV-vis spectra of the M-intermediate at one msec after a flash of light that induces photocycling. In the transition from O-640 back to BR-570 the retinal is reisomerized to the all-*trans* and the proton originally donated to Asp85 is shifted to the water on the outside of the membrane. This transition is also relatively slow and spectra taken at 5 msec after an actinic flash capture the O-intermediate. During this photocycle the pKa's of several different amino acids' protonatable groups and the Schiff base change

sequentially to pass a proton vectorially from the inside of the membrane to the outside [Rothschild, 1992]. The conformation of the retinal in the binding site has been shown in the BR-570 state to be in the all-*trans* conformation with the ring in the 6-s-*trans* conformation. Thus, the conjugated double bond system is planar [Creuzet *et al.*, 1990].

A concise summary of these results related to the structure of BR is presented in the 1990 paper of Henderson *et al.* which also presents electron diffraction data that are a landmark in the understanding of the structure of BR. This electron diffraction data is far superior to that reported in 1975. The resolution parallel to the membrane is 3.5 angstroms and about 6 angstroms perpendicular to the plane of the membrane (i.e. parallel to the long axis of the alpha helices). The diffraction data was collected at 4 K on tilted and non-tilted samples of partially dehydrated BR. The tilting of the samples allowed for more depth in the three dimensional view of the protein, albeit at relatively poor resolution. This resolution should be compared to that of X-ray diffraction of three dimensional crystals of proteins that can range to as low as 1-2 angstroms. Polypeptide chains can be delineated at 5-10 angstrom resolution. Groups of atoms can be distinguished at 2.8-4 angstrom resolution and individual atoms at around 2 angstroms. When the individual atoms can be resolved this is called atomic resolution [Stryer, 1988]. The resolution acquired from the electron diffraction studies was sufficient for Henderson and his colleagues to build a three dimensional computer model of the structure of BR. The quality of the electron diffraction data allowed accurate modeling of the relatively bulky seven TMH and the relatively electron dense retinal. The extramembranous loops were not modeled since insufficient electron density was derived for these relatively free moving loops (fig. 1.3). Since the resolution is far from 'atomic', there exists some ambiguity in the structure, especially in the arrangement of the less bulky sidechains of the amino acids in the alpha helices. This model contains 178 of BR's 248 amino acids modeled as accurately as possible. It was subsequently deposited in the Brookhaven databank of protein structures. This structure of BR has

become a working model for the protein that correlates well with the previous data [Henderson *et al.*, 1990].

Importance of BR Structure to Pharmacology. The details of the interaction between small molecules (ligands) and integral membrane receptor proteins are critical to the understanding of pharmacology at a molecular level. Recently a large group of receptors for diverse ligands has been classed together by virtue of a common hydropathy profile that predicts the existence of seven trans-membrane helical regions. These receptors are influenced by the binding of a small ligand to a ligand binding domain that is believed to be inside the barrel formed by the seven TMH. These ligands vary greatly to include, among others, the biogenic amines, retinals, endothelin and cannabinoids. Another reason these receptors are grouped together is that they bring about their intracellular response through the intermediary action of a GTP-binding regulatory protein. These receptors have thus been named the G-protein coupled receptors (GPCR) and more than seventy receptors have been included [Dohlman *et al.*, 1991; Probst *et al.*, 1992]. The group includes (with their ligands in parentheses) the mammalian opsins (retinal), α_1, α_2 (norepinephrine), β_1 and β_2 (epinephrine) - adrenergic receptors, the muscarinic receptor family (acetylcholine), the 5HT-1c and 5-HT-1a-receptors (serotonin), the substance K receptor, the endothelin receptor, D_1, D_2, D_3 receptors (dopamine), a cannabinol receptor and a functional angiotensin receptor [Probst *et al.*, 1992 and references therein]. The prototype of this group is the visual pigment, rhodopsin. Substantial evidence exists for the correctness of this structural model for the rhodopsin molecule [Hargrave *et al.*, 1983]. However, the strongest evidence for this structural motif comes from electron diffraction studies of bacteriorhodopsin (fig. 1.3). Thus, BR has become the structural prototype of this important class of receptors [Pardo *et al.*, 1992; Hibert *et al.*, 1991]. BR shares with this group a similar hydropathy profile and more importantly the ability to bind and be influenced by a small 'ligand'. Thus, the interaction of retinal with BR has become a

powerful model for the interaction of the ligand with the binding domain of the GPCR.

The utility of the BR structure as a starting point for modeling GPCR is evident from studies such as those of Hibert *et al.* (1991) in which the amino acids in the structure of BR are changed (in the computer) to the sequence of the protein under discussion. Hibert *et al.* concluded that such models 'enable structure-activity relationship studies and more rational drug design' on neurotransmitter GPCR. Pardo *et al.* (1992) advanced the use of the BR 'template' for modeling GPCR by suggesting that the linear sequence of the seven TMH need not be maintained, but that it is the geometric arrangement of the helices that should be followed. By taking the TMH as units, without regard to the linear sequence, they were able to show closer homology between BR and the GPCR. Pardo *et al.* suggest that the lack of sequence homology between BR and the GPCR is not surprising considering the large evolutionary distance between the archaebacteria and, for example, mammals. They suggest that the structural motif was conserved with the seven amphipathic TMH forming a binding pocket.

It is important to note that the similarities between BR and GPCR are believed to be at the three dimensional structural level. Even BR and rhodopsin possess very little sequence homology. Also BR is not coupled to G-proteins. Even the phototactic pigments from *Halobacterium halobium* that must communicate with the inside of the cell to effect the swimming motion of the bacterium are not believed to be coupled to G-proteins. Thus, BR is the *structural* prototype of the GPCR and rhodopsin is the best prototype, in general, of this pharmacologically important class of receptors.

In addition to this importance as a structural prototype, BR is of considerable interest due to its ability to transduce light energy into a proton gradient. It converts photon energy into chemical potential energy. This process is at least triggered if not driven by the absorption of a photon by the bound retinal co-factor [Khorana, 1988]. Recent reports indicate the potential for BR in the development of a 'biochip' that could lead to a revolution in image detection [Hong, 1986; Miyasaka *et al.*, 1992]. The image detector constructed by Miyasaka and his colleagues is termed a biomolecular sensor

and is able to react within microseconds to changes in intensity while ignoring constant light - an attribute known as differential response. This type of response is difficult to mimic using 'silicon retinas' and is important *in vivo* for activities such as predators noticing the movement of prey [Flam, 1992].

The interaction of the 'ligand', retinal with the apo-protein, bacterioopsin is significant as a model for receptor-ligand interactions in general and as an energy-transduction system. It is especially amenable to study at the molecular level because of its relative abundance, ease of manipulation and characterization, and the large amount of structural information available.

Photoaffinity Labeling of BR. Photoaffinity labeling reagents are unreactive in the dark, but when activated by light, they become highly chemically reactive and are capable of forming a covalent bond to a nearby molecule. Photoaffinity labeling reagents are normally designed to mimic the ligands of the protein of interest. By resembling the ligand of a receptor (or the substrate of an enzyme), photoaffinity labeling reagents can identify the protein in a mixture or identify a particular ligand binding site within a protein. The lack of reactivity in the dark allows the experimenter to perform basic tests on the biological activity of the ligand to show that it does bind to the native binding site. The reactive moiety of the photoaffinity labeling reagent can be revealed at any point in the experiment by initiating the photolysis. This flexibility allows manipulations of the system in the dark that may enhance specific labeling of the ligand binding site.

Several different types of photoactivatable groups are classed by the reactive intermediate produced when they are photolysed (fig. 1.7, top). One group shows the loss of molecular nitrogen to yield a carbene or nitrene. This group is thus subdivided into carbene precursors (e.g. diazo compounds and diazirines) and nitrene precursors (most often aryl azides). Another group works through radical mechanisms to label the nearby protein in a two step process. This group includes the α,β-unsaturated ketone

compounds (fig. 1.7, top and bottom). The typical reactions of the extremely reactive carbenes and nitrenes are shown in fig. 1.7, middle. Nitrenes and carbenes react similarly, but carbenes are generally more reactive than nitrenes. The most useful reaction in this scheme is labeled insertion. The ability of the reactive intermediates to insert between C-H bonds shows just how reactive they are. This C-H insertion is the most stable bond that might be formed. Other productive reactions (i.e. those that will lead to stable bonds formed with the protein) are addition to aromatic rings and reactions with nucleophiles. Dimerization reactions are not productive, but are unlikely to occur in the experiments described in this work since the retinal analog forms a 1:1 link with BR and is isolated deep inside the protein. The two step radical reactions of the α,β-unsaturated ketone groups are considerably less aggressive. In the BR system though, again due to the isolation and Schiff base link of the retinal analog in the binding pocket, the reactive group may be in contact with the protein long enough to stably label. These types of reactions have been successfully used to identify steroid receptors by photoaffinity labeling [e.g. Hearne & Benisk, 1973].

With this introduction to photoactivatable groups and with the help of Bayley (1983), it is possible to rank the reactivities of the different photoactivatable groups as follows. Aryl azides have been surpassed by the electronegatively substituted nitro- and fluoro- arylazides for ability to undergo C-H insertion [Bayley, 1983; Keana & Cai, 1988]. Carbenes are generally considered more reactive than nitrenes which makes diazo compounds and diazirines more desirable than azides. Diazirines are superior to diazo compounds since they can be activated at 365 nm [Huang *et al.*, 1982; Nakayama & Khorana, 1990], well above the normal absorbance of the aromatic amino acids of the proteins. Thus, diazirines are superior to (>) diazo compounds > electronegatively substituted aryl azides > aryl azides = unsaturated ketones > alkyl azides.

An ideal photoaffinity labeling reagent should meet the following criteria [Bayley, 1983].

• The reagent should be stable in the dark and in aqueous solution.

• The reagent should be simple to synthesize and radiolabel.

• The reagent should resemble the native ligand chemically so as to function similarly in the biological system.

• The photoactivatable group should be efficiently activated to a highly reactive intermediate at wavelengths and powers of light that do not damage the protein or the reagent itself.

• The adducts formed must be stable to the analysis conditions.

It would be extremely difficult to develop reagents that fit all of these criteria. As described in Chapter 2, several retinal analogs were designed and synthesized to possess as many of these characteristics as possible.

In designing photoactivatable retinal analogs, it is important to know from previous studies what types of chemical modifications of the retinal can be tolerated by the protein and still leave the BR analog pigment functional. Studies involving retinal analogs to investigate the retinal binding site have shown that the protein requires at least 4 conjugated double bonds in the polyene side chain and only some parts of the ring in order to function. BR will tolerate bulky modifications to the ring end of the retinal, but only minor changes to the polyene side chain and Schiff base end of the chromophore [Crouch, 1986].

On the basis of experiments with selectively hydrogenated retinals, the 'external point charge' model was proposed to account for the nearly 200 nm opsin shift [Motto *et al.*, 1980]. The 'external point charge' includes a counter-ion for the Schiff base and a negative charge near the ring portion of the retinal [Nakanishi *et al.*, 1980]. These studies along with the previous photoaffinity labeling experiments with BR indicate that the most likely section of the retinal that can be modified (and retain function of the BR analog pigment) is the cyclohexenyl ring.

The studies presented in this work were initiated prior to the publication of the landmark paper of Henderson *et al.*, 1990 and at the time when only one report of photoaffinity labeling of BR had been published [Huang *et al.*, 1982]. Since then two

reports of successful attempts to photoaffinity labeling of BR using photoactivatable retinal analogs have been published. BR is especially convenient for these studies since the retinal is covalently linked to the protein by the Schiff base at Lys216 which gives the equivalent of an extremely small K_d. Huang *et al.* (1982) showed specific labeling of Ser193 and Glu194 (fig. 1.8) using an aromatic analog of retinal (Khorana, **2**, see fig. 1.1 for structure) as the photoactivatable retinal analog. They, however, did not demonstrate the ability of the analog pigment to pump protons or to form photocycle intermediates (i.e. biological activity) before or after cross-linking. Ding *et al.* (1990) published the second report of photoaffinity labeling of BR. With their analog (Nakanishi1, **2**), they were able to demonstrate labeling of Thr121 and Gly122 (fig. 1.8). The analog pigment formed from this photoactivatable retinal was shown to pump protons at about 1/3 the efficiency of native BR. The third report also came from Nakanishi's laboratory. Boehm *et al.* (1990) reported the labeling of amino acids Ala126, Leu127, Trp137 and Trp138 with another non-aromatic retinal analog that was a carbene precursor (**4**). They showed that the BR analog pigment formed with this retinal analog functioned at about 1/3 the efficiency of native BR. Note that all of these retinal analogs contain photoactivatable groups that are carbene precursors. Also note that the labeling is spread over more than one amino acid in each site of labeling which may be due to actual labeling of these amino acids or inherent difficulties with the use of Edman degradation to identify labeled sites individually. Boehm *et al.* (1990) suggest that this spreading of the sites of labeling is due to an inherent weakness in the use of Edman degradation to identify the labeled sites. The photoactivatable retinal analogs used in the studies presented in this work were evaluated for their ability to form stable analog pigments, form photocycle intermediates, and pump protons.

Mass Spectrometric Identification of Labeled Sites. As introduced above, the identification of labeled sites using Edman degradation of isolated peptides labeled with radioactively tagged retinal analogs is less than ideal. These methods require

purification to homogeneity of the labeled peptide for unambiguous Edman sequencing - an often difficult task [Brinegar *et al.*, 1988]. The elution of the radiolabel is often spread over more than one Edman cycle which makes identification of a single labeled site nearly impossible [Boehm *et al.*, 1990]. This loss of resolution decreases the structural information that can be obtained from the labeling experiment. For example, the identification of two sequential amino acids from an Edman sequencing run as labeled sites can change the interpretation by as much as a 100 degree rotation of an alpha helix. The conditions used for Edman sequencing (as well as other protein chemistry) may also remove or degrade the label [Dohlman et al., 1988; Kaur *et al.*, 1989].

The ability of mass spectrometry to analyze polypeptides has greatly increased in the last ten years due to the introduction of three different ionization techniques that can volatilize intact peptides. These techniques for mass spectrometry of peptides and proteins have been reviewed very recently [Biemann, 1992] and will be discussed only briefly here with particular attention to their possible use in photoaffinity labeling experiments of BR. The first of these techniques was introduced by Barber *et al.* (1981) and is called fast atom bombardment (FAB) ionization. In this technique, a peptide or mixture of peptides is ionized from a liquid matrix (often glycerol) by a beam of high energy atoms or ions. Peptides undergo very little degradation in this ionization process and the protonated molecular ion $(M+H)^+$ is usually the most intense. Most peptides are amenable to fast atom bombardment MS. However, some very hydrophylic and very hydrophobic peptides are more difficult to analyze with standard FAB techniques. In general the sensitivity of fast atom bombardment MS decreases with increasing mass. At approximately six thousand daltons the sensitivity has decreased to a point that the other ionization techniques are often more useful. The accurate measurement of the mass of a peptide can answer many questions about its structure including the correctness of an amino acid sequence derived from DNA sequence, the detection of natural or biosynthetic mutations, and of most interest here

the identification of chemical modifications including photoaffinity labels. The use of MS in detection and identification of photoaffinity labeling will be further discussed below.

The other two ionization techniques have greatly expanded the mass range for analysis of peptides and large proteins with hemoglobins (~15 000 mol. wt.), albumins (~60 000 mol. wt.) and monoclonal antibodies (~150 000 mol. wt.) often being reported. Electrospray ionization extends the nominal mass range of the instrument by generating multiply charged ions. The ionization process involves the formation of tiny, usually acidic, droplets containing the sample peptide. These droplets are desolvated in in a heated capillary interfaced to the vacuum of the mass spectrometer and the sample is eventually left multiply charged and free of solvent. The other ionization technique is matrix assisted laser desorption. In this technique, the sample is crystallized with a light absorbing matrix. The sample/matrix mixture is then irradiated and the sample is ionized. It has recently been shown that mass measurements on BR and bleached BR (bacterioopsin) can be obtained using matrix assisted laser desorption (MALD)- time of flight mass spectrometry [Schey *et al.*, 1992]. MALD - time of flight mass spectrometry can distinguish these two samples, when they are run individually, that differ only by the mass of the retinal. However, these techniques could not resolve the two species in a sample that contained both [Schey *et al.*, 1992]. This method, therefore, would not be able to resolve an unlabeled BR molecule from a fraction that was mass shifted by ~300 daltons by the addition of a photoactivatable retinal analog as part of the same sample. It could be extremely useful in other aspects of identification of labeled peptides after cleavage of BR. For example the entire reaction mixture from a chemical or enzymatic cleavage could be analyzed to assure complete reaction and to look for mass shifted peptides. Since these two ionization techniques were only very recently introduced to the laboratory, they were not used in the work described here.

Since these ionization techniques result in the molecular ion and not much fragmentation, structural information on the individual peptides is lacking and must be

derived after further fragmentation. This fragmentation is achieved in tandem mass spectrometry by selecting a peptide with the first mass spectrometer and then colliding the peptide with helium. This collision imparts excess internal energy to the peptide and the peptide fragments. This process is termed collision induced dissociation. The second mass spectrometer is then used to analyze the resulting fragments. All of these product ions come from the single peptide chosen by the first mass spectrometer. These ions, thus, contain information only about the selected peptide. Fortunately, peptides consist of a linear sequence of only 20 different amino acids. With two exceptions (Leu and Ile; Lys and Gln) the amino acids have unique masses (fig. 1.9). Interpretation of fragmentations is aided by the fact that peptides tend to fragment between the individual amino acid residues in only a few different ways (fig. 1.9). This leads to only a limited number of types of sequence ions. A common nomenclature has been adopted for these ions (fig. 1.9). The ions named from the end of the alphabet result from charge retention on the C-terminal end of the peptide and those named from the beginning of the alphabet have charge retention by the N-terminal of the peptide. Ions derived from a single series allow sequence information of the peptide to be derived from the mass differences between the peaks. For example, two y series ions that differ by mass 57 indicate a glycine at that position. Multiple series are often present allowing overlapping information to further verify the structure. With practice, and especially with known cleavage specificities, the sequence of a peptide can be completely derived from its tandem mass spectrum. Under favorable conditions, complete unknowns can be sequenced [e.g. Schluter *et al.*, 1990]. Peptides for which sequence information is available make the assignments particularly straightforward since the fragment ions can be predicted from the structure (especially simply with the aid of computer applications such as MacProMass [Lee & Verumi, 1990]). Because the sequence information is dependent only on the mass of the residues, chemical modifications can often be sequence specifically identified [Biemann and Scoble, 1987; Papac *et al.*, 1992].

The method of identifying sites of labeling sequence specifically with MS/MS is

complex. Presented in fig. 1.10 is a diagrammatic representation of the analysis of one HPLC fraction that contains several peptides (P1, P2, P3) including one that is mass shifted because it is labeled (P2*). The boxes along the top are the different stages in the mass spectrometer. The three spectra shown are the MS spectrum of the peptide mixture (left) and the MS/MS spectra of the non-labeled and labeled peptide P2 (right). The MS spectrum (left) shows that the peptide is shifted by the mass of the label (M*). In the MS/MS spectrum of the labeled peptide (P2*) each peptide fragment that contains the label (e.g. ABC*) is mass shifted from the corresponding peptide (e.g. ABC) in the non-labeled MS/MS spectrum of P2 by the mass of the label (*). It is possible, although unlikely, that labeled and non-labeled versions of the same peptide would co-elute on HPLC. They are shown here together to simplify the comparison. It is also possible that the relative amounts of the labeled and non-labeled peptide could vary widely depending upon the efficiency of incorporation of the label. The depiction described in this figure has the label bound to amino acid C of the labeled peptide P2* whose sequence is ABCD.

There are two different requirements for identifying the sites of labeling in a photoaffinity labeling experiment. The labeled peptide must first be detected. Then, the site of labeling within this peptide must be identified. The use of mass spectrometry to identify sites of photoaffinity labeling has been reported [Brinegar *et al.*, 1988; Chen *et al.*, 1986]. Chen *et al.* used concomitant sequencing by Edman methods and fast atom bombardment MS to identify a site of labeling. The labeled peptide was purified chromatographically and detected by the presence of radiolabel on the photoaffinity reagent. The site of labeling was identified by Edman sequencing and a single mass spectrum confirmed the mass shift of the peptide by the mass of the label. Note that mass spectrometry was not used to identify the site of labeling nor to detect the labeled peptide, but simply confirmed their results. The work presented by Brinegar *et al.* (1988) again describes the use of MS to confirm a site of labeling already determined by the more classical methods of radiolabeling and Edman sequencing. They, however, do

confirm the sequence specific site of labeling using MS/MS with a spectrum very much like that for P2* in fig. 1.10. Note that these studies use MS and MS/MS to identify sites of labeling on a peptide already known to be labeled.

Previously, mass spectrometry has been used to map the peptides derived from CNBr cleavage of BR [Allmaier *et al.*, 1986]. Working in Biemann's lab at the Massachusetts Institute of Technology, they were able to detect nine of the ten peptides predicted from this cleavage including the highest mass peptide at ~5400 daltons. These results indicate the potential utility of this high mass fast atom bombardment MS to detect mass shifts in these peptides resulting from photoaffinity labeling. It should be emphasized that the application of these techniques to large and hydrophobic peptides is complex. The added difficulty that only a fraction of a particular peptide would be mass shifted by attachment of the photoaffinity label made the detection of labeled peptides and identification of labeled sites by MS a major undertaking.

The recent addition to MUSC of state of the art facilities for these techniques including a JEOL HX110/HX110 high mass, high performance tandem mass spectrometer encouraged the use of sophisticated applications of MS and MS/MS to the study of photoaffinity labeling of BR. The studies on peptides from BR presented in Chapter 6 represent the initial use of the JEOL HX110/HX110 mass spectrometer at MUSC. These studies were initiated late in the overall sequence of the work presented here and represent initial studies using MS in anticipation of labeled protein being derived from the rest of the studies. Also in Appendix 2, presented as an example of the power of these mass spectrometric studies, is a summary of the mass spectrometric analysis of shark immunoglobulin light chains performed with Stephen Martin in Klaus Biemann's laboratory at the Massachusetts Institute of Technology in collaboration with Sam Schluter and Jack Marchalonis.

Photoactivation. The ability to activate the photoactivatable groups of the retinal analogs without damage to the protein is a requirement for these types of experiments.

To this end, two different light sources were evaluated. The Rayonet Photochemical Reactor-100 (RPR) equipped with nominal 350 nm wavelength bulbs was used as a source of continuous wave light. A flash photolysis apparatus with a xenon flashlamp delivering broadband radiation (~200-500 nm) in approximately microsecond pulses was also employed. These two light sources are compared for emission spectra, total photon output as measured by chemical actinometry, protein damaging effects (as shown by SDS-PAGE and absorbance changes of BR), and efficiency of activation of a model compound. Both sources use a specially constructed sample cell that allows efficient exposure of the sample. These studies are fully described in Chapter 3.

Molecular Modeling used to Predict Sites of Labeling. In order to predict and evaluate photoaffinity labeled sites on BR with different retinal analogs, Henderson's model [Henderson *et al.*, 1990] was manipulated using the molecular modeling package SYBYL (TRIPOS Inc., St. Louis, MO) running on the MUSC Vax 11/785 computer (e.g. fig. 1.3). These tools allowed easy manipulation and investigation of the structure. The sets of amino acids that are predicted to be the correct distance from the retinal analog's photoactivatable moiety to be potentially labeled in these experiments served as hypotheses for the photoaffinity labeling experiments. It is hypothesized that a photoactivatable retinal analog bound in the native retinal binding site will label amino acids that were predicted to be properly situated in the three dimensional structure of the protein to be contacted by the reactive intermediate. These predictions were also carried out for the three already published photoaffinity labeling experiments of BR. These studies are described in detail in Chapter 4.

Identification of Amount of Labeling Using Radiolabeled Photoactivatable Reagent. As was suggested earlier, attempting to detect and identify sites of labeling of BR by mass spectrometry alone was an ambitious undertaking. The use of radiolabeled, photoactivatable retinal analogs and more classical biochemical techniques for detecting

amount of labeling and identifying labeled peptides was suggested early in this work. The techniques used to evaluate the ability of the two available radiolabeled retinal analogs, that formed acceptable BR analog pigments, to crosslink to BR in a photolysis dependent manner are not novel [Huang *et al.*, 1982; Ding *et al.*, 1990]. The analysis of TF4N3 was incorporated late in these studies due to the difficulty in obtaining radiolabeled TF4N3. The studies using the more classical techniques for evaluation of labeling with TF4N3 are described in detail in Chapter 5.

With this introduction, the following explicit statement of the objective, hypothesis and specific aims of this dissertation should be clear.

Objective: Define the amino acids of BR that are in close proximity to the ring of the retinal using photoactivatable retinal analogs and mass spectrometric identification of labeled sites.

Hypothesis: Identification of photoaffinity labeled sites in BR will aid in further definition of ligand/receptor interactions of the receptors belonging to the GPCR class.

Specific Aims:

1) Determine the stability and functional characteristics of BR analog pigments formed with photoactivatable retinal analogs in order to evaluate their usefulness in photoaffinity labeling experiments.

2) Define appropriate light sources and photolysis conditions for the photoactivatable moieties of the retinal analogs that form acceptable BR analog pigments.

3) Predict and evaluate photoaffinity labeled sites of BR using molecular modeling.

4) Determine if and to what extent photoactivatable retinal analogs label BR using radiolabeled versions of the retinal analogs.

5) Evaluate the use of mass spectrometry and tandem mass spectrometry to define photoaffinity labeled sites of BR sequence specifically.

The experimental investigation of these specific aims form the body of this dissertation. The results of these experiments could yield significant new information concerning the amino acids of BR that are in close proximity to, and may control the function of, the ring portion of retinal. This new information will allow evaluation of the presently well accepted model of BR put forth by Henderson *et al.* (1990). The results may also further delineate the types of interactions generally important for ligand/receptor interactions. The methodology developed may be directly applicable to similar studies with rhodopsin and eventually to the entire class of rhodopsin-like receptors.

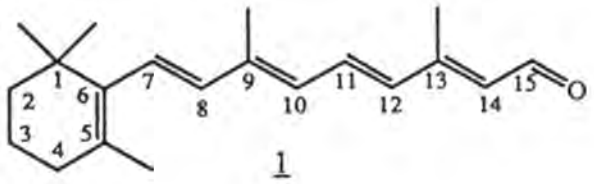

1

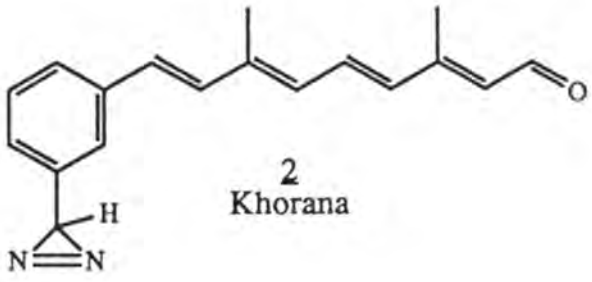

2
Khorana

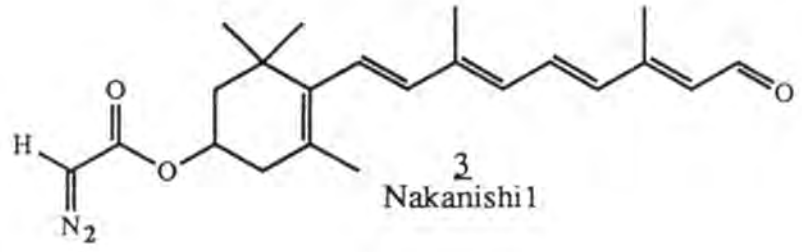

3
Nakanishi1

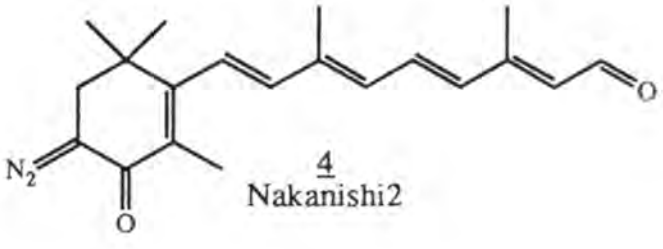

4
Nakanishi2

Figure 1.1 All-*trans* Retinal & Previously Published Photoactivatable Retinal Analogs

1: The chemical structure of all-*trans* retinal, the native chromophore of bacteriorhodopsin. The conventional numbering system of the carbon backbone is indicated. 2,3,4: Previously published photoactivatable retinal analogs.

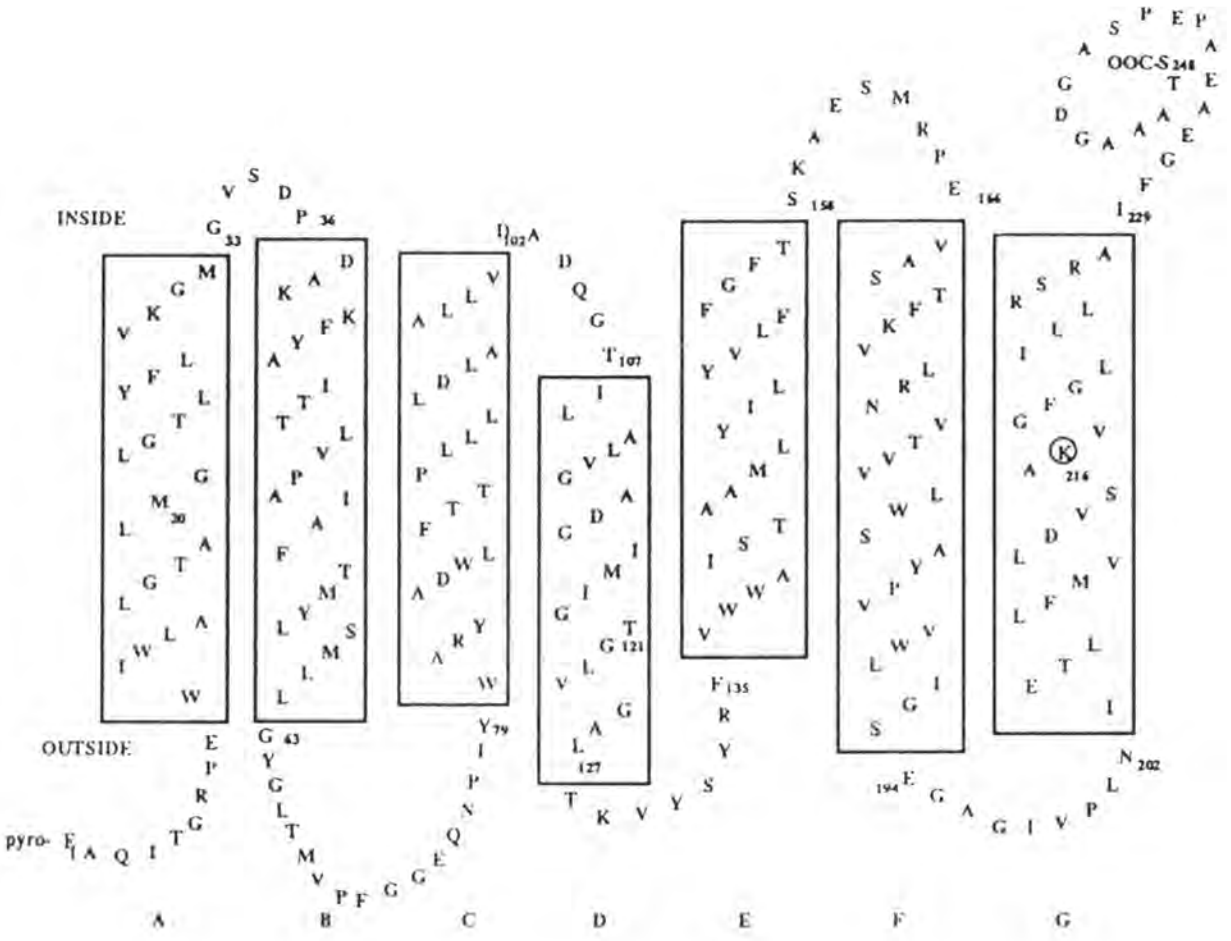

Figure 1.2 Bacteriorhodopsin, Two Dimensional Model
Two dimensional depiction of the structure of bacteriorhodopsin. The seven transmembrane helices are boxed and lettered A-G. Lysine 216 to which the retinal is bonded by a Schiff base is circled. For single letter amino acid codes, see list of abbreviations. Adapted from Henderson *et al.*, 1990.

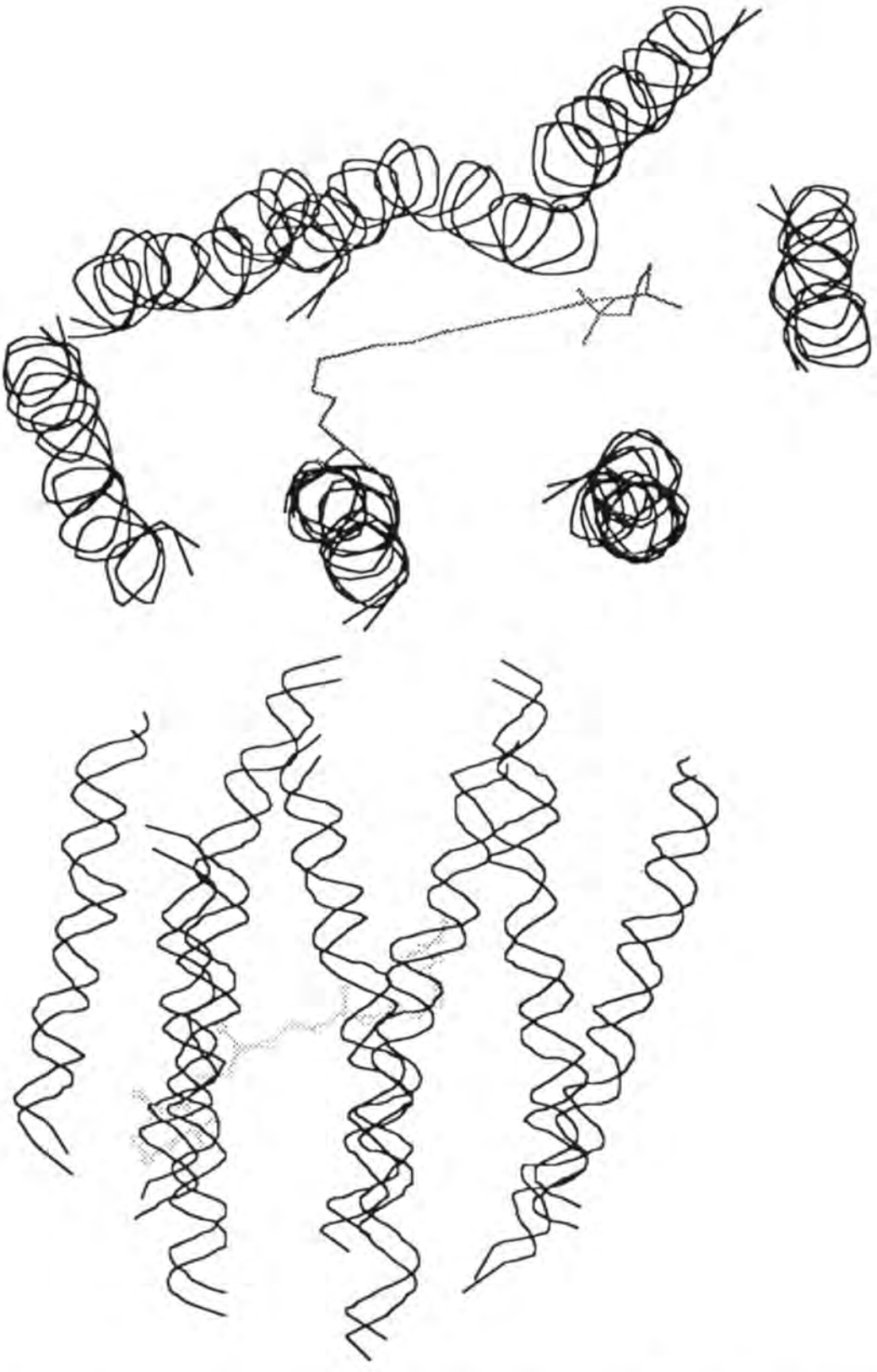

Figure 1.3 Bacteriorhodopsin, Molecular Model, Ribbon
Depictions of the three dimensional structure of bacteriorhodopsin with ribbons threaded through the α carbons of the seven transmembrane helices. Lysine 216 and retinal are shown in gray and as a ball & stick model in the bottom panel.
Adapted with SYBYL from Henderson *et al.*, 1990.

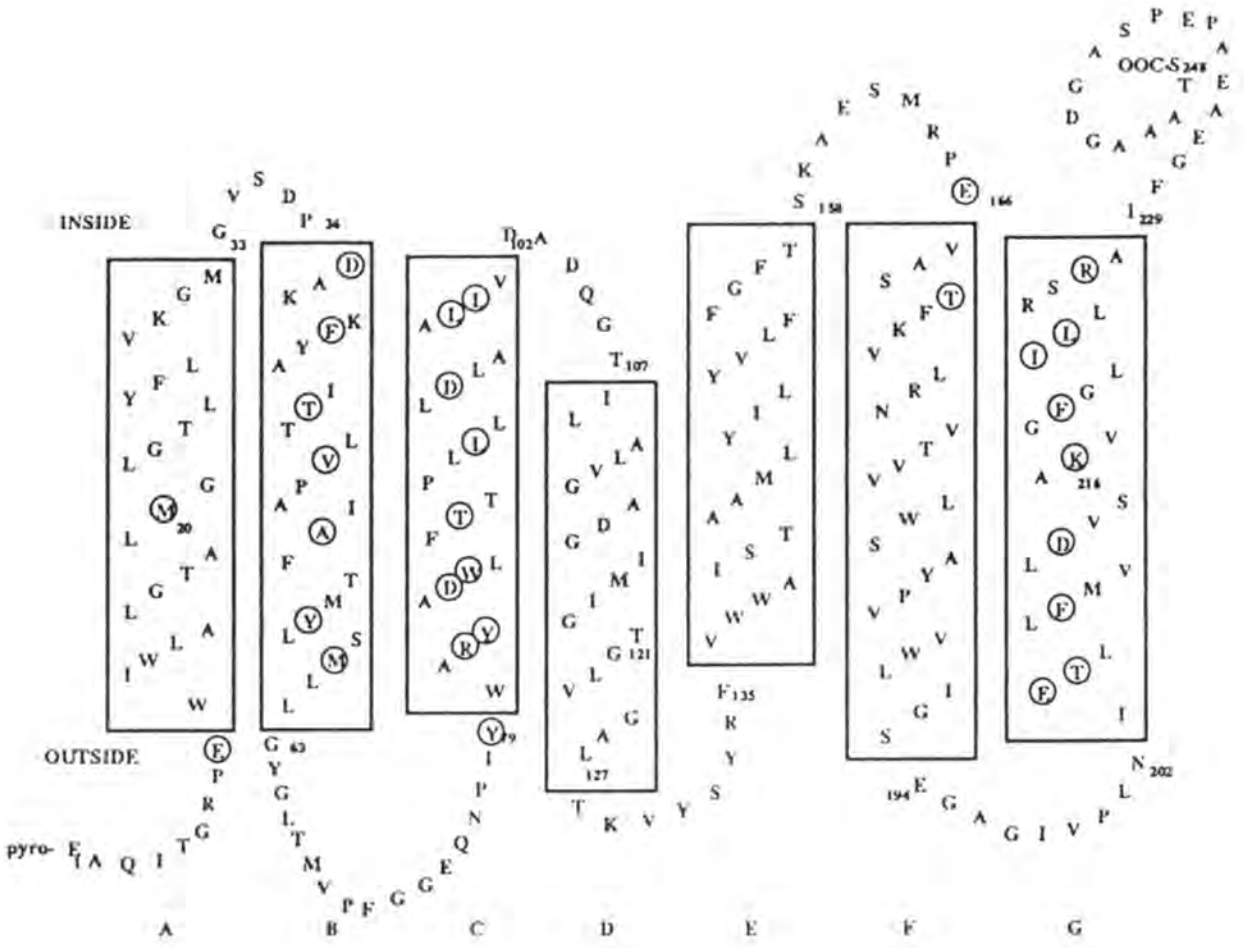

Figure 1.4 Bacteriorhodopsin, Proton Channel
Two dimensional depiction of the structure of bacteriorhodopsin. The seven transmembrane helices are boxed and lettered A-G. Lysine 216 to which the retinal is bonded by a Schiff base is circled. The other amino acids in the proton channel are also circled. Adapted from Henderson *et al.*, 1990.

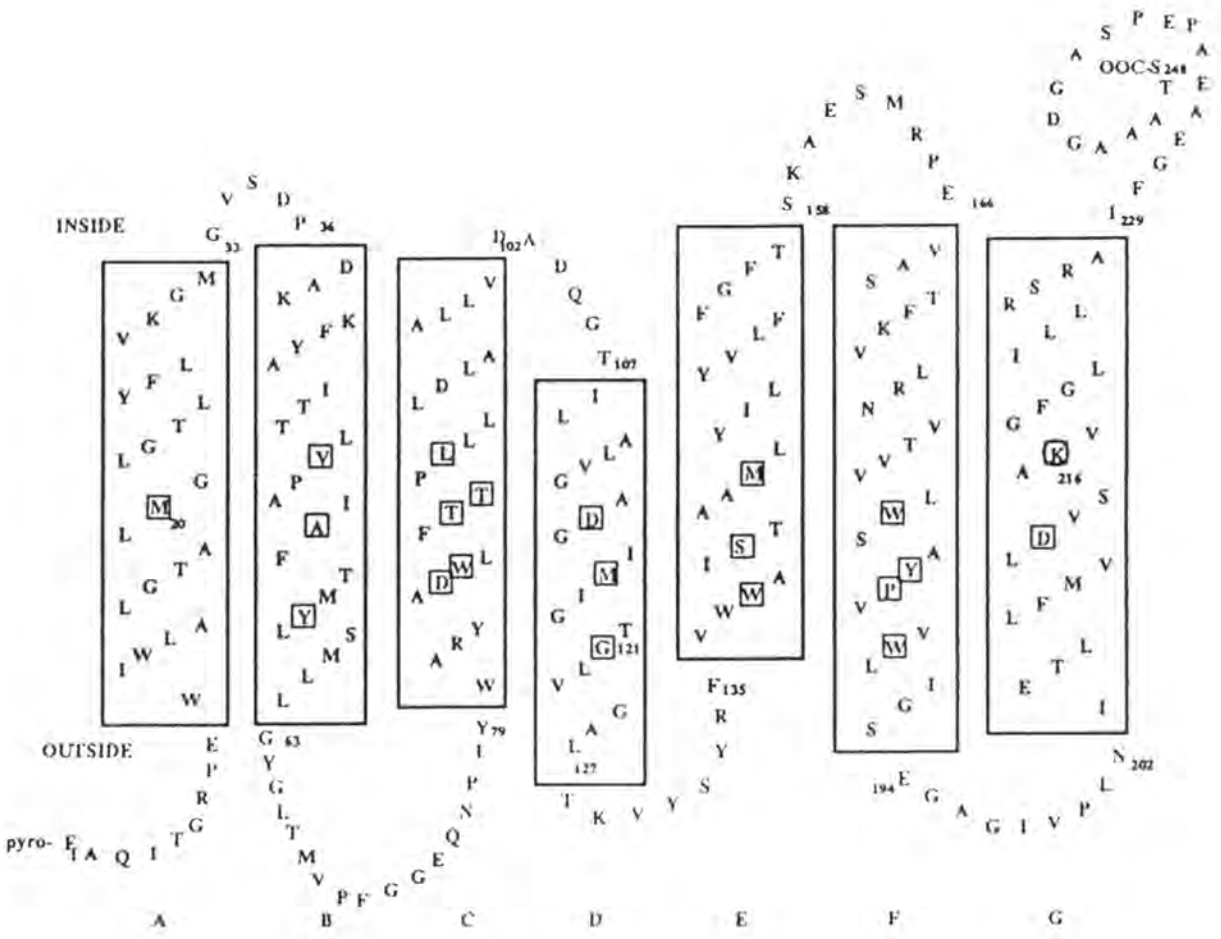

Figure 1.5 Bacteriorhodopsin, Retinal Binding Pocket
Two dimensional depiction of the structure of bacteriorhodopsin. The seven transmembrane helices are boxed and lettered A-G. Lysine 216 to which the retinal is bonded by a Schiff base is circled. Amino acids in the retinal binding pocket are in squares. Adapted from Henderson *et al.*, 1990.

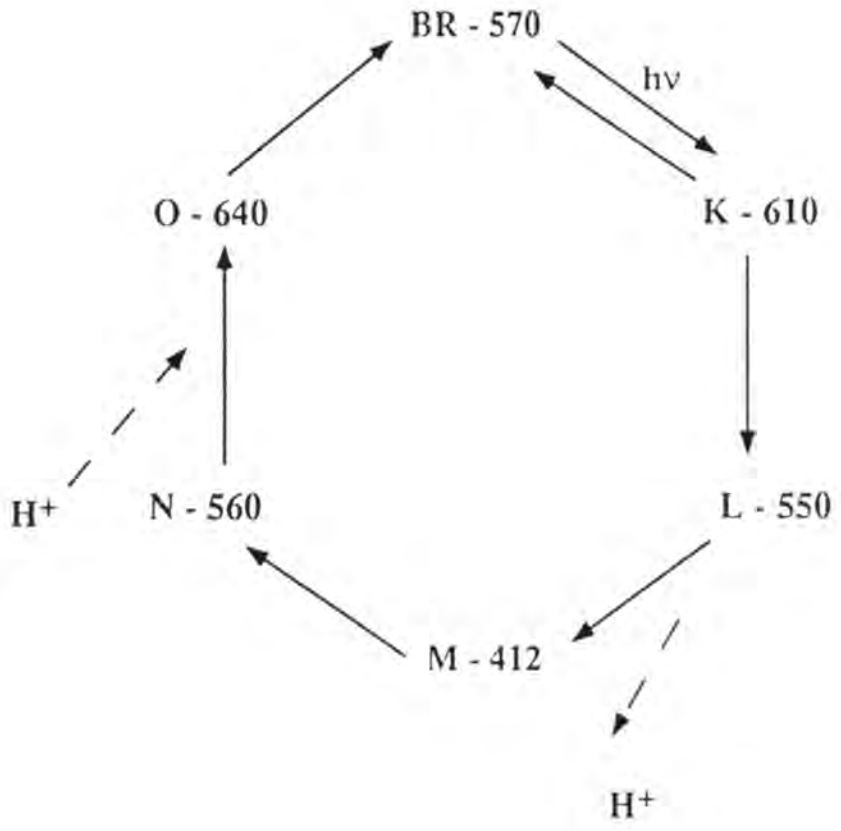

Figure 1.6 Bacteriorhodopsin Photocycle
A scheme for the photochemical cycle of BR. The cycle is initiated by light absorption by BR - 570. A proton is released on the outside and another taken up from the inside at the steps indicated. The numbers indicate the absorbance maximum of the intermediate in nanometers. Adapted from Henderson *et al.*, 1990.

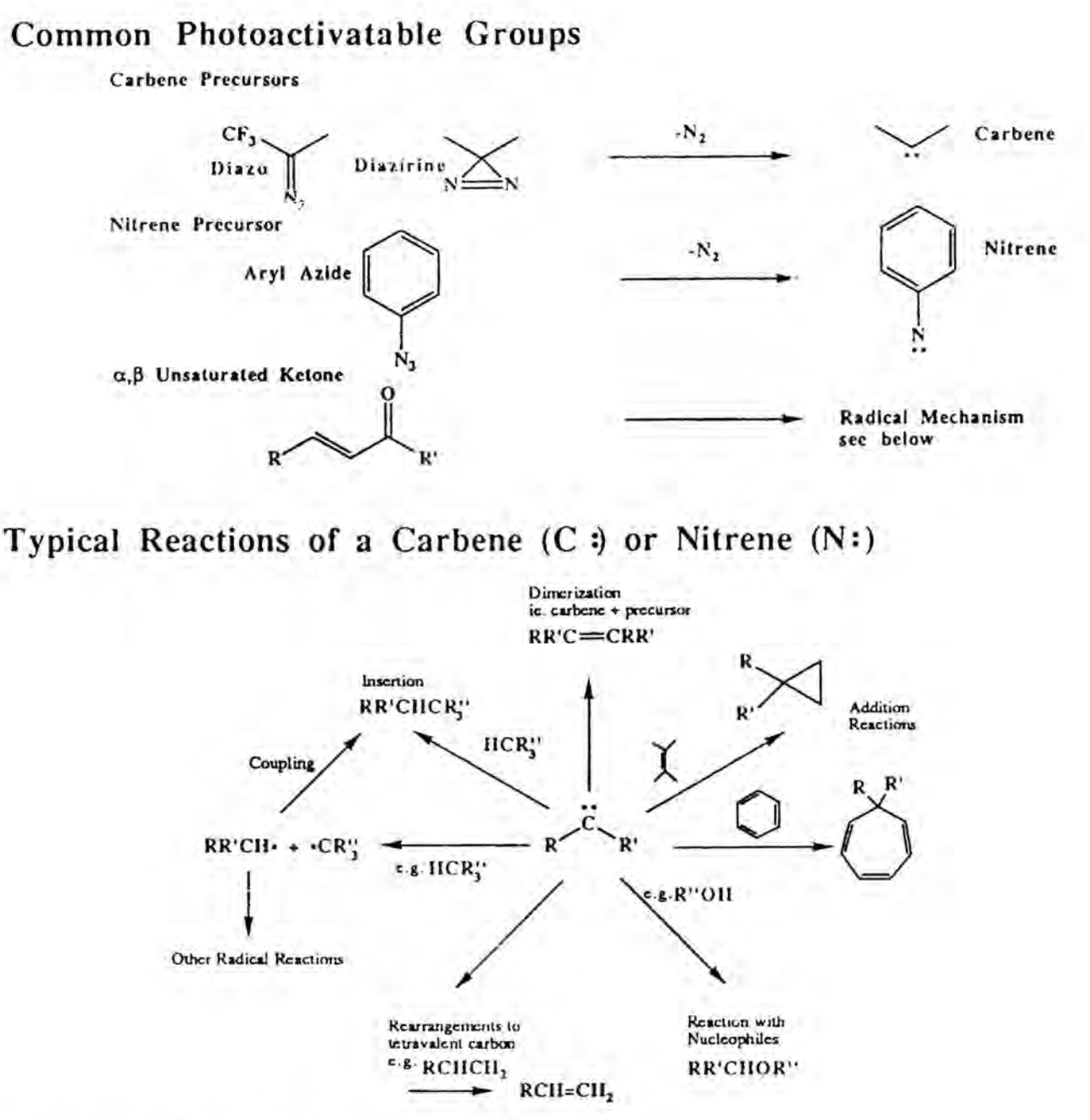

Figure 1.7 Common Photoactivatable Groups and Typical Chemical Reactions of Photoactivated Intermediates
Middle scheme shows reactions of carbenes and nitrenes. Bottom scheme shows mechanism of reaction of photoactivatible keto compounds.
Adapted from Bayley, 1983.

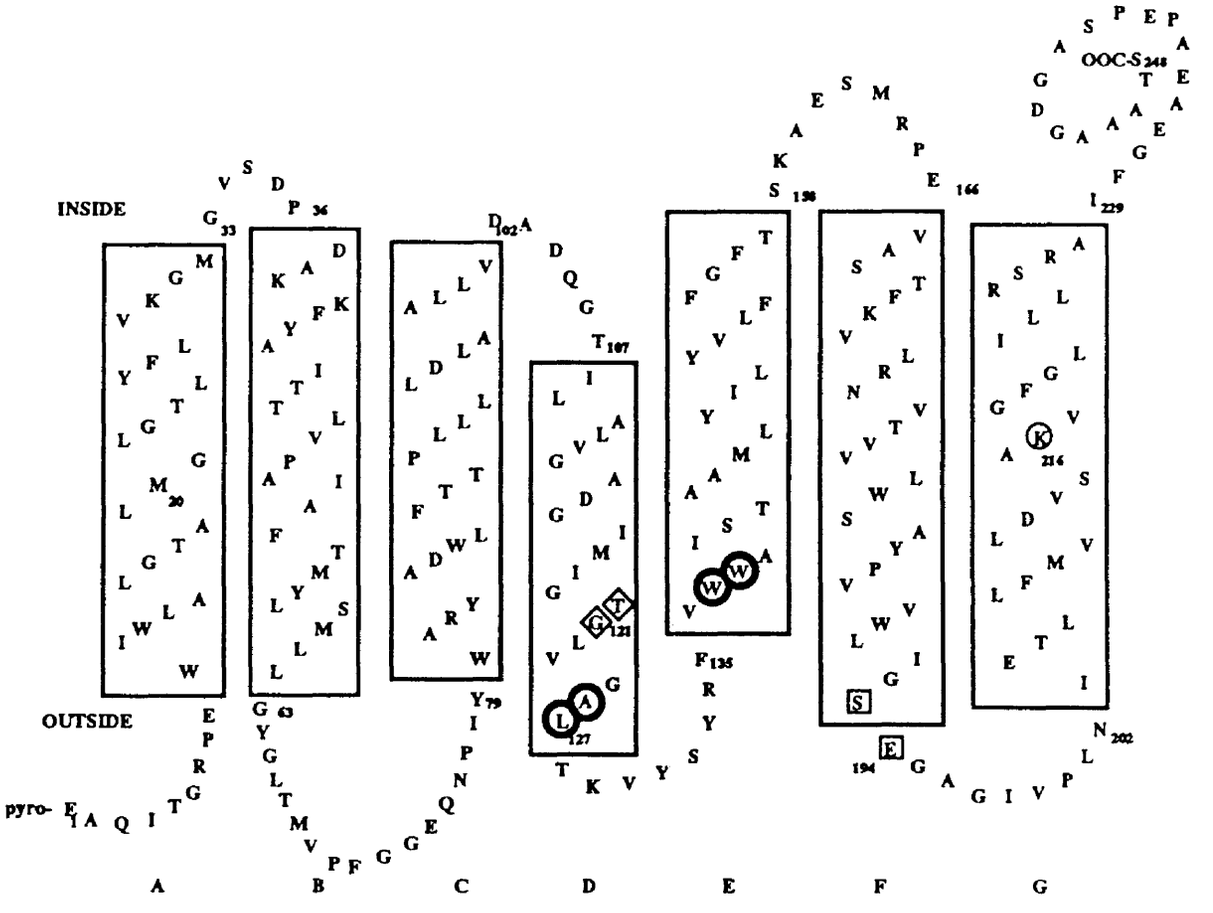

Figure 1.8 Previously Labeled Sites
Two dimensional depiction of the structure of bacteriorhodopsin. The seven transmembrane helices are boxed and lettered A-G. Lysine 216 to which the retinal is bonded by a Schiff base is circled. Ser193 and Glu194 were labeled by 2 and are boxed [Huang *et al.*, 1982]. Thr121 and Gly122 were labeled by 3 and are in diamonds [Ding *et al.*, 1990]. Ala126, Leu127, Trp137 and Trp138 were labeled by 4 and are in thick circles [Boehm *et al.*, 1990].

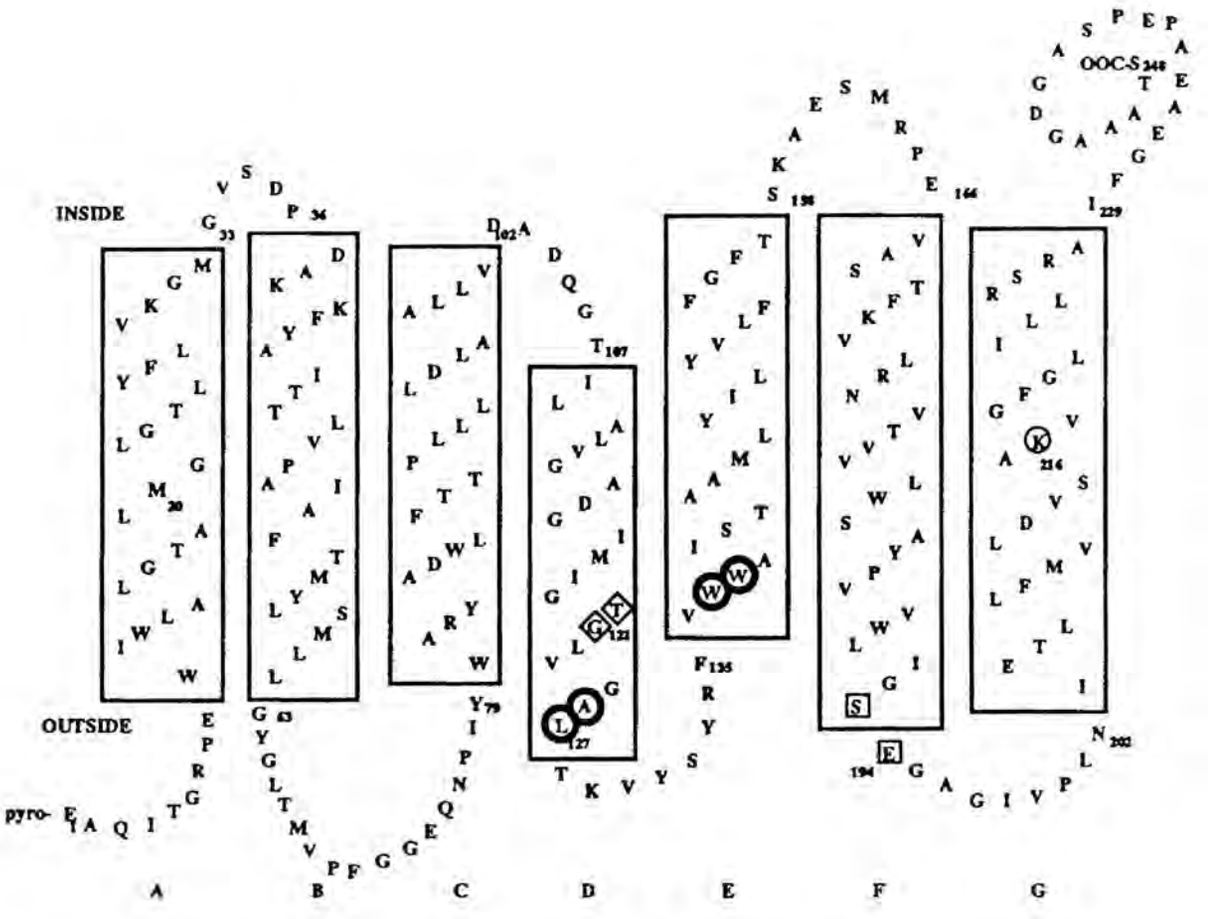

Figure 1.8 Previously Labeled Sites
Two dimensional depiction of the structure of bacteriorhodopsin. The seven transmembrane helices are boxed and lettered A-G. Lysine 216 to which the retinal is bonded by a Schiff base is circled. Ser193 and Glu194 were labeled by **2** and are boxed [Huang *et al.*, 1982]. Thr121 and Gly122 were labeled by **3** and are in diamonds [Ding *et al.*, 1990]. Ala126, Leu127, Trp137 and Trp138 were labeled by **4** and are in thick circles [Boehm *et al.*, 1990].

Fragment Ions Produced by CID from Protonated Peptides

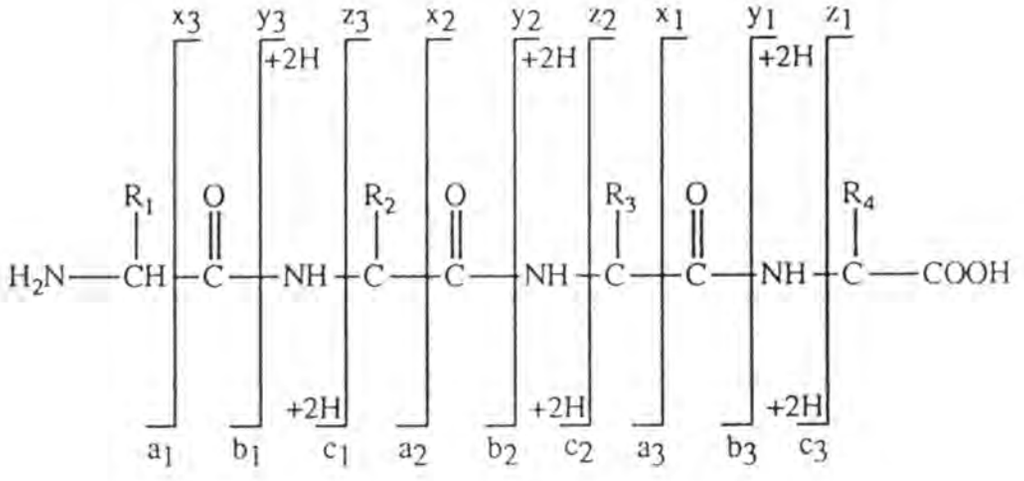

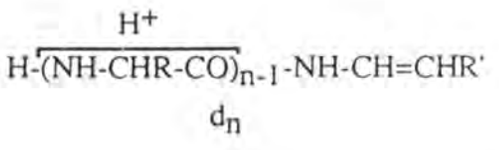

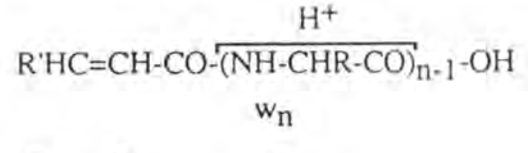

Immonium Ion
(denoted by single letter code)

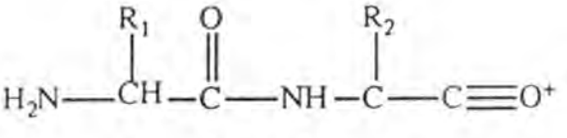

Internal Acyl Fragment Ion
(denoted by single letter code)

Amino Acid	Mass
G	57
A	71
S	87
P	97
V	99
T	101
C	103
I	113
L	113
N	114
D	115
Q	128
K	128
E	129
M	131
H	137
F	147
R	156
Y	163
W	186

Figure 1.9 CID Nomenclature and Mass of Amino Acid Residues
Adapted from Biemann, 1992.

PEPTIDES ANALYZED BY MS AND MS/MS TO DETERMINE SPECIFIC SITE(S) OF LABELING

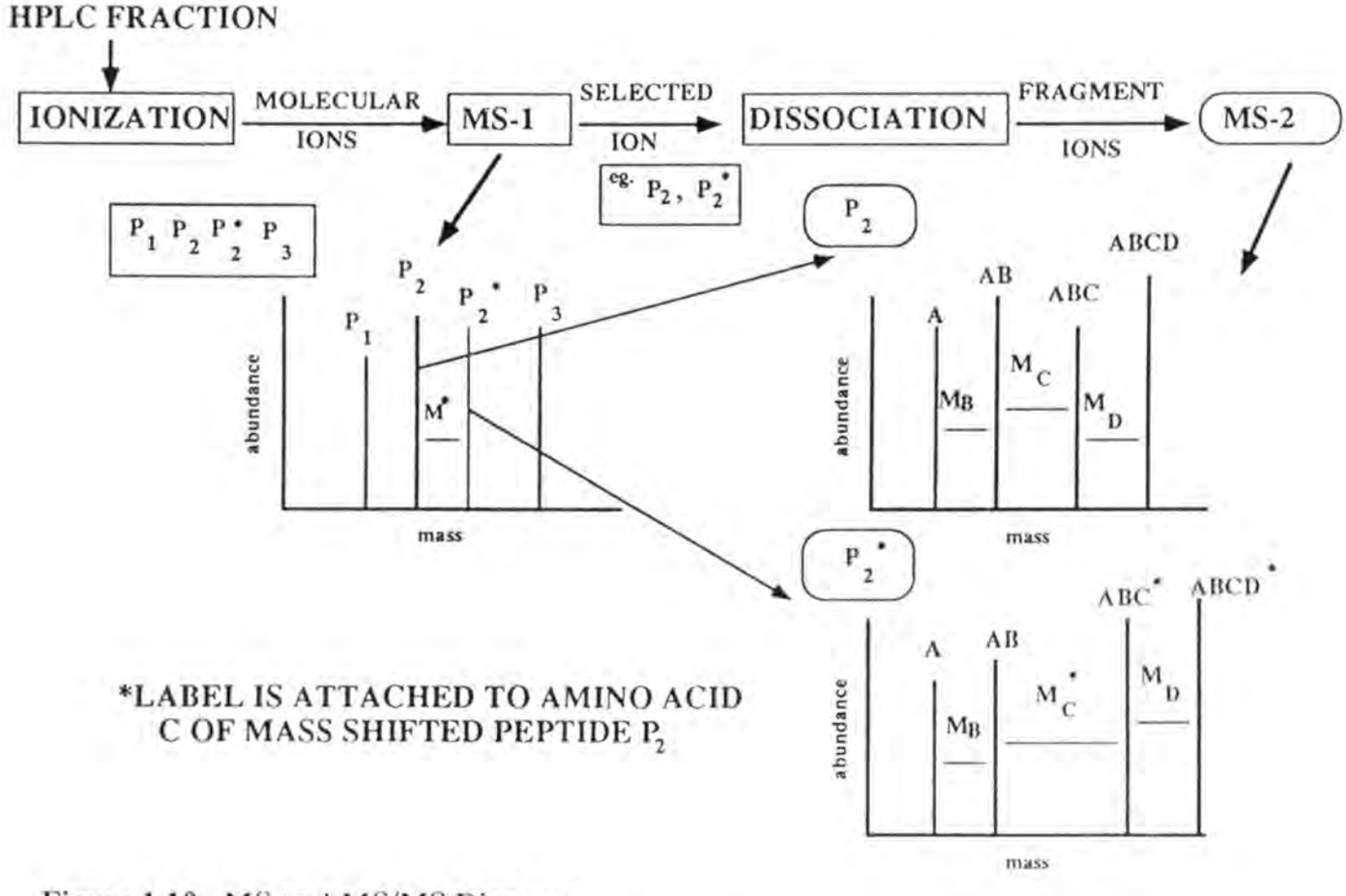

Figure 1.10 MS and MS/MS Diagram
Diagram of MS and MS/MS identification of labeled peptides. Each fraction from HPLC is analyzed by MS to determine the presence of peptides predicted from the known sequence and the cleavage method. The sequence of these peptides can be confirmed by MS/MS (P2). Unexpected peptides can be analyzed by MS/MS to show that they are the result of an unusual cleavage (not depicted) or that they have been mass shifted as the result of labeling (P2*). The MS/MS spectrum can show the site of labeling sequence specifically.

Chapter 2

Retinal Analogs and BR Analog Pigments

Portions of this chapter have been published as

Beischel, CJ, V Mani, R Govindjee, TG Ebrey, DR Knapp, and RK Crouch.

"Ring Oxidized Retinals Form Unusual Bacteriorhodopsin Analog Pigments."

Photochem. Photobiol. 54(6), 977-983, 1991

and

Beischel, CJ, V Mani, EA Cohen, DR Knapp, and RK Crouch.

"A Novel Photoaffinity Label for Bacteriorhodopsin."

Biophys. J. 57(2), 365a, 1990.

Introduction.

The use of retinals that have been modified chemically to possess a specific probe of the retinal binding site of BR has a long history in this laboratory and in others. More than fifty different retinal analogs have been tested for interaction with the protein [Crouch, 1986]. In this project, retinal derivatives that contain a photoactivatable moiety were desired. When incorporated into the protein and properly activated, these analogs should covalently link to the amino acids close to them. These retinal analogs must be designed to come as close as possible to the following characteristics of an ideal photoaffinity label for BR [adapted from Bayley, 1983].

- Easy to synthesize and radiolabel.
- Forms stable, functional BR analog pigment (i.e. biological activity)
- Stable in the dark and in aqueous solution.
- Able to be photoactivated to a highly reactive intermediate that forms a stable covalent crosslink with the protein by a wavelength and amount of light that does not damage the protein.

Compounds **5**-**12** were designed and synthesized with these criteria in mind. They were then evaluated for stable pigment formation and proton pumping function (i.e. biological activity). The chemical modifications were made to these compounds to make them potentially photoactivatable while remaining within the constraints derived from knowledge of other retinal analogs that have successfully formed stable, functional analog pigments [Crouch, 1986]. The compounds **13**-**15** were synthesized as intermediates in the synthetic schemes of the other retinal analogs and pigments were formed with these compounds since they are novel analogs. They are included here for completeness.

The analogs that are α-β unsaturated ketones were synthesized based on the precedent of using α-β unsaturated keto steroids to photolabel their receptors [Hearne & Benisk, 1973; Gronemeyer, 1985]. Compound **7** was isolated as an unexpected product of the oxidation of retinal by MnO_2. Compounds **5**,**6**,and **7** were synthesized

and purified by Dr. Venkat Mani. Compound **8** is based on the use of the classic aryl azide as a photoactivatable group. This compound was synthesized in limited quantities by Dr. Valeria Balogh-Nair at the City College of New York. The small quantity limited the analysis to pigment formation. This compound was also not radiolabeled. Compound **9**, also synthesized by Dr. Balogh-Nair, showed great promise since it has the highly reactive diazirine photoactivatable group and was supplied in sufficient quantity for many studies. However, it was not radiolabeled. Compound **10** was synthesized by Dr. Venkat Mani from compound **14**, a gift from Hoffman-LaRoche and 2-diazo-3,3,3-trifluoropropionyl chloride, commercially available from Pierce Chemical Co. It contained a carbene precursor, but did not form a stable pigment. Compound **11**, tetrafluoro-4-azidoretinal (TF4N3) was very difficult to synthesize and characterize. An outline of the synthetic scheme is included in appendix 1. This compound was originally synthesized by Dr. Venkat Mani; more recently Dr. Bernice Katz has further developed the synthesis. The model studies described in Chapter 3 are based on this potentially very useful photoactivatable group [Leyva *et al.*, 1986a, b; Keana and Cai, 1988]. This retinal analog was fully characterized as the BR analog pigment as described below. It was eventually available in tritiated form. Compound **12**, an acyclic photoactivatable retinal, was recently synthesized by Dr. John Oatis in small quantities and will soon be prepared in radiolabeled form for further evaluation. Compounds **2**,**3** and **4**, used in the previously published photoaffinity labeling experiments of BR [Huang *et al.*, 1982; Ding *et al.*, 1990], are shown in fig. 1.1 for comparison. The compounds **13**-**15** are synthetic intermediates and were analyzed to predict whether the final product would likely form pigment and in the case of **13**, pentafluororetinal, the pigment characteristics allowed discrimination of this compound and the final product of the synthesis **11**. Compound **13** was synthesized and characterized similarly to **11** and is described in the appendix. Compound **14** was a gift from Hoffman-LaRoche to Dr. Venkat Mani. He synthesized from this compound, compounds **15** and **10**. These compounds were characterized by Dr. Mani for use in these experiments.

Materials and Methods.

The methods used to evaluate the analogs as pigments are well established and described below [Crouch, 1986, Beischel *et al.*, 1991, Govindjee *et al.*, 1980].

All UV-visible spectra were recorded at room temperature using semi-micro masked cuvettes (1 ml, Markson) on a Varian Cary 2200 spectrophotometer interfaced to an IBM XT through a program in ASYST (Macmillan Software) written by DW Corson and J Reider. Incorporation of interactive graphics into the program to visually confirm the goodness of fit of the absorbance maximum determining routine were added as part of this work. Spectra were routinely recorded from 700 to 250 nm at room temperature. Unless otherwise noted, retinal analogs were dissolved in ethanol and BR analog pigments in water.

The infrared absorbance spectra of the retinal analogs were recorded on a Mattson Polaris Fourier Transform Infrared Spectrophotometer and analyzed with the dedicated ICON software. Samples of the retinals in deuterated chloroform were analyzed in a NaCl sample cell (0.1-mm path length). The sample compartment was purged with nitrogen and the spectra were recorded from 4000 to 800 cm^{-1} at 1.0 cm^{-1} resolution.

Gas chromatography-mass spectrometry (GC-MS) analyses of retinal analogs and other compounds were made on a Hewlett-Packard MSD 5970B GC-MS instrument using a fused silica capillary column containing methylsilicone as the stationary phase with He as carrier gas. Approximately 1 μg of the compound to be analyzed was injected in an ethanol solution and the temperature ramped from 50°C to 290°C in 15 minutes while repetitively scanning from 50-400 m/z.

High performance liquid chromatography (HPLC) of the retinal analogs was performed using a Varian 5000 HPLC pump and an Alltech 5μm Econosphere silica column with detection using a Waters 994 Photodiode array detector. Absorbance data were recorded from 200 - 500 nm. Solvent gradients were from 100% hexanes to 75:25 hexanes:90/10 ethyl acetate/methanol in 25 minutes.

Protonated Schiff bases of the retinal analogs were prepared by the addition of n-

butylamine (20µl, 0.5M, Sigma) in dry hexanes (Curtin Matheson) to the respective retinal in dry ethanol (~0.1 µg/ml) and allowing 15 minutes for the formation of the Schiff base which was monitored spectrally. The ethanolic solution was then acidified with trifluoroacetic acid (1 µl/ml, Pierce) and the absorbance spectrum recorded.

Bacteriorhodopsin and analog pigments. Purple membrane was purified from cultures of *Halobacterium halobium* grown in synthetic basal salt media [Gochnauer and Kushner, 1969] by the method of Becher and Cassim (1975) with an additional sucrose gradient purification (30-60% sucrose, 100,000 g, 17 h). Bleached membrane was prepared by a modification of the method of Tokunaga *et al.* (1977). Purple membrane was bleached by exposure to bright white light at 37°C in a solution of 1 M NH_2OH, 0.1 M NaCl and 10 mM Tris buffer (pH 9.5) for ~4 h. Retinyloximes were removed by hexane washes. The analog pigments were formed by the incremental addition of a concentrated ethanolic solution of the retinal analogs to bleached membrane in distilled water with stirring and the absorbance spectra were recorded using bleached purple membrane as the reference. The retinal analog was added until no further change in the absorbance maximum of the analog pigment occurred. The final concentration of ethanol was <1%. Stability of the pigment to hydroxylamine was measured by the addition of 20 ml of 1 M NH_2OH (pH 7) to the pigment and observation of the absorbance over several hours. Possible displacement of the retinal analog by all-*trans* retinal was determined by addition of a three-fold molar excess of all-*trans* retinal to the analog pigment. Absorbance was monitored over several hours with specific attention to an increased absorbance at 558 nm, the maximum of the native retinal based pigment.

Samples were irradiated with a fiber optics directed microscope illuminator (Dyonics, 150 W). Reversible light adaptation was accomplished by a 2 min exposure of the pigments to white light (100 mW/cm^2) from the same source. Dark adaptation was monitored until no further shift in the absorbance maximum occurred.

Extraction of retinals. Pigments formed with tritiated retinals (~1 mg) were pelleted (100 000 g, 20 min) and the supernatant decanted and counted as below. The pigment

was solubilized with 1 M NH_2OH (100 µl), 10% SDS (25 µl), and sodium phosphate buffer (50 mM, pH 9.5, 175 µl). Methanol (300 µl) was added to the mixture which was then vortexed and heated at 40°C (10 min). The retinals were extracted 2X with 500 µl of dichloromethane. Samples were counted in Aquasol-2 (5 ml, DuPont).

Photocycle intermediates and proton pumping. (These experiments were performed by Dr. Rajni Govindjee and Dr. Tom Ebrey at the University of Illinois - Urbana-Champaign, Department of Biophysics according to Govindjee *et al.*, 1980.) Flash-induced absorbance changes of the pigments were measured with a kinetic spectrometer in 100 mM KCl pH 7.0. The actinic flash was from a Nd-YAG laser (532 nm, 7 ns: Quanta Ray DCR 11). Proton release and uptake were observed by measuring the absorbance changes of the pH sensitive dye, pyranine. The light-induced difference spectra were measured with an optical multichannel analyzer system (Princeton Instruments Corp., Princeton, NJ). Each difference spectrum is an average of 16 flashes.

The number, trivial and systematic names of the retinal analogs that were synthesized for these studies are presented for completeness and ease of future reference.

5, 4-oxoretinal, [9-(3'-oxo-2',6',6'-trimethyl-1'-cyclohexenyl)-3,7-dimethyl-2,4,6,8-nonatetraenal].

6, 2,3 dehydro 4-oxoretinal, [9-(3'-oxo-2',6',6'-trimethyl-1',4'-cyclohexadienyl)-3,7-dimethyl-2,4,6,8-nonatetraenal].

7, Dioxocyclopentenylretinal, [9-(3',4'-dioxo-2',5',5'-trimethyl-1'-cyclopentenyl)-3,7-dimethyl-2,4,6,8-nonatetraenal].

8, VBN-I, [9-(4-azido-2,6-dimethylphenyl)-3,7-dimethyl-2,4,6,8-nonatetraenal].

9, VBN-II, [9-(4-(1-diazirino-2,2,2-trifluoroethyl)-2,6-dimethylphenyl)- -3,7-dimethyl-2,4,6,8-nonatetraenal]

10, FRED, [9-(2,3,6-trimethyl-4-(1-oxo-2-diazo-3,3,3-trifluoropropoxy)phenyl)-3,7-dimtheyl-2,4,6,8-nonatetraenal].

11, TF4N3, [9-(4-azido-2,3,5,6-tetrafluorophenyl)-3,7-dimethyl-2,4,6,8-nonatetraenal]

12, Acyclicretinal, [5',9'-dimethyl-2'-isopropyl-11-oxo-3',5',7',9'-undecatetraenyl-2-diazo-3,3,3-trifluoropropanoate].

13, Pentafluororetinal, [9-(2,3,4,5,6-pentafluorophenyl)-3,7-dimethyl-2,4,6,8-nonatetraenal].

14, Hydroxyretinal, [9-(4-hydroxy-2,3,6-trimethylphenyl)-3,7-dimethyl-2,4,6,8-nonatetraenal].

15, Methoxyretinal, [9-(4-methoxy-2,3,6-trimethylphenyl)-3,7-dimethyl-2,4,6,8-nonatetraenal].

Results.

4-Oxoretinals (5,6,7). 4-Oxoretinal **2**, 2,3 dehydro-4-oxoretinal **6**, and dioxocyclo-pentenylretinal **7** are formed from the prolonged exposure of all-*trans* retinal **1** to activated manganese dioxide. Only the all-*trans* isomers were isolated. The UV-vis, infrared, mass and NMR spectra of these three oxoretinals [Williams and Mani, 1991] confirm the structures as depicted in fig. 2.1. Compounds **5** , **6** and **7** show an intense absorbance in their infrared spectra consistent with the presence of carbonyl function(s) other than the conjugated aldehyde as determined by comparison with the infrared spectrum of all-*trans* retinal **1**. Compound **7** has another carbonyl peak in its infrared spectrum corresponding to the second ring carbonyl. They each display an absorbance maximum greater than 350 nm consistent with their extended conjugation. However, the cyclopentenyl derivative **7** has a λ_{max} significantly red shifted from the λ_{max} of most retinals (435 nm *vs*. 380 nm, fig. 2.2). The absorbance data for the retinals and the corresponding protonated Schiff bases are shown in figure 2.10. Interestingly, whereas the λ_{max} of the unprotonated Schiff base of **7** remains strongly red shifted by 81 nm from that of retinal **1**, the λ_{max} of the protonated Schiff base of **7** (455 nm) is close to that for retinal itself (444 nm).

All three oxoretinals form stable analog pigments with bacterioopsin (fig. 2.2). The properties of these pigments and those of regenerated BR are summarized in figure 2.10. The absorbance maxima for these three pigments are all similar in spite of the differences in the absorbance of the retinals. The cyclopentenyl retinal **7** has a smaller "opsin shift" (Motto *et al.*, 1980) than the other oxopigments (2 600 *vs.* 4 400 cm^{-1}). The rate of formation of pigment from dioxocyclopentenylretinal **7** is comparable to that of all-*trans* retinal whereas pigment formation with the other two oxoretinals **5** and **6** is considerably slower ($t_{1\backslash 2}$ of 5 min as compared with $t_{1\backslash 2}$ of <1 min). The oxoretinal analog pigments have absorbance maxima blue shifted about 50 nm from that of native BR. The pigments formed are all reasonably stable to the addition of hydroxylamine, as

no significant loss of pigment was observed after 60 min in the presence of 20 mM hydroxylamine. Likewise, addition of all-*trans* retinal to the oxoretinal analog pigments did not result in a decrease in absorbance at the pigments' maxima or an increase in absorbance at 558 nm, the maximum of dark-adapted BR.

Exposure of the three oxoretinal pigments to the white light source which reversibly light adapts (2 min, 10 nm red shift) native BR resulted in an irreversible ~20 nm blue shift in their respective absorbance maxima which was complete after 15 min irradiation. After 1 h in the dark, the previously illuminated pigments of **5** and **6** showed 4-8 nm red shifts which were reversible upon 2 min illumination (fig. 2.2, bottom panel). However, incubation of the illuminated oxoretinal **7** pigment in the dark for up to two weeks did not result in any change in its λ_{max} (fig. 2.3).

The flash-induced difference spectra of the illuminated and non-illuminated **5** and **6** based pigments show a decrease in absorbance near the absorbance maximum of the pigment and an increase near 370-410 nm (fig. 2.4, 2.5). The flash induced difference spectra in the millisecond time scale of illuminated and non-illuminated pigment **5** (fig. 2.6) are somewhat different. The non-illuminated form (fig. 2.6, top) shows a decrease in absorbance at 470 nm, an 'M'-like intermediate at ~370 nm, and a small increase in absorbance at 550 nm. These changes decay very slowly. The illuminated sample (fig. 2.6, bottom) has a smaller 'M' and a larger increase at 550 nm. Again these changes persist even 200 ms after the flash.

Figure 2.4 shows the proton release and reuptake for **5** after an actinic flash measured with the pH sensitive dye, pyranine. Under these conditions proton reuptake kinetics were close to those of the decay of 'M'. Similar results were seen for the analog pigments from **6** (fig. 2.5), but the proton pumping was reduced from that observed in the regenerated bacteriorhodopsin (fig. 2.4, right). These results are summarized in figure 2.10.

Extraction of the tritiated retinals from irradiated and non-irradiated samples of the 4-oxoretinal **5** analog pigment showed that ~3% (97.4±0.8% extracted-irradiated,

97.3±0.8% extracted-non-irradiated) of the radiolabel remained with the protein in all cases, regardless of light exposure.

The data pertaining to the characterization of the rest of the retinal analogs and the BR analog pigments derived from them are summarized in fig. 2.10. These data are supported by several hundred UV-vis absorbance spectra recorded and analyzed over the course of these studies. Several of these spectra are presented in appendix 1. The results from these characterizations are summarized below and are discussed in the subsequent section with particular emphasis on the retinal analogs that were shown to be particularly promising as BR photoaffinity labels.

*VBN-I and VBN-II (**8** and **9**).* VBN-I (**8**) was synthesized in very limited quantities and is very unstable. The analog has a λ_{max} of 360 nm in ethanol and fairly rapidly forms a BR analog pigment with a λ_{max} of 472 nm which reversibly light/dark adapts. VBN-II (**9**) has a λ_{max} of 370 nm in ethanol and fairly rapidly forms a BR analog pigment with a λ_{max} of 480 nm. This analog pigment is fairly stable to competition with ATR and hydroxylamine. The analysis of the functional capabilities of this analog pigment is shown in figure 2.9 which should be compared with the same analysis for regenerated BR (fig. 2.7). This analog pigment shows a small 'M'-type intermediate at 1 ms after the flash. The 'O' intermediate is minimally present at best. The 'M' decay kinetics are similar to those of regenerated BR. However the measurement of proton pumping showed no indication of proton release/reuptake as measured by the pH sensitive dye, pyranine. Also it can be seen that the irradiated and non-irradiated pigment are virtually identical in these analyses. This compound was not available in radiolabeled form.

*Fred (**10**).* Compound **10** was nicknamed 'Fred.' It has a λ_{max} of 369 nm in

ethanol and forms a BR analog pigment at only 460 nm. This analog pigment was unstable to ATR and hydroxylamine.

*TF4N3 (**11**).* Tetrafluoro-4-azidoretinal was extremely difficult to synthesize and characterize. This compound has a λ_{max} of 390 nm in ethanol and rapidly forms a BR analog pigment at 517 nm which permanently shifts to 510 nm after irradiation at 350 nm. The functional characterization of this pigment is shown in fig. 2.8. This analog pigment shows a substantial 'M'-like intermediate at 1 ms after the flash and a less obvious, but significant 'O'-like intermediate at 5 ms after the flash. The kinetic spectra show robust formation of the 'M'-intermediate and substantial proton pumping estimated to be about 40% that of BR (fig. 2.7).

*Acyclicretinal (**12**).* Compound **12** has a λ_{max} in ethanol of 360 nm; not unusually low, considering it has one less double bond. The analog BR pigment forms fairly rapidly at 450 nm. This pigment is fairly stable to competition with ATR and hydroxylamine.

*Compounds **13**,**14**, and **15**.* These compounds were synthetic intermediates in the syntheses of the above compounds. Their characteristics as BR analog pigments are included here since they are novel retinal analogs and for completeness. Their characteristics are summarized in figure 2.10.

Discussion.

Khorana, Nakanishi1 and Nakanishi2 (2,3,4). The characteristics of these three retinals and their BR analog pigments are included for comparison to the presently studied analogs. Compound **2** is an aromatic retinal analog without the methyl groups on the ring. Huang *et al.* (1982) did not report on the ability of this analog pigment to function (i.e. to pump protons). Interestingly, it was Boehm *et al.* (1990) who reported that this BR analog pigment was "nonfunctional". Compound **4** does however have an excellent photoactivatable group in the diazirine. Compound **3** was more recently used to photoaffinity label BR by Ding *et al.* (1990). This non-aromatic retinal analog is very similar to retinal. The analog pigment formed with this compound does pump protons at about 50% - 100% the efficiency of native BR [Sen *et al.*, 1982; Ding *et al.*, 1990]. Compound **4** was also recently reported from Nakanishi's laboratory. This compound was shown to form a stable BR analog pigment that was capable of pumping protons at about 1/5 the efficiency of native BR [Boehm *et al.*, 1990]. The characteristics of these retinal analogs and their BR analog pigments are summarized in fig. 2.10 along with the original data for the other retinal analogs derived from this work. The sites labeled by these three retinal analogs are analyzed by molecular modeling as described in chapter 4.

4-Oxoretinals (5,6,7). The formation of structurally altered retinals from the prolonged exposure of all-*trans* retinal (or retinol) to manganese dioxide has been previously reported. Wald (1948) observed a product he tentatively identified as 4-oxoretinal. Recently, Colmenares and Liu (1991) report the loss of a carbon in the side chain upon reaction of retinal with excess manganese oxide. In this laboratory we have isolated three compounds from this reaction, one of which is the 4-oxoretinal as reported by Wald.

The oxoretinals form stable BR pigments. The increased rate of formation of the dioxocyclopentenylretinal **7** pigment as compared with the other two oxoretinals **5** and **6** pigments may be due to the 6-s-*trans* conformation in solution found in **7** in contrast to the 6-s-*cis* solution conformation of the other two oxoretinals and to all-*trans* retinal itself [Honig *et al.*, 1971]. The native chromophore in BR has been established to be in

the 6-s-*trans* conformation [Creuzet *et al.*, 1991]. The small opsin shift (2600 cm^{-1}) calculated for pigment **7** may be due to a similar solution and pigment conformation.

These derivatized retinals **5**, **6** and **7** are in the binding site of the native chromophore in BR as shown by the failure of added all-*trans* retinal to produce a pigment at 560 nm. These analog pigments, similar to BR, are also stable to hydroxylamine. The absorbance data for the oxoretinal **5** analog pigment are in agreement with that previously reported [Sumper and Herrmann, 1976]. The 40-50 nm blue shifts in these three oxoretinal analog pigments can be explained by a disruption of the interaction of the conjugated double bond system with the 'external point charge' by the electronegative substituents on the ring of the retinal analogs at position 4. The similarity between the two pigments based on oxoretinal **5** and oxoretinal **6** indicates the lack of importance of the double bond between carbons 2 and 3, further supporting the notion that an 'external point charge' interacts with retinal near the 4 position.

These analog pigments have an unusual response to white light showing a significant, permanent blue shift rather than the well known metastable red shift associated with light adaptation of native BR (fig. 2.3). Once transformed by white light, the oxoretinal **5** and oxoretinal **6** based pigments show a metastable red shift upon dark adaptation of 4-8 nm which is reversible (fig. 2.2, 2.3). To our knowledge these are the first bacteriorhodopsin pigments known to light and dark adapt 'backwards'. The irradiated and non-irradiated forms of **5** and **6** show flash induced difference spectra (fig. 2.4, 2.5) similar to BR. However, the 'M'-intermediate decay kinetics and proton uptake (fig.2.4, 2.5) are much slower than in BR.

It was initially thought that this permanent shift induced by white light of pigment **5** might be due to the chromophore ring crosslinking with the protein. However, the extent of radiolabel in retinal extractions from these pigments is equal and near quantitative for photolysed and non-photolysed samples which does not support the idea that a crosslink had formed. If crosslinking to the protein has occurred, the linkage is evidently unstable to the extraction procedure.

Further investigation into the photochemistry of the 4-oxoretinal analog indicates that it was unlikely to be a good photoaffinity label due to the relative lack of reactivity of the photoactivated intermediate derived from this highly conjugated keto compound [Calvert and Pitts, 1966]. Photolysis would yield the n->π^* transition at long wavelengths (low energy) for this ketone in conjugation with the extended π system of the retinal sidechain. This transition would be of considerably lower energy than the photoactivated intermediate of the $\alpha-\beta$ unsaturated keto steroids that have only one double bond in conjugation with the ketone. Besides this low reactivity the radical formed would have to undergo an intersystem cross in order to label the protein. This intersystem cross is required for spin coupling of the radical pair in the mechanism of labeling by these types of compounds (see fig. 1.7) The extra time required for this intersystem cross would likely move the radical pair away from each other leading to a second hydrogen abstraction instead of combination of the radical pair. It would also be possible for the radical derived to be delocalized throughout the extended conjugation which could lead to reactivity at any number of carbons. A final consideration is that the low energy photoactivated analog may simply decay back to the ground state without undergoing any type of intermolecular reaction. Thus, in retrospect, the extended conjugation of this retinal analog renders it unlikely to form a highly reactive intermediate on photolysis.

Williams and Mani (1991) speculated that the α,β-dicarbonyl moiety of dioxocyclopentenylretinal 7 is similar to arginine modifying reagents making it potentially useful as a chemical crosslinking reagent. The unusual irreversible shift upon exposure to white light and the unusual 'M'-intermediate spectra (fig. 2.6) of the oxoretinal 7 analog pigment may be indicative of a photocycle dependent modification. This notion of an analog pigment covalently linked to the protein at both the Schiff base and ring end of the retinal would be consistent with its unusual properties. However, using 7 tritiated at C-11 and C12, we consistently extract ~95% of the retinals from both illuminated and non-illuminated analog pigments. The failure to demonstrate

crosslinking may be due to the inability of the dioxocyclopentenylretinal to form crosslinks under the conditions tested or to the instability of a crosslink to the extraction conditions.

VBN-I and VBN-II (8 and 9). VBN-I was made in very limited quantities, is very unstable, and possesses an unsubstituted aryl azide. Because of these drawbacks, it was not further evaluated. VBN-II is a very stable compound that has an excellent photoactivatable group - the carbene precursor, trifluoromethyldiazirine [Bayley, 1983]. This compound forms a good BR analog pigment which, unfortunately, does not pump protons to any appreciable extent (fig. 2.9). This lack of function is not unusual for aromatic retinal analogs [Crouch, 1986]. There is also no indication of change in characteristics between the irradiated and non-irradiated pigments. The need for radioactively labeled retinal analogs to assess crosslinking limited the further usefulness of this compound for these studies.

Fred (10). This compound possesses a good photoactivatable group (the trifluoromethyl-2-diazopropionyl moiety), but forms a very unstable BR analog pigment. This lack of stability indicates a poor interaction with the retinal binding site. However, the absorbance shift from 369 nm to 460 nm from the chromophore in solution to the BR analog pigment indicates at least a partial binding. These indications of only a minimal interaction with the retinal binding site encouraged the discontinuation of the analysis of this compound.

TF4N3 (11). This compound proved to be one of the most difficult to synthesize and characterize, but was promising due to its excellent photoactivatable group [Keana and Cai, 1988] and its unusual ability as an aromatic retinal analog, to form a partially functional BR analog pigment. The large opsin shift (from 390 nm in solution to 517 nm as the BR analog pigment) showed the interaction of this retinal with the native retinal binding site. The BR analog pigment formed with this compound was also stable to competition with ATR and to bleaching with hydroxylamine in the dark. These characteristics as well as a 40% proton pumping efficiency indicate that this retinal analog is binding well to the native retinal binding site. This retinal analog eventually

was available in a radiolabeled form and was further characterized for its ability to crosslink to BR under different photolysis conditions (see Chapter 5).

*Acyclicretinal (**12**).* This compound contains an excellent photoactivatable group (trifluorodiazopropionate, Chowdry *et al.*, 1976) and is not aromatic. It has been previously shown that acyclic retinals can form functional BR analog pigments [Crouch, 1986]. This compound was only recently synthesized and will be evaluated for its ability to crosslink to organic solvents and when prepared in a radiolabeled form to crosslink to BR.

*Compounds **13**,**14**, and **15**.* These three aromatic analogs were analyzed to help to determine if the final product of the syntheses would likely form functional BR analog pigments. As is the case with most aromatic retinal analogs, these three compounds formed analog pigments that did not function well. Compounds **14** and **15** formed unstable analog pigments as did the final product of this synthesis Fred (**10**). The pentafluororetinal (**13**) analog pigment functioned less well than its azide substituted derivative TF4N3 (**11**). The analog pigment absorbance maximum of **13** was >50 nm different from that of **11** which allowed a simple use of BR pigment formation to test for the successful substitution of the para-fluorine with azide from the pentafluororetinal in a different synthetic scheme than that presented in the appendix.

In summary, the most useful of these retinal analogs for further study is the radiolabeled form of TF4N3 (**11**). 4-Oxoretinal (**5**) and 2,3 dehydro-4-oxoretinal (**5**), although potentially photoactivatable, show no indication of stable crosslink formation to the protein despite their unusual pigment characteristics. VBN-II (**9**) is an excellent compound, but was not available in radiolabeled form.

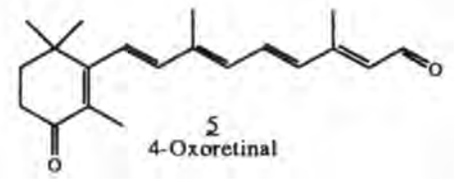

5
4-Oxoretinal

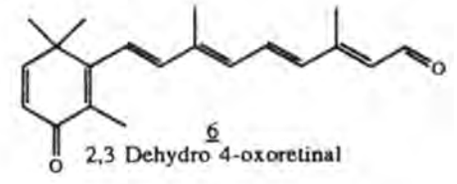

6
2,3 Dehydro 4-oxoretinal

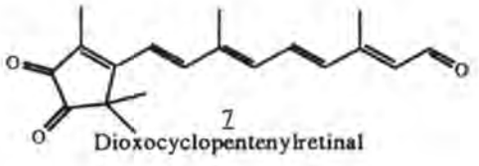

7
Dioxocyclopentenylretinal

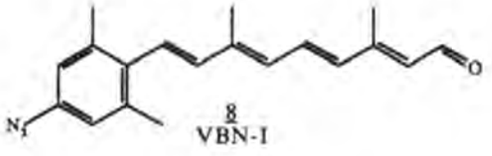

8
VBN-I

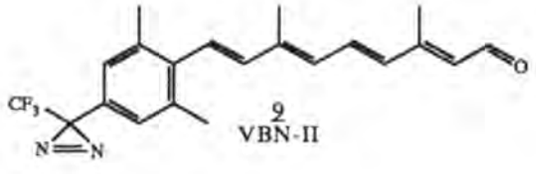

9
VBN-II

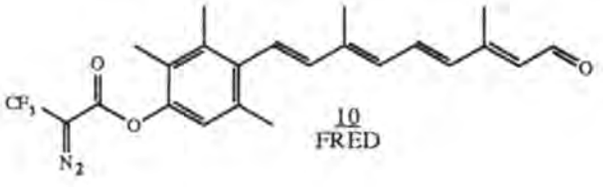

10
FRED

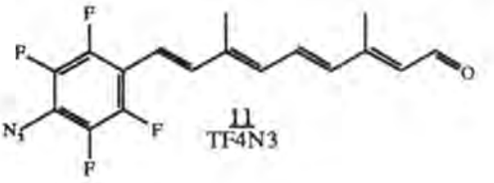

11
TF4N3

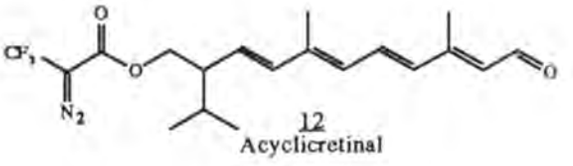

12
Acyclicretinal

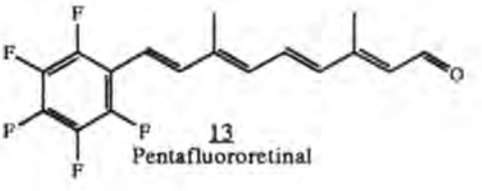

13
Pentafluororetinal

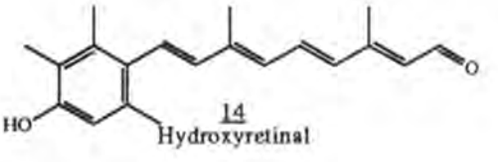

14
Hydroxyretinal

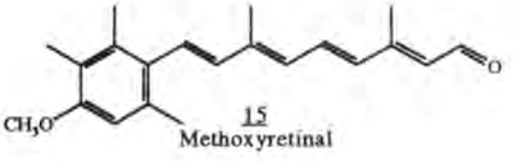

15
Methoxyretinal

Figure 2.1 Retinal Analog Structures
Chemical Structures of Retinal Analogs Evaluated as BR Analog Pigments

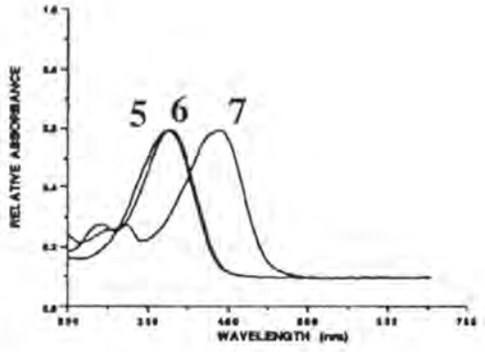

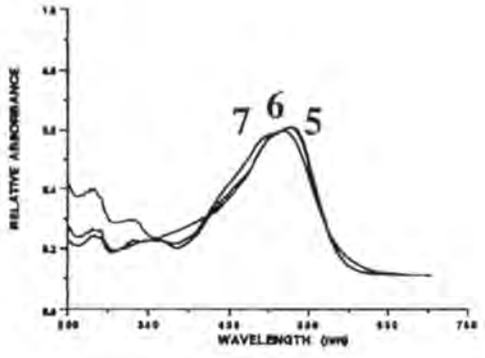

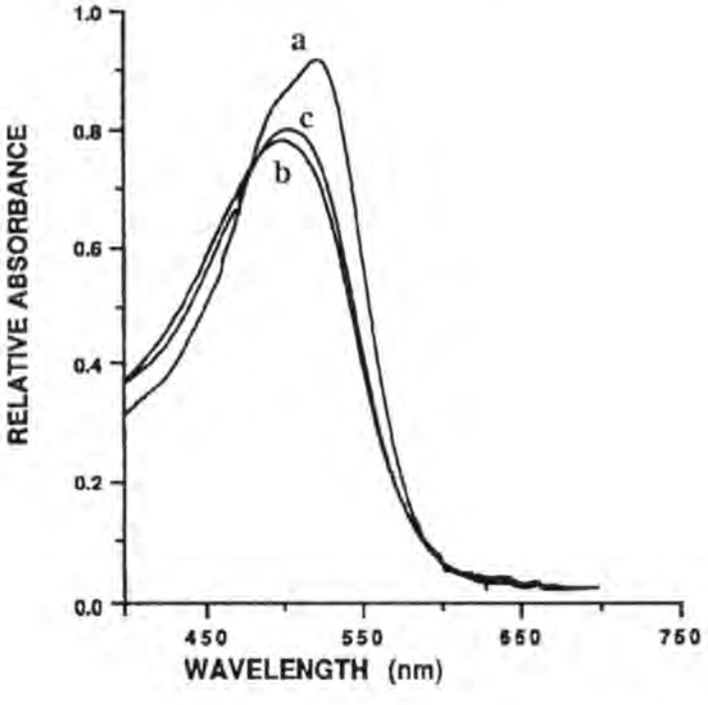

Figure 2.2 UV-vis Spectra of Oxoretinals and Analog Pigments
Top panel: Absorbance spectra of oxoretinals 5,6,7 in ethanol. Middle panel: as BR analog pigments in water. Spectra have been normalized. Bottom panel: Absorbance spectra of BR analog pigment **5** before illumination (a), after illumination (b), and illuminated/dark adapted (c).

Pigment Chromophore	Pigment λ_{max}
Retinal **1**	558 nm $\underset{\text{dark}}{\overset{h\nu}{\rightleftharpoons}}$ 568 nm
4-Oxoretinal **5**	524 nm $\xrightarrow{h\nu}$ 502 nm $\underset{h\nu}{\overset{\text{dark}}{\rightleftharpoons}}$ 506 nm
2,3-Dehydro-4-oxoretinal **6**	522 nm $\xrightarrow{h\nu}$ 500 nm $\underset{h\nu}{\overset{\text{dark}}{\rightleftharpoons}}$ 508 nm
Dioxocyclopentenyl-retinal **7**	515 nm $\xrightarrow{h\nu}$ 500 nm $\underset{h\nu}{\overset{\text{dark}}{\rightleftharpoons}}$ 500 nm

Figure 2.3 Pattern of LA/DA for Oxoretinal Analog Pigments
Scheme of light adaptation/dark adaptation for retinal **1** and the oxoretinals **5**,**6**,**7**, based analog pigments.

4-Oxoretinal

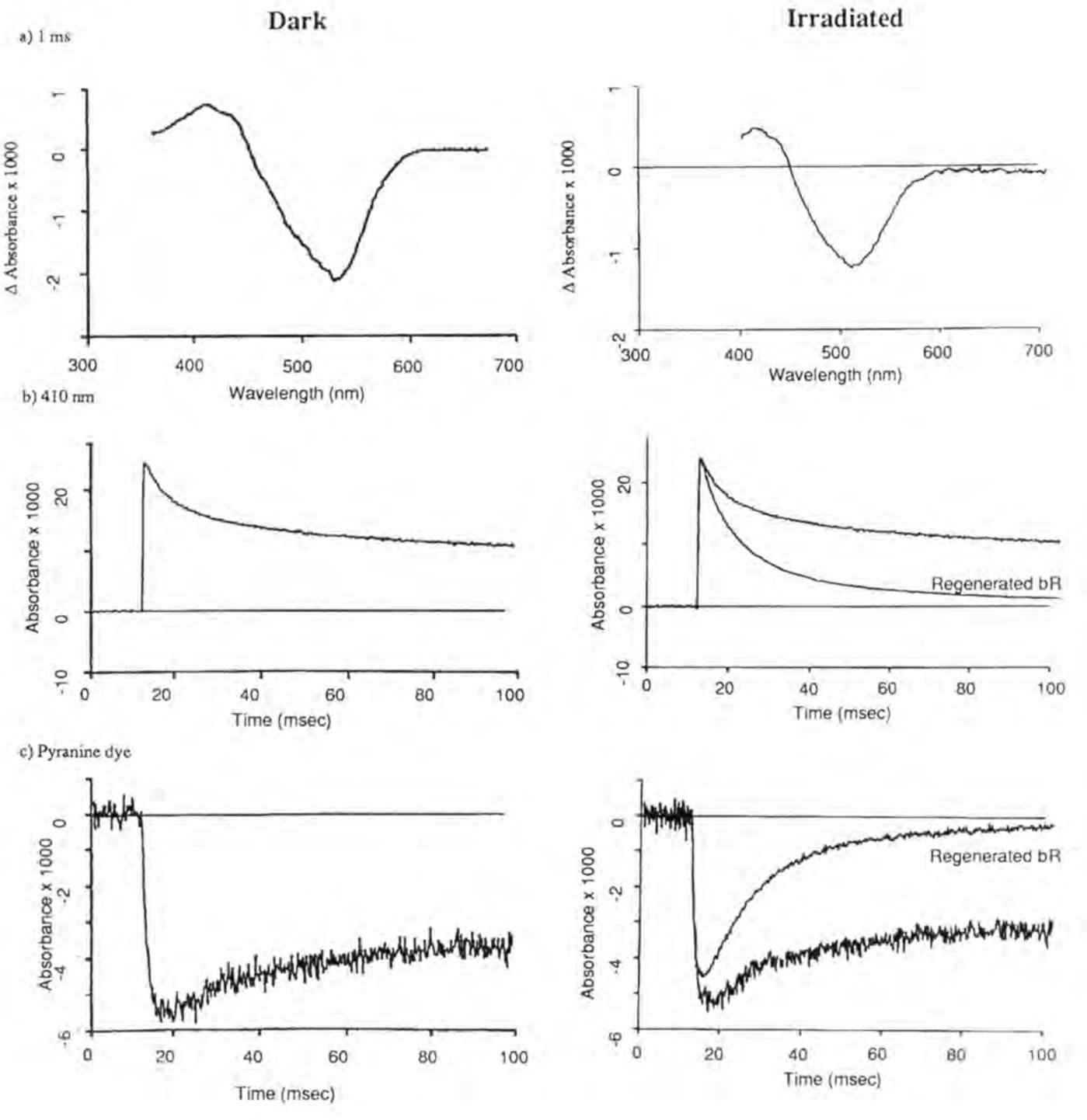

Figure 2.4 4-Oxoretinal Pigment Kinetic Spectra
Right side: Flash induced absorbance changes of regenerated BR and oxoretinal **5** based pigment after irradiation with white light. The traces were normalized at their maxima to facilitate comparison of the kinetics. Left side: Flash induced absorbance changes of **5** based pigment without irradiation with white light. Top panels: Flash induced difference spectra 1 ms after the actinic flash. Middle panels: 'M'-type intermediate kinetics measured at 410 nm. Bottom panels: Proton release and reuptake as detected by absorbance changes in the pH sensitive dye, pyranine.

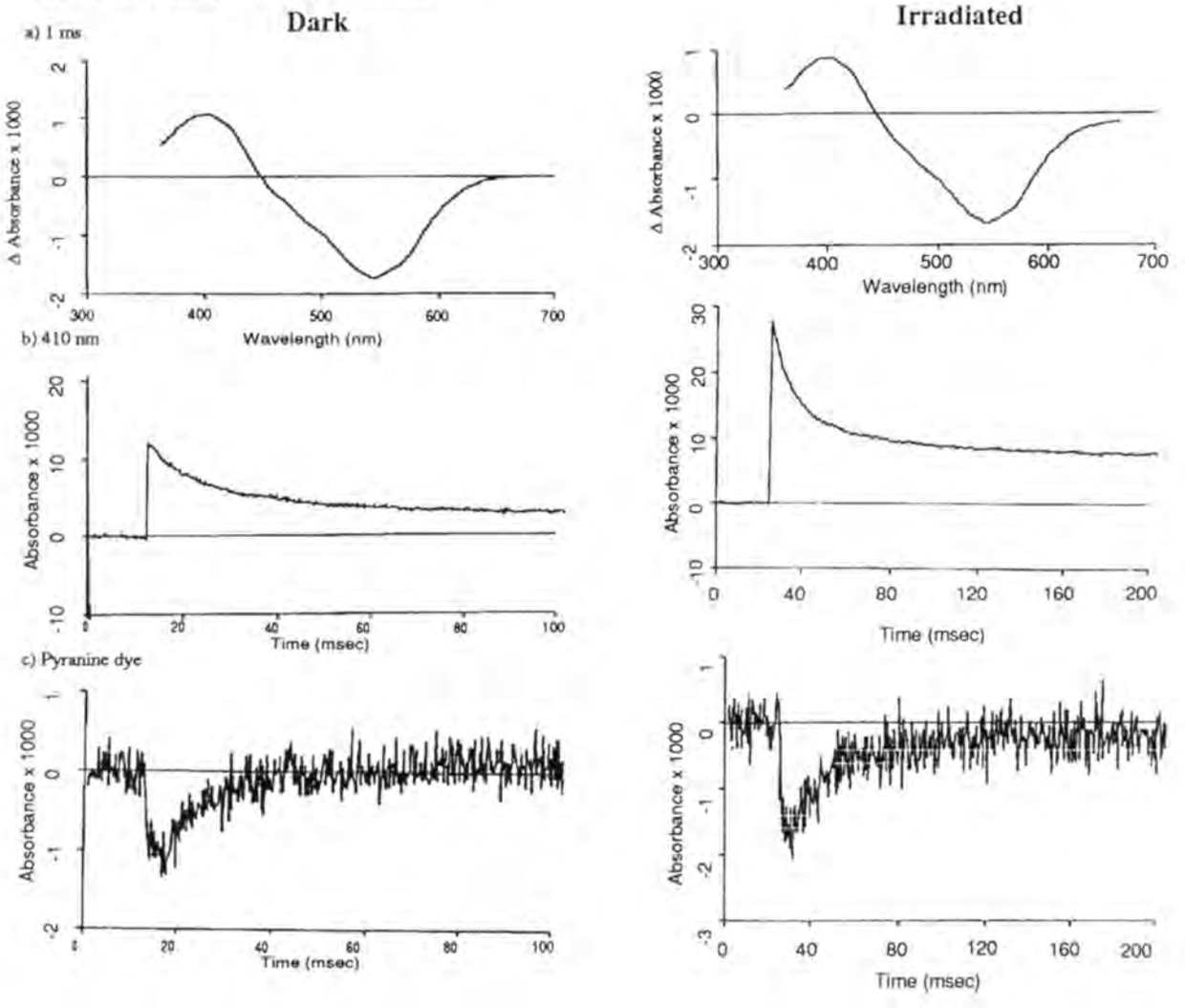

Figure 2.5 2,3-dehydro-4-oxoretinal Pigment Kinetic Spectra
Right side: Flash induced absorbance changes of oxoretinal **6** based pigment after irradiation with white light. Left side: Flash induced absorbance changes of **6** based pigment without irradiation with white light. Top panels: Flash induced difference spectra 1 ms after the actinic flash. Middle panels: 'M'-type intermediate kinetics measured at 410 nm. Bottom panels: Proton release and reuptake as detected by absorbance changes in the pH sensitive dye, pyranine.

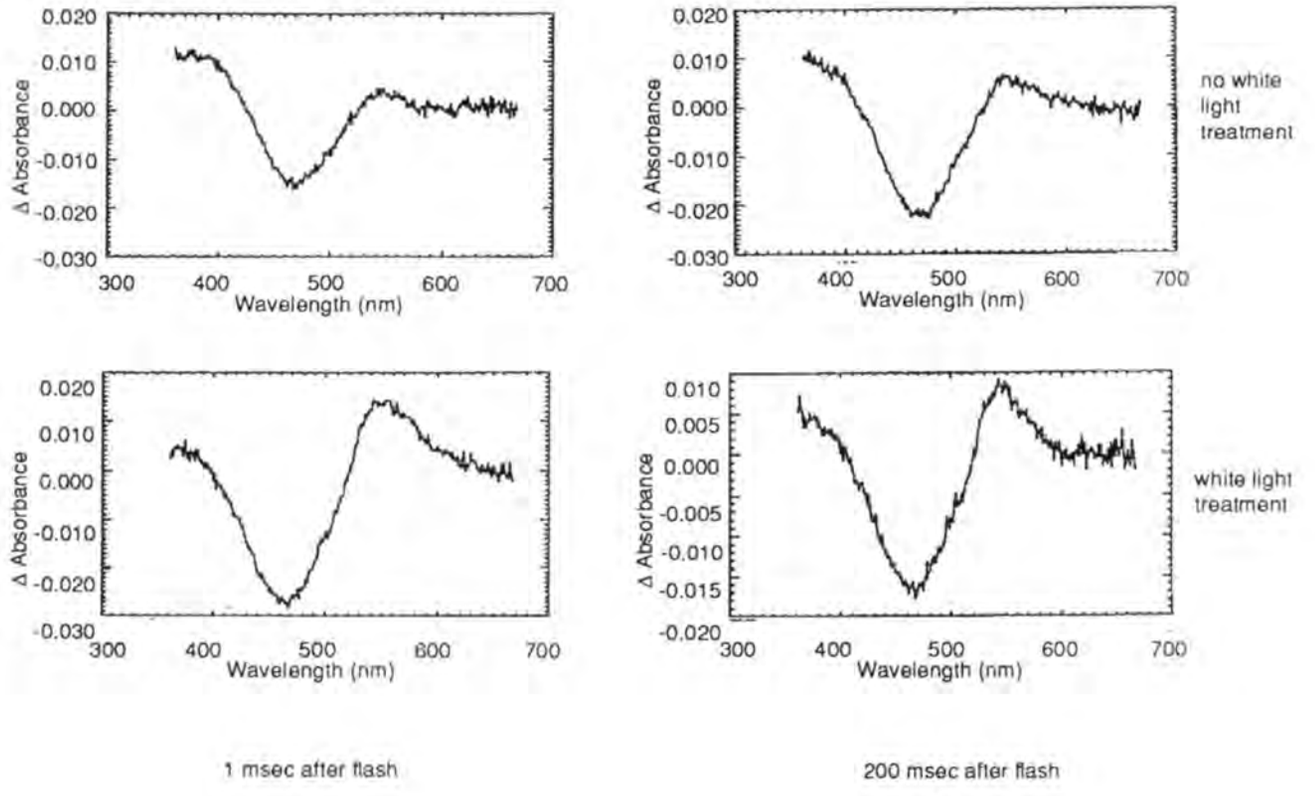

Figure 2.6 Dioxocyclopentenylretinal Kinetic Spectra
Flash induced difference spectra of oxoretinal 7 based pigment. Top panel: non-irradiated, 1 ms (left spectrum) and 200 ms (right spectrum) after the actinic flash. Bottom panel: irradiated, 1 ms (left) and 200 ms (right) after the actinic flash.

Regenerated Bacteriorhodopsin

a) 1ms

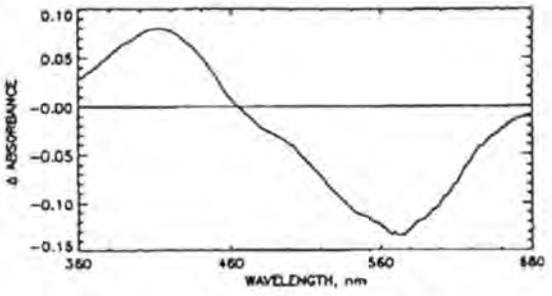

b) 5 ms

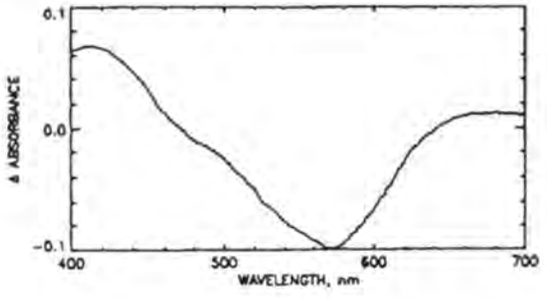

c) 410 nm

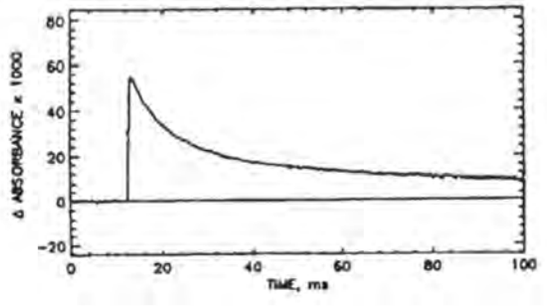

d) pyranine dye

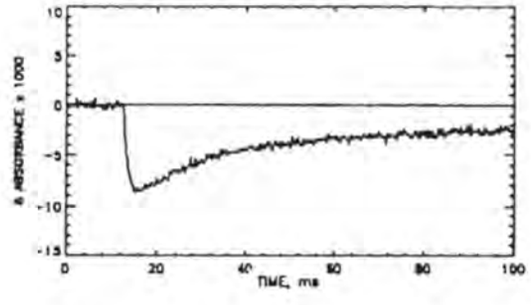

Figure 2.7 Regenerated Bacteriorhodopsin Kinetic Spectra
Flash induced absorbance changes of regenerated BR as positive control for those in figures 2.8 and 2.9. a) Difference spectrum 1 ms after flash, the 'M' intermediate. b) Difference spetrum 5 ms after the flash, the 'O' intermediate. c) Flash induced absorbance changes at 410 nm, 'M' intermediate kinetics. d) Proton release and reuptake as detected by the pH sensitive dye, pyranine.

TF4N3

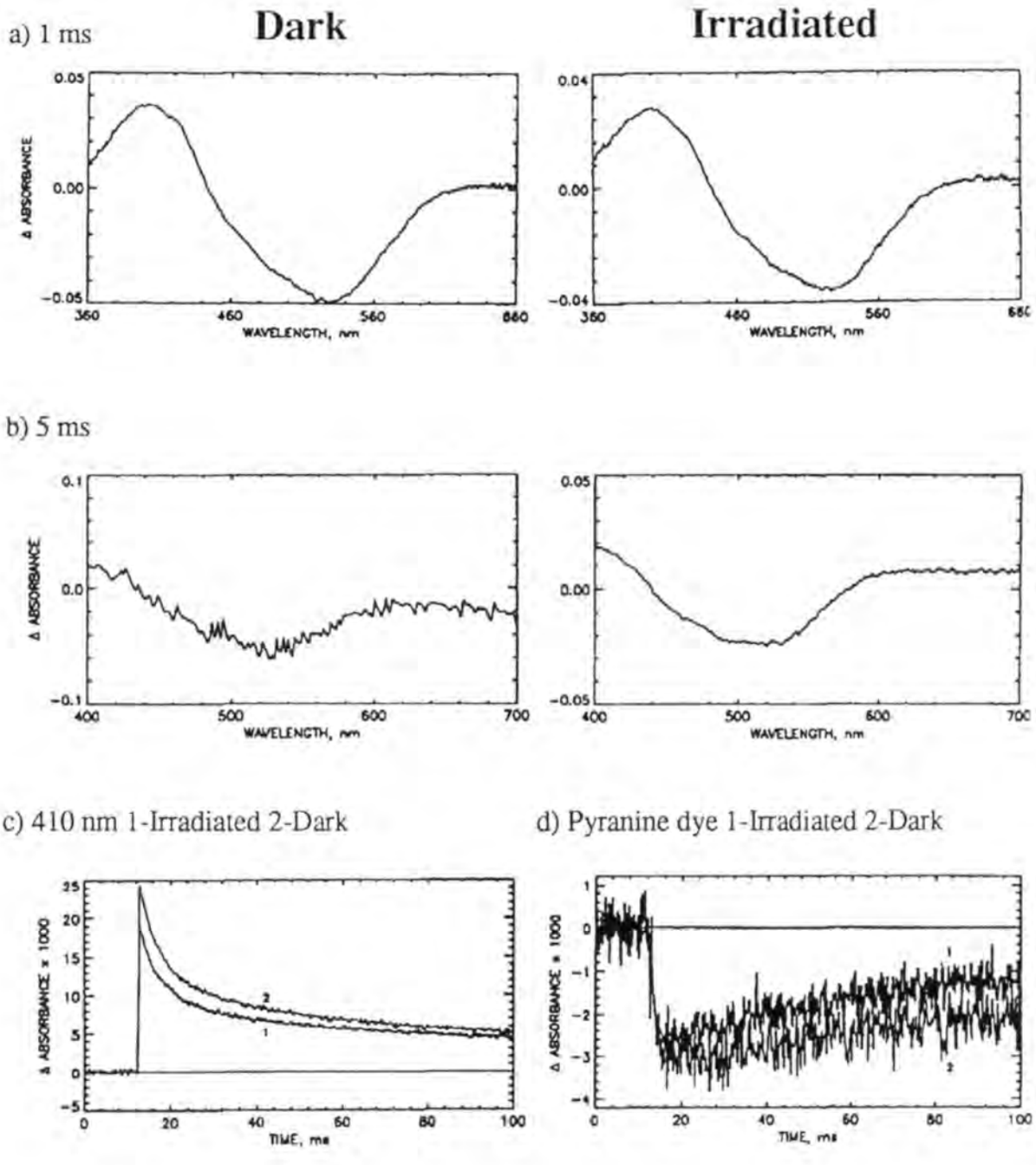

Figure 2.8 TF4N3 Pigment Kinetic Spectra
Flash induced absorbance changes of TF4N3 **11** analog pigment before (a+b, Left) and after (a+b, Right) irradiation at 350 nm for 10 min in the RPR-100.
a) Difference spectra 1 ms after flash. b) Difference spectra 5 ms after the flash. c) Flash induced absorbance changes at 410 nm, (1-irradiated, 2-dark) d) Proton release and reuptake as detected by the pH sensitive dye, pyranine (1-irradiated, 2-dark).

VBN-II

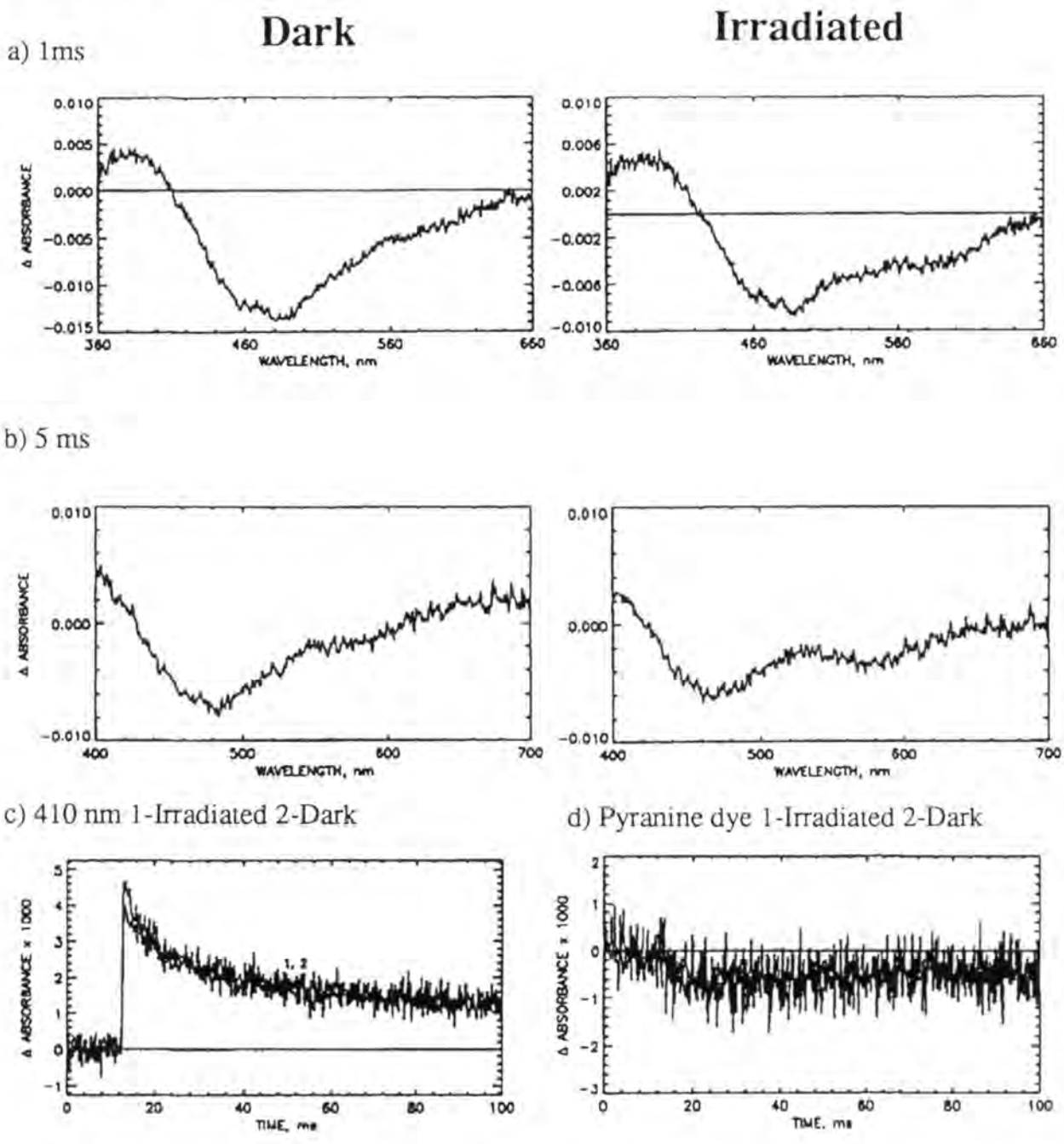

Figure 2.9 VBN-II Pigment Kinetic Spectra
Flash induced absorbance changes of VBN-II **9** analog pigment before (a+b, Left) and after (a+b, Right) irradiation at 350 nm for 10 min in the RPR-100.
a) Difference spectra 1 ms after flash. b) Difference spectra 5 ms after the flash. c) Flash induced absorbance changes at 410 nm, (1-irradiated, 2-dark) d) Proton release and reuptake as detected by the pH sensitive dye, pyranine (1-irradiated, 2-dark).

Chromophore	Name	ABS Max EtOH	PSB ABS Max EtOH	Pigment DA/LA	t1/2 formation	Stability NH2OH/ATR	M - intermediate ABS Max	Proton Pumping
1	Retinal	378	444	558/568	***	***/***	412	***
2	Khorana	370	N/A	470	N/A	N/A	N/A	N/A
3	Nakanishi1	380	N/A	525	N/A	N/A	410	**
4	Nakanishi2	385	N/A	497	N/A	N/A	N/A	**
5	4-Oxoretinal	378	425	524#	**	**/**	420	*
6	2,3 Dehydro-4-oxoretinal	380	426	522#	**	**/**	420	*
7	Dioxocyclopentenylretinal	435	455	515 #	***	**/**	unusual	0
8	VBN-I	360	N/A	472/478	**	N/A	N/A	N/A
9	VBN-II	370	N/A	480	**	**/**	400	0
10	FRED	369	N/A	460	**	*/*	390	*
11	TF4N3	390	unstable	517	***	**/**	400	**
12	Acyclicretinal	360	N/A	450	**	*/*		
13	Pentafluororetinal	360	407	456	*	*/*	unusual	*
14	Hydroxyretinal	386	456	491	*	*/*	390	*
15	Methoxyretinal	382	450	490	**	*/*	390	*

Figure 2.10 Summary of characteristics of retinal and retinal analogs and their BR pigments. N/A= not available.
Data for Khorana is from Huang et al., 1982, for Nakanishi1, from Ding et al., 1990 and for Nakanishi2, from Boehm et al., 1990.
see fig. 2.3.

Chapter 3

Model Photolysis

Portions of this chapter have been published as

Beischel, CJ, SK Moore, RK Crouch, and DR Knapp.

"A Versatile Flash Photolysis Apparatus."

Rev. Sci. Instrum. 63(3), 2069-2072, 1992.

Introduction.

Once the BR analog pigment is formed and characterized it is necessary to photoactivate the analog to produce the reactive intermediate and effect labeling of the protein. The reactive intermediates are usually products of the loss of molecular nitrogen from different photoactivatable moieties. Photoactivated diazirines and trifluorodiazopropionates form carbenes; aryl azides and fluorinated aryl azides form nitrenes. These highly reactive intermediates are capable of C-H bond insertion, other stable bond formations and unstable formations. In order to efficiently photoactivate the retinal analogs described in Chapter 2, it is important to determine the appropriate photolysis conditions.

These experiments are commonly done using continuous wave irradiation of samples with UV light. Photoactivation of reagents is often accompanied by nonspecific photolytic or heat induced damage to the protein or other biological system under study, especially if the wavelength of irradiation corresponds with the absorbance of the protein. It has been observed that the use of flash photolysis in place of CW-UV irradiation causes less protein damage [Ji, 1979]; therefore, the use of flash photolysis can be advantageous in such experiments.

Short duration UV flashes can be obtained from gas discharge flashlamps or from UV lasers. Flashlamp sources are significantly less expensive than laser sources. Commercially available photoflash units have been used for flash photolysis experiments [Kiehm and Ji, 1977]. Larger photon fluxes can be delivered with shorter duration flashes using xenon flashlamps fired by high voltage power supplies and rapid discharge capacitors, but this type of apparatus can present greater safety hazards in the laboratory in terms of potential for UV exposure, flashlamp explosion, and electrical shock. A xenon flashlamp apparatus is commercially available including flashlamp enclosures with mirror and lens assemblies to yield focused beams of light (e.g., from Xenon Corporation, Woburn, MA). A sample cell where the sample solution is contained in an annular chamber surrounding a linear flashlamp has been described [Matheson, *et al.*, 1977]. This type of apparatus has the advantage of giving uniform

exposure of the entire sample and of making maximal utilization of the UV light. Believing that such an apparatus would be effective in activating the retinal analogs described in Chapter 2 and being unable to locate a commercial source, an apparatus was designed and constructed. Design elements include a lamp enclosure/sample cell incorporating safety features to minimize the potential hazards from UV exposure, lamp explosion, and electrical shock and the versatility to use chemical solution filters and temperature control. The sample cell design incorporates a series of concentric annular chambers of different path lengths (1 mm or 2 mm in the present design) which can be used for sample solutions, circulating temperature control fluids, or wavelength selecting filter solutions. The lamp enclosure/sample cell was used with a commercially available power source, but designs for construction of suitable power sources have been reported [e.g., Wegrzyn *et al.*, 1989]. This chapter describes the lamp enclosure/sample cell and compares it with a commonly used CW source in terms of photon flux as measured by chemical actinometry and photolysis of a model aryl azide compound (fig. 3.1 and 3.2).

Materials and Methods.

Materials. Ferric chloride, potassium oxalate monohydrate, ferrous sulfate, sodium acetate, sodium azide, cyclohexane, pentafluorobenzaldehyde, dimethylformamide and 1,10-phenanthroline were reagent grade (Aldrich, Milwaukee, WI) and used without further purification. The organic solvents were stored over molecular sieves.

Tetrafluoro–4–azidobenzaldehyde (TFABA) was prepared by a modification of the method of Keana and Cai (1988). Pentafluorobenzaldehyde was allowed to react with a 1.5 molar excess of sodium azide in dimethylformamide for 6 hours at room temperature [Beischel *et al.*, 1990]. The product was confirmed as TFABA by UV, IR, and gas chromatography–mass spectrometry (fig. 3.2, top panel).

Continuous wave apparatus. A Rayonet Photochemical Reactor RPR–100 (New England Ultraviolet), equipped with sixteen type 3500Å lamps (350 nm) was used with the same sample cell as used in the flash apparatus (see below).

Flashlamp and power source. A Xenon Corporation (Woburn, MA) Model N–734D line source flashlamp was used. This linear flashlamp has a 3 mm bore and a 75 mm arc length. The flashlamp was fired by a Xenon Corp. Model M–457A Micropulser configured with a 0.2 F capacitor to deliver 10 J at 10 kV and having a repetition rate of up to 30 Hz. For the experiments described here, 10 J flashes were employed under manual control.

Flashlamp housing and sample cell. (This apparatus was designed by Daniel R. Knapp and constructed by Cliff Harvey.) The flashlamp housing and sample cell are shown in fig. 3.4. The housing is constructed from 5 in outer diameter, 0.125 in wall aluminum tubing (A) mounted on a 9 in x 7 in x 2 in aluminum chassis (B) with a disc of 0.75 in thick bakelite (C). The interior of the aluminum tubing is polished to give a reflective surface. Another disc of bakelite forms a cover (D) on which is mounted the connector removal mechanism and safety interlock switches (E,F) (Microswitch SM series subminiature switches, Newark Electronics, Chicago, IL). The chassis bottom is covered with a sheet of 1/4 in Plexiglass. Switch E is closed when the enclosure cover is in place, and switch F is closed when the flashlamp power connector is in place.

Switches E and F are wired in series with the safety interlock circuit of the M–457A Micropulser which prevents the firing of the flash circuit unless both the cover is on and the connector attached. The flashlamp (G) is mounted at the bottom end (flashlamp cathode) in a Superior Electric Supercon type RS50GR receptacle (Newark Electronics, Chicago, IL) which has been drilled out for a tight fit on the 0.280 in Flashlamp end terminal. This connector is connected with 14 ga copper wire to a Supercon type RP50GR pin connector mounted on the chassis base (H). The connections are covered with RTV Silicone Rubber (Newark Electronics, Chicago, IL) to reduce corona discharge. The chassis pin connector mates with the socket connector on the cable supplied with the Micropulser. The top flashlamp terminal connects to a custom made 0.280 in brass collet mounted in the enclosure cover. The collet is tightened with the threaded pin taken from a Supercon RP50GR connector using a hollow 7/16 in nutdriver (XceLite HS–14). The pin then connects to the Supercon RP50GB connector on the Micropulser cable. The cable connector is mounted in a Delrin cylinder with exterior grooves machined to match levers (I) taken from a household corkscrew device. The levers are used to remove the tightly fitting connector.

The sample cell (detail shown in fig. 3.5) is constructed from four 65 mm lengths (J) of concentric quartz tubing (Quartz Scientific, Fairport Harbor, OH). Tubing sizes of 15 mm id, 18 mm od; 22 mm id, 25 mm od; 27 mm id, 30 mm od; and 34 mm id, 37 mm od give three concentric cylindrical chambers 2 mm, 1 mm, and 2 mm thick. The lengths of tubing are press fitted into 2.5 mm deep grooves in end pieces (K) machined from 1/2 in thick Teflon discs. Each endpiece contains an 11 mm diameter center hole through which passes the flashlamp. Connections to the chambers are made through 1/4–28 threaded holes (L) designed to mate with flange type tubing connectors (Alltech No. 2022, State College, PA) or plugs (Alltech No. 80089). A cylindrical support (M) cut from a plastic beaker holds the cell at the proper height to align with the flashlamp arc.

Ferrioxalate actinometry. The dose of UV radiation delivered to the 1 mm sample compartment by the continuous wave and flash sources was compared using potassium

ferrioxalate (KFOX) actinometry as described by Hatchard and Parker (1956) (fig. 3.1, top). Several suggested modifications to this original procedure were incorporated and tested using standard ferrous solutions (Calvert and Pitts, 1966; Kurien, 1971; Cabral *et al.*, 1977; Boman and Demas, 1981; Kirk and Namasivyam, 1983) (fig. 3.3, top). The cell was filled with 0.15 M KFOX (0.1 N H_2SO_4) and exposed to either CW or flash UV radiation. Aliquots (20 µl) were removed after various amounts of UV exposure (time for CW source; number of flashes for flash source) and allowed to react for one hour with the following: 1,10–phenanthroline (400 µl, 1%, 0.025 N H_2SO_4; 7–fold molar excess over 0.15 M ferric/ferrous ion concentration), 1.5 M sodium acetate (30 µl), 0.05 N H_2SO_4 (550 µl). The absorbance at 510 nm was measured using a Varian CARY 2200 spectrophotometer using the same mixture minus the KFOX as reference.

Photolysis of TFABA. A 1.5×10^{-7} M solution of TFABA in cyclohexane was exposed to either the CW or flash light source. Periodically in time or number of flashes, samples of the solution were analyzed by gas chromatography–mass spectrometry (Hewlett Packard 5970B) to determine the amount of the cyclohexane addition product, (fig. 3.2, bottom) 4–cyclohexylaminotetrafluorobenzaldehyde (TFCBA) formed.

Photolysis of pigments. Bacteriorhodopsin analogs and pigments are irradiated in the same sample cuvettes as described above. The pigments are kept cold by placing the RPR in the cold room and filling the center of the sample cell with ice. At all times the sample is separated from ice cold water by only a 1 mm thick quartz cylinder. The sample cell is cooled in the flash apparatus by placing the cell in a plastic beaker that has had a hole cut in the bottom. The beaker is then filled with ice and again the sample is always separated from ice cold water by only a 1 mm thick quartz cylinder.

Results.

The photon dose measured by KFOX actinometry was plotted versus time or number of flashes and found to be linear with time in the CW source up to approximately 50 s exposure and with number of flashes in the flash source up to about 25 flashes. Under the conditions used, the photon doses measured in the linear region were 7.3×10^{17}/s for the CW source and 7.6×10^{17}/flash for the flash source (fig. 3.3, bottom).

The photolysis of TFABA, as indicated by the production of the cyclohexane insertion product TFCBA, reached a maximum after about 40 s of CW irradiation and after about 10 flashes. No other significant products were observed indicating near quantitative conversion of the TFABA to the cyclohexane insertion product. See fig. 3.6 for an example of the GC-MS data.

Discussion.

The apparatus depicted in fig. 3.4 provides a convenient, safe, and versatile method of performing flash photolysis experiments on solutions and incorporates provisions for temperature control via circulating thermostatted fluids and the use of solution wavelength filters. Key design features in the described apparatus were for protection of the operator from the hazards of UV exposure, lamp explosion, and electrical shock. The lamp and sample cell are enclosed in a light tight cylindrical container which also provides protection in the event of lamp explosion. The cover plate, while light tight, is loose fitting and would be blown off in the event of explosion and allow debris to be directed vertically. Safety interlock switches which are wired in series with the safety interlock circuitry of the Micropulser unit prevents activation of the high voltage circuitry unless the cover is on the enclosure and the top electrical lead is attached. A key feature of the apparatus is the collet type upper flashlamp terminal connector. Insertion and removal of the concentric sample cell requires opening of an electrical connection to the flashlamp. Due to the requirement for a high current, low resistance connection, the connectors supplied on the Micropulser cables require a tight force fit. Repeated attachment and removal of such a connector presents a risk of breakage of the relatively expensive flashlamp. We therefore employed the concept of a "zero insertion force" connector which is tightened after insertion with no stress applied to the lamp terminal. This was accomplished by machining a brass collet, similar to those used on machine tools, sized to fit the 0.28 in lamp terminal. The collet is tightened with a 1/4–28 threaded hex bolt/connector pin (part N in fig. 3.4) from a Supercon type pin connector. The connector pin mates directly with the Supercon connector on the Micropulser cable. Since this high current connection also fits tightly, a means of removing it without transferring stress to the flashlamp was needed. A removal mechanism was fabricated using lever arms from a household corkscrew device to remove the connector with a smooth vertical force.

The photon flux delivered to the sample cell by the flashlamp was compared to that delivered to the same cell in a commonly used CW irradiation apparatus using

KFOX actinometry. Lamps delivering predominant radiation centered around 350 nm were used in the CW source since this wavelength is commonly used to photolyze electronegatively substituted aryl azide compounds and diazirines. The quantum yield of the KFOX actinometer and the emission characteristics of the two light sources as a function of wavelength are shown in fig. 3.5, bottom. The actinometry measurements showed that the total flux delivered in 1 sec of CW exposure could be obtained from a single flash with 10J delivered to the flashlamp. Since the duration of the flash is on the order of 2 μs, the flash source is more than 10^5 as intense per unit time. The sample exposure, therefore, is less than 10^{-5} as long with the flash source as with the CW source for the same UV flux delivered.

Since fluorinated aryl azides have been suggested as excellent photoactivatable groups and since TF4N3 retinal (**8**) possesses this functionality, photolysis of a model fluorinated arylazide (TFABA) was used as a model to compare the CW and flash sources. Photolysis of TFABA in cyclohexane yields a single C–H insertion product, TFCBA. The maximum production of TFCBA required about 4 times the photon flux from the CW source as from the flash. This result suggests that the nominal 350 nm lamps in the CW source do not deliver the optimal wavelength for photolysis of the aryl azide. In summary, the described apparatus provides a convenient, versatile, and safe means of employing high flux, short duration flash photolysis on solution samples.

It requires five times the number of flashes needed to activate the model compound to induce noticeable damage to the protein. However, at even very long exposures to the CW source using 350 nm light, no noticeable protein damage was detected. These results suggest that the protein damage is done by short wavelength light which is further supported by the fact that 254 nm wavelength bulbs in the Rayonet Reactor sharply decreased the absorbance of BR at 570 nm over only fifteen minutes irradiation (data not shown). It may be possible to replace the expensive quartz cylinders in the sample cell with Pyrex cylinders. Pyrex glass absorbs light < 300 nm and is less fragile than quartz. Since photoactivation can be induced by light > 300 nm

in wavelength, as shown by the CW source, glass cylinders may be an inexpensive alternative to the easily broken quartz cylinders. The shielding of the sample from light < 300 nm may also decrease protein damage.

As evidenced in the emission spectra in fig 3.5, the flash apparatus has a wide emission spectrum with high flux in the UV (<340 nm). With these characteristics, the flash apparatus should activate nearly any of the photoactivatable groups described here. The RPR-100 reactor with the 350 nm bulbs should activate the fluorinated arylazides and diazirines very specifically with less damage to protein than the flash apparatus. These two sources were used in attempts to photoactivate TF4N3 as described in Chapter 5.

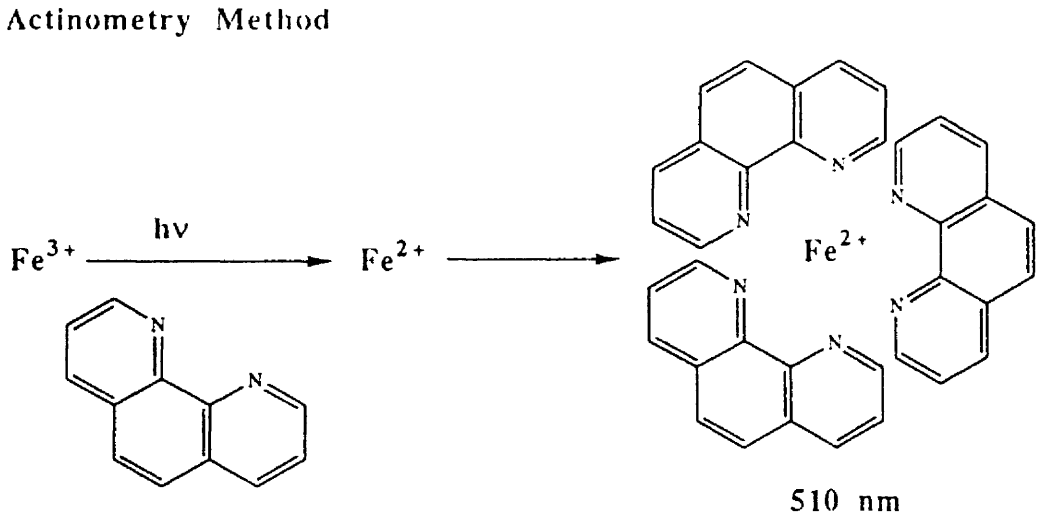

Figure 3.1 Actinometry
Diagram of chemical actinometry method. Potassium ferrioxalate solution absorbs light converting ferric ion to ferrous ion which is complexed by 1,10 phenanthroline. This 3:1 complex is red (510 nm).

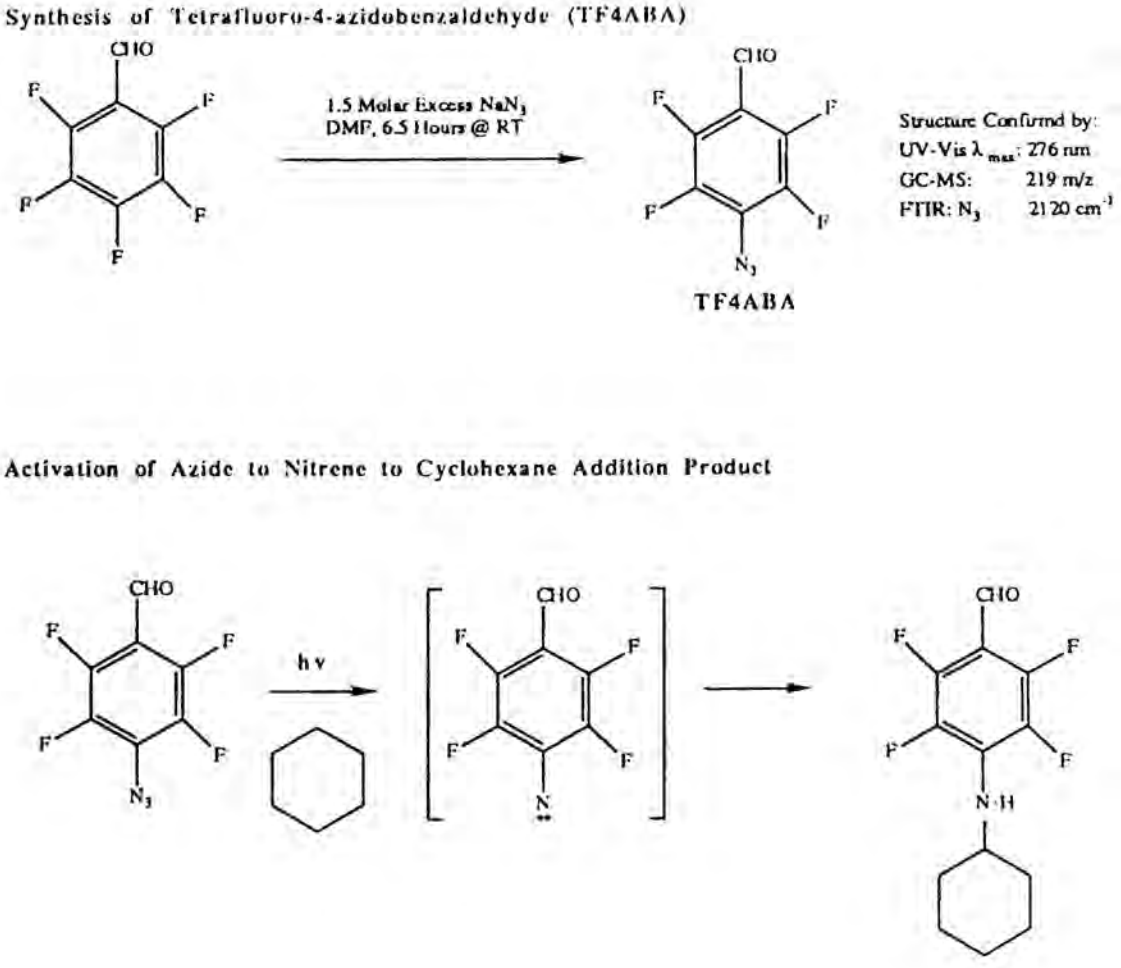

Figure 3.2 Model Photolysis
Top panel: Synthesis of tetrafluoro-4-azidobenzaldehyde from pentafluorobenzaldehyde with sodium azide. Successful synthesis was confirmed spectrally.
Bottom panel: Diagram of the photoactivation of TF4ABA in cyclohexane leading to the desired C-H insertion derived cyclohexane addition product, TFCBA.

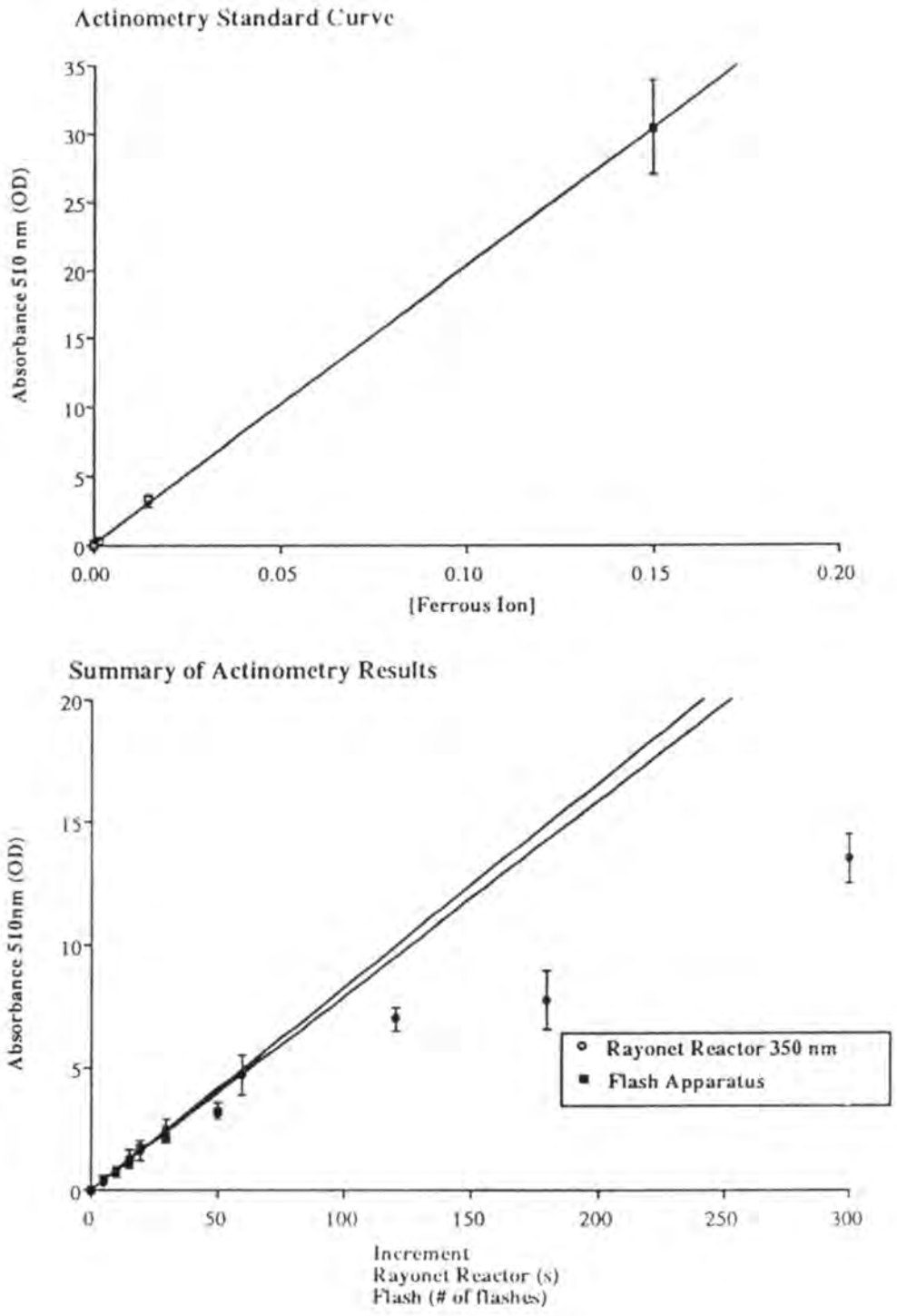

Figure 3.3 Actinometry Results

Top panel: Actinometry standard curve from standard solutions of ferrous ion. See materials and methods section for modifications of the published procedure required for these results. Bottom panel: Summary of actinometry results for the RPR-100 with 16, 350 nm bulbs and for the flash apparatus with 10 kV flashes. The plotted lines were chosen since the linearity of of the actinometric methods decreases at high total photon count.

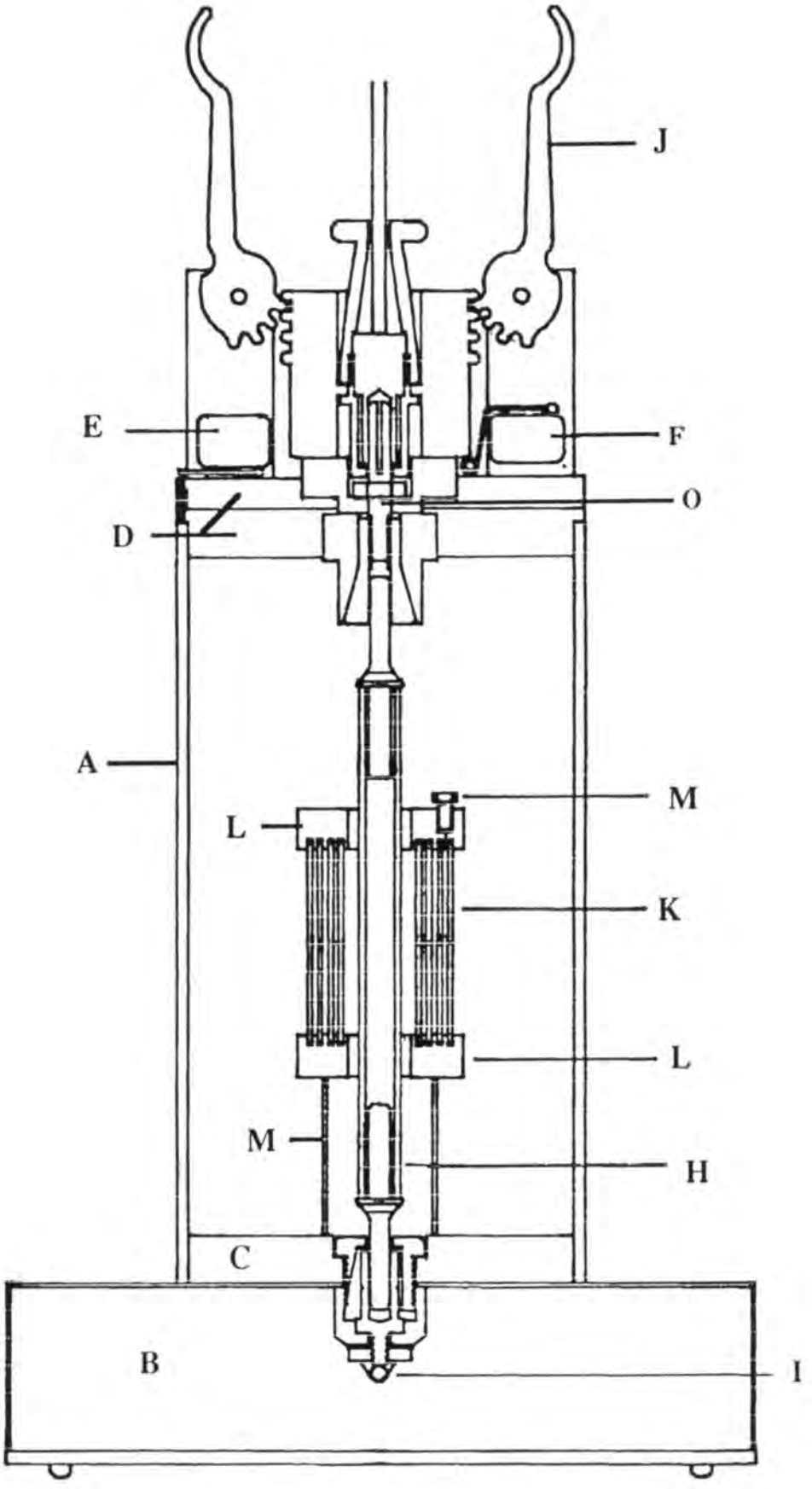

Figure 3.4 Flash Apparatus
Diagram of coronal section of flash photolysis apparatus. See text for descriptions of lettered items.

Detail of Sample Cell

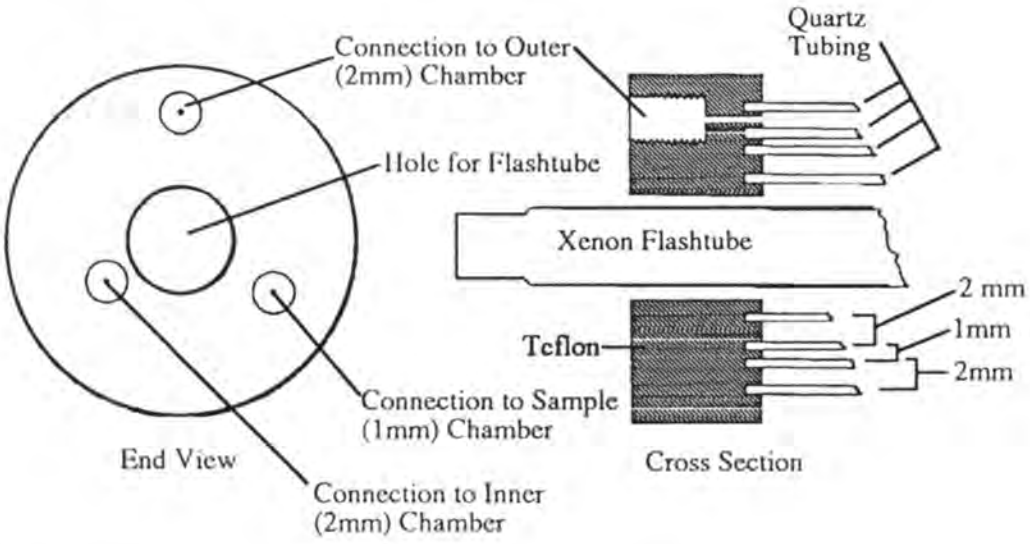

Emission Spectra and Quantum Yield

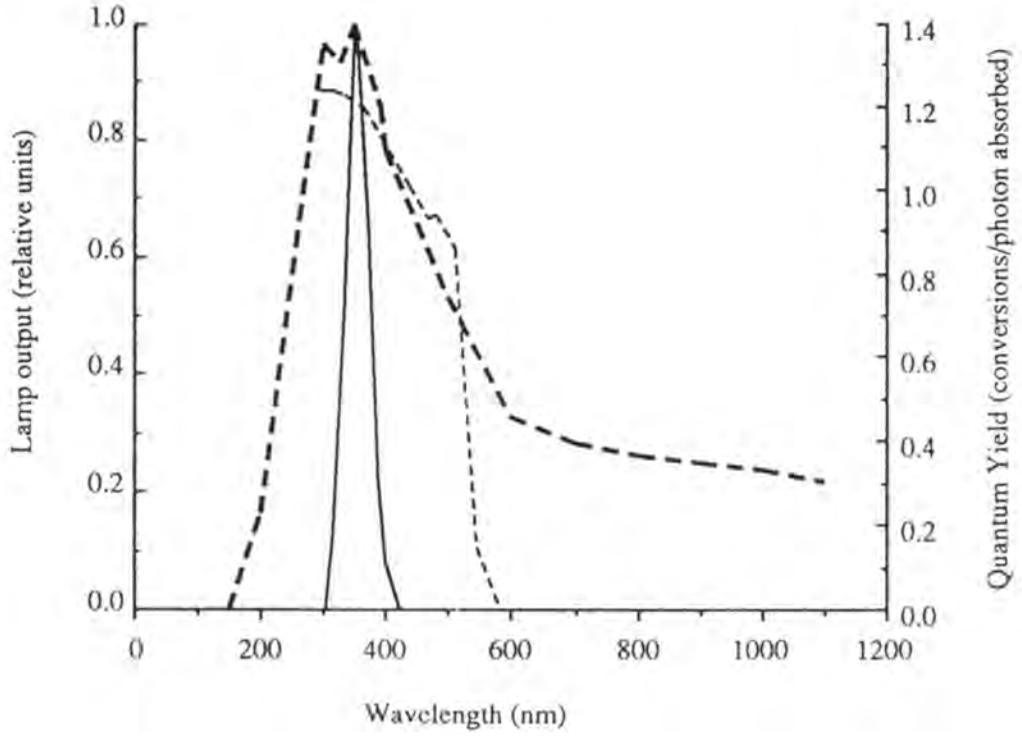

Figure 3.5 Sample Cell and Emission Spectra
Top panel: End view and cross-sectional view of sample cell depicted in figure 3.4. The end view shows access points to the different annular chambers formed by the four quartz cylinders that fit tightly into grooves in the top and bottom teflon bases. Bottom panel: Emission spectra of the flash lamp (heavy dashed line), the RPR-100 350 nm lamps (solid line), and the quantum yield of the actinometry method (light dashed line). Emission spectra adapted from manufacturers' literature. Quantum yield adapted from Calvert & Pitts, 1966.

GC-MS of TF4ABA and Cyclohexane Addition Product at 30 s Photolysis with the RPR-100 at 350 nm.

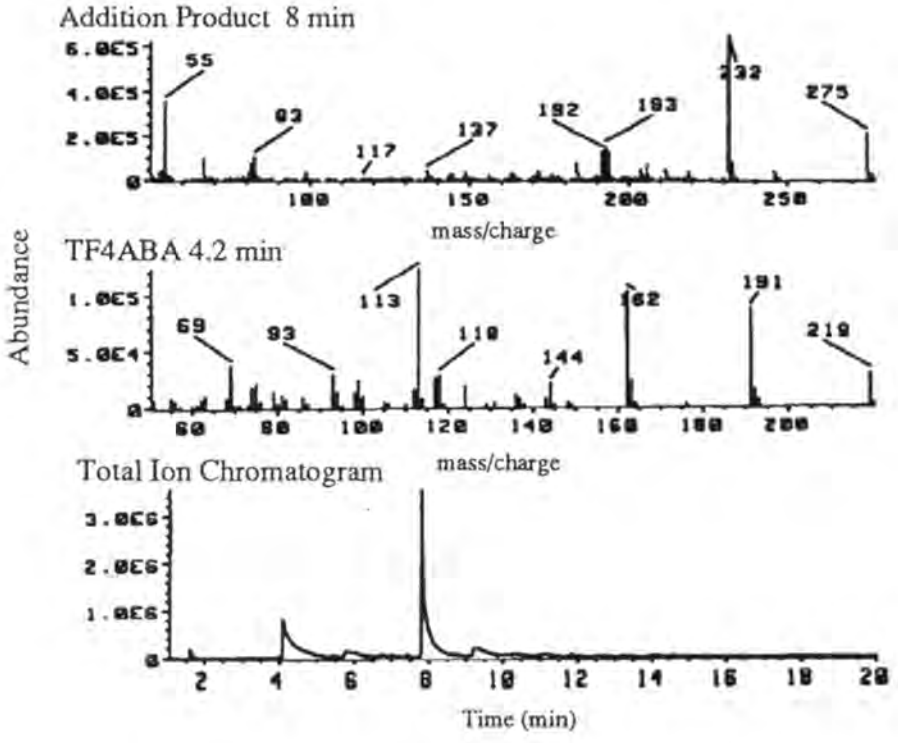

Figure 3.6 Example of Model Photolysis Results
This figure shows the gas chromatography - mass spectrometry confirmation of the C-H insertion derived product from the photolysis of TF4ABA in cyclohexane. GC-MS data from the 30 s time point indicating ~60% conversion of the azide (TF4ABA, 4.2 min, mass=219) to the cyclohexane addition product (TFCBA, 8 min, mass=275).

Chapter 4

Prediction and Evaluation of Photoaffinity Labeled Sites in BR Using Molecular Modeling

Portions of this chapter will be submitted for publication as

Beischel, CJ, K Gray, ES Hazard, RK Crouch, and DR Knapp.

"Prediction and Evaluation of Photoaffinity Labeled Sites in Bacteriorhodopsin using Molecular Modeling."

J. Mol. Graph., manuscript in preparation.

Introduction.

Bacteriorhodopsin has 248 amino acids, each of which is at least potentially a site of labeling for photoactivatable retinal analogs. It is important to be able to predict and interpret the many possible labeled sites. Predictions define the expected experimental results as a small set of amino acids likely to be labeled. These predictions form the basis of the hypothesis that a photoactivatable retinal analog in the native retinal binding site will label one or more of the amino acids in the set. Interpretation includes whether experimental results are consistent with the predictions and evaluation of the models used to make the predictions. The use of sophisticated computer programs for molecular graphics allows insights and measurements on these complex molecules as well as building of accurate models of less complicated molecules such as retinal analogs. The tools of molecular modeling are used to visualize this complex protein and to predict experimental results.

Henderson *et al.* (1990) published and subsequently deposited in the Brookhaven protein crystal data bank coordinates of a molecular model for BR based on cryo-electron diffraction studies. This widely accepted model serves as the basis for the following predictions.

By using Henderson's model in our dynamic, room temperature system it is possible to test the accuracy of this model that is based on studies done at 4 K on partially dehydrated PM. To keep the interpretation of these types of studies simple, it is important to make as few assumptions as possible. If amino acids are labeled that are outside the predicted sets, it implies that the predictions were incorrectly made, that the model is poor or that the labeling experiment did not work as planned. Three increasingly restrictive assumptions were made as to the placement of the retinal analog in the native retinal binding site of BR. Each assumption requires the retinal analog to be more and more precisely restricted to the native retinal binding site. These methods are applied to four different photoactivatable retinal analogs.

Materials and Methods.

Materials. The necessary equipment for these studies include a desktop computer (Macintosh IIsi) networked to the university VAX 11/785 and the Biomolecular Computing Resource software that includes the molecular modeling software SYBYL by Tripos (St. Louis, MO). The desktop computer must also run the terminal emulation application for SYBYL, NITRO (Tripos). For graphics manipulation on a smaller scale and for a variation on graphics output, an application called Nanovision (ACS Software, American Chemical Society, William R Light, generously purchased by DW Corson) was used. Slide output was done using Powerpoint (Microsoft) and a Montage (Presentation Technologies, Santa Cruz, CA) slidemaker.

Methods. It is not the intent of this methods section to explain the general use of the Macintosh as a terminal for the Vax or of the SYBYL molecular modeling package. Some important commands or subsections of SYBYL particular to this work are capitalized and explained in this section. The atomic coordinates of the bacteriorhodopsin model of Henderson were imported into SYBYL from the Brookhaven crystal data bank (Biopolymer Brookhaven In). The model is fully manipulatable in SYBYL. This structure is the working model for these predictions. The crystal structure of Vitamin A (retinol) was imported from the SYBYL fragment library as was that of lysine (Build Molecule Fragment Fragment_name Get). The Vitamin A is in the 6-s-*trans* configuration as it has been shown to be in the protein [Creuzet *et al.*, 1991]. The lysine-retinal protonated Schiff base structure was 'synthesized' in SYBYL. This basic structure was compared to the same structure lifted from the Henderson model. The retinal was then modified to model the photoactivatable retinal analogs that have previously been used to label BR and the labels that are being synthesized for this project. Using the Measure Distance command in SYBYL the distances between different atoms in the modeled analogs were measured. Three distances were measured for each analog: from the alpha carbon of the lysine (#1) to the photoactivated carbene or nitrene, from the Schiff base nitrogen (#2) to the photoactivated carbene or nitrene, and from carbon 6 of the retinal analog (#3) to the

photoactivated group (fig. 4.1). These distances were used to define sets of amino acids that are within a reasonable distance to be labeled by the photoactivated analogs. A large sphere of the distance measured plus 3 angstroms had a smaller sphere of the distance minus three angstroms subtracted from it. For example, the SYBYL command to define a set of amino acids between ten and fifteen angstroms from the Schiff base lysine is Define Dynamic_Set Substructure {Sphere(Lys216.NZ,15)}-{Sphere(Lys216.NZ,10)} Setname Comment. To list the amino acids in the resulting set the command List Local Setname Full is used. Any amino acid residue that has an atom in this defined volume is made part of the set. This manipulation defined a set of amino acids that were close to the photoactivatable group assuming free movement about the atom used for the measurement. Also defined was a set of amino acids on the 'outside' of the helixes in Henderson's model. This set was defined by choosing an amino acid that pointed directly to the center of the bundle and defining its rotation to be 0 degrees. One hundred degrees was added or subtracted for each step in the amino acid sequence and any amino acid that was between 101 degrees and 259 degrees was determined to be outside the helix and unlikely to be labeled. Each amino acid in the α-helix was assumed to be 100 degrees from the preceding amino acid [Stryer, 1988]. This set of amino acids was subtracted from each of the predicted sets to leave three predicted sets for each retinal analog (Define Static_Set Substructure {Setname}-{Outside} Setname Comment). In order to more correctly analyze the results of Huang *et al.* (1982), it was necessary to build their labeled amino acids onto Henderson's structure. Ser193 and Glu194 were added to Gly192 as an α-helix and alternatively as a random coil (using the Picking menu Biopolymer, Edit Molecule, Add to Chain subsections). This was necessary because Henderson's model contains only the amino acids for which he had sufficient electron density to model (i.e. those in the transmembrane helixes). The two new models were used in the evaluation of the analog Khorana **2**.

Movement of molecular graphics files from SYBYL to Nanovision or most other

molecular graphics packages requires the use of the Biopolymer Brookhaven Out Filename commands. This series of commands writes the chosen structure from the SYBYL format into the standard Brookhaven database format that is readable by Nanovision. Graphics output of the NITRO window to a Macintosh PICT file is done simply from the File Menu of the NITRO terminal emulation software.

Results and Discussion.

The amino acids in the set 'Outside' that are predicted to be oriented away from the retinal binding site are depicted in an end-on view in Fig. 4.2. The three sets from Nakanishi1 **3** are depicted graphically in figures 4.3-4.6. Set #3 and the labeled sites for Khorana **2** are shown in fig. 4.7 on an especially extended version of Henderson's model that contains Ser193 and Glu194 in an α helical conformation. The results of labeling with Nakanishi2 **4** are shown in fig. 4.8 along with the amino acids of set #3 for this retinal analog. The sequence of BR, the amino acids in the structure, the amino acids determined to be outside the barrel of BR, the measurements and the three sets for four different analogs are summarized in Fig 4.9. The two models of retinal, one lifted from Henderson's model and that obtained from the fragment library are very similar and the measurements made on these models were nearly identical (data not shown). The model derived from the fragment library was used in the measurements presented here.

The prediction of the labeled sites was made with a minimum of assumptions. The first is the use of Henderson's model as the working model. This assumption implies the accuracy of this model of BR that was derived from two dimensional crystals at liquid nitrogen or liquid helium temperatures. Henderson's model correlates well with the rest of the biophysical data derived from studies of BR at various temperatures. This includes an excellent correlation with the studies done using site-directed mutants of BR that have defined certain amino acids that are believed to be important for tuning of the absorbance spectrum of retinal and for proton pumping function [Khorana, 1988].

The assumption was made that the retinal analogs would form a Schiff base with Lys216 and not with other amino groups. This assumption is based on the extensive literature on BR analog pigments in which the retinal analogs that form BR analog pigment bind to Lys216. A Schiff base formed with another amino group will not be stable because it will not be in the very special environment that surrounds Lys216. The

opsin shift indicates that the Schiff base-retinal link is protonated and that it is being influenced by the known counterion. The protonation and counterion contribute most of the influence for the opsin shift [Motto *et al.*, 1980]. The BR analog pigments described here are stable and display a considerable opsin shift indicating that the retinals are interacting with a similar environment as is the native retinal that has been shown to be Schiff base linked to Lys216 [Bayley *et al.*, 1981].

It is also assumed that since the retinal and the analogs are believed to be in the center of the seven transmembrane helixes that the amino acids on the outside (i.e. near the lipid membrane, the hydrophobic half of the amphipathic helix) will not be labeled by the photoactivated intermediate. It is much more likely that the reactive intermediate would label a site on the inside. This assumption allowed the exclusion of 69 amino acids from the total of 178 amino acids in the structure (fig. 4.2). Note that 70 of the original 248 amino acids have been deleted by Henderson's results. He did not model the amino acids for which he did not have sufficient electron density. The 70 excluded residues form the more freely moving extramembranous loops. Ser193 and Glu194 are in these loops, but were added in two different motifs in order to more thoroughly evaluate the results of Huang *et al.* (1982).

Three sets were defined for each retinal analogs. These sets identified amino acids that were an appropriate distance from the three centers of rotation to come into contact with the photoactivated intermediate (fig. 4.1). The three sets show increasing restriction of the movement of the retinal analog in the protein. The three sets were defined assuming free movement about the α carbon of Lys216 (#1) allowing the entire retinal, Schiff base and lysine sidechain to move, about the Schiff base nitrogen (#2) allowing movement of only the retinal, and about carbon 6 of the retinal (#3) allowing movement only around the ring end of the retinal analog. This last assumption is reasonable because it is believed that the retinal and thus the very similar analogs are tightly held by the protein around the retinal side chain [Crouch, 1986]. The second assumption relies on the stability of the position of the lysine side chain. The first

assumption depends only on the stability of the helixes.

A plus or minus three angstrom volume was chosen for several reasons. Measurements on the retinal-lysine combination lifted from Henderson's model varied slightly from our model developed from the crystal structures. It is assumed that the retinal analogs bind in the 6-s-*trans* conformation. Changing this ring-side chain orientation can change the measurements on the analogs slightly. The hydrogen atoms are not included in Henderson's structure which gives another approximately one angstrom size around most amino acid sidechains. The bond formed would have a length of about 1.5 angstroms. This room for variation led to the choice of a rather large volume - 6 angstroms thick - as potentially contacted by the photoactivated intermediate.

The three previously used labels were included in this analysis to test the validity of the analysis and the likelihood that these analogs labeled sites in the native retinal binding pocket (fig. 4.1). The experiments of Huang *et al.* (1982) showed the labeling of Ser193 and Glu194 (Arrow, fig. 4.7; Boxed and Shaded, fig. 4.9) with an aromatic analog of retinal (**2**). These two amino acids are not in Henderson's model. Since not enough electron density was available to model them, they are believed to be part of the freely moving extramembranous loops. It is likely [Henderson *et al.*, 1990] that this label was incompletely in the binding site consistent with its small opsin shift and the unreported functional state of the analog pigment. (It should be noted that Huang *et al.* (1982) did not report the functional characterization of the BR analog pigment formed with **2**. However, Boehm *et al.* (1990) stated that the BR analog pigment formed with **2** was "nonfunctional".) When this analog was tested with two models of BR that had Ser193 and Glu194 built on as α-helix and random coil, these two amino acids were still not in the specified volume. In fact, the hydroxyl of the Ser193 was ~4 angstroms beyond the larger sphere and the terminal oxygen of Glu194 was ~7 angstroms beyond the larger sphere (fig. 4.7). These amino acids are 12-16 angstroms from the number six carbon of the retinal as placed by Henderson.

The experiments of Ding *et al.* (1990) using the retinal analog (**3**) showed labeling of Thr121 and Gly122 (Arrow, fig. 4.6; Boxed, fig. 4.9). These sites are in all of the sets predicted by this analysis indicating the likely placement of this analog in the native retinal binding pocket. Since the BR analog pigment of Nakanishi1 (**3**) is functional, it is believed that this analog fits well into the native site. (It should be noted that Ding *et al.* (1990) reported 100% efficiency in proton pumping of the BR analog pigment formed with **3** as compared to positive control. Whereas, Sen *et al.* (1982) stated that the analog pigment was 50% functional. This difference could be explained by the use of optically pure **3** in the experiments of Ding *et al.* (1990).)

Evaluation of the labeled sites reported using the retinal analog Nakanishi2 **4** [Boehm *et al.*, 1990] was more complex. Of the four amino acids labeled (Ala126, Leu127, Trp137 and Trp138 (fig. 4.8)), only Trp138 was predicted to be properly situated to be contacted by the carbene derived from photolysis of **4**. The labeling of Ala126 and Leu127 is particularly interesting since these amino acids possess aliphatic sidechains. Assuming labeling of the sidechains, the ability of the carbene to insert into the very stable C-H bonds may indicate very close contact between the carbene and these sidechains. The limitations of the use of Edman degradation to determine labeled sites when fairly high resolution structural information is desired is highlighted by the labeling of these two amino acids. Leu127 was labeled, but is oriented, in the model, to the outside of the helices where it may interact with the lipid bilayer as one might expect for a very hydrophobic amino acid such as leucine. The labeling of these amino acids shows a limitation in the model suggesting a rotation of helix D to turn Ala126 and Leu127 toward the retinal binding site. Or, as suggested by Boehm *et al.* (1990), the labeling of Leu127 may arise from incomplete cleavage or elution during each cycle of the Edman sequencing when Ala126 primarily contained the radiolabel. They also, very reasonably, suggest the movement of the retinal analog in the binding site as reason for distribution of the sites of labeling on these two amino acids. The modeling performed here favors the first argument involving incomplete Edman cycling. However, it should be emphasized that neither of these sites is well situated to be labeled by this retinal

analog, if the analog binds in the retinal binding site as modeled by Henderson. These two amino acids are located very near the cytoplasmic end of helix D indicating that this retinal analog, similar to Khorana **2** must be oriented with its ring much closer to the cytoplasmic surface than the native retinal. This lack of ability to completely bind to the hydrophobic binding pocket of the retinal ring may be due to the addition of the polar photoactivatable groups.

The labeling of Trp137 and Trp138 by Nakanishi2 **4** is also very interesting. The model and the predictions presented here clearly indicate the proximity of the ring of retinal to Trp138 in the retinal binding pocket. However, if the previous argument about the smearing of the radiolabel in the Edman cycling holds, one must assume that the primary labeling was to Trp137. These amino acids are separated by a 100 degree rotation around helix E. These inconsistencies emphasize the need for determination of the exact amino acid(s) labeled for proper evaluation of labeling in this high resolution context. It would be possible to reorient helix E to place the two tryptophans in close proximity to the ring end of the retinal. It should be emphasized that small variations in the model as suggested by this particular result may not be warranted considering the difficulty in interpretation of the data.

The labeling of these four amino acids by **4** and of Ser193 and Glu194 by **2** indicate the difficulty inherent in the chemical modification of retinal with retention of binding to the native retinal binding site. One fairly simple interpretation of these results is that these two retinal analogs, due to the modifications of their rings, fit only well enough in the retinal binding site to form the Schiff base and that the ring end of these analogs was not capable of completely fitting into the retinal binding site. Thus, these retinal analogs labeled amino acids between the retinal binding site and the cytoplasmic surface of the protein.

The fact that these amino acids were not identified even in set #1 for each of these retinal analogs may indicate an overly rigid interpretation of the model. The assumption for set #1 required rigid retention of the relative positions of the alpha helices. It is possible that the the binding of a retinal analog, that does not fit well into the ring end of

the binding pocket, to the epsilon amino group of Lys216 may shift the relative positions of the alpha helices allowing contact between the reactive intermediate, still tethered to Lys216, with the amino acids that have been shown to be labeled.

From this discussion, it may be concluded that the retinal analog Nakanishi1 **3** fit best into the binding site as modeled by Henderson *et al.* (1990) and that the retinal analogs Khorana **2** and Nakanishi2 **4** did not fully fit into the ring end of the retinal binding site. This qualitative description of the ability of these retinal analogs to occupy the retinal binding site correlates with the ability of the BR analog pigments to function as a light driven proton pump. The functional characterization of the BR analog pigment formed with Khorana **2** indicates poor proton pumping (in Boehm *et al.*, 1990). This retinal labeled amino acids that are the greatest distance from the retinal binding site in Henderson's model. The retinal analog Nakanishi1 **3** showed function at about 50%-100% (see above) of the level of native BR and labeled amino acids in Henderson's model well situated to be in contact with the reactive intermediate. The retinal analog Nakanishi2 **4** showed function at about 1/5 the level of native BR and labeled amino acids an intermediate distance from the retinal binding site in the model. Thus, function of these retinal analogs as BR analog pigments correlates roughly with the labeling of amino acids near the native retinal binding site in the model. Overall these predictions show the utility of the model for evaluation of other experimental results and the utility of photoaffinity labeling experiments to evaluate the model.

Predictions were made for the most promising of the retinal analogs in these studies. The results from the predictions using TF4N3 **11** show the likely labeling of Thr121 and Ser141 if this retinal analog fits well into the retinal binding site as was suggested by the ~40% efficiency of proton pumping determined during the functional characterization of the analog pigment.

These studies demonstrate the power of molecular modeling for prediction of experimental results. These predictions form the basis of the hypothesis that the amino acids in these sets would be labeled by a retinal analog bound in the native retinal

binding site. More sophisticated applications of molecular modeling are being used to aid in rational drug design with BR being used as the basis for modeling members of the class of GPCR [Stone, 1992; Hibert *et al.*, 1991; Pardo *et al.*, 1992].

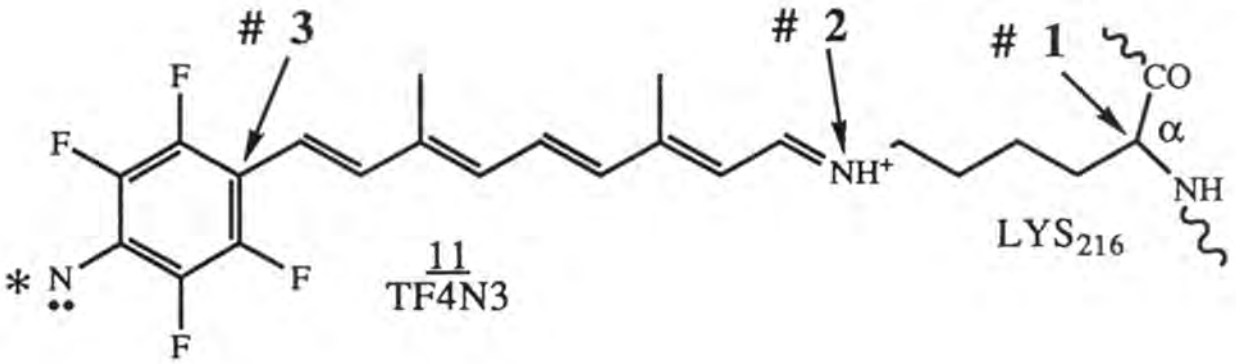

11
TF4N3

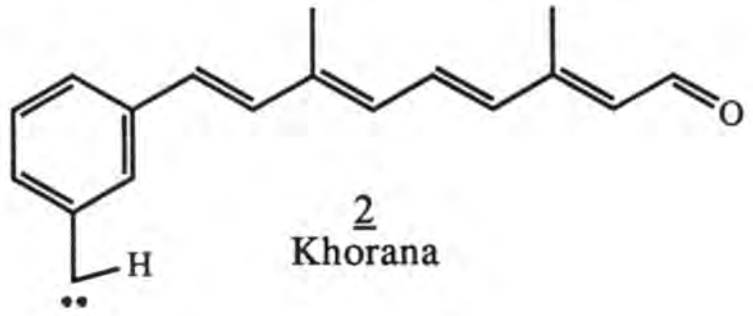

2
Khorana

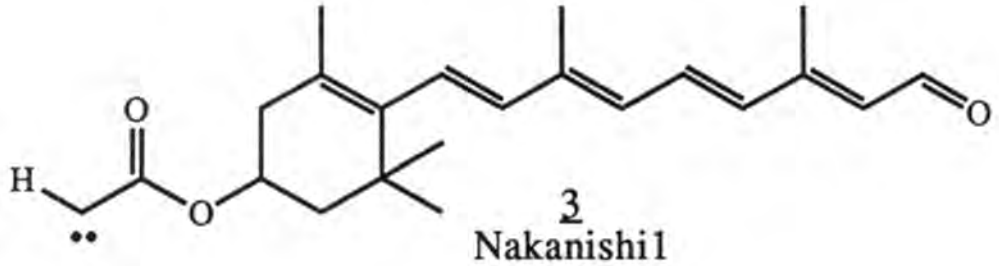

3
Nakanishi1

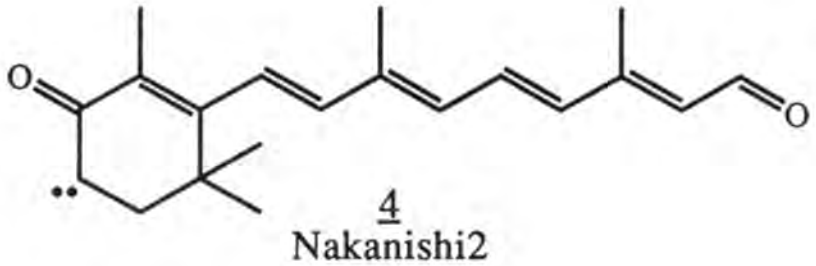

4
Nakanishi2

Figure 4.1 Photoactivated Intermediates of Retinals 2,3,4,11.
Each retinal analog is shown as its highly reactive intermediate produced by photoactivation. Indicated on the top compound are the centers of rotation for the 3 different sets of sites of labeling. The sets are based on measurements from #1, #2 and #3 to the reactive group (*). These centers of rotation were used for each analog.

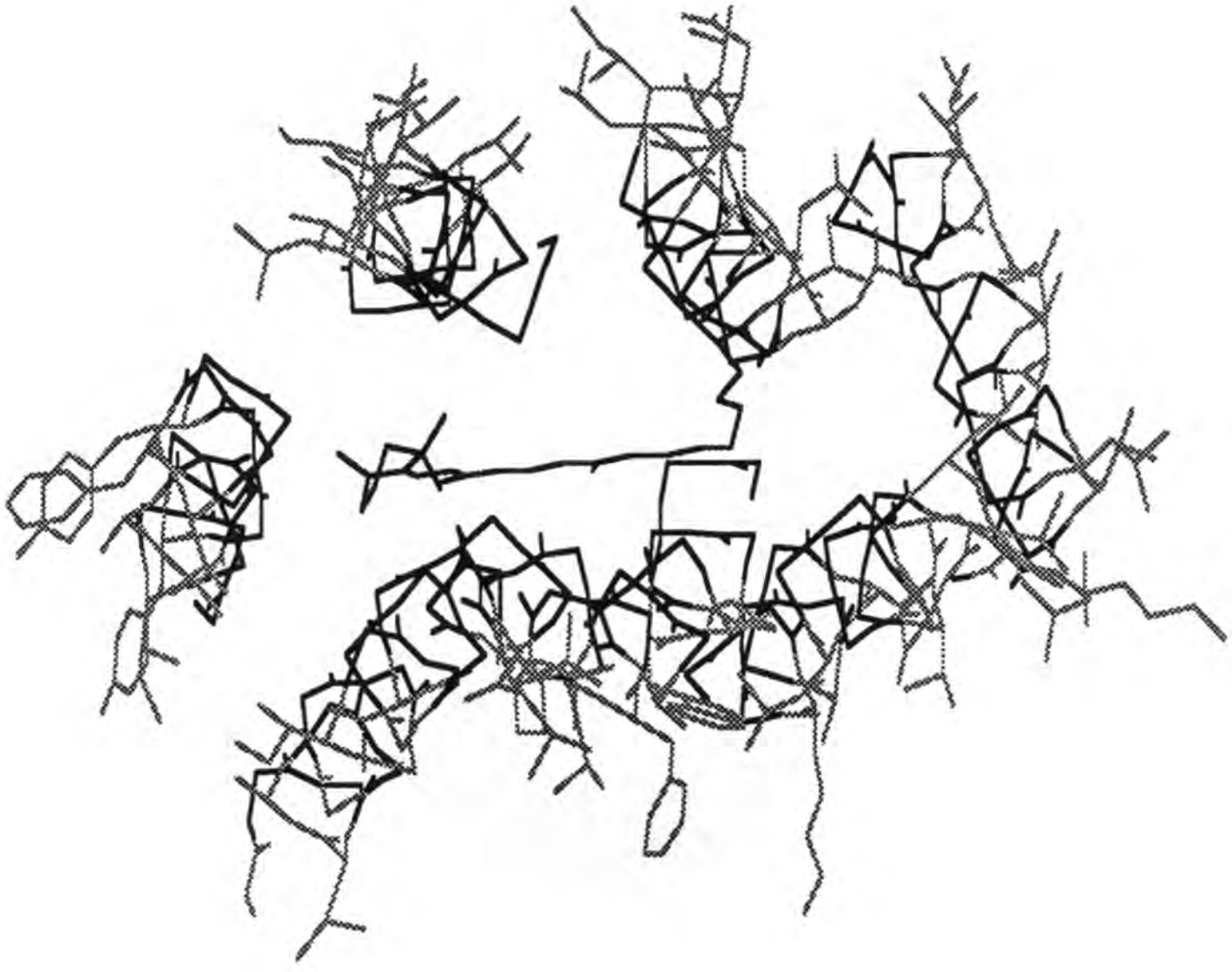

Figure 4.2 Outside
This view, from the cytoplasmic side, of BR's 7 transmembrane helices from SYBYL depicts in gray and full sidechains the amino acids that were chosen as outside the barrel of BR and unlikely to be labeled by any photoactivatable analog of retinal. These amino acids were excluded from the predicted sites of labeling.

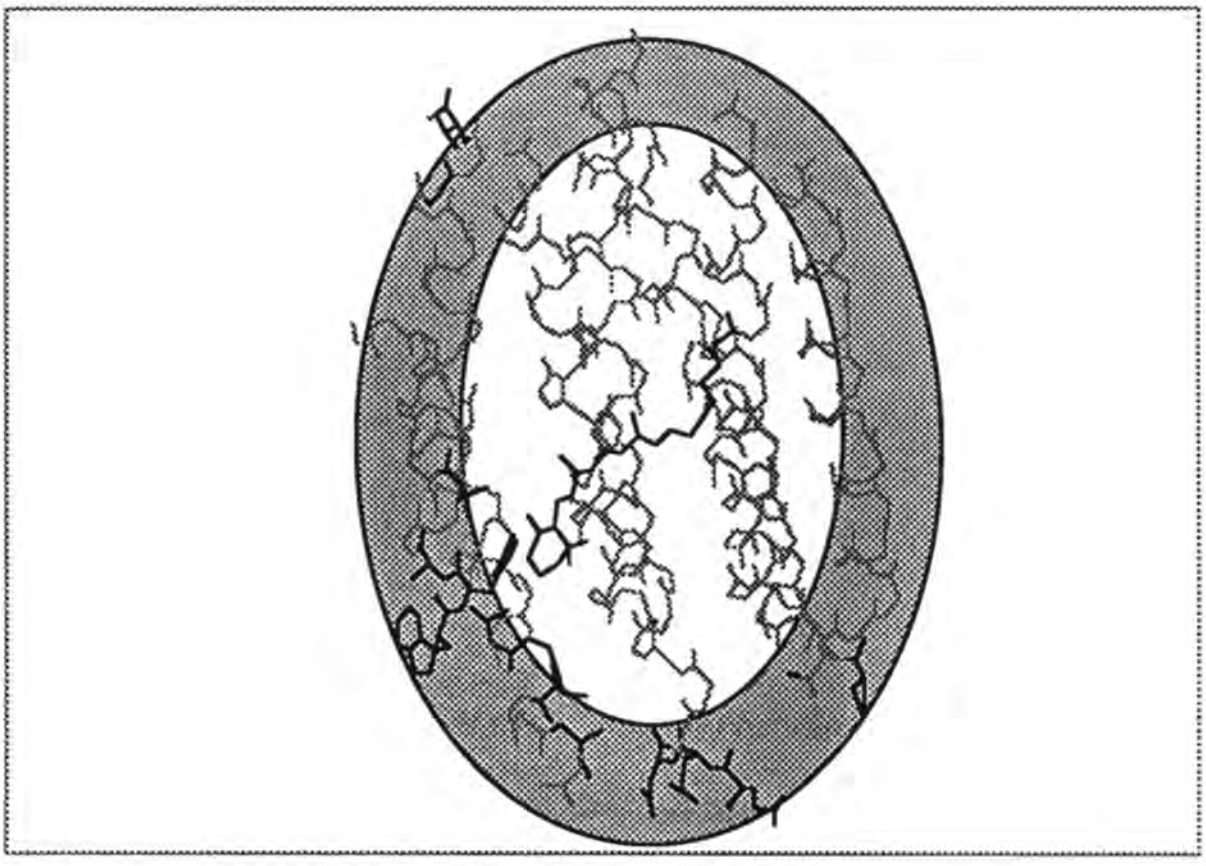

Figure 4.3 Nakanishi1 Set #1
Side view of BR from SYBYL indicates in black the set of amino acids predicted to be labeled by **3** if rotation is allowed of the entire lysine side chain and retinal about the α-carbon of Lys 216.

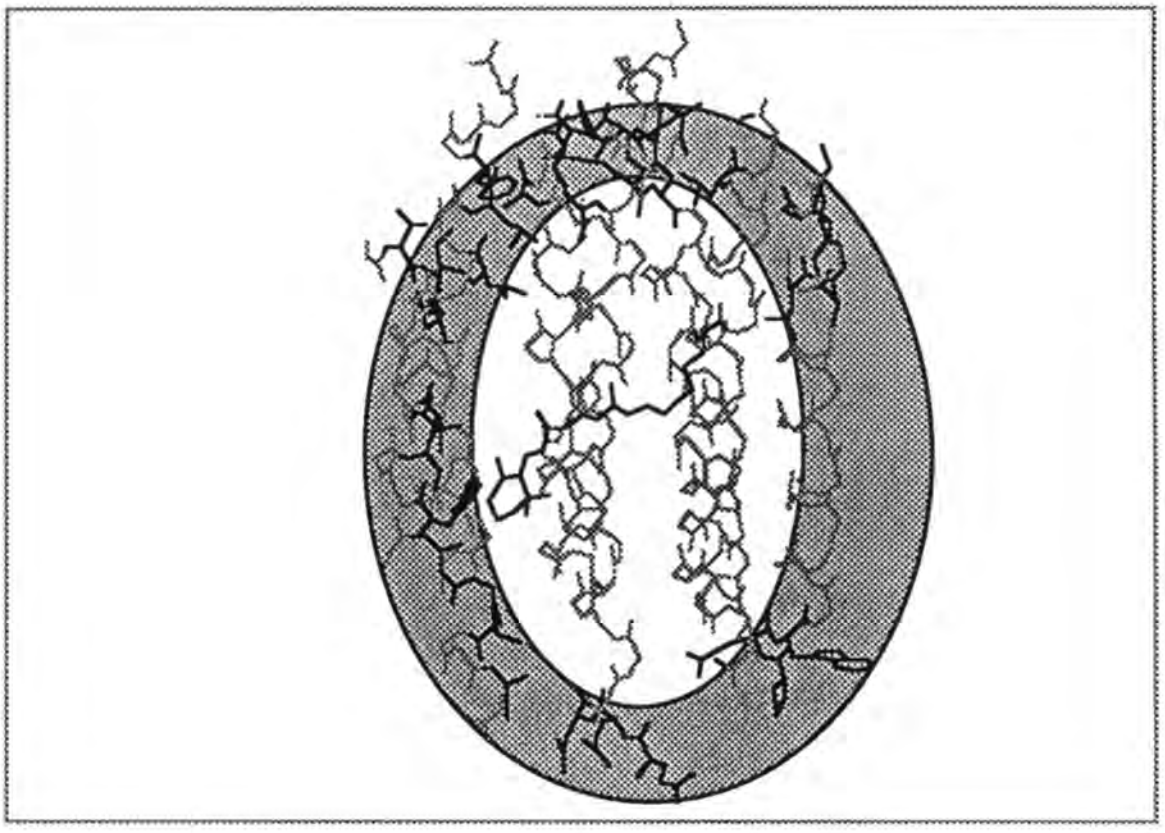

Figure 4.4 Nakanishi1 Set #2
Side view of BR from SYBYL indicates in black the set of amino acids predicted to be labeled by **3** if rotation is allowed of the retinal analog about the nitrogen of the Schiff base.

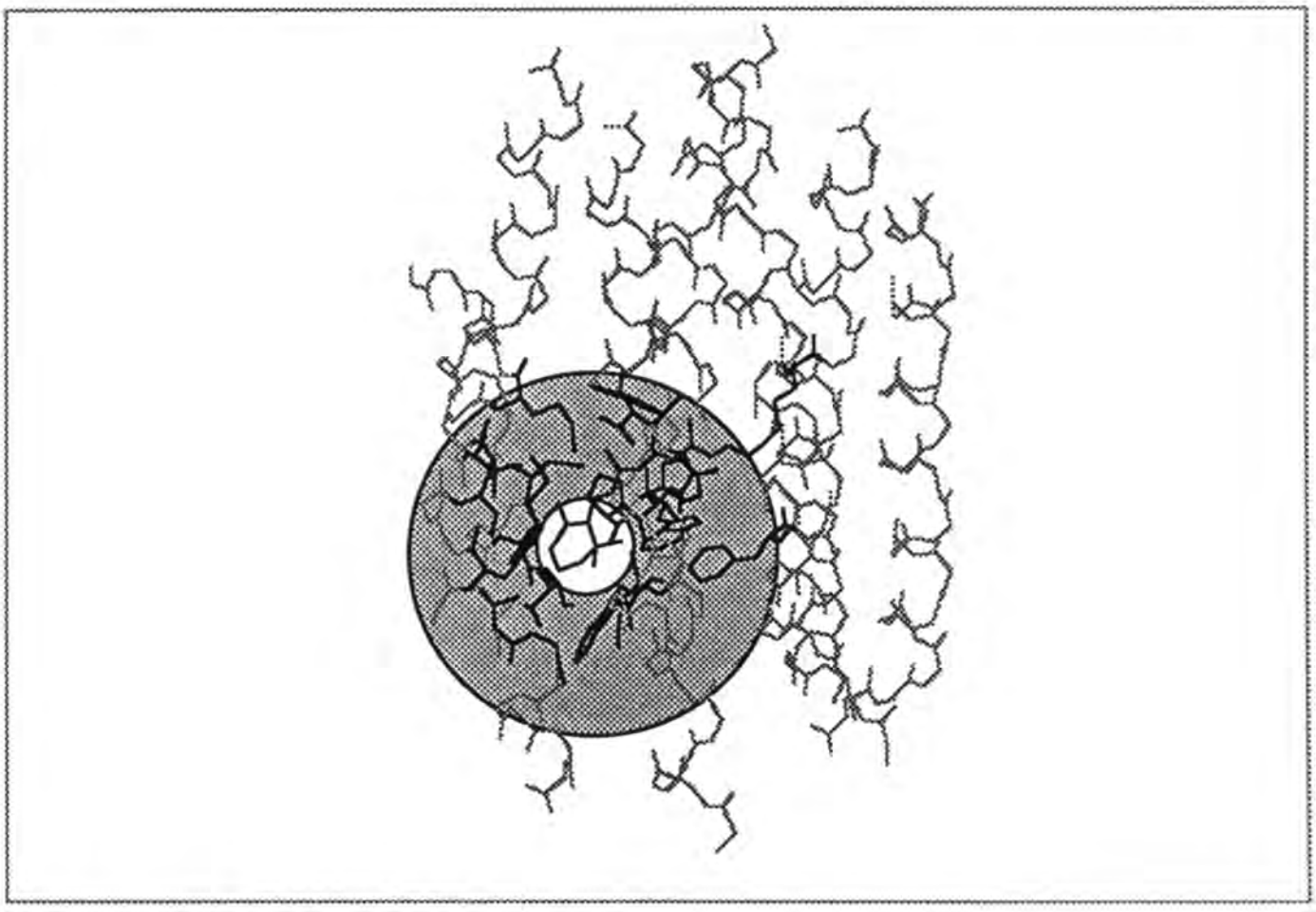

Figure 4.5 Nakanishi1 Set #3
Side view of BR from SYBYL indicates in black the set of amino acids predicted to be labeled by **3** if rotation is allowed only of the ring of the retinal analog about carbon 6 as numbered in retinal **1** (fig. 1.1).

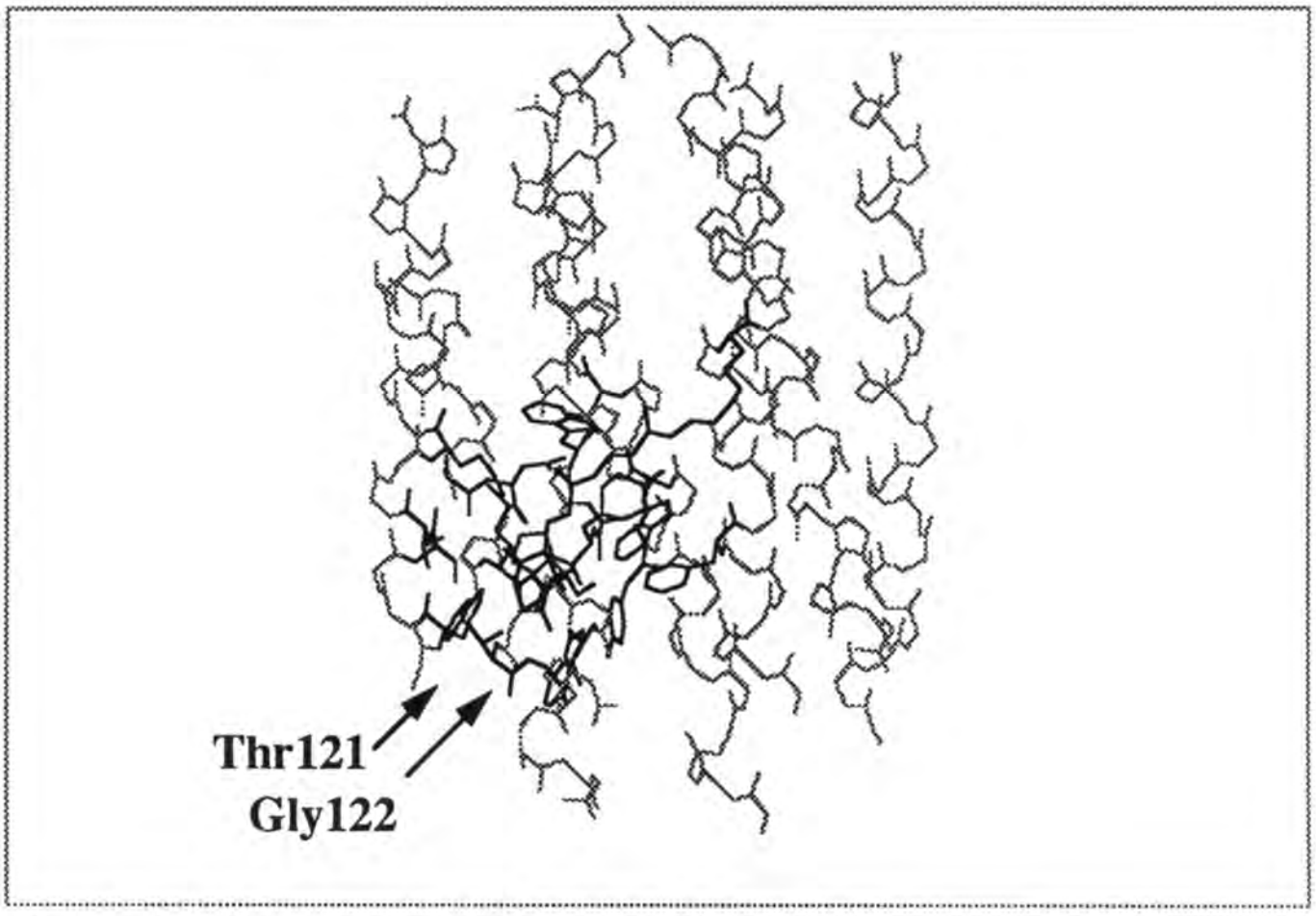

Figure 4.6 Nakansihi1's Labeled Sites
Side view of BR from SYBYL indicates in black the amino acids that were labeled by **3** in the experiments by Ding *et al.*, 1990. These two amino acids, Thr121 and Gly122, are in all three sets of predicted labeling sites for this retinal analog. The amino acids in dark gray are the other amino acids in set #3 from the predictions.

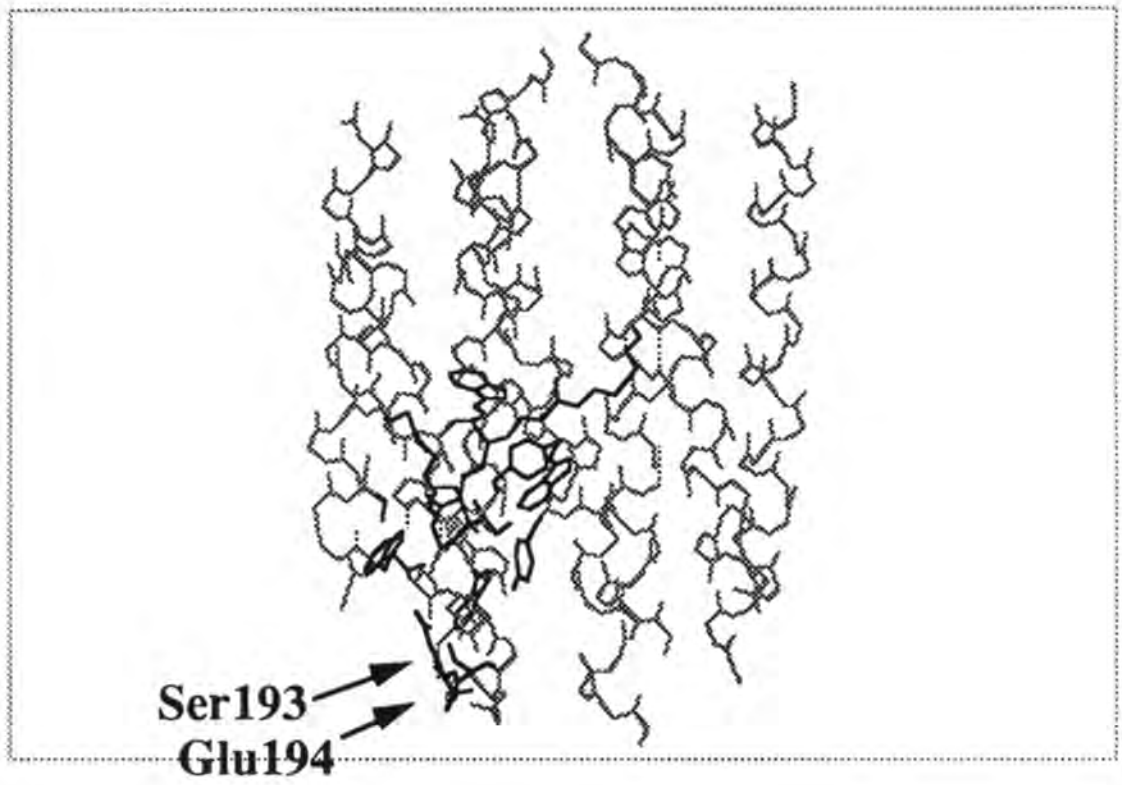

Figure 4.7 Khorana's Labeled Sites
Side view of BR from SYBYL indicates in black the amino acids that were labeled by **2** in the experiments of Huang *et al.*, 1982. These two amino acids, Ser193 and Glu194, are NOT in any of the sets of predicted labeling sites for this retinal analog. The amino acids in dark gray are the amino acids in set #3 from the predictions.

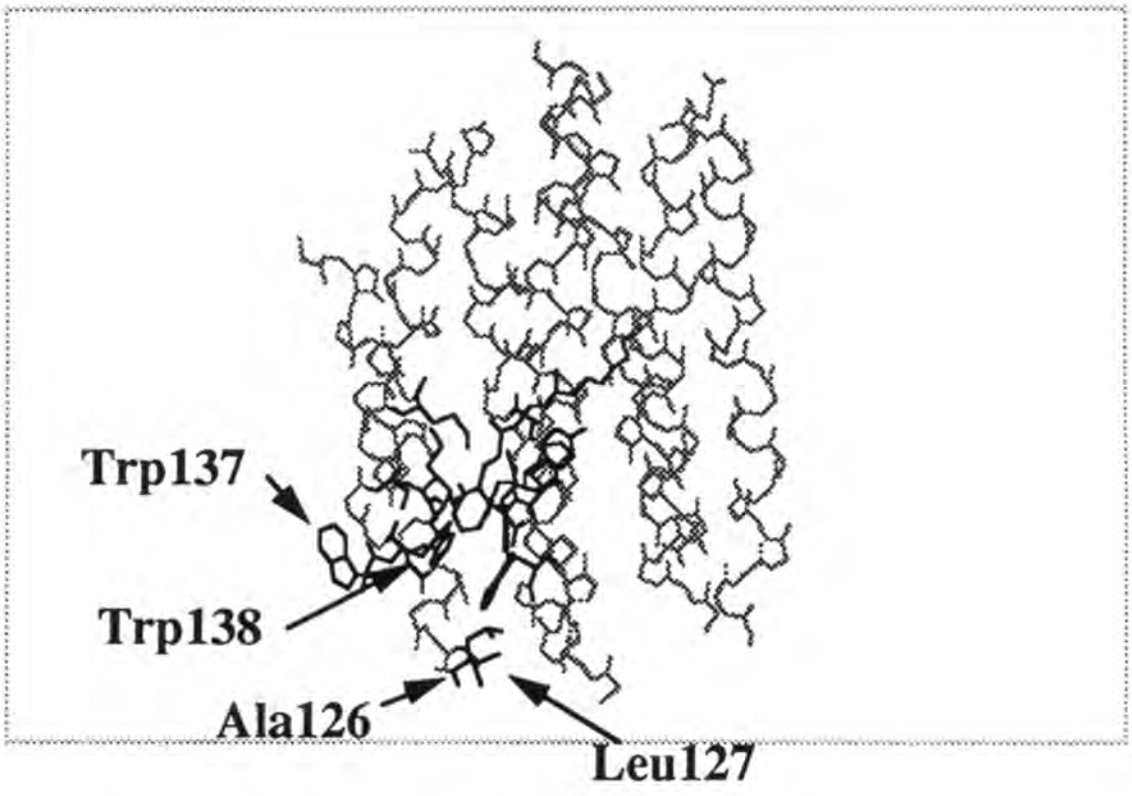

Figure 4.8 Nakansihi2's Labeled Sites
Side view of BR from SYBYL indicates in black the amino acids that were labeled by **4** in the experiments by Boehm *et al.*, 1990. Of the four labeled amino acids (Ala126, Leu127, Trp137, and Trp138) only Trp138 was predicted to be labeled. Trp138 was a member of all three sets predicted for this retinal analog. The amino acids in dark gray are the amino acids in set #3 from the predictions.

Figure 4.9 Table of Predicted Sets for Selected Retinal Analogs

This large table is a summary of the results of the studies described in this chapter. The first column shows the complete amino acid sequence of BR. The second column shows those amino acids that are included in the structure from Henderson *et al.*, 1990. The third column are those amino acids excluded from the predicted sets because they are believed to be oriented towards the outside of BR (see figure 4.2). The fourth column then indicates the possibilities for the predicted sets, i.e. those amino acids in Henderson's structure that are oriented toward the inside of the barrel of BR. The remainder of the table is in sets of three columns indicating the members of the three different predicted sets for the indicated retinal analogs. Also the measurements from the center of rotation to the reactive moiety are indicated in angstroms near the top of each column.

				Khorana 2			Naka1 3			Naka2 4			TF4N3 11		
bR sequence	aa in structure	outside excluded	Inside	alpha C	Lys N	Ret C6	alpha C	Lys N	Ret C6	alpha C	Lys N	Ret C6	alpha C	Lys N	Ret C6
				19.313	13.826	3.868	23.326	17.739	5.841	19.852	15.514	3.427	21.446	15.849	3.279
pGLU1															
ALA2															
GLN3															
ILE4															
THR5															
GLY6															
ARG7															
PRO8	PRO8		PRO8	PRO8			PRO8	PRO8		PRO8			PRO8		
GLU9	GLU9		GLU9	GLU9	GLU9			GLU9		GLU9	GLU9		GLU9		
TRP10	TRP10		TRP10	TRP10	TRP10			TRP10		TRP10	TRP10		TRP10	TRP10	
ILE11	ILE11	ILE11													
TRP12	TRP12		TRP12		TRP12						TRP12			TRP12	
LEU13	LEU13		LEU13		LEU13										
ALA14	ALA14	ALA14													
LEU15	LEU15	LEU15													
GLY16	GLY16		GLY16												
THR17	THR17		THR17												
ALA18	ALA18	ALA18													
LEU19	LEU19		LEU19												
MET20	MET20		MET20												
GLY21	GLY21	GLY21													
LEU22	LEU22	LEU22													
GLY23	GLY23		GLY23		GLY23										
THR24	THR24		THR24		THR24									THR24	
LEU25	LEU25	LEU25													
TYR26	TYR26		TYR26		TYR26			TYR26			TYR26			TYR26	
PHE27	PHE27		PHE27		PHE27						PHE27			PHE27	
LEU28	LEU28		LEU28		LEU28			LEU28			LEU28			LEU28	
VAL29	VAL29	VAL29													
LYS30	LYS30		LYS30					LYS30							
GLY31	GLY31		GLY31					GLY31							
MET32	MET32	MET32													
GLY33	GLY33	GLY33													
VAL34															
SER35															
ASP36															
PRO37															
ASP38	ASP38		ASP38	ASP38						ASP38			ASP38		
ALA39	ALA39		ALA39	ALA39				ALA39		ALA39					
LYS40	LYS40	LYS40													
LYS41	LYS41		LYS41					LYS41			LYS41			LYS41	
PHE42	PHE42		PHE42		PHE42			PHE42			PHE42			PHE42	
TYR 43	TYR 43		TYR 43		TYR43						TYR43			TYR43	
ALA44	ALA44	ALA44													
ILE45	ILE45		ILE45												
THR46	THR46		THR46												
THR47	THR47	THR47													
LEU48	LEU48	LEU48													
VAL49	VAL49		VAL49												
PRO50	PRO50		PRO50												
ALA51	ALA51	ALA51													
ILE52	ILE52		ILE52												
ALA53	ALA53		ALA53												
PHE54	PHE54	PHE54													
THR55	THR55	THR55													
MET56	MET56		MET56												
TYR57	TYR57		TYR57												
LEU58	LEU58	LEU58													
SER59	SER59	SER59													
MET60	MET60		MET60												
LEU61	LEU61	LEU61													
LEU62	LEU62	LEU62													
GLY63	GLY63		GLY63	GLY63	GLY63		GLY63	GLY63		GLY63	GLY63		GLY63	GLY63	
TYR64															
GLY65															
LEU66															
THR67															
MET68															
VAL69															
PRO70															
PHE71															
GLY72															
GLY73															
GLU74	GLU74		GLU74				GLU74	GLU74							
GLN75	GLN75		GLN75				GLN75	GLN75							
ASN76	ASN76		ASN76				ASN76	ASN76			ASN76				
PRO77	PRO77	PRO77													
ILE78	ILE78		ILE78	ILE78	ILE78					ILE78	ILE78		ILE78	ILE78	
TYR79	TYR79		TYR79	TYR79	TYR79					TYR79			TYR79	TYR79	
TRP80	TRP80	TRP80													
ALA81	ALA81	ALA81													
ARG82	ARG82		ARG82												
TYR83	TYR83		TYR83			TYR83			TYR83			TYR83			
ALA84	ALA84	ALA84													
ASP85	ASP85		ASP85												
TRP86	TRP86		TRP86			TRP86			TRP86			TRP86			TRP86
LEU87	LEU87	LEU87													
PHE88	PHE88	PHE88													
THR89	THR89		THR89												
THR90	THR90		THR90						THR90						
PRO91	PRO91	PRO91													
LEU92	LEU92		LEU92												
LEU93	LEU93		LEU93												
LEU94	LEU94		LEU94												
LEU95	LEU95	LEU95													
ASP96	ASP96		ASP96		ASP96									ASP96	
LEU97	LEU97		LEU97		LEU97						LEU97			LEU97	
ALA98	ALA98		ALA98		ALA98			ALA98			ALA98			ALA98	
LEU99	LEU99	LEU99													
LEU100	LEU100		LEU100					LEU100							
VAL101	VAL101		VAL101	VAL101						VAL101			VAL101		
ASP102															
ALA103															
ASP104															
GLN105															

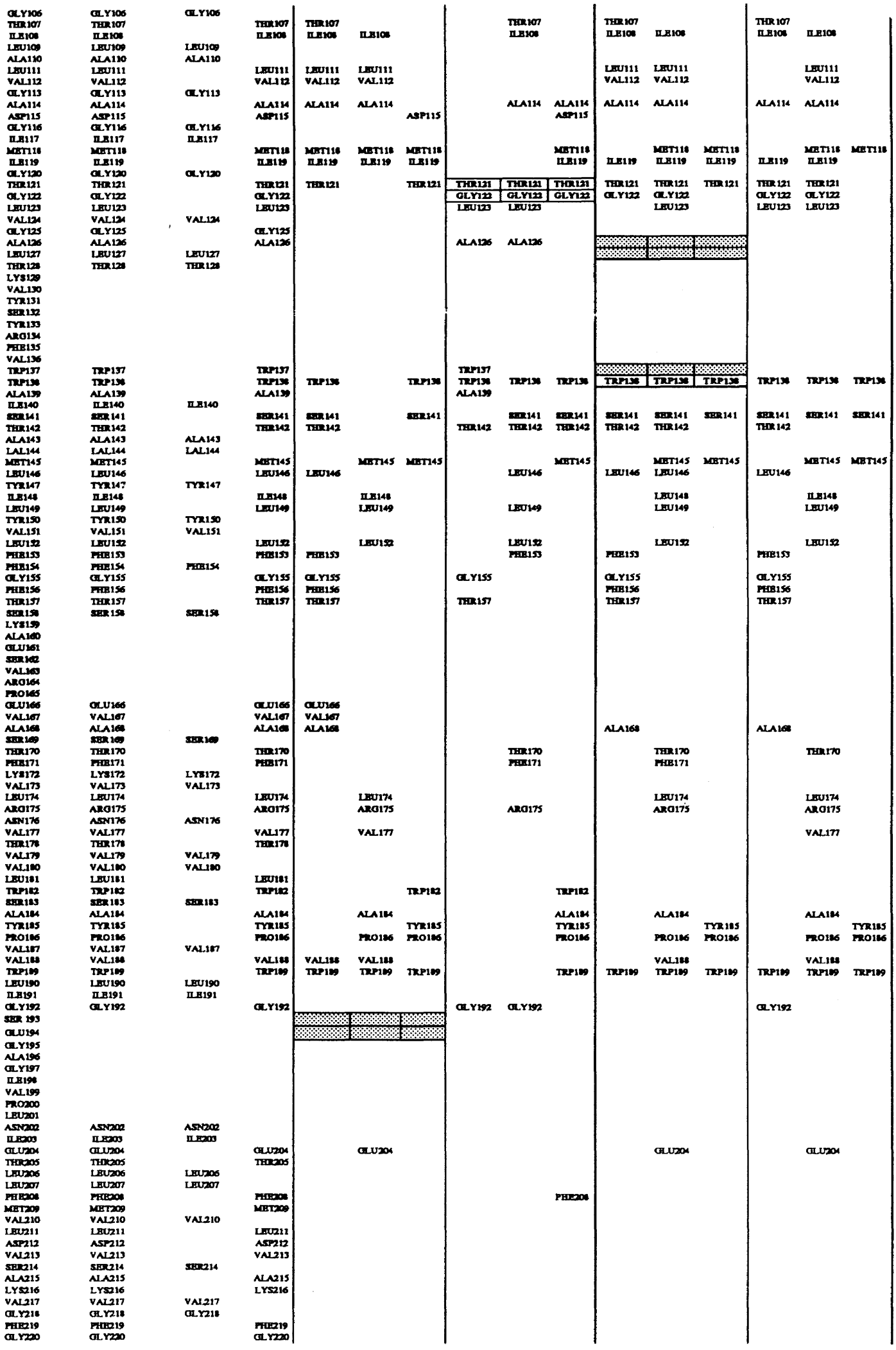
GLY106 GLY106 GLY106
THR107 THR107 THR107 THR107 THR107 THR107 THR107 THR107
ILE108 ILE108 ILE108 ILE108 ILE108 ILE108 ILE108 ILE108 ILE108 ILE108
LEU109 LEU109 LEU109
ALA110 ALA110 ALA110
LEU111 LEU111 LEU111 LEU111 LEU111 LEU111 LEU111 LEU111 LEU111
VAL112 VAL112 VAL112 VAL112 VAL112 VAL112 VAL112 VAL112 VAL112
GLY113 GLY113 GLY113
ALA114 ALA114 ALA114 ALA114 ALA114 ALA114 ALA114 ALA114 ALA114 ALA114
ASP115 ASP115 ASP115 ASP115 ASP115
GLY116 GLY116 GLY116
ILE117 ILE117 ILE117
MET118 MET118 MET118 MET118 MET118 MET118 MET118 MET118 MET118 MET118 MET118
ILE119 ILE119 ILE119 ILE119 ILE119 ILE119 ILE119 ILE119 ILE119 ILE119 ILE119
GLY120 GLY120 GLY120
THR121 THR121 THR121 THR121 THR121 THR121 THR121 THR121 THR121 THR121 THR121 THR121
GLY122 GLY122 GLY122 GLY122 GLY122 GLY122 GLY122 GLY122 GLY122 GLY122 GLY122 GLY122
LEU123 LEU123 LEU123 LEU123 LEU123 LEU123 LEU123 LEU123 LEU123 LEU123 LEU123 LEU123
VAL124 VAL124 VAL124
GLY125 GLY125 GLY125
ALA126 ALA126 ALA126 ALA126 ALA126
LEU127 LEU127 LEU127
THR128 THR128 THR128
LYS129
VAL130
TYR131
SER132
TYR133
ARG134
PHE135
VAL136
TRP137 TRP137 TRP137 TRP137
TRP138 TRP138 TRP138 TRP138 TRP138 TRP138 TRP138 TRP138 TRP138 TRP138 TRP138 TRP138 TRP138
ALA139 ALA139 ALA139 ALA139
ILE140 ILE140 ILE140
SER141 SER141 SER141 SER141 SER141 SER141 SER141 SER141 SER141 SER141 SER141 SER141 SER141
THR142 THR142 THR142 THR142 THR142 THR142 THR142 THR142 THR142 THR142
ALA143 ALA143 ALA143
LAL144 LAL144 LAL144
MET145 MET145 MET145 MET145 MET145 MET145 MET145 MET145 MET145 MET145 MET145
LEU146 LEU146 LEU146 LEU146 LEU146 LEU146 LEU146 LEU146 LEU146 LEU146
TYR147 TYR147 TYR147
ILE148 ILE148 ILE148 ILE148 ILE148
LEU149 LEU149 LEU149 LEU149 LEU149 LEU149 LEU149 LEU149
TYR150 TYR150 TYR150
VAL151 VAL151 VAL151
LEU152 LEU152 LEU152 LEU152 LEU152 LEU152 LEU152 LEU152
PHE153 PHE153 PHE153 PHE153 PHE153 PHE153 PHE153 PHE153
PHE154 PHE154 PHE154
GLY155 GLY155 GLY155 GLY155 GLY155 GLY155 GLY155 GLY155
PHE156 PHE156 PHE156 PHE156 PHE156 PHE156 PHE156 PHE156
THR157 THR157 THR157 THR157 THR157 THR157 THR157 THR157
SER158 SER158 SER158
LYS159
ALA160
GLU161
SER162
VAL163
ARG164
PRO165
GLU166 GLU166 GLU166 GLU166
VAL167 VAL167 VAL167 VAL167
ALA168 ALA168 ALA168 ALA168 ALA168 ALA168
SER169 SER169 SER169
THR170 THR170 THR170 THR170 THR170 THR170 THR170 THR170
PHE171 PHE171 PHE171 PHE171 PHE171 PHE171
LYS172 LYS172 LYS172
VAL173 VAL173 VAL173
LEU174 LEU174 LEU174 LEU174 LEU174 LEU174
ARG175 ARG175 ARG175 ARG175 ARG175 ARG175 ARG175
ASN176 ASN176 ASN176
VAL177 VAL177 VAL177 VAL177 VAL177 VAL177
THR178 THR178 THR178
VAL179 VAL179 VAL179
VAL180 VAL180 VAL180
LEU181 LEU181 LEU181
TRP182 TRP182 TRP182 TRP182 TRP182 TRP182
SER183 SER183 SER183
ALA184 ALA184 ALA184 ALA184 ALA184 ALA184 ALA184 ALA184 ALA184 ALA184
TYR185 TYR185 TYR185 TYR185 TYR185 TYR185 TYR185 TYR185 TYR185 TYR185 TYR185
PRO186 PRO186 PRO186 PRO186 PRO186 PRO186 PRO186 PRO186 PRO186 PRO186 PRO186 PRO186
VAL187 VAL187 VAL187
VAL188 VAL188 VAL188 VAL188 VAL188 VAL188 VAL188 VAL188 VAL188 VAL188
TRP189 TRP189 TRP189 TRP189 TRP189 TRP189 TRP189 TRP189 TRP189 TRP189 TRP189 TRP189 TRP189
LEU190 LEU190 LEU190
ILE191 ILE191 ILE191
GLY192 GLY192 GLY192 GLY192 GLY192 GLY192 GLY192 GLY192
SER 193
GLU194
GLY195
ALA196
GLY197
ILE198
VAL199
PRO200
LEU201
ASN202 ASN202 ASN202
ILE203 ILE203 ILE203
GLU204 GLU204 GLU204 GLU204 GLU204 GLU204 GLU204 GLU204
THR205 THR205 THR205
LEU206 LEU206 LEU206
LEU207 LEU207 LEU207
PHE208 PHE208 PHE208 PHE208 PHE208
MET209 MET209 MET209
VAL210 VAL210 VAL210
LEU211 LEU211 LEU211
ASP212 ASP212 ASP212
VAL213 VAL213 VAL213
SER214 SER214 SER214
ALA215 ALA215 ALA215
LYS216 LYS216 LYS216
VAL217 VAL217 VAL217
GLY218 GLY218 GLY218
PHE219 PHE219 PHE219
GLY220 GLY220 GLY220

LEU221	LEU221	LEU221					
ILE222	ILE222		ILE222	ILE222		ILE222	ILE222
LEU223	LEU223		LEU223	LEU223	LEU223	LEU223	LEU223
LEU224	LEU224	LEU224					
ARG225	ARG225	ARG225					
SER226	SER226		SER226		SER226		
ARG227							
ALA228							
ILE229							
PHE230							
GLY231							
GLU232							
ALA233							
GLU234							
ALA235							
PRO236							
GLU237							
PRO238							
SER239							
ALA240							
GLY241							
ASP242							
GLY243							
ALA244							
ALA245							
THR246							
SER247							

Chapter 5

Evaluation of Labeling with Radiolabeled Tetrafluoro-4-azidoretinal, A Photoactivatable Retinal Analog.

Introduction.

The objective of the experiments described in this chapter was to determine *if* and to *what extent* radiolabeled photoactivatable retinal analogs would crosslink to BR as a function of amount of irradiation. The work described in the preceding chapters sets the basis for these experiments. Formation and characterization of the analog pigments showed the 'biological activity' for the retinal analogs indicating their abilities to mimic the characteristics of the retinal based pigment. The model photolysis studies gave two viable alternatives for irradiation of the retinal analog pigments. It is shown here that the amount of light necessary to activate the model compound does not cause significant damage to the protein. The molecular modeling studies predict which sites in the protein are likely to be labeled. It is critical to show that the analogs do crosslink to the protein in a light dependent manner. These experiments are modeled after those reported in the successful experiments of Huang *et al.* (1982) and Ding *et al.* (1990). (The determination of amount of crosslinking by Boehm *et al.* (1990) was not described at length.) Critical to the described experiments is the availability of radiolabeled, photoactivatable retinal analog. This involves the synthesis from commercially available tritiated retinol (C-11 and C-12 are tritiated) or the introduction of a tritium at the C-15 position by an extra reduction/oxidation cycle using sodium borotritiide as the reducing agent [Huang *et al.*, 1982; Boehm *et al.*, 1990]. It would be more desirable to radiolabel the analog closer to the photoactivatable group to decrease the risk of the radiolabel being cleaved from the photoactivated moiety during protein manipulations, thus separating the chemically reactive end from the 'reporter', radiolabeled end of the retinal analog [Dohlman *et al.*, 1990; Ding *et al.*, 1990]. In fact, Ding *et al.* (1990) explicitly stated that the ester linkage between the photoactivatable group and the rest of the retinal was cleaved quantitatively in the CNBr cleavage step. Thus, it was critical for their experiments that the radiolabel was proximal to the ester linkage.

The methods used are based on those of Huang *et al.* (1982) and Ding *et al.* (1990). However, some modifications were made due to the presence of isomeric impurity of the radiolabeled version of TF4N3 (**10**). Purification of the all-*trans* isomer

was not undertaken because the amount of total radiolabeled TF4N3 synthesized was extremely small (~70 μg). Since this compound was isomerically impure, it was necessary to bind the non-specifically bound retinal analog with fatty acid free BSA. Thus, the isomers of TF4N3 that do not form a BR analog pigment (i.e. other than the all-*trans* isomer) were bound to BSA instead of being non-specifically bound to BR. The presence of excess BSA also gave an internal control for the ability of TF4N3 to crosslink to proteins in a photolysis dependent manner. In other words, the excess BSA bound the TF4N3 which did not form a BR analog pigment and acted as a scavenger of activated TF4N3 nitrene.

The methods used here included improvements in technique beyond those used in the successful experiments of Huang *et al.* (1982) and Ding *et al.* (1990). A competitive block with cold ATR was incorporated. Since in these samples the retinal binding site was occupied by the native ATR, the radiolabeled TF4N3 could not form a BR analog pigment and would be bound to the excess BSA in the photolysis mixture. The amount of photolysis was varied from no photolysis to ten times the amount that was necessary to completely activate the model compound for TF4N3 as described in Chapter 3 using both of the light sources. Once photolysed most of the excess BSA was removed by decanting the supernatant after centrifugation. Then, separation of the residual BSA from BR and the separation of non-crosslinked retinal analog from BR was accomplished with SDS-PAGE. Two identical gels were run simultaneously. One of the gels was cut into slices, and each slice was assayed for radioactivity. The other gel was stained with Coomassie, photographed, treated with scintillant to prepare for fluorography, exposed to X-ray film and analyzed as the fluorograph.

As described below, these methods were evaluated using reduced tritiated BR (RTBR) and non-reduced tritiated BR (Hot BR) as positive and negative controls. Reduced tritiated BR was made by the regeneration of BR with tritiated ATR (~10 mCi/mmol) and reduction of the Schiff base using the methods of Bayley *et al.* (1981) and Peters *et al.* (1976). Analysis of the non-reduced form showed that the SDS-PAGE completely cleaved the Schiff base and separated the retinal from BR. Analysis with

RTBR as aliquots from different time points in the reduction reaction showed the techniques utility in detecting small amounts of radiolabel associated with BR.

It should be emphasized that these experiments were limited by the total amount, the limited purity, and the relatively low specific activity (~10 mCi/mmol) of the radiolabeled TF4N3 retinal analog. However, the studies of Huang *et al.* (1982) and Ding *et al.* (1990) indicated the possibility of successful determination of percent labeling with a single time course of photolysis experiment. Huang *et al.* (1982) and Ding *et al.* (1990) showed a time of photolysis dependent increase in radioactivity associated with BR with a single time course of photolysis study.

Unfortunately, VBN-II (**6**) could not be used in similar studies since it was not available in radiolabeled form. As described in the next chapter, attempts to determine sites of labeling without radiolabeled analogs have been unsuccessful.

Materials and Methods.

A comparison of the methods described here with those of the three reported successful photoaffinity labeling experiments of BR is shown in fig. 5.5. The two major differences are in the specific activities of the retinal analogs and the presence of 1% BSA in the photolysed sample in the studies presented here. The specific activity of Khorana **2** was 10 fold higher than that used here. The specific activity of Nakanishi1 **3** was similar to TF4N3 **11** (~10 mCi/mmol). Its low specific activity was a major reason for the synthesis of Nakanishi2 **4** at 4800 mCi/mmol, some 480 times higher than their previous report of photoaffinity labeling of BR. The use of BSA to bind non-specifically bound isomers of TF4N3 was necessary as described above. However, leaving the BSA in the photolysis mixture is more controversial. The BSA did serve as a control for the ability of photoactivated radiolabeled TF4N3 to bind to proteins in general. A similar argument is that BSA would scavenge the photoactivated intermediates of radiolabeled TF4N3 that were not in the retinal binding site. The use of scavengers for photoactivated intermediates was suggested by Bayley (1983). The main argument for removing the BSA by decanting the supernatant after centrifugation *before* photolysis is that the large amount of BSA may shield the photoactivatable group of TF4N3 from the activating photons. Although possible, this shielding would likely be overcome by the large amount of total photolysis described in the experiments below. The best method for overcoming the potential troubles caused by the BSA is synthesis of isomerically pure photoactivatable retinal analogs thus obviating the use of BSA altogether. The very difficult synthesis of this retinal analog, which was made even more difficult by the addition of the two steps necessary for radiolabeling, made the preparation of isomerically pure radiolabeled TF4N3 extremely difficult. Partial removal of the BSA by centrifugation before photolysis is a reasonable alternative. However, the very limited amount of radiolabeled TF4N3 limited the analysis to the experiments presented below.

Materials. The following materials and suppliers were used in the experiments described in this chapter. Tritiated TF4N3 retinal analog was prepared by Bernice Katz

at a specific activity of ~10 mCi/mmol. The extinction coefficient was estimated at 50 000 using that of phenylretinal [Bayley *et al.*, 1981]. Bleached BR with 280/570 ratio ≤ 3 when regenerated with ATR was used to form the analog pigments. ATR (Sigma) freshly dissolved in ethanol and its concentration checked was used to bind to the retinal binding site in the blocking experiments. Tritiated ATR (~10 mCi/mmol) was used in the negative and positive control samples. The sample cell discussed in Chapter 3 with a 1 mm path length was used for the photolysis. The two light sources (Flash Apparatus or RPR-100) were used to irradiate the samples. One percent fatty acid free BSA (Sigma) in water was used to non-specifically bind excess retinal and retinal analogs . The scintillation cocktail used was Aquasol-2 (DuPont) and the counts determined in a scintillation counter (Beckman 100SC). SDS-PAGE was performed using a Bio-Rad mini-gel apparatus and 12.5% precast minigels (BioRad) according to the manufacturer's suggestions. Gel slices were solubilized with Solvable (DuPont). KCl (1 M, Sigma) was used to visualize the protein bands on the gel that was sliced and counted [Bergman and Jornvall, 1987]. Before fluorography the gels were treated with En^{3}Hance (DuPont). The treated gels were exposed to X-ray film (X-Omat, Kodak) or Hyperfilm (Amersham).

Methods. Pigment Formation. An analog pigment was formed as described in Chapter 2 with tritiated TF4N3 retinal. Additional tritiated TF4N3 was added until there was spectral evidence for an excess of TF4N3 over BR. This excess was shown by an increase in the absorbance due to the retinal analog free in solution (~390 nm) with no further increase in the absorbance from the analog pigment (~520 nm). An equivalent amount of 'blocked' pigment was formed by a treatment with a 2 fold excess of non-radiolabeled ATR (by absorbance over the previously determined amount of ATR necessary to regenerate BR from this amount of bleached BR) before addition of the radiolabeled TF4N3 retinal. These pigments were allowed to incubate at 4 C for 1 hour. Then, the samples were diluted with 1% BSA (10 mg/ml) to 4 ml. The final [BR] was 0.1 mg/ml, ~4 μM. The pigment/BSA mixture was then placed in the cooled sample

cell.

Photolysis. Three separate experiments were performed. The first sample was photolysed from 0-30 min in the RPR at 350 nm at 4 C. A second sample was photolysed from 0-240 min in the RPR at 350 nm at 4 C. A third sample was photolysed using the flash apparatus from 0-100 flashes at 10 kV at 4 C. One ml aliquots were removed at appropriate intervals. The irradiation was repeated with the 'blocked' pigment (that had been pretreated with excess ATR) for the first and third samples. Due to a lack of tritiated TF4N3, this control was not performed for the longer irradiation at 350 nm. The samples were then centrifuged (20 000g, 30 min) to pellet the pigment (most of the BSA remains in the supernatant). The supernatant was decanted to a scintillation vial and counted in 10 mL of Aquasol-2. Some BSA, as will be evident below, remained with the BR pellet thus allowing evaluation, by SDS-PAGE, of any radiolabel covalently linked to the BSA concurrently with the analysis of BR.

SDS-PAGE. The pellets were resuspended in standard SDS-PAGE sample buffer. They were sonicated for 15 minutes in an ultrasonic water bath and then heated to 70 C for 2 minutes. Sonication and heat are necessary to solubilize the BR in the sample buffer. The complete solubilization allows the BR to run as a monomer by SDS-PAGE. It was necessary to have BR run as a single band to optimize the chances for detecting small amounts of radioactivity associated with BR. If the BR was not sonicated and heated, it ran as monomers, dimers and trimers thus spreading any potential counts associated with BR over three separate bands. It also should be noted that Huang *et al.* (1982) heated their BR samples to 100 C in one of their assays of crosslinking. The samples were then loaded (~10 μg on each lane, ~2000 cpm) on two identical minigels. The same amount of sample that was loaded was added directly to a scintillation vial. Aquasol-2 (10 mL) was added and the samples counted in the liquid scintillation counter. This value was taken as the total amount loaded on each gel and used as the denominator in calculation of percent radiolabel remaining associated with BR. The gels were run at 200 V for ~40 min. In two cases the dye front was not run off of the bottom of the gel and the high counts associated with the dye front (fig. 5.1b and fig.

5.2b) indicate that the highly lipophilic retinals run with the SDS at the dye front. This should not be taken as a labeling of the lipids from the BR samples as one would not expect SDS-PAGE to separate retinals alone from photoactivated retinals covalently linked to lipids. Also, these high counts in the dye front were also seen in the negative and positive controls which did not contain photoactivatable compounds. One of the twin gels was fixed, stained in Coomassie and destained. The other gel was stained with 1 M KCl [Bergman and Jornvall, 1987] to visualize the protein bands. As experience was gained fewer and fewer slices were necessary for successful isolation of the BSA and BR containing gel pieces. The gel was sliced by lane and by band, and the pieces were removed to vials. The proteins were solubilized from the gel slices using Solvable according to manufacturer's directions by addition of 500 µl of Solvable to the gel slices and heating to 50 C for three hours. To these solubilized slices, Aquasol-2 (10 mL) was added and the samples were counted in the scintillation counter. The stained gel was treated with En^{3}Hance (a scintillant, according to the manufacturer's suggestions) and exposed to X-ray film (X-Omat or Hyperfilm) for 1 week at 193 K. The impregnation of the gel with scintillant increases the efficiency of conversion of the decay of the tritium to exposure of the X-ray film. The counts were analyzed for an irradiation dependent increase in counts associated with the BR band [Ding *et al.*, 1990; Huang *et al.*, 1982]. The X-ray film was developed and analyzed similarly.

Later, non-radiolabeled TF4N3 retinal was analyzed similarly to the model studies of TF4ABA in organic solvents. The retinal analog was dissolved in cyclohexane or dioxane and photolysed in the RPR at 350 nm. Aliquots were taken at different time points and analyzed by GC-MS as described for the retinals in Chapter 2 or by FAB-MS by Kelly Thornburg or by direct probe electron impact ionization with the help of Ken Patrick. The spectra were analyzed for a photolysis dependent change in mass, especially for the addition of the organic solvent to the photoactivated intermediate. The masses of interest were 351 m/z (TF4N3, azide), 323 (TF4N3, nitrene), 325 (TF4N3, amine, NH_2) or 323+mass of solvent (TF4N3 nitrene + solvent).

Results and Discussion.

Positive Control (fig. 5.1). These methods were evaluated using positive and negative control samples made from bleached BR that was regenerated with tritiated ATR. The negative control sample was, simply, this regenerated pigment in which the retinal was bonded through the normal protonated Schiff base to Lys216. The positive control sample was this tritiated BR that had had the Schiff base reduced to form a non-hydrolyzable bond [Bayley *et al.*, 1981] and was subsequently referred to as RTBR. This linkage is stable to all of the protein manipulations subsequently used. The results of the positive control SDS-PAGE and slicing and counting are shown in fig. 5.1. The percent reduction of the Schiff base at the 90 min timepoint was estimated at 12% (see fig. 5.1 lane 8, fig. 5.2 lane 10). These studies also showed that the normal Schiff base was completely cleaved under these conditions and that the tritiated retinal was separated from the BR (see Lane 1, fig. 5.3). It is interesting to note that sodium borohydride treatment of BR cleaves the protein into two pieces, one of which contains Lys216 and hence the radiolabeled retinal attached by the reduced Schiff base [Ding *et al.*, 1990]. This cleavage accounted for the two small bands found on gels below the BR band in the RTBR lanes and for the additional faint spot in the fluorographs corresponding to the smaller band. The 90 min RTBR was used in subsequent gels as a positive control and was labeled RTBR. Since the amount of radiolabel associated with BR was easily detected even after only 5 minutes of reduction and since the specific activity of the ATR used in these control studies is similar to that of the TF4N3 used in the photolysis studies, the limit of detection was estimated at <5%. This detection limit should be sufficient to detect labeling in studies of photoaffinity labeling of BR. Using similar techniques, Huang *et al.* (1982) reported 20% labeling; Ding *et al.* (1990) estimated 25-30% labeling; Boehm *et al.* (1990) reported 15%.

The tritiated TF4N3 was made by Dr. Bernice Katz at a specific activity of ~10 mCi/mmol. Because this compound was isomerically impure, it was important to bind the isomers of TF4N3 that would only non-specifically associate with BR (i.e. any isomer that is not all-*trans*) with BSA and control for non-specific labeling by including

blocking the retinal binding site with non-radiolabeled ATR in one set of samples. It was hoped that a time of photolysis dependent increase in the amount of radioactivity associated with BR would be observed [Huang *et al.*, 1982; Ding *et al.*, 1990]. Both light sources were used in attempts to photoactivate the tritiated TF4N3 bound to BR.

Flash Photolysis (fig. 5.2). The results of the flash photolysis are shown in fig 5.2. This figure shows the Coomassie stained SDS-PAGE gel of the separation of the residual BSA from BR and the radioactivity counts associated with the different samples and bands (fig. 5.2b). The blocking with ATR procedure was efficient as shown by the fact that the radioactivity associated with the BR pellet was much lower in the blocked samples than in the non-blocked samples (335±49 cpm vs. 1609±160 cpm, respectively). The percent of radioactivity associated with BR in the blocked samples was not calculated because the total counts loaded were so low. The positive control shows the detection of the radioactivity associated with BR in lane 10. Lanes 2-5 show a slight increase in percent radioactivity associated with BR with increasing number of flashes. This change was from 0.7% to 1.7% - a possible labeling of only 1%. Lane 5 and Lane 9 show multiple bands due to protein damage from the high number of flashes (100 flashes). This protein degradation was not surprising considering the high amount of UV light emitted by the flash lamp. It should be emphasized that the sample was kept at 4 C throughout the photolysis which suggests that this protein degradation was likely light induced rather than heat induced.

Photolysis at 350 nm (figs. 5.3 and 5.4). The results of the 350 nm photolysis are shown in fig 5.3 (0-30 min) and fig. 5.4 (0-240 min). These figures show the Coomassie stained SDS-PAGE gel of the separation of the residual BSA from BR and the radioactivity counts associated with the different samples and bands (figs. 5.3b, 5.4b). The blocking with ATR procedure was efficient as shown at the shorter irradiation times shown in fig. 5.3 by the fact that the radioactivity associated with the BR pellet was much lower in the blocked samples than in the non-blocked samples (352±27 cpm vs. 1591±179 cpm, respectively). The percent of radioactivity associated with BR in the blocked samples was not calculated because the total counts loaded were

so low. The positive control with RTBR is shown in lane 1 of fig. 5.4 with 9.8% of the loaded radioactivity associated with BR. The amount of radioactivity associated with BR in the non-blocked photolysed samples ranges from 0% to 1.3%. This indicates that very little if any TF4N3 crosslinked to BR even after this extended photolysis.

These studies indicate that little or no significant labeling of BR occurred with radiolabeled TF4N3 under the conditions described when the estimate of limit of detection of a significant increase over time of photolysis was set at <5%. This limit of detection is relatively high due to the relatively low specific activity of the radiolabeled TF4N3. The results presented were corroborated by fluorography performed on identical gels. The fluorographs showed only the bands from the positive control lanes and no other bands. It should be emphasized that despite the low specific activity, these experiments would have shown labeling of the protein if the efficiency of labeling had been similar to previously published reports of photoaffinity labeling of BR. Using similar techniques, Huang *et al.* (1982) reported 20% labeling; Ding *et al.* (1990) estimated 25-30% labeling; Boehm *et al.* (1990) reported 15%. Both light sources were used and at a wide range of total photolysis to maximize chances of success. Significant protein damage occurred only after more than 50 flashes (5X that required to completely activate the model compound, fig. 5.2, lane 5+9).

There are several possible reasons for this lack of success in labeling BR with this photoactivatable retinal analog.

The excess BSA in the photolysis samples shielded the TF4N3 from the necessary photons for activation of the azide to the nitrene. As discussed above in the methods section, the use of BSA was necessary to bind the isomeric impurities in the radiolabeled TF4N3. Photolysing the samples before centrifugation to remove most of the BSA may have allowed the high concentration of BSA to absorb much of the light during photolysis. However, the extended photolysis times and the short path length in the sample cell (1 mm) should overcome these possible shielding effects. The best solution to this possible difficulty with BSA would be synthesis of pure radiolabeled all-

trans TF4N3. The other reasonable alternative of removing most of the BSA by centrifugation *before* photolysis was not performed due to the lack of radiolabeled TF4N3.

The nitrene resulting from the photolysis of TF4N3 was not sufficiently reactive to efficiently bind to BR. This possibility depends on the differences in reactivity between the nitrene resulting from photolysis of the model compound TF4ABA and that of the full retinal (TF4N3). As described in Chapter 3, the TF4ABA, the benzaldehyde, efficiently crosslinked to the inert organic solvent cyclohexane in a photolysis dependent manner. Recently, similar model photolysis studies with TF4N3 in cyclohexane and dioxane have been performed to investigate the possible lack of reactivity of the nitrene derived from photolysis of TF4N3. These studies have shown only the amine (NH_2, mass 325) in the photolysed samples. These results indicate that, unlike the benzaldehyde, the full retinal analog does not, when photolysed, react with the solvent through C-H insertion. The formation of the amine is likely due to the triplet derived abstraction of hydrogens from the solvent. This reaction requires much less reactivity and is one of the products of reaction of many of the highly fluorinated aryl azides that have been synthesized as potential photoactivatable groups [Leyva *et al.*, 1986a,b, 1989; Keana *et al.*, 1988, 1990; Cai *et al.*, 1992, Soundarajan *et al.*, 1990]. In fact the high yield of the C-H insertion derived product with the benzaldehyde (TF4ABA) was remarkable. This success with TF4ABA indicating the reactivity of polyfluorinated aryl azides encouraged the many attempts to synthesize the full retinal analog containing this photoactivatable group.

There is some theoretical and experimental evidence that suggests that the chemistry of the para position of the ring of the benzaldehyde may be considerably different from that of the retinal analog in which the aldehyde is separated from the aromatic ring by an extended conjugated double bond system. Assuming that the groups closest to the ring have the most effect, it should be noted that the aldehyde and the conjugated system have different electron affinities. The aldehyde is more electron withdrawing than the conjugated double bond system [Hansch *et al.*, 1973]. The difference in chemistries of

the para position of the ring of pentafluorobenzaldehyde and of pentafluororetinal was demonstrated by the relative ease of substitution of the para fluorine with sodium azide. The substitution reaction at the benzaldehyde level is quantitative (see appendix 1) and was successfully completed by even the most inexperienced organic chemist. The para fluorine could not be substituted with azide after the retinal sidechain had been added [Bernice Katz, personal communication]. Fujjii *et al.* (1989) had difficulty substituting the para fluorine of pentafluorotoluene, but no trouble with the benzaldehyde. This difference in chemistries would also affect the reactivity of the resulting nitrene. The photolysis conditions were certainly adequate to activate the model benzaldehyde to a highly reactive nitrene, but may not have activated the full retinal analog to a highly reactive intermediate. It should be noted that the reports suggesting the use of polyfluorinated aryl azides as photoactivatable groups have studied highly fluorinated aryl azides that have electron withdrawing groups para to the azide [Leyva *et al.*, 1986a,b, 1989; Keana *et al.*, 1988, 1990; Cai *et al.*, 1992, Soundarajan *et al.*, 1990].

It has also been suggested that the extended conjugation of the retinal sidechain influences the reactivity of the nitrene [MS Platz, personal communication]. The nitrene in TF4N3 is in conjugation with the extended π system of electrons formed by the ring and the sidechain. This conjugation allows delocalization of the electrons of the nitrene. This delocalization is further supported by the resonance structures that can be drawn for the nitrene in which the electrons can be moved throughout the conjugation. Thus, the nitrene from the full retinal analog, in comparison to that of the benzaldehyde, may be considerably less reactive. This difference in reactivities is supported by the formation of the C-H insertion product upon photolysis of the benzaldehyde in cyclohexane and the formation of the amine on photolysis of the full retinal analog in cyclohexane. It should be noted that the photoactivated intermediates of the successful photoaffinity labeling experiments of BR using Khorana **2**, Nakanishi1 **3**, and Nakanishi2 **4** were highly reactive carbenes (instead of the less reactive nitrenes) that were NOT in conjugation with the double bond system of the retinal sidechain.

If these differences are the reason for lack of labeling, the problem is inherent in the

structure of the retinal analog. To overcome this possibility, other photoactivatable retinal analogs must be developed.

TF4N3 is not bound in the native retinal binding site. The BR analog pigment formed with TF4N3 showed a reasonable opsin shift and partial functioning which strongly supports its placement in the native retinal binding pocket. This pocket has the ring end of retinal buried in the TMH. However, the aromatic analog, Khorana (**10**) labeled Ser193 and Glu194 which are modeled to be extramembranous. Thus it is possible that, despite the opsin shift, and the partial functioning of the TF4N3 BR analog pigment, the ring end of TF4N3 actually labeled the water or lipids surrounding BR in the purple membrane. Again, this possibility is inherent to the structure of the retinal analog. The solution is design and synthesis of superior retinal analogs.

The analog itself was unstable to the aqueous environment used for pigment formation and never made it into the protein intact. With the general difficulty in characterizing this retinal analog, it would be extremely difficult to perform experiments to test this possibility. Again, the solution is different retinal analogs.

The crosslink formed was unstable to the analysis conditions. This is an unfortunate possibility since the conditions of this assay for crosslinking are very mild in comparison to those used in the further work-up of the protein for analysis of sites of labeling.

The radiolabel was cleaved from the photoactivatable group. Again this possibility is unfortunate considering the relatively mild conditions of the crosslinking assay. It is well known that retinal is a labile compound [Bownds, 1967] and that labeling experiments have been ruined by such cleaving of the reporter radiolabel [Dohlman *et al.*, 1988]. The solution to this problem is the incorporation of the radiolabel into the retinal analog on an atom close to the carbene or nitrene [Ding *et al.*, 1990].

In summary, the formation of these crosslinks (labeling) is the point of these experiments. This lack of labeling makes the kinetic spectroscopy studies of the irradiated and non-irradiated form of the TF4N3 analog pigment simple to interpret,

since no difference was noted. In the final chapter, several suggestions are made to improve the likelihood of success of these experiments. These suggestions do not involve modification of the methods of assaying for crosslinking or of the photolysis conditions. These suggestions are for the synthesis of new retinal analogs that incorporate necessary design improvements as mentioned above.

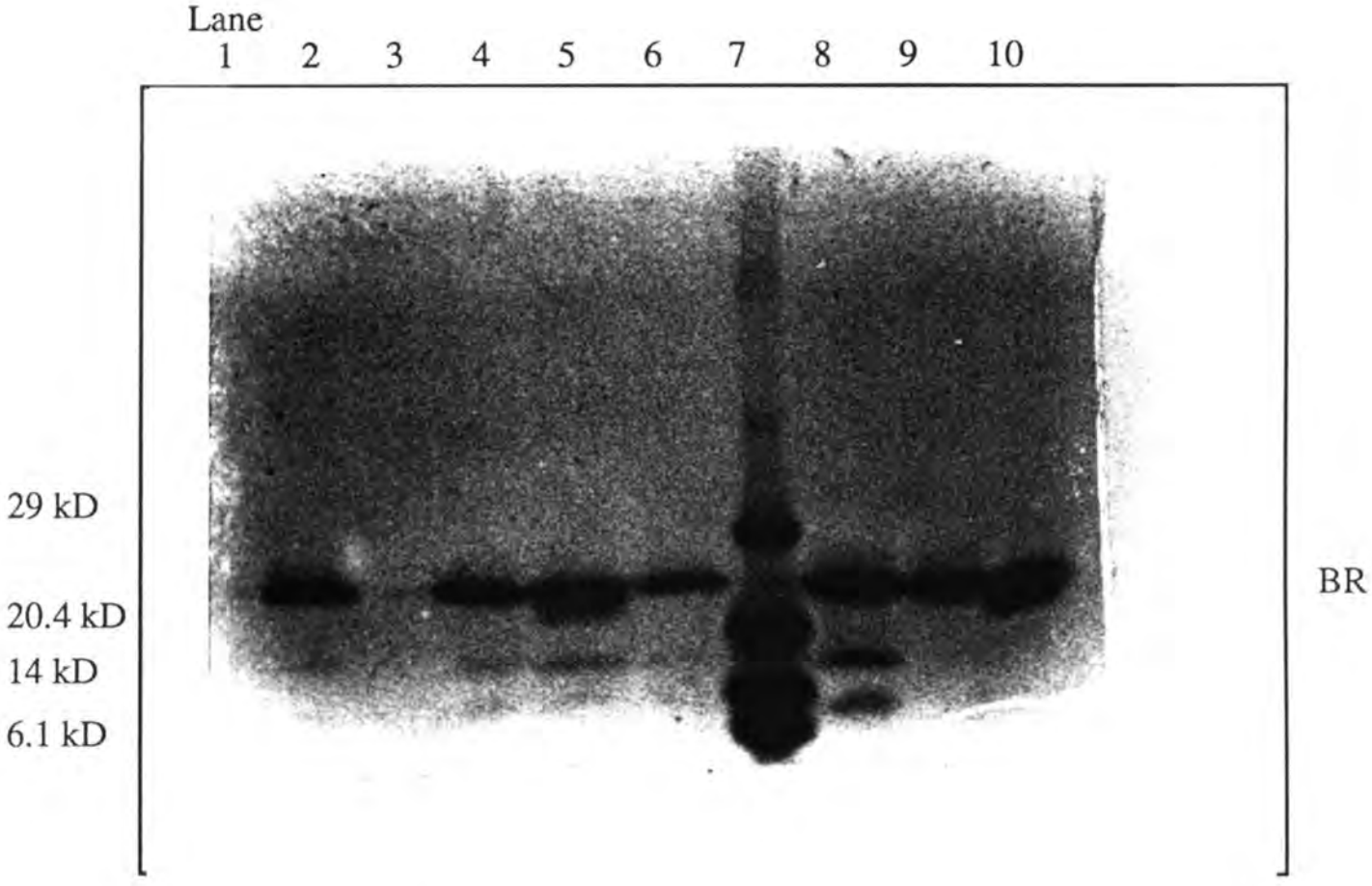

	Sample	cpm BR/cpm loaded (%)	
Lane 1	Blank	-----	
Lane 2	RTBR at 5 min	7.2	(67/927)
Lane 3	Blank	-----	
Lane 4	RTBR at 15 min	8.7	(78/900)
Lane 5	Cold Reduced BR	-----	
Lane 6	RTBR at 30 min	13.5	(77/571)
Lane 7	MW standards	-----	
Lane 8	RTBR at 90 min	11.5	(240/2080)
Lane 9	RTBR at 0 min	0.2	(2/1046)
Lane 10	Cold PM	-----	

Figure 5.1 SDS-PAGE of Reduced Tritiated BR
Top panel: Photograph of coomassie stained gel. Each lane was loaded with ~10 μg of the sample indicated in the key. The gel was run, sliced and counted as described in materials and methods.
Bottom panel: The results are expressed as (%) radioactivity associated with BR/ Total radioactivity loaded in that lane with the cpm values (with background subtracted) in parantheses.

	Lane 1	Lane 2	Lane 3	Lane 4	Lane 5	Lane 6	Lane 7	Lane 8	Lane 9	Lane 10
Sample	BR	3H BR	3H BR	MW	3H BR	BR	3H BR	Blank	3H BR	Blank
Reduction		0 min	90 min		30 min	90 min	15 min		5 min	
Loaded	25	1071	2105	25	596	26	925	24	952	
Gel slice 1	29	28	29	26	33	27	31	25	32	
Gel Slice 2	28	28	29	23	28	26	25	27	27	
BSA	27	31	33	28	28	29	32	26	25	
BSA	28	27	31	32	24	26	28	28	23	
Gel slice 5	30	26	33	26	25	22	28	26	29	
Gel slice 6	27	29	29	26	29	25	27	28	25	
BR	25	28	44	43	63	24	40	40	30	
BR	26	26	130	33	43	29	58	31	62	
BR	28	27	145	29	50	30	59	33	54	
Dye Front	29	214	236	71	80	30	110	71	167	

Background Loaded = 25
Background BR = 78
BR-Background/Loaded-Background
2/1046 240/2080 77/571 78/900 67/927

Figure 5.1b Raw cpm Data from SDS-PAGE of Reduced Tritiated BR
Gel was sliced, solubilized, added to scintillation cocktail and counted.

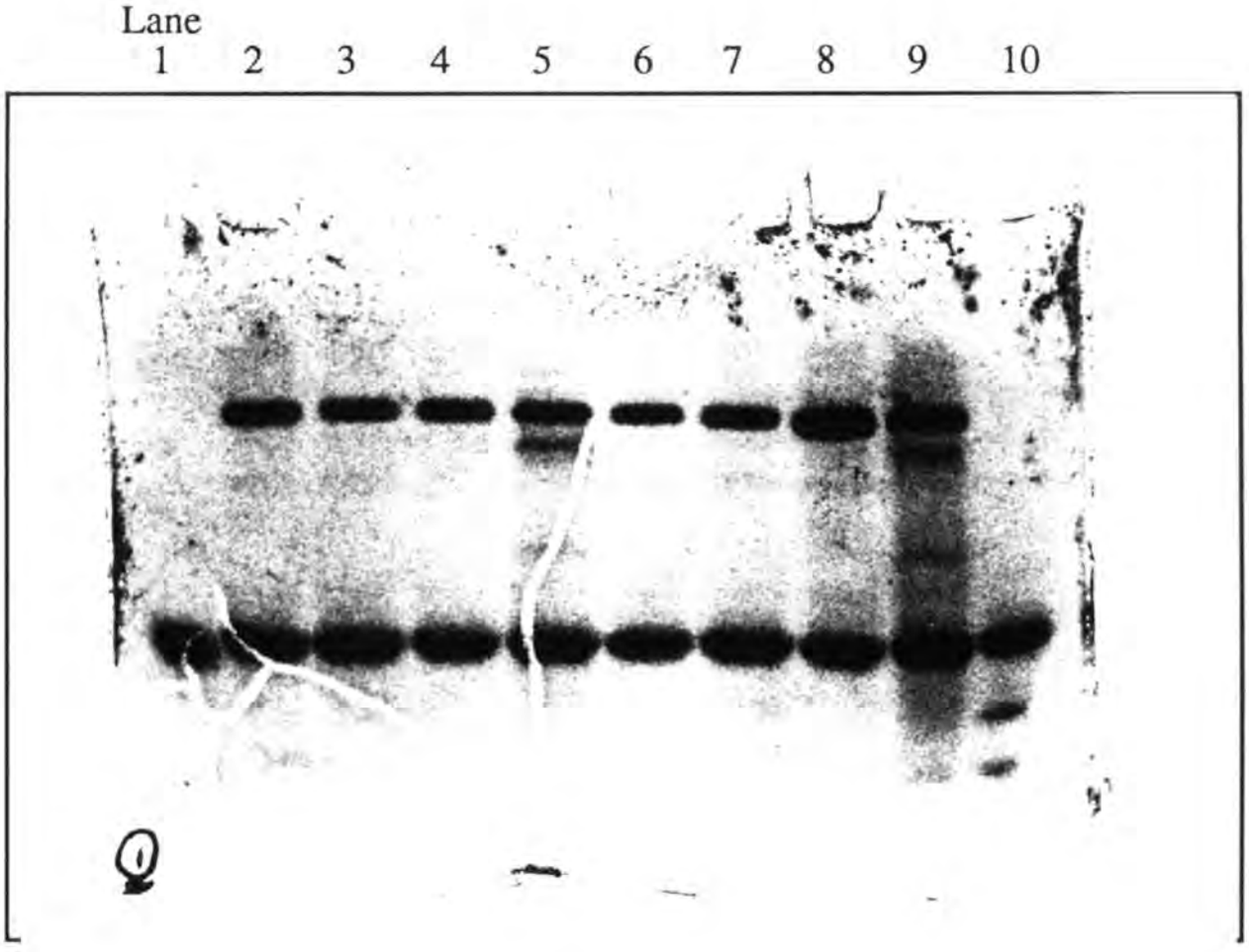

	Sample	cpm BR/cpm loaded (%)	
Lane 1	Cold BR	-----	
Lane 2	0 Flash	0.7	(12/1721)
Lane 3	1 Flash	1.1	(16/1492)
Lane 4	10 Flash	1.2	(18/1418)
Lane 5	100 Flash	1.7	(29/1723)
Lane 6	0 Flash - Blocked	-----	(8/254)
Lane 7	1 Flash - Blocked	-----	(7/306)
Lane 8	10 Flash - Blocked	-----	(5/298)
Lane 9	100 Flash - Blocked	-----	(12/373)
Lane 10	RTBR at 90 min	14.2	(103/725)

Figure 5.2 SDS-PAGE of Flash Photolysis with Radiolabeled TF4N3
Top panel: Photograph of coomassie stained gel. Each lane was loaded with ~10 μg of the sample indicated in the key. The gel was run, sliced and counted as described in materials and methods.
Bottom panel: The results are expressed as (%) radioactivity associated with BR/ Total radioactivity loaded in that lane with the cpm values (with background subtracted) in parantheses.

	Lane 1	Lane 2	Lane 3	Lane 4	Lane 5	Lane 6	Lane 7	Lane 8	Lane 9	Lane 10
Pretreatment	None	None	None	None	None	Excess ATR	Excess ATR	Excess ATR	Excess ATR	None
Sample	BR	0 Flashes	1 Flash	10 Flashes	100 Flashes	0 Flashes	1 Flash	10 Flashes	100 Flashes	RTBR
Loaded	27	1748	1492	1445	1750	281	333	325	400	752
Comb	43	41	42	34	31	30	33	27	33	28
BSA	28	53	60	50	46	37	36	28	34	27
BSA	30	36	37	42	39	29	23	24	33	29
BR	26	33	35	31	34	24	28	26	27	32
BR	25	30	32	38	46	35	30	30	36	122
Dye Front	28	310	416	396	358	110	79	85	106	115
Supernatant		5896	6147	6214	6051	15520	15726	15233	14418	

Background Loaded = 27
Background BR = 51
BR-Background/Loaded-Background

12/1721	16/1492	18/1418	29/1723	8/254	7/306	5/298	12/373	103/725

Figure 5.2b Raw cpm Data from SDS-PAGE of Flash Photolysis
Gel was sliced, solubilized, added to scintillation cocktail and counted.

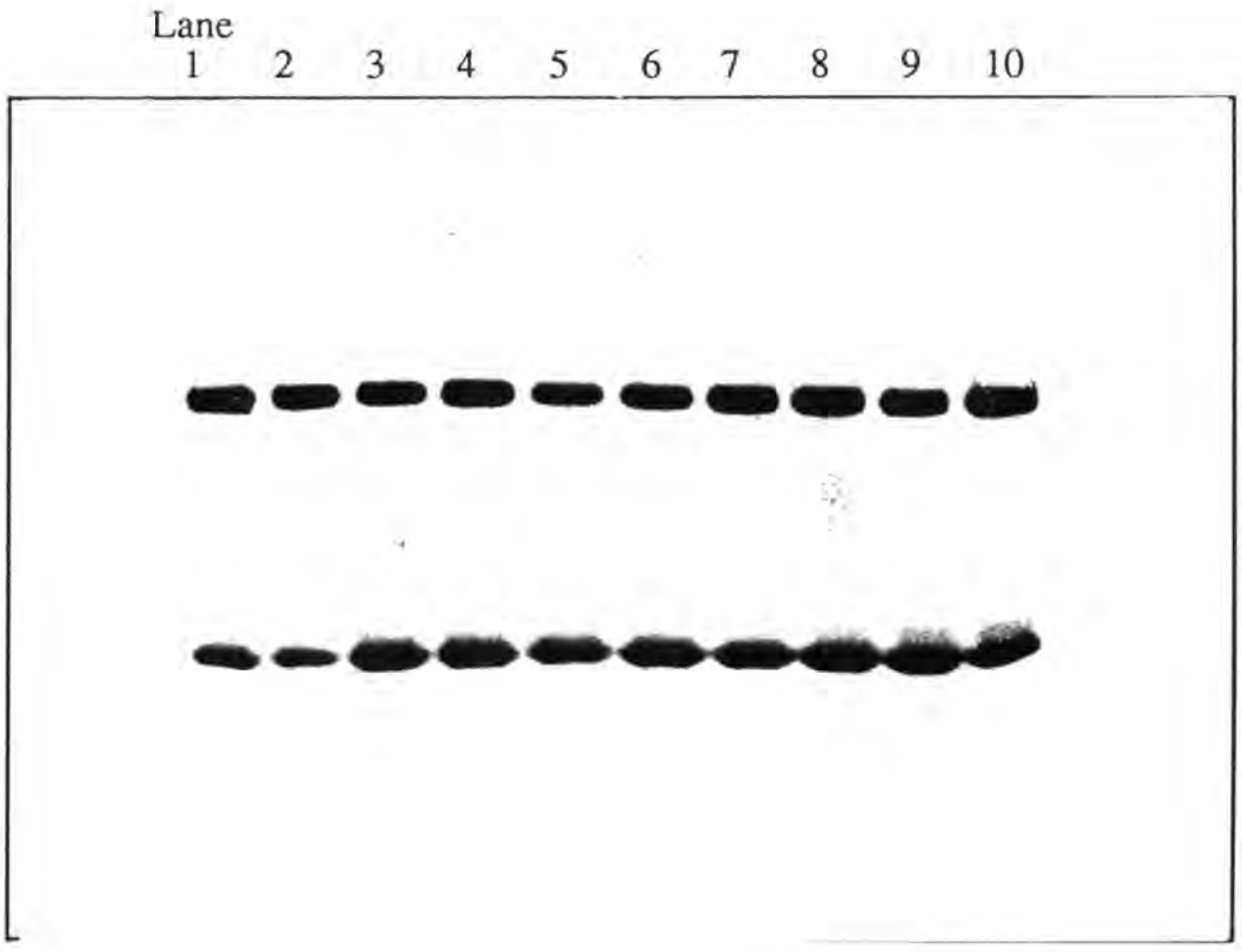

	Sample	cpm BR/cpm loaded (%)	
Lane 1	Tritiated BR	0.8	(7/853)
Lane 2	BR	-----	
Lane 3	0 min RPR - Blocked	-----	(12/295)
Lane 4	10 min RPR - Blocked	-----	(13/350)
Lane 5	30 min RPR - Blocked	-----	(8/324)
Lane 6	0 min RPR	0.6	(10/1516)
Lane 7	2 min RPR	0.5	(8/1527)
Lane 8	5 min RPR	0.0	(0/1816)
Lane 9	10 min RPR	0.5	(9/1714)
Lane 10	30 min RPR	0.8	(11/1390)

Figure 5.3 SDS-PAGE of 350 nm Photolysis with Radiolabeled TF4N3
Top panel: Photograph of coomassie stained gel. Each lane was loaded with ~10 μg of the sample indicated in the key. The gel was run, sliced and counted as described in materials and methods.
Bottom panel: The results are expressed as (%) radioactivity associated with BR/ Total radioactivity loaded in that lane with the cpm values (with background subtracted) in parantheses.

	Lane 1	Lane 2	Lane 3	Lane 4	Lane 5	Lane 6	Lane 7	Lane 8	Lane 9	Lane 10
Pretreatment	None	None	Excess ATR	Excess ATR	Excess ATR	None	None	None	None	None
Sample	Hot BR	BR	0 min	10 min	30 min	0 min	2 min	5 min	10 min	30 min
Loaded	882	29	324	379	353	1545	1556	1845	1743	1419
Gel slice 1	26	27	21	81	90	33	104	29	29	34
BSA	26	24	20	26	32	29	29	33	46	33
BSA	28	31	29	48	33	22	29	23	34	21
Gel slice 4	25	21	21	64	31	26	23	29	25	25
Gel slice 5	37	34	22	39	82	29	20	26	52	23
Gel slice 6	34	25	23	33	39	24	23	29	29	39
BR	24	39	25	36	27	30	31	24	36	28
BR	33	28	37	27	31	30	27	26	23	33
Gel Bottom	24	27	32	22	50	68	26	32	36	35
Supernatant	2424	26	11750	11589	12198	5142	5346	3426	4140	5161
Background Loaded = 29										
Background BR = 67										
BR-Background/Loaded-Background										
	7/853		12/295	13/350	8/324	10/1516	8/1527	0/1816	9/1714	11/1390

Figure 5.3b Raw cpm Data from SDS-PAGE of 350 nm Photolysis
Gel was sliced, solubilized, added to scintillation cocktail and counted.

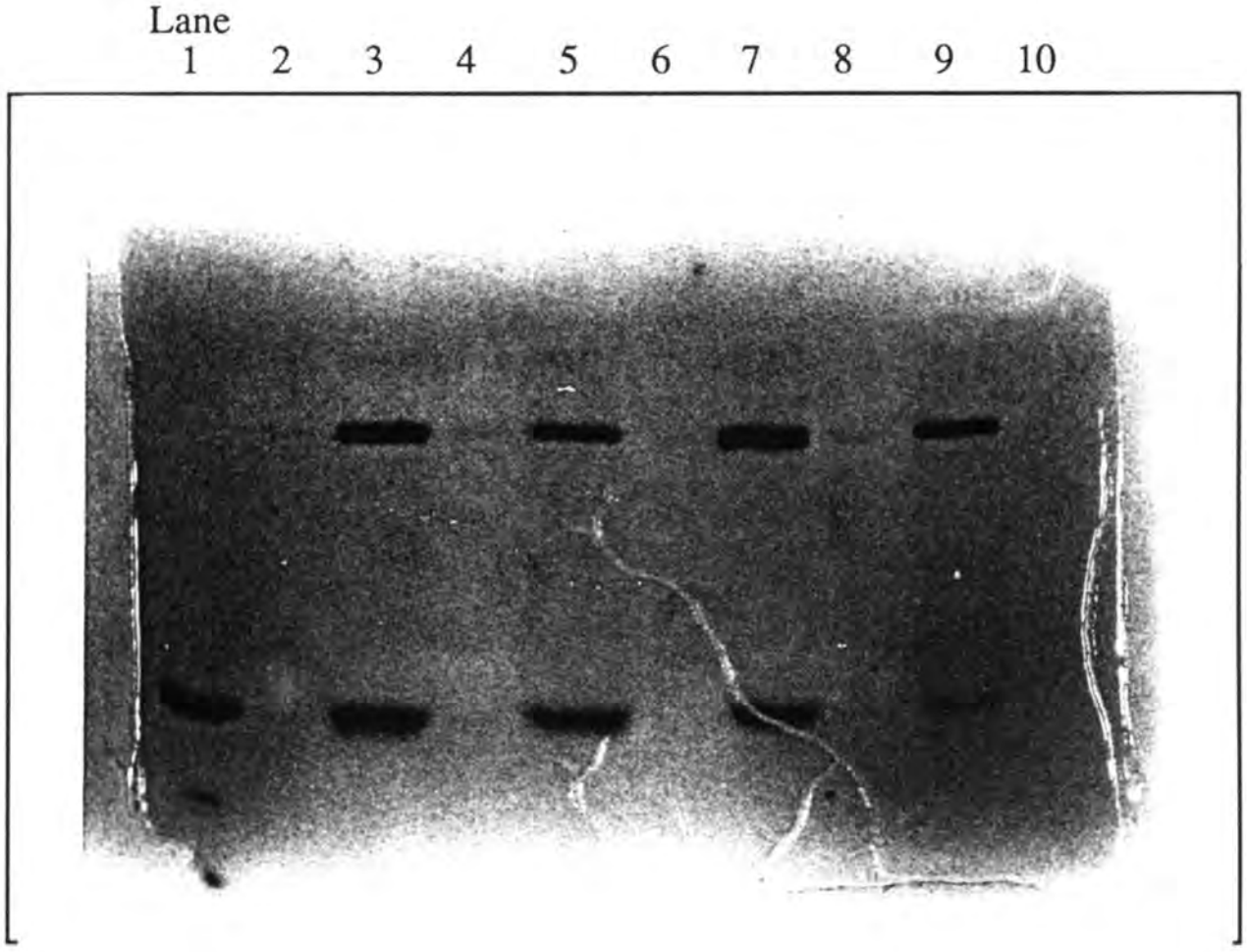

	Sample	cpm BR/cpm loaded (%)	
Lane 1	RTBR at 90 min	9.8	(147/1494)
Lane 2	Blank	-----	
Lane 3	0 min RPR	0.0	(0/2379)
Lane 4	Blank	-----	
Lane 5	60 min RPR	1.3	(22/1627)
Lane 6	Blank	-----	
Lane 7	120 min RPR	0.7	(10/1330)
Lane 8	Blank	-----	
Lane 9	240 min RPR	0.2	(1/762)
Lane 10	Blank	-----	

Figure 5.4 SDS-PAGE of 350 nm Photolysis with Radiolabeled TF4N3
Top panel: Photograph of coomassie stained gel. Each lane was loaded with ~10 μg of the sample indicated in the key. The gel was run, sliced and counted as described in materials and methods.
Bottom panel: The results are expressed as (%) radioactivity associated with BR/ Total radioactivity loaded in that lane with the cpm values (with background subtracted) in parantheses.

	Lane 1	Lane 2	Lane 3	Lane 4	Lane 5	Lane 6	Lane 7	Lane 8	Lane 9	Lane 10
Sample	RTBR (90)	Blank	0 min	Blank	60 min	Blank	120 min	Blank	240 min	Blank
Loaded	1555		2440		1688		1391		763	
BSA	35		79		63		55		46	
BR	208		61		83		71		62	
Supernatant			11389		12521		8308		5976	
Background Loaded = 61										
Background BR = 61										
BR-Background/Loaded-Background										
	147/1494		2/2379		22/1627		10/1330		1/762	

Figure 5.4b Raw cpm Data from SDS-PAGE of 350 nm Photolysis
Gel was sliced, solubilized, added to scintillation cocktail and counted.

Retinal Analog	Extinction Coefficient	Specific Activity	Absorbance Maximum Retinal/Pigmen
TF4N3 (11)	~50 000	~ 10 mCi/mmol	390 nm (EtOH)/ 517 nm
Khorana (2)	~50 000	120 mCi/mmol	394 nm (MeOH)/ 470 nm
Nakanishi1 (3)	49 000	~ 10 mCi/mmol	360 nm (hexane)/ 535 nm
Nakanishi2 (4)	50 500	4800 mCi/mmol	385 nm (MeOH)/ 497 nm

Retinal Analog	Proton Pumping Efficiency	Photolysis Conditions	Irradiation
TF4N3 (11)	40%	4 C, 0.1 mg/ml BR, 10 mg/ml BSA, water	350 nm (0-240 min), Flash (0-100)
Khorana (2)	? ("nonfunctional" Boehm et al., 1990)	?T, 0.4-1.4 mg/ml BR, water	365 nm, 10 min
Nakanishi1 (3)	50% (Sen et al., 1982), 100% (Ding et al., 1990)	4 C, ?[BR], water	254 nm, 10 min
Nakanishi2 (4)	20%	4 C, 0.39 mg/ml BR, water	254 nm, 2 min

Retinal Analog	Assay of Crosslinking	% Labeled	Amino Acids Labeled
TF4N3 (11)	10 ug, SDS-PAGE slice and count, 70 C, 2 min	< 5%	
Khorana (2)	4 ug, SDS-PAGE slice and count & Ethanol Precip. 100 C, 5min	30%	Ser193, Glu194
Nakanishi1 (3)	3 ug SDS-Page slice and count	25-30%	Thr121, Gly122
Nakanishi2 (4)	SDS-PAGE ?	15%	Ala126, Leu127, Trp137, Trp138

Figure 5.5 Comparison of Photoaffinity Labeling Experiments of BR

The extinction coefficients of 11 and 2 were estimated from that of phenyl retinal (Bayley et al., 1981).

Huang et al. did not report the proton pumping efficiency of the BR analog pigment of 2. However, Boehm et al. described it as nonfunctional.

Data derived from Huang et al, 1982; Ding et al., 1990; Sen et al., 1982; Ok et al., 1988; Boehm et al., 1990.

Chapter 6

Peptide Analysis of Bacteriorhodopsin using Mass Spectrometry:

Introduction.

The objective of the studies presented in this chapter is to evaluate the use of mass spectrometry and tandem mass spectrometry to detect and identify sites of photoaffinity labeling of bacteriorhodopsin. Mass spectrometry and tandem mass spectrometry (MS/MS) offer potential advantages over the classical Edman methods [Biemann and Martin, 1987]. The use of MS and MS/MS to identify modified proteins is well established [Biemann and Scoble, 1987; Biemann, 1992]. The recent addition to MUSC of state of the art facilities for these techniques encouraged sophisticated application of MS to protein structure experiments on BR. MS/MS can identify amino acid modifications sequence specifically [Kaur *et al.*, 1989; Chen *et al.*, 1989]. (In order to gain experience in the mass spectrometric analysis of peptides and proteins before the installation of the new tandem mass spectrometer at MUSC, preliminary studies were performed on shark immunoglobulin light chains at the Massachusetts Institute of Technology. The results of these studies are presented in appendix 2.)

The first step in the mass spectrometric analysis of BR is cleavage of the protein into smaller peptides. BR, however, is resistant to most cleavage methods when it is in the form of purple membrane where it is still embedded in a lipid bilayer. Delipidation of the protein is necessary before cleavage. Once delipidated, BR can be dissolved in 70% formic acid and cleaved with CNBr. The mixture of the resulting ten peptides is amenable to tryptic cleavage in a normal tryptic buffer. Before the first chemical cleavage, delipidated BR is not soluble in the buffers most often used for tryptic digestion. After tryptic digestion the final mixture of peptides is ready for HPLC fractionation and then for mass spectrometric analysis. The samples from the analog pigment made with VBN-II (**9**) that had been photolysed were also subjected to mass spectrometric study and the results were analyzed for mass shifts of the predicted peptides consistent with the mass of this retinal analog.

Mass spectrometric analysis of BR was used initially to confirm the sequence of the protein. This work was performed before the introduction of fast atom bombardment as an ionization technique. The methods relied on derivitization of the peptides for gas

chromatographic mass spectrometric analysis. These methods were particularly useful for identification of the pyroglutamic acid as the N-terminal amino acid in BR [Khorana *et al.*, 1979; Gerber and Khorana, 1982]. After the introduction of fast atom bombardment ionization, Khorana's and Biemann's lab collaborated again on the use of mass spectrometry to confirm the sequence of BR, but this time on mutants of the protein produced by molecular biological techniques. Allmaier *et al.* (1986) and Martin (personal communication) showed the mass spectra of nine of the ten peptides derived from the CNBr cleavage.

The mass spectral studies presented in this chapter were performed as initial studies of BR on the newly installed JEOL HX110/HX110 mass spectrometer at MUSC. These mass spectrometric studies were performed only late in the overall studies presented here and were not emphasized since detection of a labeled peptide by other means was deemed necessary for the successful use of MS for identifying the site(s) of labeling.

Materials and Methods.

Materials. The following materials and instruments were used in these analyses. Sephadex LH-20 (Pharmacia) was used to delipidate BR. CNBr, NBA, glycerol, and thioglycerol were obtained from Aldrich. Ethanol was used as an HPLC solvent (UV-grade, Pierce). Formic Acid was used to dissolve BR (Sigma). Trifluoroacetic acid (Sequencing grade, Pierce) was used in the HPLC solvents. Trypsin was obtained from Boehringer-Manheim. The gradient HPLC system consisted of two Waters 510 HPLC pumps, a Waters gradient controller, a Waters 994 Photodiode array detector, a Waters 441 fixed wavelength detector (214 nm), a Vydac (Hesperia, CA) C_4 and C_{18} reversed-phase HPLC column, and a Waters UK6 injector. A Speed-Vac Concentrator was used to remove solvents. A JEOL HX110/110 High Performance/High Mass Tandem Mass Spectrometer (JEOL, Japan) was used for mass spectrometric analysis and a computer program that runs on Macintosh computers, MacProMass [Lee and Vemuri, 1990] was used to aid in analysis of the data.

Methods. BR. Delipidation. The lyophilized pigment was resuspended in a small amount of 88% formic acid and then diluted to 70:30 ethanol:88% formic acid. The sample was then loaded on a pre-equilibrated Sephadex LH-20 column (50x2cm) and eluted with 70:30 ethanol:88% formic acid. The fractions were analyzed by UV-vis spectrophotometry and the protein containing samples (absorbance at 280 nm) were pooled and the solvent evaporated in a Speed-Vac Concentrator [Gerber *et al.*, 1979].

CNBr Cleavage. The delipidated protein was dissolved in a small amount of 88% formic acid and sonicated until in solution. This sonication also warmed the sample to aid in solubilization. Typically about 5 mg of protein was dissolved in ~1 mL of 88% formic acid. Once solubilized, the solution was diluted to 70% formic acid. No tryptamine was added since the tryptamine was shown to discolor the solution and cause confusion when analyzed using photodiode array detection. A 500 fold molar excess of CNBr over the number of methionines was added as a solution in 70% formic acid. The reaction solution was purged with nitrogen and wrapped in foil. The CNBr must

be fresh. The sample was then stirred for 24 hours at room temperature then diluted two fold with water and lyophilized twice to remove the excess CNBr.

Cleavage with CNBr and Trypsin. Although the CNBr digestion goes to completion the HPLC fractionation of some of these very hydrophobic peptides was difficult; therefore, the tryptic digestion was carried out after the CNBr procedure without intermediate HPLC separation. The dried CNBr derived peptides were resuspended in 1% SDS with heat and sonication. The solution was diluted 1:13 with 100 mM ammonium carbonate buffer. One percent by weight of trypsin was added in 0.01% TFA. The reaction mixture was incubated at 37 C for 5 hours and then lyophilized. The method for use of trypsin in the presence of small amounts of SDS was that of Bosserhoff *et al.* (1989).

Fractionation by HPLC. The separations were performed on a Waters gradient system using a Vydac C_4 reversed-phase HPLC column with a small guard column containing the same solid phase. The solvents were A: water with .1% TFA B: ethanol .07% TFA. The gradient used was initial 100% A, 0-5 minutes 25% B, 5-60 minutes 25-100% B, 60-70 minutes 100% B, 70-80 minutes 100% B - 100% A. Flow rate was .75 mL per minutes with detection at 214 nm and spectra taken from 200-500 nm by the 994 detector.

Mass Spectrometry To the fractions collected from the HPLC approximately 1µl of glycerol was added, the samples vortexed and frozen with liquid nitrogen. The samples were placed in a Speed-Vac Concentrator and excess solvent removed. The freezing and use of glycerol decreased the sample loss to the walls of the tubes. Once concentrated, a small amount (1-5 µl) of 5-10% of acetic acid was added to each tube and the sample vortexed to mix.

The samples were analyzed with a JEOL HX110/HX110 Tandem Mass Spectrometer consisting of two double focusing mass spectrometers of EBEB geometry with a mass range of 14000 daltons. Molecular weight determinations were done in MS-1 at resolution 1500. The samples were applied to the probe tip and ionized by bombardment with 18 kV cesium ions. Single stage analysis was performed with an

accelerating voltage of 10 kV. If no sample related ions were observed a small amount of p-nitrobenzyl alcohol (NBA) was added to the sample surface and the analysis repeated.

Tandem Mass Spectrometry. Peptides of interest that were in the proper mass range were analyzed by MS/MS to determine their primary sequence and any modifications that may indicate labeling [Biemann and Scoble, 1987]. The MS/MS experiments were performed with the collision cell operated at 3 kV filled with helium sufficient to attenuate the ion current of the ^{12}C monoisotopic peak by 70%. Once the tandem mass spectra were recorded they were interpreted manually with the aid of the known sequence of BR as manipulated by MacProMass [Lee and Vemuri, 1990].

Results and Discussion.

The delipidation, cleavage, and HPLC fractionation of the resulting peptides showed similar results to those previously published [Gerber *et al.*, 1979]. The delipidation column completely separated the lipid-like retinal which was yellow from the protein which absorbed at 280 nm. CNBr and tryptic cleavage yielded HPLC profiles that showed many peptide peaks consistent with efficient cleavage. All fractions from several HPLC runs of CNBr cleaved and CNBr/trypsin cleaved BR were analyzed by MS. Representative mass spectra of the many taken are shown in the figures. The results of these initial studies are summarized in fig. 6.1 and 6.2.

Ten peptides ranging in mass from ~450 to 5400 are predicted to result from CNBr cleavage of BR. The predicted fragments are shown in fig. 6.1 and listed in fig. 6.2. Tryptic and CNBr digestion leads to many fragments as depicted in fig. 6.1. Those peptides that were found are indicated on fig. 6.1 and listed in fig. 6.2. Some sections of BR were identified by peptides derived from more than one cleavage. Three of the peptides' sequences were confirmed by MS/MS including one peptide (BR sequence 24-32, mass 1023, fig. 6.3, bottom) that was the result of an unusual cleavage between glycine and threonine. Some representative MS spectra are shown in fig. 6.4 through fig. 6.9. Two of the three confirming MS/MS spectra are shown in fig. 6.3 including the spectrum that confirms the sequence of the unusual cleavage fragment. The peptides that were found are all below 2600 mass showing a predilection for the HPLC recovery or ionization of the smaller peptides.

Overall 49% of the amino acids in BR were identified by MS. Nine percent of the protein was sequenced by MS/MS. Two unusual cleavage sites were identified. One was a cleavage between Asp and Pro which is known to be acid labile [Allen, 1981]. The other unusual cleavage was between Gly and Thr. The sequence of the peptide derived from this latter cleavage was confirmed by tandem mass spectrometry (fig. 6.3, bottom). Attempts to identify any mass shifted peptides in the sample from photolysed VBN-II (**9**) pigment were unsuccessful due to the complexity of the spectra. These results of these initial studies indicate the general utility of MS and MS/MS for analysis

of BR.

However, as can be seen in the spectra presented in fig. 6.4, the MS spectra are very complex making identification of the peaks difficult. Each of the peaks in these spectra were analyzed to determine if they were derived from unusual cleavages or from obvious modifications of the protein. Each mass was searched through the sequence of BR using MacProMass to determine possible unusual cleavages. Each was also searched as the Homoserine and the Homoserine Lactone - the two possible products of Met after the CNBr cleavage. It was expected that the peptides containing Thr or Ser may be formylated during the delipidation and CNBr cleavage steps and shifted in mass by a multiple of 28. The unassigned peaks were also checked against spectra derived from just the matrix as sample on the probe tip. The difficulty in assigning even some of the rather large peaks shows that finding a labeled peptide of possibly low abundance would be very difficult. Another possible complication is that the label could be partially degraded [Bownds, 1967; Dohlman *et al.*, 1988]. This degradation, if uniform, would shift the expected mass of the labeled peak. If non-uniform this degradation would spread a possibly already small signal over several peaks making them even more difficult to identify.

The identification of only the smallest peptides indicates an inherent favoring of these peptides in one or more steps in the analysis. The larger peptides may be inefficiently recovered from the HPLC, may stick to the plastic of the tube, may be inefficiently ionized in the matrices chosen, or inefficiently detected in the mass spectrometer. Most of these possible complications were controlled for by routine analysis of bovine insulin at mass > 5000. This control showed that the sample manipulations and the mass spectrometry worked well for insulin, a water soluble hormone, but the large peptides derived from BR are extremely hydrophobic. Thus, peptide mapping shows unexpected complexity with many minor, hard to identify peaks which decreases the usefulness of peptide mapping as a detection method for moderately labeled peptides.

The simplest way to improve the utility of mass spectral analysis is to use

radiolabeled, photoactivatable retinal analogs that would allow identification of the area of the chromatogram in which labeled peptides elute. Focusing to one area of the chromatogram, if not one peptide, would greatly simplify these analyses. This technique has been successfully used on a soluble protein [Chen *et al.*, 1986]. A possible control study that could be used to troubleshoot the methods would be confirmation of Lys216 as the site of the Schiff base linkage to retinal using RTBR. These studies may further the development of the method, but would contribute very little new knowledge since the identification of Lys216 as the linkage site is firmly established.

The results of this mass spectrometric analysis of BR indicate that these methods are useful for mapping much of BR, that MS/MS is useful for sequencing peptides from BR and that these methods in general would be most useful in analysis of a peptide that is known to be labeled.

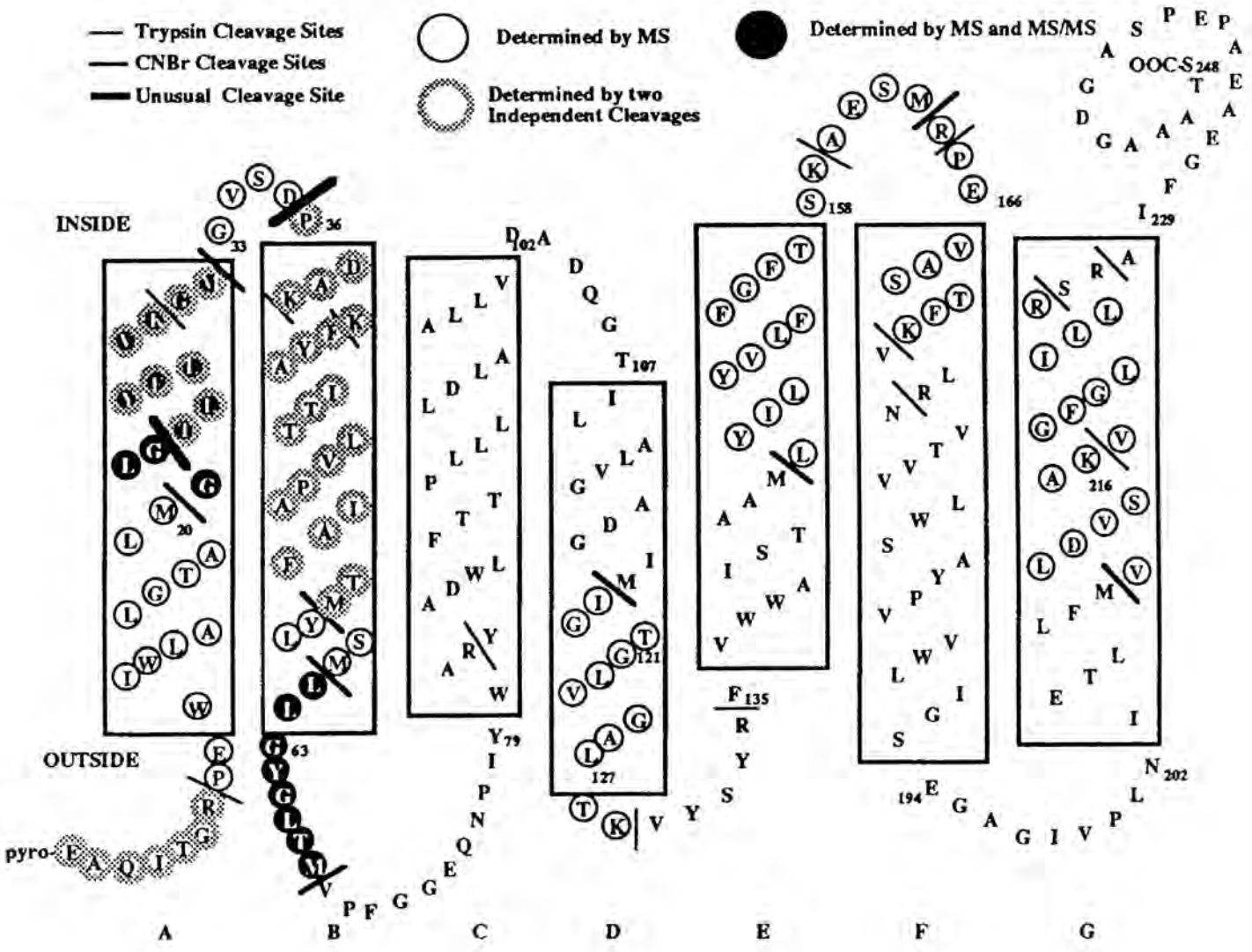

Figure 6.1 Summary of Mass Spectrometry Results
Graphic summary of MS and MS/MS results on a two dimensional model of BR (see figure 1.2). The predicted and unusual sites of cleavage are indicated as well as the peptides found by MS and confirmed by MS/MS.

CNBr Fragments

Number	Fragment	Expected Mass (MH+)	Observed Mass (MH+)
1	1-20	2190.2	2190.8
2	21-32	1250.7	1251.4*
3	33-56	2508.3	2508.9
4	57-60	465.2	465.1
5	61-68	819.5	819.2*
6	69-118	5397.8	
7	119-145	2913.6	
8	146-163	2081.1	2081.9
9	164-209	5036.8	
10	210-248	3843.0	

CNBr/Trypsin Fragments

Number	Fragment	Expected Mass (MH+)	Observed Mass (MH+)
1	1-7	756.4	756.9
12	119-129	1029.6	1029.2
17-18	164-172	1034.6	1034.1
21	210-216	731.4	731.0
22	217-225	987.6	987.1
21-22	210-225	1700.0	1699.5

Unusual Cleavage Fragments

Fragment	Sequence	Expected Mass (MH+)	Observed Mass (MH+)
24-32	(G)TLYFLVKGHsl	1023.6	1023.3*
37-56	(D)PDAKKFYAIT TLVPAIAFTHsl	2150.2	2150.9

* Sequence Confirmed by MS/MS

Figure 6.2 MS & MS/MS of Peptides from BR
Hsl = Homoserine lactone

Figure 6.3 MS/MS of Two Peptides from Bacteriorhodopsin

Top panel: MS/MS spectrum of CNBr3 confirming the sequence of this peptide that is a predicted product of CNBr cleavage of BR. Bottom panel: MS/MS spectrum of BR sequence 24-32 resulting from an unusual cleavage between glycine and threonine. The sequence was suspected from a search of the sequence of BR and is confirmed by this MS/MS spectrum. For symbol identification, refer to Biemann and Martin (1987).

MS/MS of CNBr3 819.2 (MH+)
LLGYGLTHomoserine Lactone

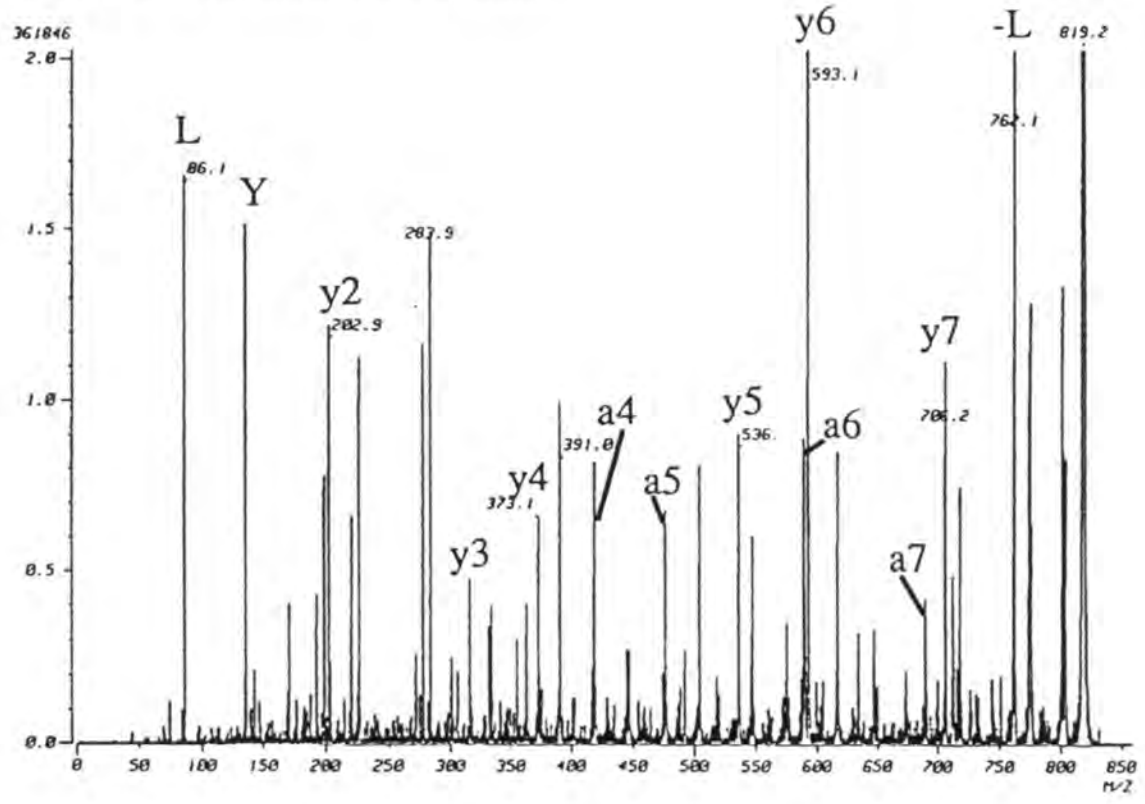

MS/MS of partial CNBr2 (24-32) 1023.3 (MH+)
(G)TLYFLVKGHomoserine Lactone

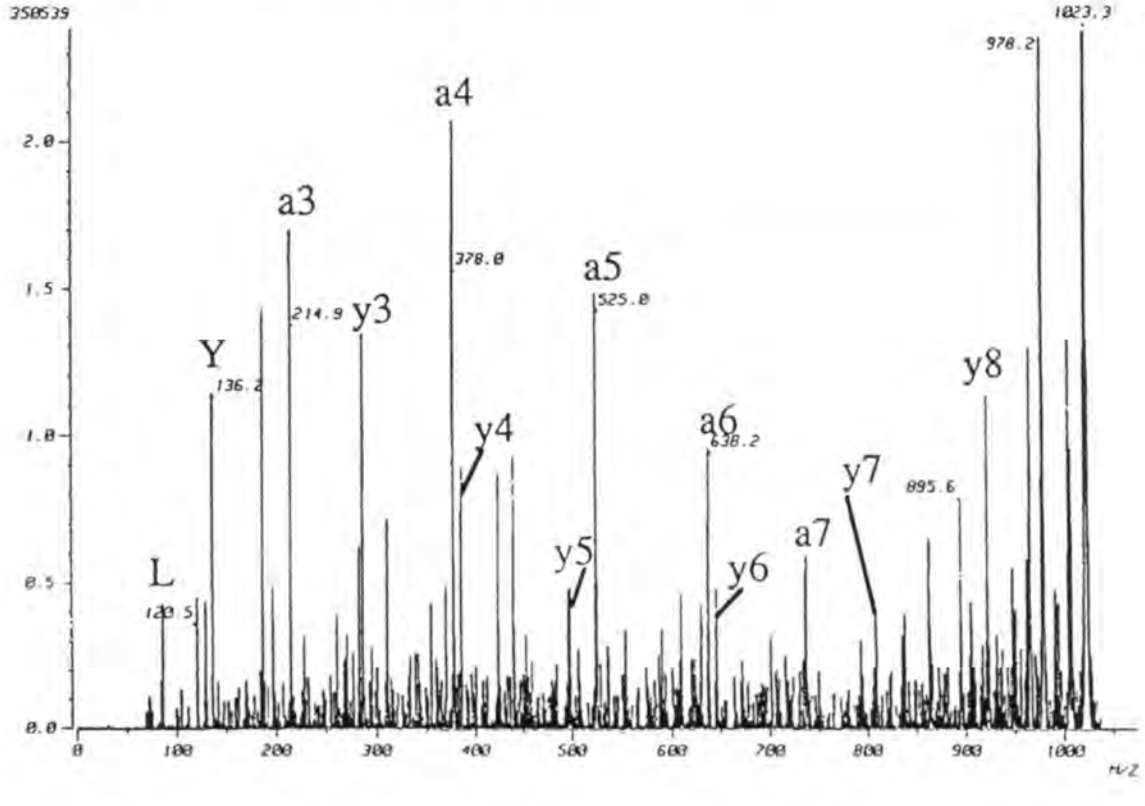

CNBr2 and CNBr3

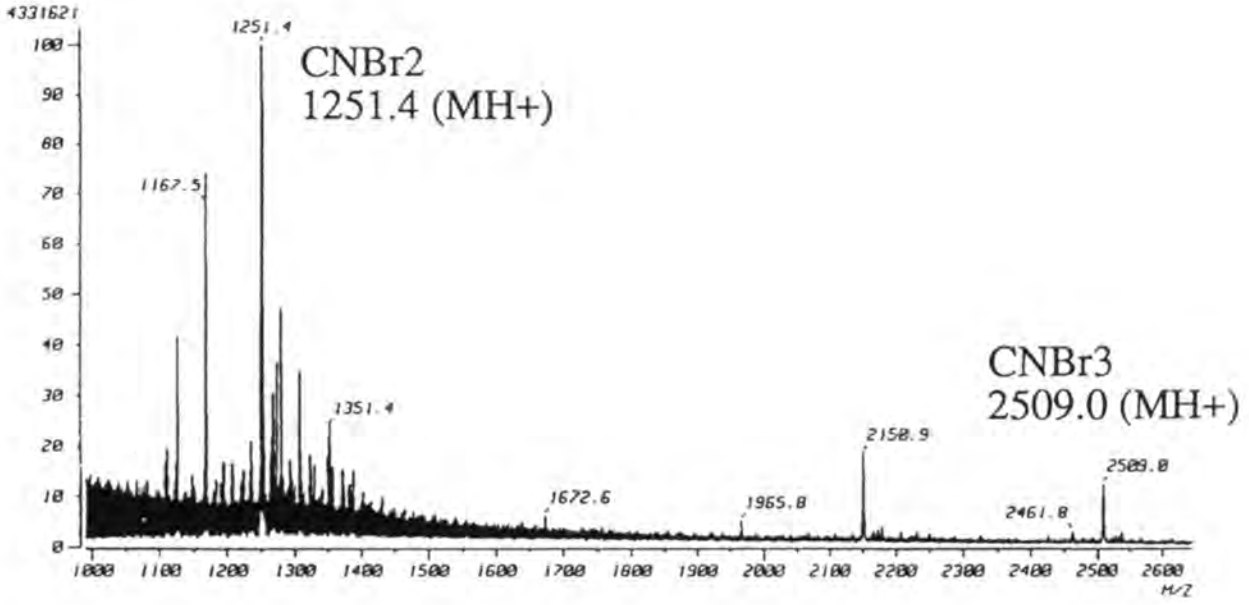

CNBr2 1251.4 (MH+)
GLGTLYFLVKGHomoserine Lactone

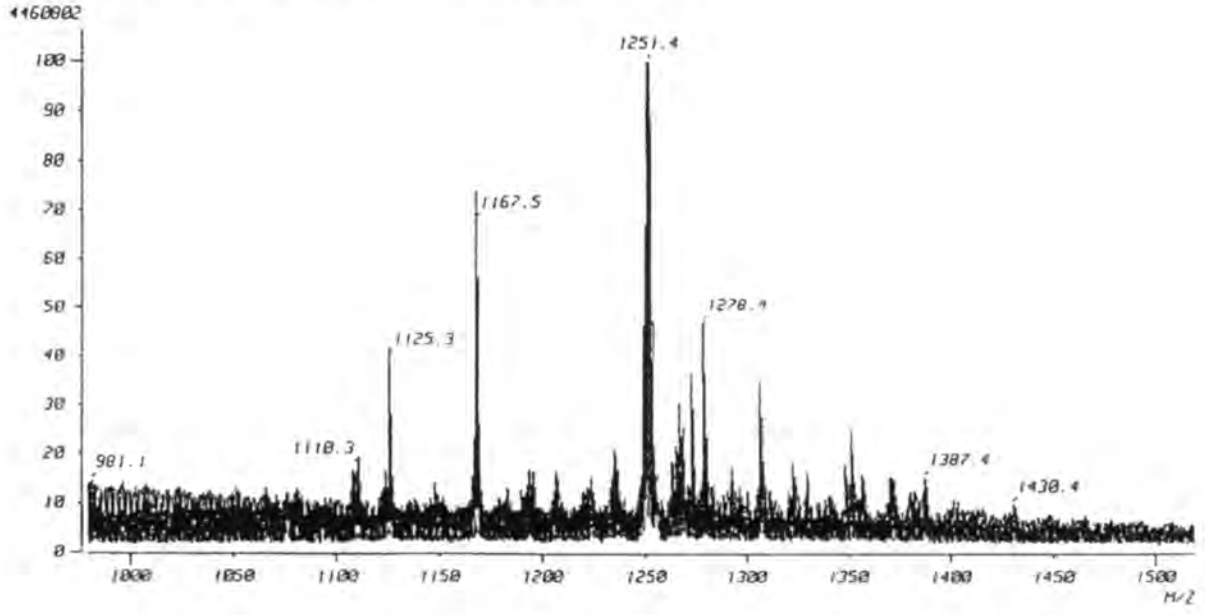

Figure 6.4 MS of Bacteriorhodopsin Peptides - A
MS of CNBr/Trypsin cleavage fragments of BR.
Top panel: HPLC fraction containing CNBr2 at 1251 m/z and CNBr3 at 2509 m/z. Unidentified peaks are not labeled.
Bottom panel: CNBr2 in a different HPLC fraction. Note complexity of spectrum from a single HPLC peak.

CNBr3 2508.99 (MH+)
GVSDPDAKKFYAITTLVPAIAFTHomoserine Lactone

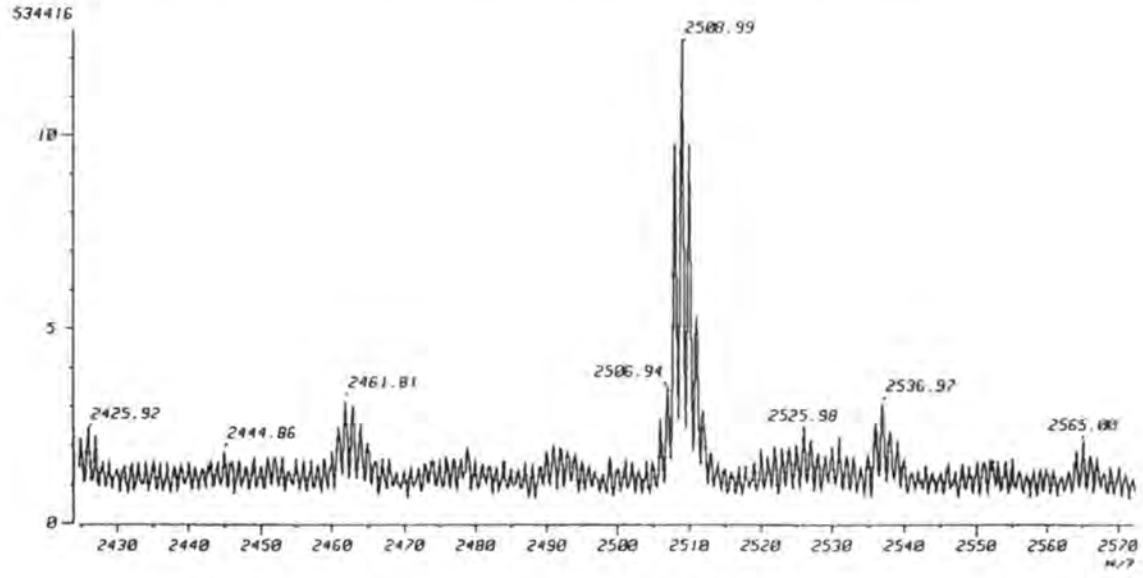

Tryptic Peptide (1-7)
756.9 (MH+)
pyrEAQITGR

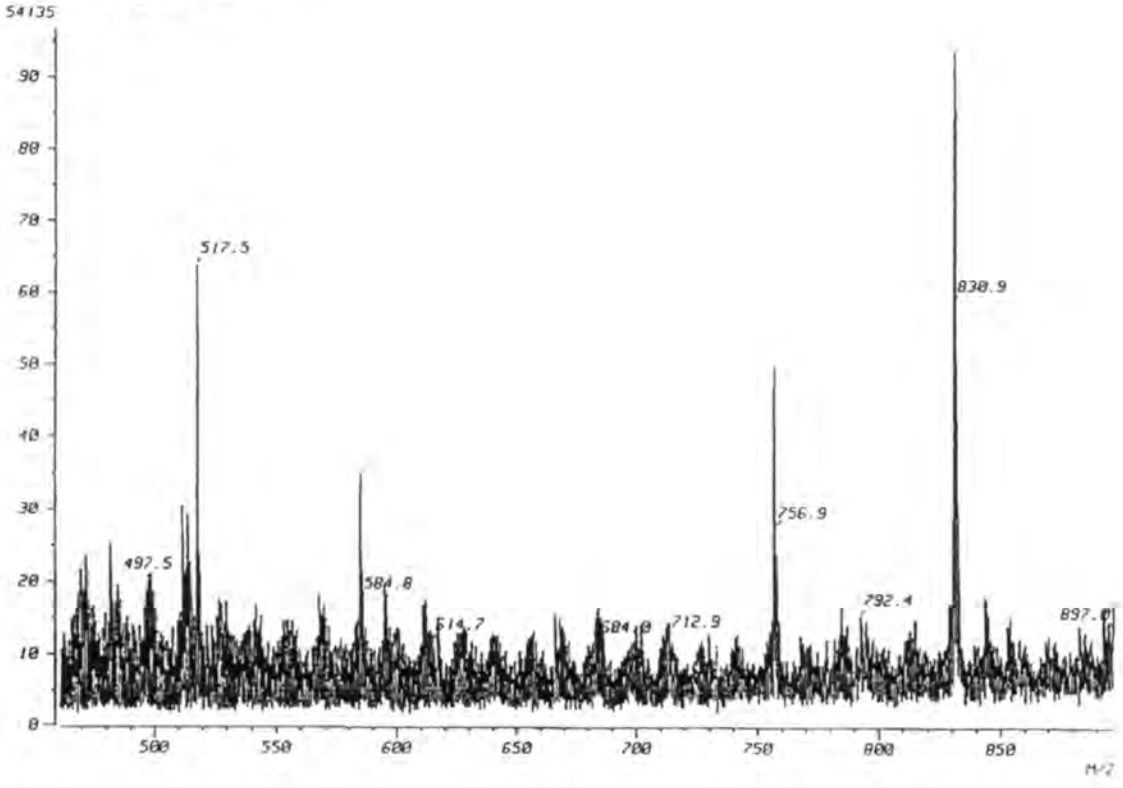

Figure 6.5 MS of Bacteriorhodopsin Peptides - B
MS of CNBr/Trypsin cleavage fragments of BR.
Top panel: MS of CNBr3 at 2509 m/z which is the largest of the 10 CNBr fragments found. Bottom panel: MS of tryptic fragment 1 with the sequence from 1-7 of BR.

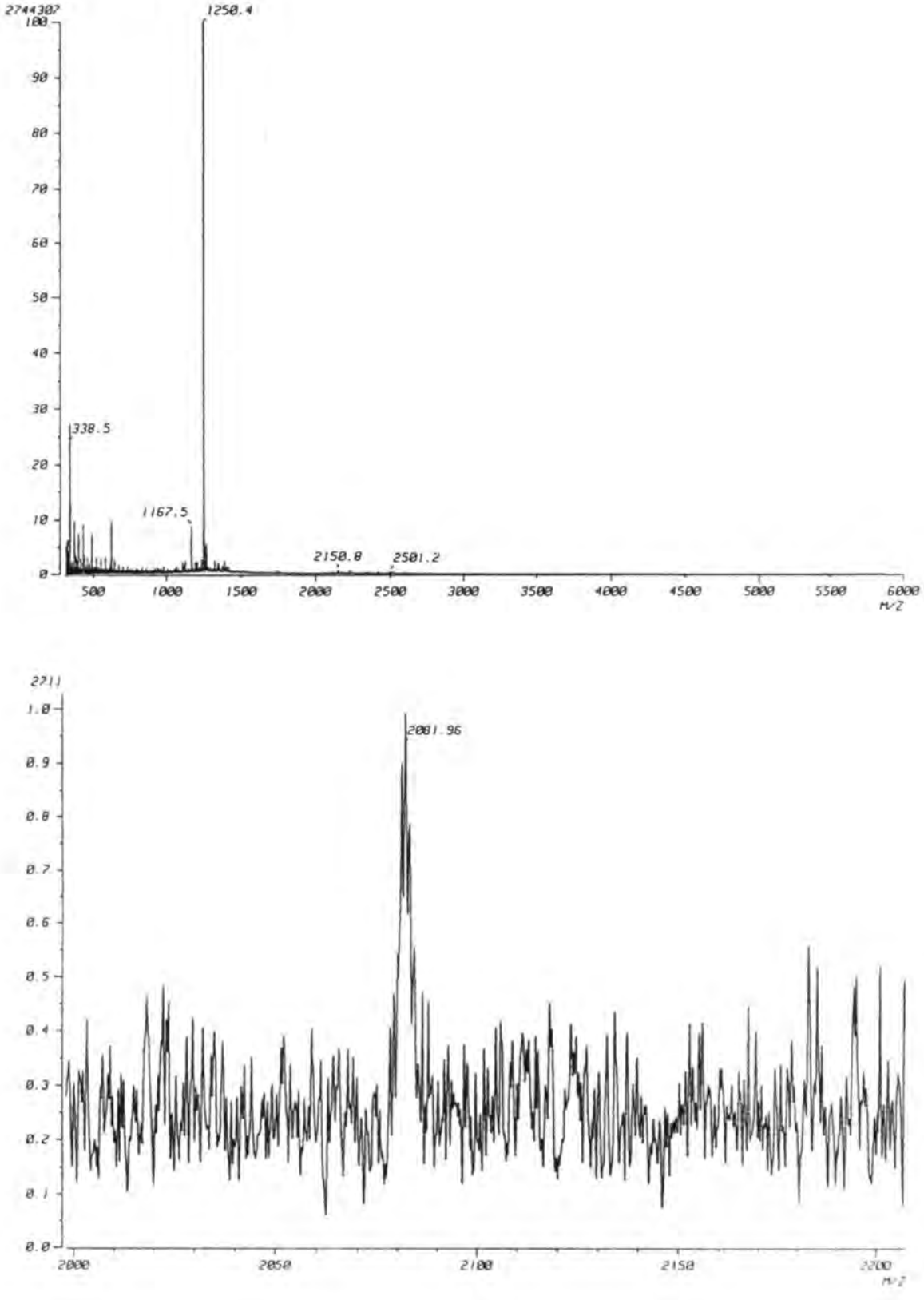

Figure 6.6 MS of BR Peptides - C

Top panel: MS of CNBr2 at 1250.4 m/z; Bottom panel: MS of CNBr8 at 2081.9 m/z

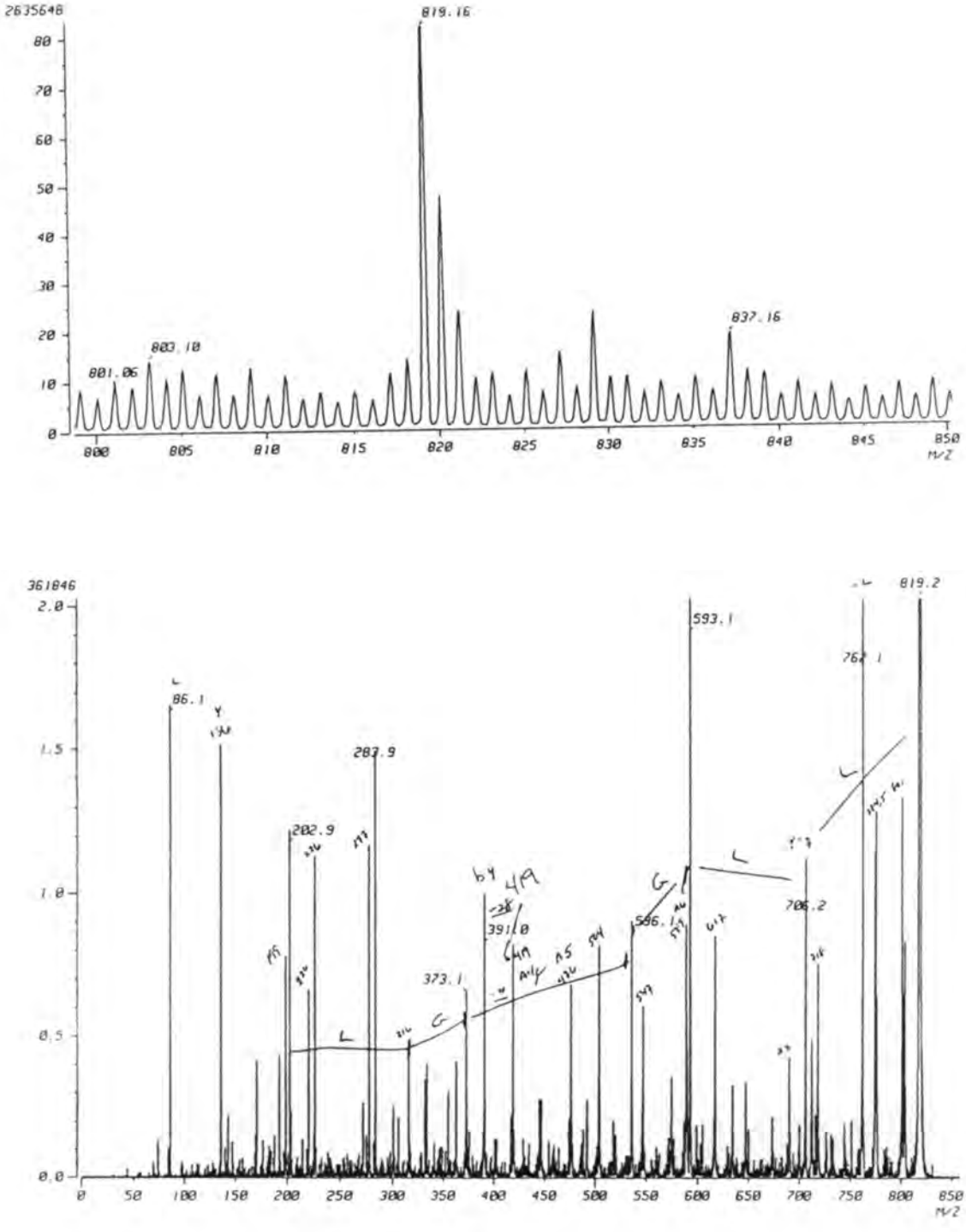

Figure 6.7 MS and MS/MS of CNBr5

Top panel: MS of CNBr5 at 819.2 m/z; Bottom panel: MS/MS of CNBr5

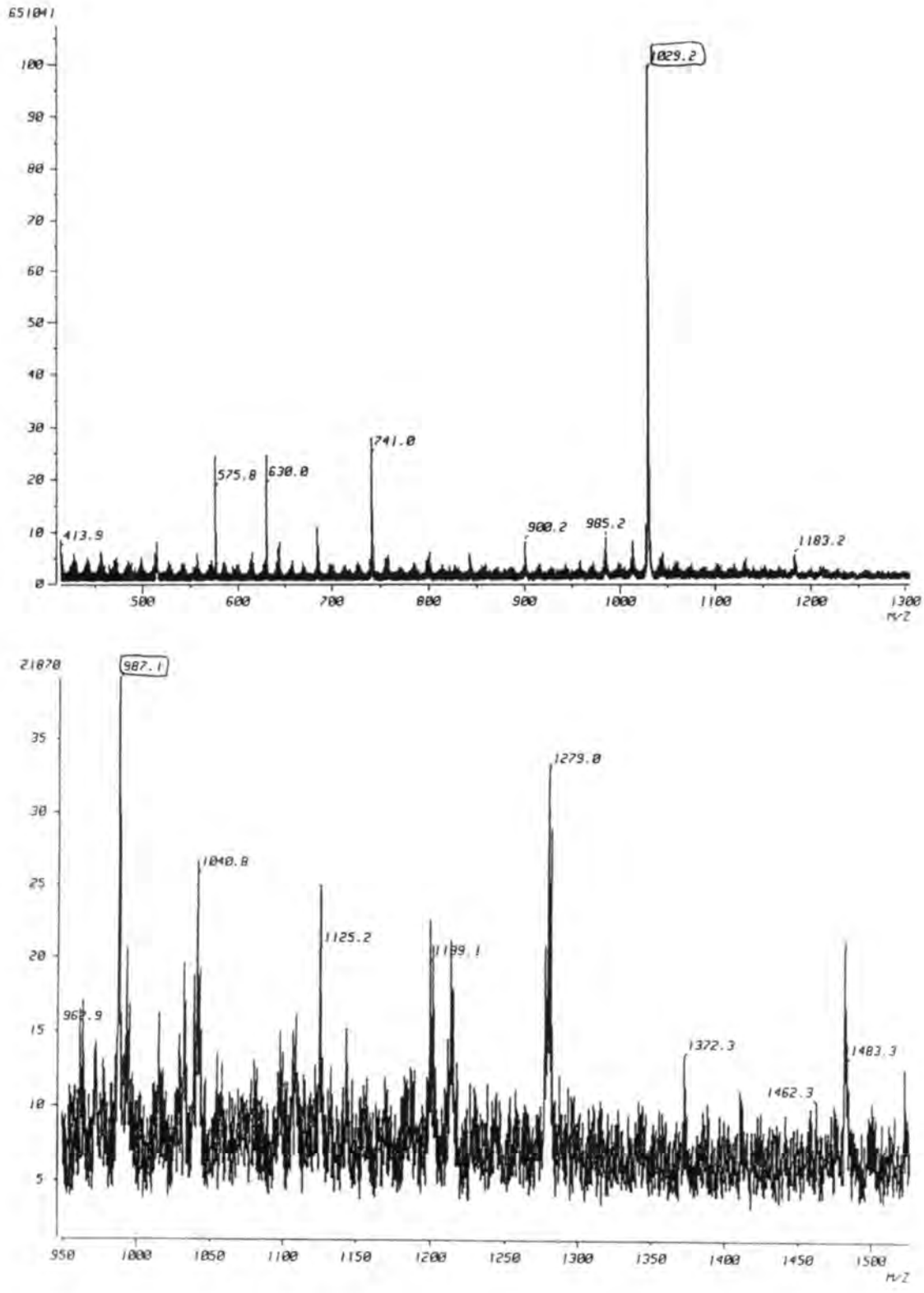

Figure 6.8 MS of Tryptic Fragments of BR

Top panel: MS of peptide 119-129 at 1029.2 m/z of sequence IGTGLVGALTK;

Bottom panel: MS of peptide 217-225 at 987.1 m/z of sequence VGFGLILLR.

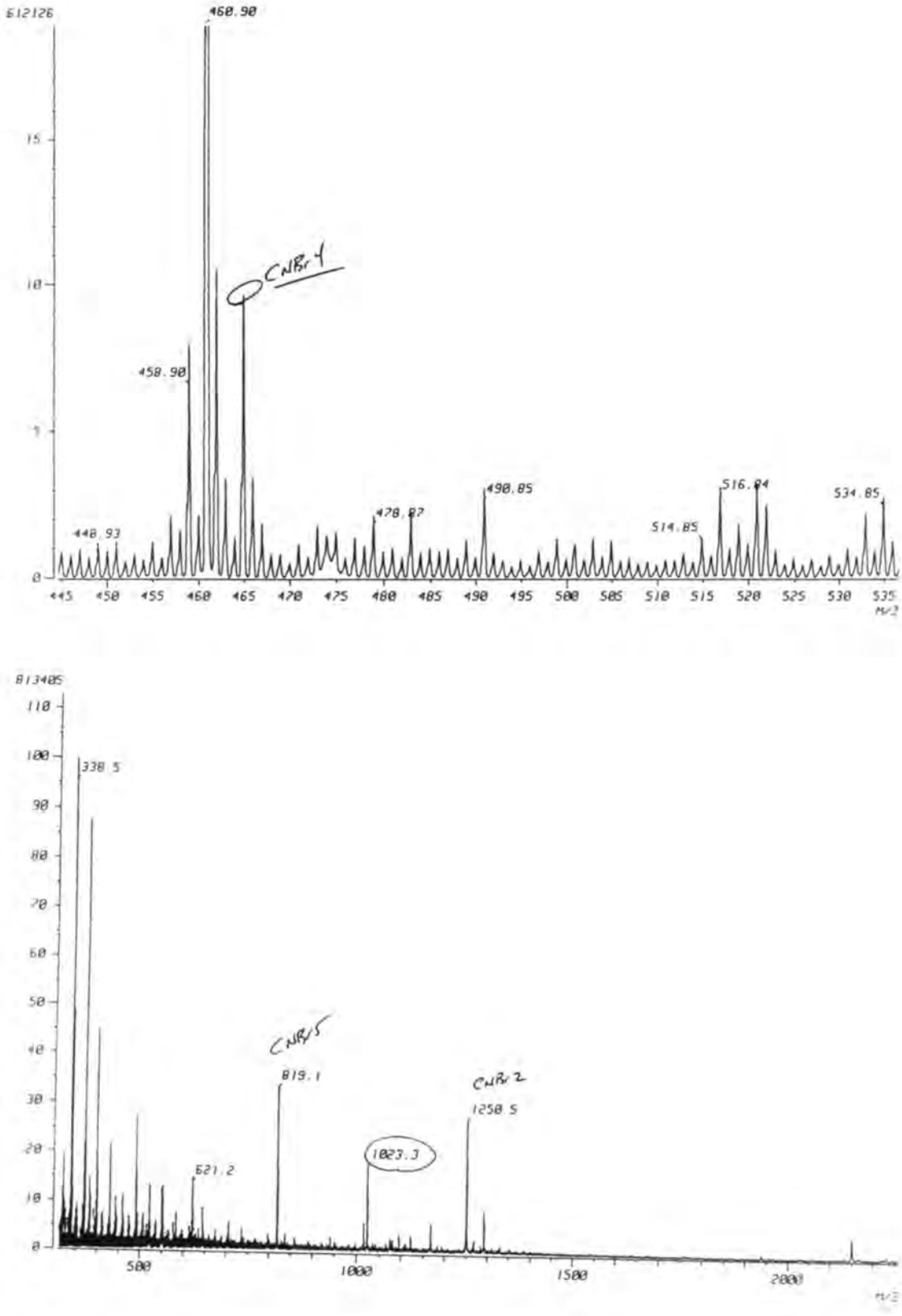

Figure 6.9 MS of BR Peptide - D

Top panel: MS of CNBr4 at 465.1 m/z; Bottom panel: MS of CNBr5 at 819.1 m/z, CNBr2 at 1250.5 m/z and a partial peptide of CNBr2 at 1023.3 m/z with sequence (G)TLYFLVKGHomoserine lactone.

Chapter 7

Summary of Results and Suggestions for Future Work

Eleven different retinal analogs were analyzed as their BR analog pigments. Eight of these retinal analogs were photoactivatable and their analysis as BR analog pigments determined which were suitable for further investigation.

A new flash photolysis apparatus was compared to a continuous wave source. These two light sources were compared by chemical actinometry, ability to activate a newly synthesized model compound, and likelihood of inducing protein damage. Both light sources activated the model compound at total photon counts that induced no noticeable damage to BSA or BR. Both sources were used to activate the retinal analog based on the model compound.

Techniques for prediction of photoaffinity labeled sites in BR were developed using molecular modeling as a tool. These methods were then used to test the previously published accounts of photoaffinity labeling of BR. The results suggest that the retinal analog of Huang *et al.* (1982) was not fully in the retinal binding site of BR when it was activated and labeled the protein. However, the experiments of Ding *et al.* (1990) show labeling of sites very near the photoactivatable group when the analog is placed in the native retinal binding pocket. Analysis of the results of Boehm *et al.* (1990) indicate that this retinal analog labeled amino acids that were intermediate between those of Huang *et al.* and Ding *et al.* for being near the native retinal binding site as modeled by Henderson *et al.* (1990).

It was determined by preliminary studies that radiolabeled retinal analogs would be necessary to determine the extent of labeling after photolysis. The two retinal analogs that were made in radiolabeled form that formed stable and partially functional BR analog pigments (4-oxoretinal **5** and TF4N3 **11**) were tested for their ability to form stable crosslinks with the protein upon photolysis. With an estimate of the limit of detection of <5%, it was determined that neither of these retinal analogs formed significant amounts of a stable crosslink to the protein on photolysis. In retrospect it was realized that the conjugation of the photoactivatable group with the rest of the retinal analog likely rendered the photoactivated intermediates from these two retinal analogs insufficiently reactive to label the protein in high yields.

In anticipation of labeled protein, mass spectrometric analysis of BR was undertaken. This analysis required delipidation, cleavage of the protein by chemical and enzymatic means, separation of peptides by HPLC and analysis by MS and MS/MS. Forty-nine percent of the protein was identified by MS and 9% was sequenced by MS/MS. Two unusual cleavage sites were identified and one of them was confirmed by MS/MS. These experiments emphasized the need for radioactive tracer to be incorporated in the retinal analog to focus the use of mass spectrometry to analysis of a certain region of the HPLC chromatogram if not to a particular peptide.

The major difficulty in these attempts to photoaffinity label BR was the extreme difficulty in the synthesis and characterization of photoactivatable retinal analogs. With this in mind and the fact that a great deal of effort that is not described in these chapters went into isolation and characterization of the retinal analogs in fig. 2.1, it is critical to suggest improvements in the design of the retinal analogs that would make them easier to synthesize and the photoactivated intermediates derived from them more reactive. New and improved retinal analogs are required that would be more likely to be useful in photoaffinity labeling experiments of BR.

What is the 'ideal' photoactivatable retinal analog? The photoactivatable group *must not* be in conjugation with the retinal sidechain. The retinal analog should be non-aromatic. Aromatic rings are sterically very different from cyclohexenyl rings. This is a larger change in structure than may be immediately obvious. Aromatic retinal analogs that function (pump protons) as the BR analog pigments are unusual [Crouch, 1986]. The partial functioning displayed by the TF4N3 pigment was pleasantly surprising. The ideal retinal analog should contain a carbene precursor as a photoactivatable group since carbenes are more reactive than nitrenes and have been most successful in studies on BR and rhodopsin [Huang *et al*, 1982; Ding *et al.*, 1990; Nakayama and Khorana, 1990; Boehm *et al.*, 1990]. The retinal analog should be radiolabeled to a high specific activity on an atom near the photoactivatable group. The high specific activity would aid in identification of even small amounts of labeling. The radiolabel on a proximate atom

would decrease the possibility of the degradation of the label leading to separation of the radiolabel from the photoactivatable group [Dohlman *et al.*, 1988; Ding *et al.*, 1990]. This ideal retinal analog must be relatively simple to synthesize so as to be available in sufficient quantities for complete and timely characterization. The retinal analog Nakanishi (**11**) is an excellent analog for all of the above reasons (except for possibly ease of synthesis and high specific activity, see below). This analog labeled Thr121 and Gly122 that are perfectly placed in the retinal binding pocket to be labeled by this analog. When synthesized as the optically pure compound, Ding *et al.* (1990) showed that Nakanishi1 **3** formed a BR analog pigment that pumped protons as efficiently as the regenerated (with ATR) BR. It should be noted that the results of the photoaffinity labeling experiments were reported eight years after the initial report [Sen *et al.*, 1982] with an intermediate report on the synthesis of the optically active compound [Ok *et al.*, 1988]. These reports are from the laboratory of the world's premier retinal chemist.

Two retinal analogs are being synthesized here that have great potential for being excellent photoaffinity labels for BR. One is the acyclicretinal (**12**, fig.7.1) that contains the excellent photoactivatable group, trifluoromethyldiazoproprionate [Chowdry *et al.*, 1976], is not aromatic and has already been shown to form a BR analog pigment. Several acyclic retinals have been shown to form functional BR analog pigments [Crouch, 1986]. The BR analog pigment formed with this acyclic retinal **12** is currently being tested for its functional characteristics. This retinal analog has recently been shown to form stable crosslinks to cyclohexane when photolysed in solution [John Oatis, personal communication]. One potential drawback of this retinal analog is the relatively labile ester linkage between the photoactivatable group and the rest of the retinal. For greatest utility this compound should be made radioactive with ^{14}C in the trifluoromethyldiazoproprionyl moiety.

The other retinal analog is very similar to this acyclic retinal but is based on valine (**16**, fig. 7.1). This analog has an amide linkage to the photoactivatable group that can be methylated to the tertiary amide. The radiolabeling of this compound can be easily

obtained by purchase of the readily available radiolabeled valine. As a result the radiolabel would be attached to the photoactivatable group by a very stable linkage.

From the current studies, a flow chart for the most efficient approach to photoaffinity labeling experiments of BR can be designed (fig. 7.2). The inherent linearity in the design of these studies is one of the greatest difficulties in achieving the final goal. Each step must be successfully completed before the next step can be reasonably approached. Also, it should be noted that when a decision step fails, one must return to the very beginning of the flow chart. This linearity and lack of branching points makes the initial steps particularly crucial. The design, synthesis and full characterization of a potential photoactivatable retinal analog must be completed before it is reasonable to proceed with the next steps. Several times in the present studies incompletely chemically characterized retinal analogs were characterized as the BR analog pigments only to be redone when the completed chemical characterization showed that the retinal analog being analyzed was other than that expected. For example, one product of many attempts to synthesize TF4N3 **11** was the 4-ethoxytetrafluorophenylretinal analog. This compound formed a BR analog pigment similar to TF4N3, but was, of course, not photoactivatable.

Next, the fully characterized retinal analog must be shown to be both a good retinal analog by testing as the BR analog pigment AND contain a good photoactivatable group by analysis of photolysis in organic solvents. Both of these steps must be completed satisfactorily before the preparation of the radiolabeled compound is undertaken. As was learned in these experiments, the full retinal analog may act considerably differently in the photolysis studies than an easier to synthesize model compound. It is therefore suggested that the photolysis in organic solvents experiments be performed with the full retinal analog. These two steps are presently underway for the acyclic retinal **12**.

After the retinal analog has been shown to form a good BR analog pigment and been shown to contain an excellent photoactivatable group, it should be prepared in radiolabeled form with the radioactive atom being stably linked to the photoactivatable

group. The higher the specific activity, the higher the sensitivity for detecting labeling will be. At the very least, 10 mCi/mmol is required. Photolysis can then be performed under conditions shown to be adequate by the studies of the particular retinal analog in organic solvents.

The amount of labeling as determined by radioactivity associated with BR after cleavage of the Schiff base and separation of the retinals from the protein must be determined. A labeling of at least 15% would allow comparison with the previously reported photoaffinity labeling of BR that showed labeling from 15-30%. This amount of labeling would also facilitate determination and interpretation of the labeled amino acids.

Once labeled protein has been obtained, a three pronged approach to determining sites of labeling using Edman degradation, amino acid analysis and mass spectrometry is suggested. The use of an in-line β–counter would be particularly useful for focusing the experiments on a certain area of the chromatogram derived from HPLC analysis of the cleaved protein. Amino acid analysis can confirm which peptide of those derived from the cleavage of the protein contains the radiolabel. Edman degradation has the drawbacks of being rarely able to identify a single amino acid as the labeled site in a peptide [Boehm *et al.*, 1990]. This is especially troublesome when photoaffinity labeling is being used in this "higher resolution" context. However, it has been successfully used in all of the previous photoaffinity labeling experiments on BR and rhodopsin. Mass spectrometry has the potential advantage over Edman degradation described in Chapter 1 of identifying a single labeled amino acid site, but is unproven as the sole technique for identifying photoaffinity labeled sites. These three techniques should prove complementary in identification of labeled sites.

The overall objective of these experiments - to photoaffinity label BR and to determine sites of labeling - has not yet been reached. Several intermediate objectives were achieved and these studies suggest possible modifications that will increase the

chances for overall success. The major difficulty in these studies was the difficulty in synthesis of the labile photoactivatable retinal analogs. It is hoped that the retinal analogs presently being synthesized will, with the foundation laid by this work, provide interesting structural information on the retinal binding site of bacteriorhodopsin and contribute to the knowledge of drug-receptor interactions by further elucidating the interactions of this 'ligand' with its 'receptor'.

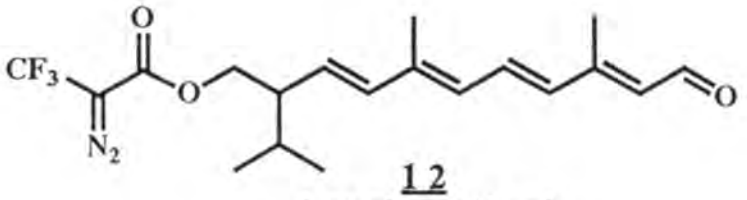

12
Acyclicretinal

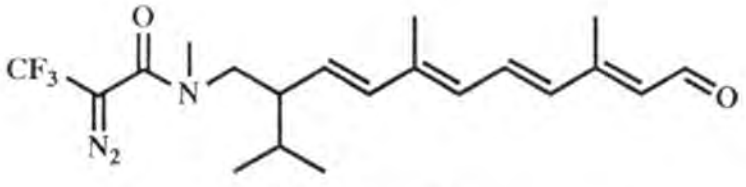

16
Valine Based Retinal

Figure 7.1 Photoactivatable Retinal Analogs Presently Being Synthesized These two retinal analogs possess the excellent photoactivatable group, trifluoromethyl diazopropanoate that is NOT in conjugation with the retinal sidechain.

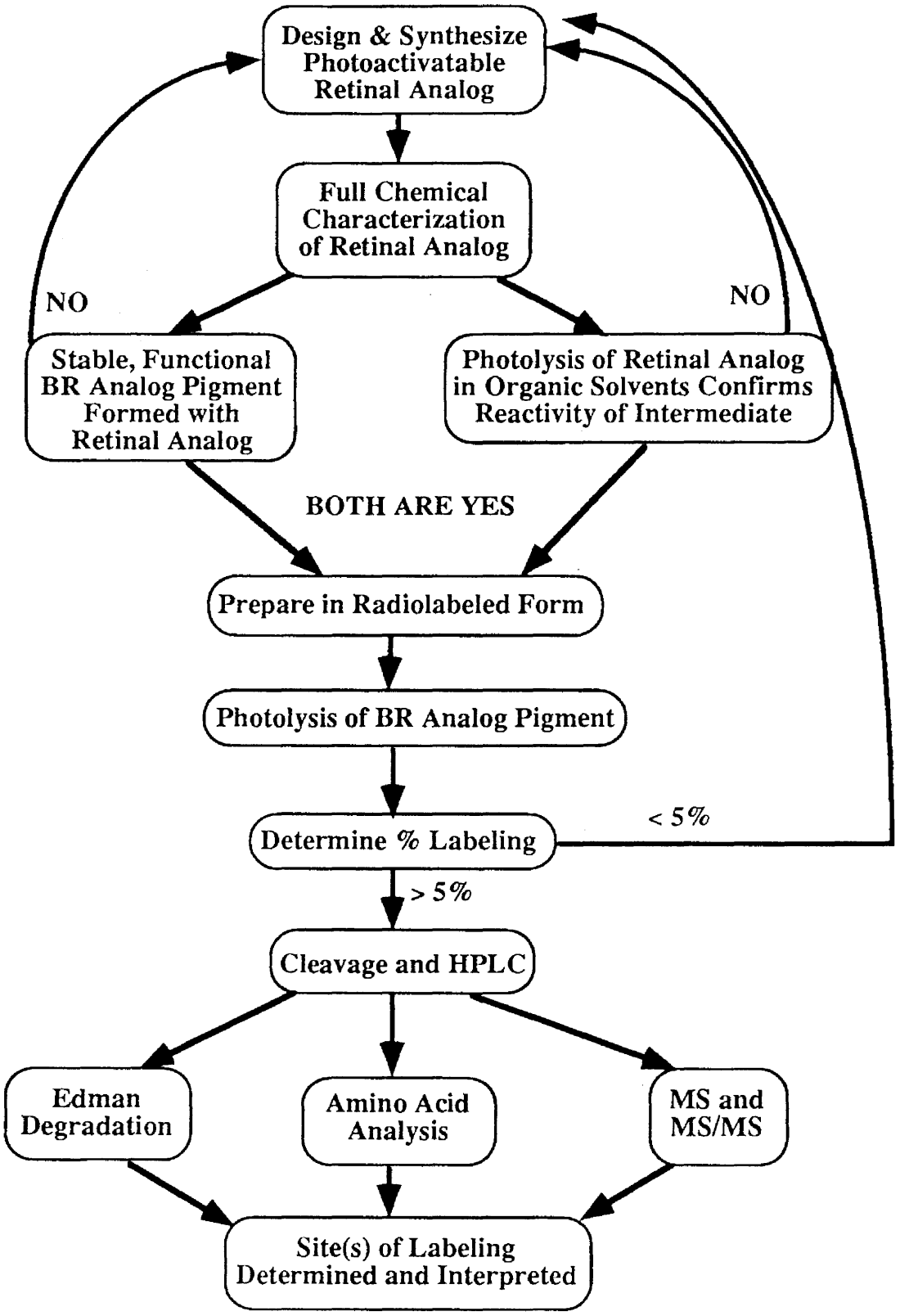

Figure 7.2 Suggested Critical Path For Photoaffinity Labeling of BR
The flow chart represents the suggested most efficient path to photoaffinity labeling of BR using photoactivatable retinal analogs.

List of References

Allen, G. "Sequencing of Proteins and Peptides." In Laboratory Techniques in Biochemistry and Molecular Biology Vol. 9, Elsevier/North Holland Biomedical Press, New York, 1981, p55.

Allmaier, G, BH Chao, HG Khorana, and K Biemann. "The Determination of the Location and Nature of Amino Acid Substitution in Biosynthetic Bacterioopsin." 34th Annal Conference on Mass Spectrometry and Allied Topics. 308-309, 1986.

Barber, M, RS Bordoli, RD Sedgewick, and AN Tyler. "Fast Atom Bombardment (F.A.B.): A New Ion Source for Mass Spectrometry." J. Chem. Soc. Chem. Comm. 325-327, 1981.

Bayley, HB. Photogenerated Reagents in Biochemistry and Molecular Biology, New York: Elsevier, 1983.

Bayley, H, R Radhakrishnan, KS Huang and HG Khorana. "Light Driven Proton Translocation by Bacteriorhodopsin Reconstituted with the Phenyl Analog of Retinal." J. Biol. Chem. 256(8), 3797-3801, 1981.

Bayley, H, K Huang, R Radhakrishnan, AH Ross, Y Takagaki, and HG Khorana. "Site of Attachment of Retinal in Bacteriorhodopsin." Proc. Natl. Acad. Sci. USA, 78(4), 2225-2229, 1981.

Becker, BM and JY Cassim. "Improved Isolation Procedures for the Purple Membrane of Halobacterium halobium." Prep. Biochem. 5, 161-178, 1975.

Beischel, CJ, V Mani, EA Cohen, DR Knapp, and RK Crouch "A Novel Photoaffinity Label for Bacteriorhodopsin." Biophys J, 57, 365a, 1990.

Beischel CJ, V Mani, R Govindjee, TG Ebrey, DR Knapp, and RK Crouch "Ring Oxidized Retinals Form Unusual Bacteriorhodopsin Analogue Pigments." Photochem. Photobiol. 54(6), 977-983, 1991.

Beischel CJ, SK Moore, RK Crouch, and DR Knapp "A Versatile Flash Photolysis Apparatus." Rev. Sci. Instrum. 63(3), 2069-2072, 1992.

Bergman, T, H Jornvall. "Electroblotting of Individual Polypeptides from SDS/Polyacrylamide Gels for Direct Sequence Analysis." Eur. J. Biochem. 169, 9-12, 1987.

Biemann, K. "Mass Spectrometry of Peptides and Proteins." Annu. Rev. Biochem. 61, 977-1010, 1992.

Biemann, K and H.A. Scoble. "Characterization by Tandem Mass Spectrometry of Structural Modifications in Proteins." Science 237, 992-998, 1987.

Biemann,K and SA Martin. "Mass Spectrometric Determination of the Amino Acid Sequence of Peptides and Proteins." Mass Spectrometry Reviews 6, 1-76, 1987.

Boehm, MF, MA Gawinowicz, A Foucault, F Derguini, and K Nakanishi. "Photoaffinity Labeling of Bacteriorhodopsin with [15-^{3}H]-3-Diazo-4-keto-all-*trans*-retinal." J. Am. Chem. Soc. 112, 7779-7782, 1990.

Boman, WD and JN Demas "Ferrioxalate Actinometry: a Warning on Its Proper Use." J. Phys. Chem. 80(21) 2434–2435, 1981.

Bosserhoff, A, J Wallach, and RW Frank. "Micropreparative Separation of Peptides Derived from Sodium Dodecyl Sulfate-Solubilized Proteins." J Chrom. 473, 71-77, 1989.

Brinegar, AC, G Cooper, A Stevens, CH Hauer, J Shabanowitz, DF Hunt, and JE Fox. "Characterization of a Benzyladenine Binding-Site Peptide Isolated from a Wheat Cytokinin-Binding Protein: Sequence Analysis and Identification of a Single Affinity-Labeled Histideine Residue by Mass Spectrometry." Proc. Natl. Acad. Sci. USA. 85, 5927-5931, 1988.

Bownds, D. "Site of Attachment of Retinal in Rhodopsin." Nature 216, 1178-1181,1967.

Cabral, MLPF, JCN Ferreira, and DE Nicodem. "The Use of .15M Potassium Ferrioxalate as a Chemical Actinometer." Molecular Photochemistry 8(3), 213–214, 1977.

Cai, SX, DJ Glenn, JFW Keana. "Toward the Development of Radiolabeled Fluorophenyl Azide-Based Photolabeling Reagents: Synthesis and Photolysis of Iodinated 4-Azidoperfluorobenzoates and 4-Azido-3,5,6-trifluorobenzoates." J.Org.Chem. 57, 1299-1304, 1992.

Calvert, JG and JN Pitts, Jr. "Chemical Actinometers for the Determination of Ultraviolet Light Intensities". In Photochemistry Wiley, New York, 1966, pp. 780–786.

Chen, S, TD Lee, K Legesse, and JE Shively. "Identification of the Arylazido-b-alanyl-NAD+_Modified Site in Rabbit Muscle Glyceraldehyde-3-phosphate

Dehydrogenase by Microsequencing and Fast Atom Bombardement Mass Spectrometry." Biochemistry. 25, 5391-5395, 1986.

Chowdry,V and FH Westheimer. "Photoaffinity Labeling of Biological Systems." Ann Rev. Biochem. 48, 293-325, 1979.

Chowdry, V, R Vaughan, and FH Westheimer. "2-Diazo-3,3,3-trifluoropropionyl chloride: Reagent for Photoaffinity Labeling." Proc. Natl. Acad. Sci. USA. 73(5), 1406-1408, 1976.

Colmenares, LU and RHS Liu. "An Unexpected C-19 Product of the Reaction of Retinal with MnO2. Structure Characterization and Bacteriorhodopsin Analogs." Tetrahedron Lett. 1991.

Creuzet, F, A McDermott, R Gebhard, K van der Hoef, M Spijker-Assink, J Herzfeld, J Lugtenburg, M Levitt, and R Griffin. "Determination of Membrane Protein Structure by Rotational Resonance NMR: Bacteriorhodopsin." Science 251, 783-786, 1991.

Crouch, RK. "Studies of Rhodopsin and Bacteriorhodopsin using Modified Retinals." Photochem. Photobiol. 44, 803-807, 1986.

Crouch, RK, V Mani, C Beischel, and P Goletz. "A Cautionary Note: Retinol in Liposomes Can Auto-oxidize to Form Retinal." Investigative Ophthalmology & Visual Science 31/4, 112, 1990.

Ding, W, A Tsipouras, H Ok, T Yamanato, MA Gawinowicz, and K Nakanishi. "Photoaffinity Labeling of Bacteriorhodopsin." Biochemistry 29, 4898-4904, 1990.

Dohlman, HG, MG Caron, and RJ Lefkowitz. "A Family of Receptors Coupled to Guanine Nucleotide Regulatory Proteins." Biochemistry 26, 2657-2664, 1987.

Dohlman, HG, MG Caron, CD Strader, N Aimlaiky, and RJ Lefkowitz. "Identification and Sequence of a Binding Site Peptide of the β2-Adrenergic Receptor." Biochemistry 27, 1813-1817, 1988.

Dohlman, HG, J Thorner, MG Caron, and RJ Lefkowitz. "Model Systems for the Study of Seven-Transmembrane Segment Receptors." Annu. Rev. Biochem. 60, 653-688, 1991.

Dunn, R, J McCoy, M Simsek, M Majumdar, SH Chang, UL RajBhandary, and HG Khorana. "The Bacteriorhodopsin Gene." Proc. Natl. Acad. Sci. USA. 78, 6744-6748, 1981.

Engelman,DM, R Henderson, AD McLachlan, and BA Wallace. "Path of the Polypeptide in Bacteriorhodopsin." Proc. Natl. Acad. Sci. USA 77, 2023-2027, 1980.

Fedan, JS, GK Hogaboom, and JP O'Donnell. "Photoaffinity Labels as Pharmacological Tools." Biochemical Pharmacology 33, 1167-1180, 1984.

Findlay, J and E Eliopoulos. "Three-Dimensional Modelling of G Protein-linked Receptors." TIPS. 11, 492-499, 1990.

Flam, F. "Getting an Eyeful of Biomolecules." Science 255, 289, 1992.

Freedman, DH. "Bytes of Life." Discover November, 67-72, 1991.

Fujjii, S, Y Maki, and H Kimoto. "Nucleophilic Substitution of Pentafluorobenzene with Imidazole." J. Fluor. Chem. 43, 131-144, 1989.

Gerber, GE, RJ Anderegg,WC Herlihy, CP Gray, K Biemann, and HG Khorana. "Partial Primary Structure of Bacteriorhodopsin: Sequencing Methods for Membrane Proteins." Proc. Natl. Acad. Sci. USA 76, 227-231, 1979..

Gerber, GE and HG Khorana. "Primary Structure of Bacteriorhodopsin: Sequencing Methods for Membrane Proteins." Methods in Enzymology. 88, 56-74, 1982.

Gochnauer, MB and DJ Kushner. "Growth and Nutrition of Extremely Halophilic Bacteria." Can. J. Microbiol. 15, 1157-1165, 1969.

Govindjee, R, TG Ebrey, and AR Crofts. "The Quantum Yield of Proton Pumping by the Purple Membrane of Halobacterium Halobium". Biophys. J. 30, 231-242, 1980.

Gronemeyer,H. "Photoaffinity Labelling of Steroid Hormone Binding Sites." TIBS. July:264-267, 1985.

Hansch, C, A Leo, SH Unger, KH Kim, D Nikaitani, and EJ Lien. "'Aromatic' Substituent Constants for Structure-Activity Correlations." Journal of Medicinal Chemistry., 16(11), 1207-1216, 1973.

Hargrave, PA, JH McDowell, DR Curtis, JK Wang, E Juszczak, SL Fong, JK Mohana Rao, and P Argos. "The Structure of Rhodopsin." Biophys. Struct. Mech. 9, 235-244, 1983.

Hatchard, CG and CA Parker. "A New Sensitive Actinometer II. Potassium Ferrioxalate as a Standard Chemical Actinometer." Proc. R. Soc. London, Ser. A. 235, 518–536, 1956.

Hearne, M and WF Benisk. "Use of a Solid-phase Photoaffinity Reagent to Label a Steroid Binding Site: Application to the Δ5 -3-ketosteroid Isomerase of Pseudomonas testosteroni." Biochem. 26, 7511-7521, 1973.

Henbest, HB, ERH Jones and TC Owen. "Studies in the Polyene Series. Part II. Oxidation of Vitamin A1 and Retinene1 by Manganese Dioxide." J. Chem Soc. 4909-4912, 1957.

Henderson, R, JM Baldwin, TA Ceska, F Zemlin, E Bechmann and KH Downing. "Model for the Structure of Bacteriorhodopsin Based on High-resolution Electron Cryo-microscopy." J. Mol. Biol. 213, 899-929, 1990.

Henderson, R and Unwin, PAH. "Three Dimensional Model of Purple Membrane obtained by Electron Microscopy." Nature. 257, 28-33, 1975.

Heyn, MP, J Westerhausen, I Wallat, and F Seiff. "High-sensitivity Neutron Diffraction of Membranes: Location of the Schiff Base End of the Chromophore of Bacteriorhodopsin." Proc. Natl. Acad. Sci. USA. 85, 2146-2150, 1988.

Hibert, MF, ST Kallmeyer, A Bruinvels, and J Hoflack. "Three Dimensional Models of Neurotransmitter G-Binding Protein-Coupled Receptors." Molecular Pharmacology 40, 8-15, 1991.

Hong, FT. "The Bacteriorhodopsin Model Membrane System is a Prototype Molecular Computing Element." Biosystems 19, 223-236, 1986.

Honig, B, BS Hudson, BS Sykes and M Karplus. "Ring Orientation in β-ionone and Retinals." Proc Natl. Acad. Sci USA 68, 1289-1293, 1971.

Huang, KS, R Radhakrishnan, H Bayley, HG Khorana. "Orientation of Retinal in Bacteriorhodopsin as Studied by Cross-linking using a Photosensitive Analog of Retinal." J. Biol. Chem. 257, 13616-13623, 1982.

Johnson, RS and K Biemann. "The Primary Structure of Thioredoxin from *Chromatium vinosum:* Determined by High Performance Tandem Mass Spectrometry." Biochemistry. 26, 1209-1214, 1987.

Johnson, RS, SA Martin, K Biemann, JT Stults and JT Watson. "Novel Fragmentation Process of Peptides of Collision-induced Decomposition in a Tandem Mass Spectrometer: Differentiation of Leucine and Isoleucine." Analyt. Chem. 59, 2621-2625, 1987.

Kaur, S, D Hollander, R Haas, and AL Burlingame. "Characterization of Structural Xenobiotic Modifications in Proteins by High Sensitivity Tandem Mass Spectrometry." J. Biol. Chem. 264, 16981-16984, 1989.

Keana, JFW and SX Cai. "Functionalized Perfluorophenyl Azides: New Reagents for Photoaffinity Labeling." J. Fluor. Chem. 43, 151–154, 1988.

Keana, JFW and SX Cai. "New Reagents for Photoaffinity Labeling: synthesis and Photolysis of Functionalized Perfluorophenyl Azides." J. Org. Chem. 55,

3640-3647, 1990.

Khorana, HG. "Bacteriorhodopsin, a Membrane Protein that Uses Light to Translocate Protons." J. Biol. Chem. 263, 7439-7442, 1988.

Khorana, HG, GE Gerber, WC Herlihy, CP Gray, RJ Anderegg, K Nihei, and K Biemann. "Amino Acid Sequence of Bacteriorhodopsin." Proc. Natl. Acad. Sci. USA 76, 5046-5050, 1979.

Kiehm, DJ and TH Ji. "Photochemical Crosslinking of Cell Membranes." J. Biol. Chem. 252, 8524–31, 1979.

Kirk, AD and C Namasivyam. "Errors in Ferrioxalate Actinometry." Anal. Chem. 55, 2428-2429, 1983.

Kurien, KC. "A Modification to the Ferrioxoalate Actinometer." J. Chem Soc. (B). 2081-2082, 1971.

Lee, TD and S Vemuri. "MacProMass: A Computer Program to Correlate Mass Spetral Data to Peptide and Protein Structures." Biomed. Env. Mass Spec. 19, 639-645, 1990.

Leyva, E, MS Platz, G Persy, and J Wirz. "Photochemistry of Phenyl Azide: The Role of Singlet and Triplet Phenylnitrene as Transient Intermediates." J. Am. Chem. Soc. 108, 3783-3790, 1986a.

Leyva, E, MJT Young, and MS Platz. "High Yields of Formal CH Insertion Products in the Reactions of Polyfluorinated Aromatic Nitrenes." J. Am. Chem. Soc. 108, 8307-8309, 1986b.

Leyva, E, D Munoz, MS Platz. "Photochemsitry of Fluorinated Aryl Azides in Toluene Solution and in Frozen Polycrystals." J. Org. Chem. 54, 5938-5945, 1989.

Lugtenburg, J, MS Szweykowska, C Heeremans, JA Pardoen, GS Harbison, J Herzfeld, RG Griffin, SO Smith, and RA Mathies. "Mechanism for the Opsin Shift of Retinal's Absorption in Bacteriorhodopsin." J Am. Chem. Soc. 108, 3104-3105, 1986.

Marti, T, SJ Rosselet, H Otto, MP Heyn, and HG Khorana. "The Retinylidene Schiff Base Counterion in Bacteriorhodopsin." J. Biol. Chem. 266(28), 18674-18683, 1991.

Martin, SA, CE Costello, K Biemann. "Optimization of Experimental Procedures for Fast Atom Bombardment Mass Spectrometry." Analyt. Chem. 54, 2362-2368, 1982.

Matheson Jr., RR, HE Van Wart, AW Burgess, LI Weinstein, and HA Scherage. "Study of Protein Topography with Flash Photolytically Generated Nonspecific Surface Labeling Reagents: Surface Labeling of Ribonuclease A." Biochemistry 16, 396–403, 1977.

Miyasaka, T, K Koyama, and I Itoh. " Quantum Conversion and Image Detection by a Bacteriorhodopsin-Based Artificial Photoreceptor." Science 255, 342-344, 1992.

Nakanishi,K, V Balogh-Nair, M Arnaboldi, K Tsujimoto, and B Honig. "An External Point-charge Model for Bacteriorhodopsin to Account for its Purple Color." J. Am. Chem. Soc. 102, 7945-7947, 1980.

Nakayama, TA and HG Khorana. "Orientation of Retinal in Bovine Rhodopsin Determined by Crosslinking Using a Photoactivatable Analog of 11-*cis*-Retinal. J. Biol. Chem. 265(26), 15762-15769, 1990.

Ok, H, C Caldwell, DR Schroeder, AK Singh, and K Nakanishi. "Synthesis of Optically Active 3-diazoacetylretinals with Triisopropylphenylsulfonyl-hydrazone." Tetrahedron Letteers., 29(19), 2275-2278, 1988.

Ovchinnikov, YA, NG Abdulaev, MY Feigina, AV Kiselev, and NA Lobanov. "The Protein Sequnce of Bacteriorhodopsin." FEBS Lett. 100, 219-224 , 1979.

Papac, DI, KR Thornburg, EE Bullesbach, RK Crouch, and DR Knapp. "Palmitylation of a G-Protein Coupled Receptor; Direct Analysis by Tandem Mass Spectrometry." J. Biol. Chem. in press, 1992.

Pardo, L., J. A. Ballesteros, R. Osman, and H Weinstein. "On the Use of the Transmembrane Domain of Bacteriorhodopsin as a Template for Modeling the Three-dimensional Structure of Guanine Nucleotide-binding Regulatory Protein-coupled Receptors." Proc. Natl. Acad. Sci. USA, 89, 4009-4012, 1992.

Peters, J, R Peters, W Stoeckenius. "A Photosensitive Product of Sodium Borohydride Reduction of Bacteriorhodopsin." FEBS Letters. 61(2) 128-134, 1976.

Pinney, KG, KE Carlson, BS Katzenellenbogen, JA Katzenellenbogen. "Efficient and Selective Photoaffinity Labeling of the Estrogen Receptor using Two Nonsteroidal Ligands that Embody Aryl Azide or Tetrafluoroaryl Azide Photoreactive Functions." Biochemistry 30(9) 2421-31, 1991.

Rosenshein, IL, JJ Marchalonis. "The Immunoglobulins of Carcharrhine Sharks: A Comparison of Serological and Biochemical Properties." Comp. Biochem Physiol. 86B, 737, 1987.

Rothschild, KJ. "FTIR Difference Spectroscopy of Bacteriorhodopsin: Toward a Molecular Model." J. Bioenerg. Biomem. 24(1),147-167, 1992.

Schey, KL, DI Papac, DR Knapp, and RK Crouch. "Matrix-assisted Laser Desorption Mass Spectrometry of Rhodopsin and Bacteriorhodopsin." Biophys J., *in press*, 1992.

Schluter SF, CJ Beischel, SA Martin, and JJ Marchalonis. "Sequence Analysis of Homogeneous Peptides of Shark Immunoglobulin Light Chains by Tandem Mass Spectrometry: Correlation with Gene Sequence and Homologies among Variable and Constant Region Peptides of Sharks and Mammals." Molecular Immunology 27 (1), 17-23, 1990.

Sen, R, TS Widlanski, V Balogh-Nair, and K Nakanishi. "Photoaffinity Labeling of Bacteriorhodopsin with 3-([1-14C]Diazoacetoxy)-trans-retinal." J. Am. Chem. Soc. 105, 5160-5162, 1983.

Soundarajan, N and MS Platz. "Descriptive Photochemistry of Polyfluorinated Azide Derivatives of Nethyl Benzoate." J. Org. Chem. 55:2034-2044, 1990.

Stone, R. "Biology Approaches the Teraflop Era." Science. 256, 440-442, 1992.

Stryer, L. Biochemistry. New York: WH Freeman and Company, 1988, p.26.

Sumper, M and G Herrmann. "Biosynthesis of Purple Membrane: Control of Retinal

Synthesis by Bacterioopsin." FEBS Lett. 71, 333-336, 1976.

Taylor, CA, Jr., HE Smith, and BJ Danzo. "Photoaffinity Labeling of Rat Androgen Binding Protein." Proc. Natl. Acad. Sci. USA 77:234-238, 1980.

Tokunaga, F, R Govindjee, TG Ebrey, and RK Crouch. "Synthetic Pigment Analogues of the Purple Membrane." Biophys. J. 19, 191-198, 1977.

Torres, MJ, J Zayas, and MS Platz. "A Formal CH Insertion Reaction of an Aryl Nitrene into an Alkyl CH Bond. Implications for Photoaffinity Labeling." Tet. Lett. 27, 791-794, 1986.

Wald G. "The synthesis from Vitamin A1 of "Retinene1" and of a New 545 mμ Chromogen Yielding Light-sensitive Products." J. Gen. Physiol. 31, 489-505, 1948.

Wegryzn, J, G Patonay, and I Warner. "Versatile Power Supply Circuit for Xenon Flashlamps." Rev. Sci. Instrum. 60(1), 90–95, 1989.

Williams, TC and V Mani. "Design of a Helix-bundle Cross-link: NMR and UV-visible Spectroscopic Analyses and Molecular Modeling of Ring-oxidized Retinals." Biochemistry 30, 2976-2988, 1991.

Appendix 1

Synthesis of TF4N3

and

Spectra of Retinal Analogs

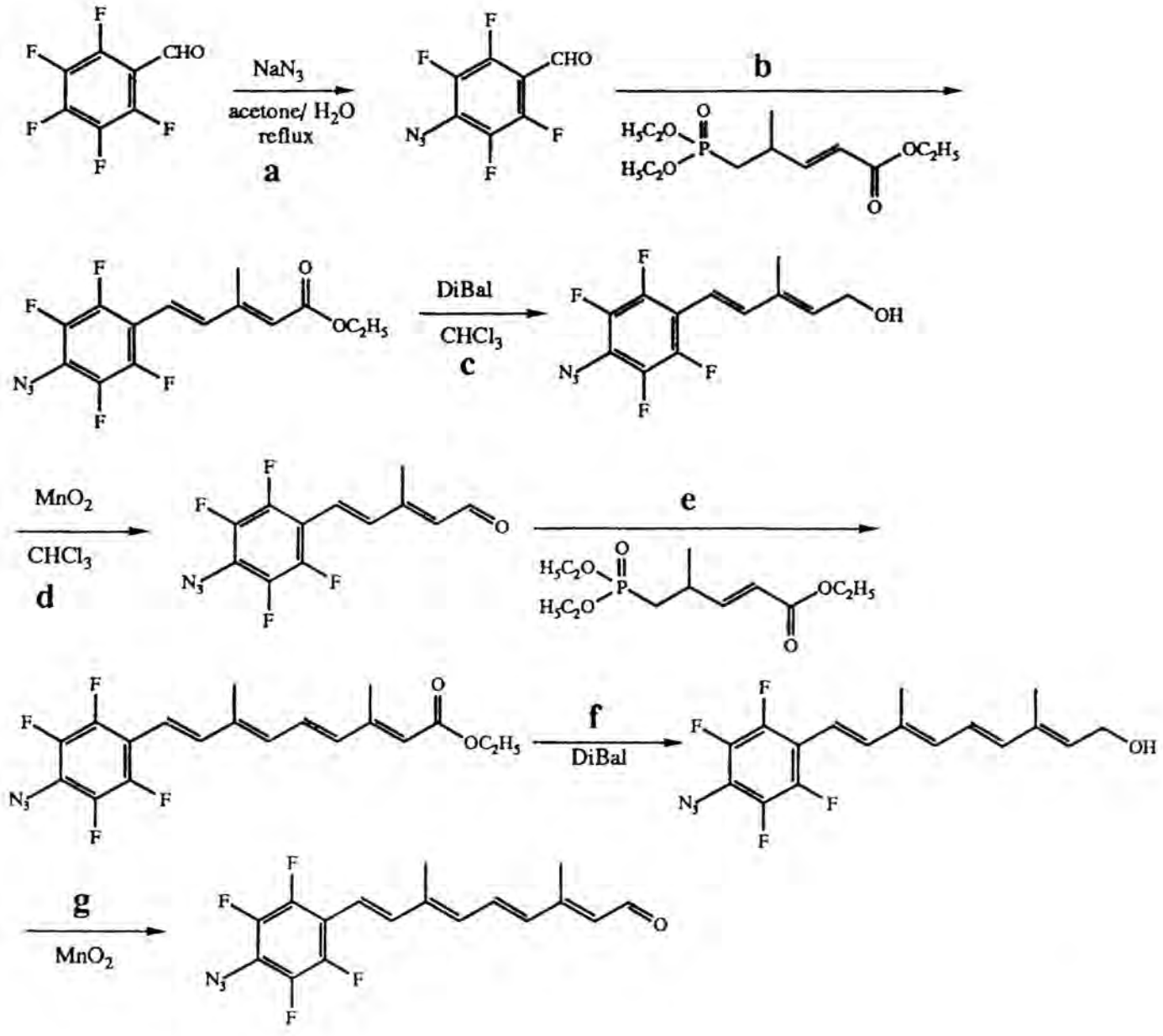

Figure A1.1 Synthetic Scheme for TF4N3

Synthesis of TF4N3 ***11***:

Step a: Pentafluorobenzaldehyde (Aldrich, 2.4 g, 12.2 mmol) was refluxed with sodium azide (Aldrich, 0.8 g, 12.3 mmol) in 26 ml acetone:water 3:1 for seven hours. The product was extracted with ether twice. The extract was dried with magnesium sulfate (anhydrous, Sigma). The ether is evaportaed under a stream of nitrogen.

Yield=100%. UV=250 nm. IR=2130 cm^{-1}.

Step b: TF4ABA (2.17 g, 10 mmol) was reacted with triethyl-3-methyl-4-phosphocrotonate (Aldrich, 2.64 g, 10 mmol) in 12 mL sodium bis(trimethylsilyl)amide (1.0 M, Aldrich) in tetrahydrofuran. The phosphocrotonate and base were allowed to react for 0.5 h at room temperature. TF4ABA in freshly distilled THF was added and stirred overnight at room temperature. Water was added to quench the reaction and the product was extracted with petroleum ether, dried with magnesium sulfate and evaporated under argon. The precipitate was dissolved in the least amount of 50% ethyl acetate:hexanes and purified by passage through silica gel and eluting with 10% ethyl acetate:hexanes. The pure fractions were crystalline solids.

Yield=30%. UV=250 nm. IR=2137cm^{-1}. MS=303m/z (amine).

Step c: The ester was dissolved in chloroform and twice the moles of ester of DiBal (Aldrich, 1.0 M in chloroform) was added slowly with stirring at 0 C. When the ester was fully reacted (absent by TLC), water was added to precipitate aluminum. It was filtered, extracted with chloroform, dried with magnesium sulfate, and evaporated with argon. The residue was dissolved in 50% ethyl acetate:hexane and purified through a silica column eluted with 35% ethyl acetate:hexane. The purified fractions were combined and evaporated to dryness.

Yield=68%. UV=305 nm. IR= 2127cm^{-1}.

Step d: The alcohol was dissolved in chloroform. Manganese dioxide which was sonicated in deionized water for 24 hours, filtered and dried in an oil bath under house vaccuum was added. One gram of manganese dioxide was used per 0.1 g of alcohol. The mixture was stirred at room temperature overnight, filtered through celite, dried with magnesium sulfate and dried with argon. The solid was dissolved in 50% ethyl acetate:hexanes and separated on a silica column with 10% ethyl acetate:hexanes. The trans isomer was used for the next step.

Yield=63%. UV=358 nm. IR=2127cm^{-1}.

Step e: Same as step b. Yield=82%. UV=378 nm.

Step f: Same as step c. Yield=65% UV=357 nm.

Step g: Same as step d. Yield=63%. UV=390 nm.

Further separation of the isomers was done on a preparative HPLC silica column (Econosphere 5μm) to obtain the all-*trans*. The following characterizations were performed on the *trans* isomer: UV-vis, MS, IR, proton NMR, fluorine NMR.

UV=390 nm

MS=323m/z (nitrene), 325m/z (amine)

IR=2122cm^{-1}

fluorine NMR=two peaks in AA'XX' pattern

proton NMR - showed predominately all-*trans* isomer

UV-vis absorbance maximum in ethanol (nm)

compound	pentafluoro	azido
benzaldehyde	235	250
C-5 ester	304	317
C-5 alcohol	282	305
C-5 aldehyde	316	358
C-10 ester	360	383
C-10 alcohol	345	363
C-10 aldehyde	370	390

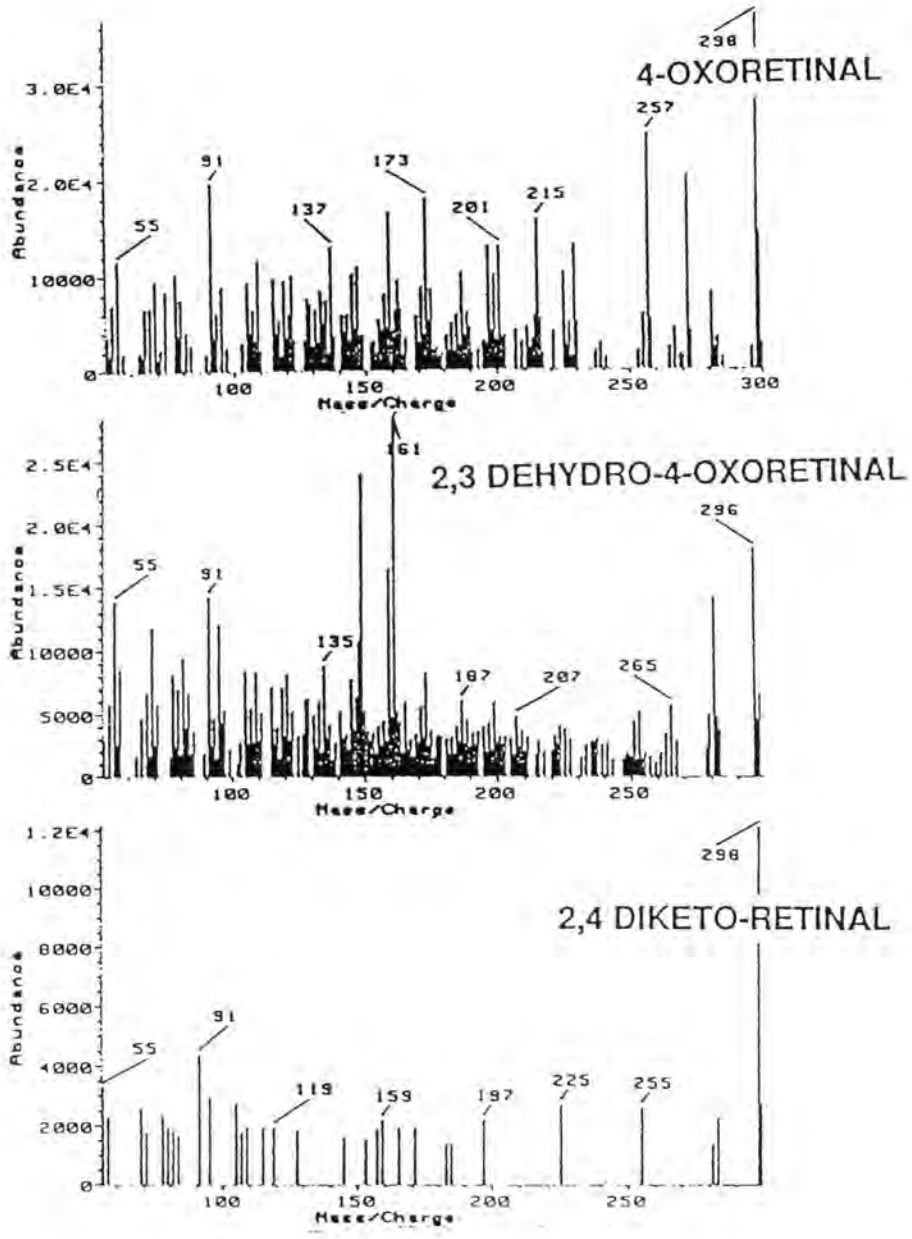

Figure A1.2 Mass Spectra of Oxoretinals 5,6,7

Mass spectra of **5** (top: 298 m/z), **6** (middle: 296 m/z) and **7** (bottom:298 m/z).

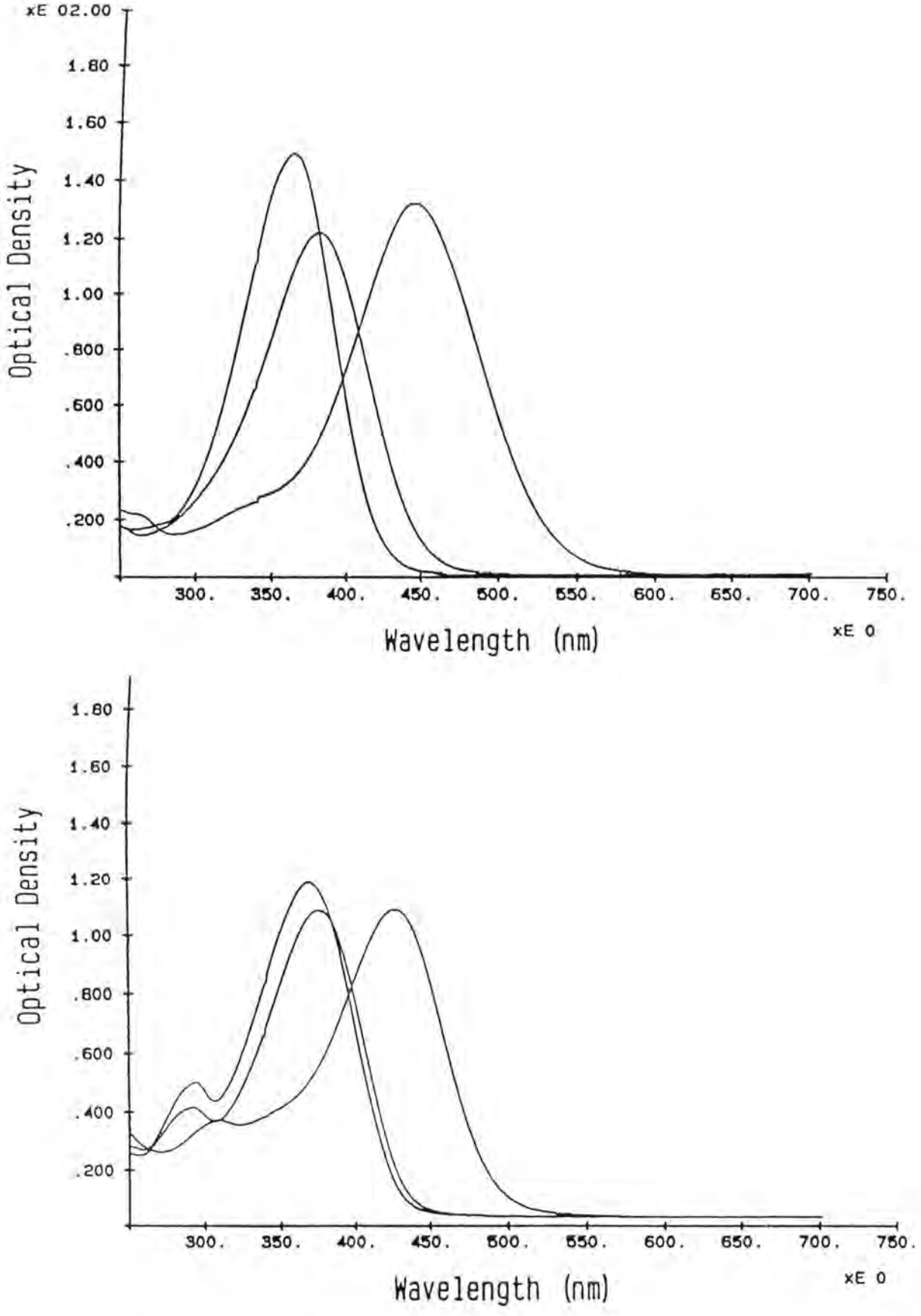

Figure A1.3 Protonated Schiff Base Formation for 1 and 5

UV-vis spectra of formation of protonated Schiff base of retinal (top,**1**) and 4-oxoretinal (bottom, **5**). The aldehyde of each has an absorbance maximum at ~380 nm, the Schiff base with n-butylamine is blue shifted, and the protonated Schiff base is red shifted.

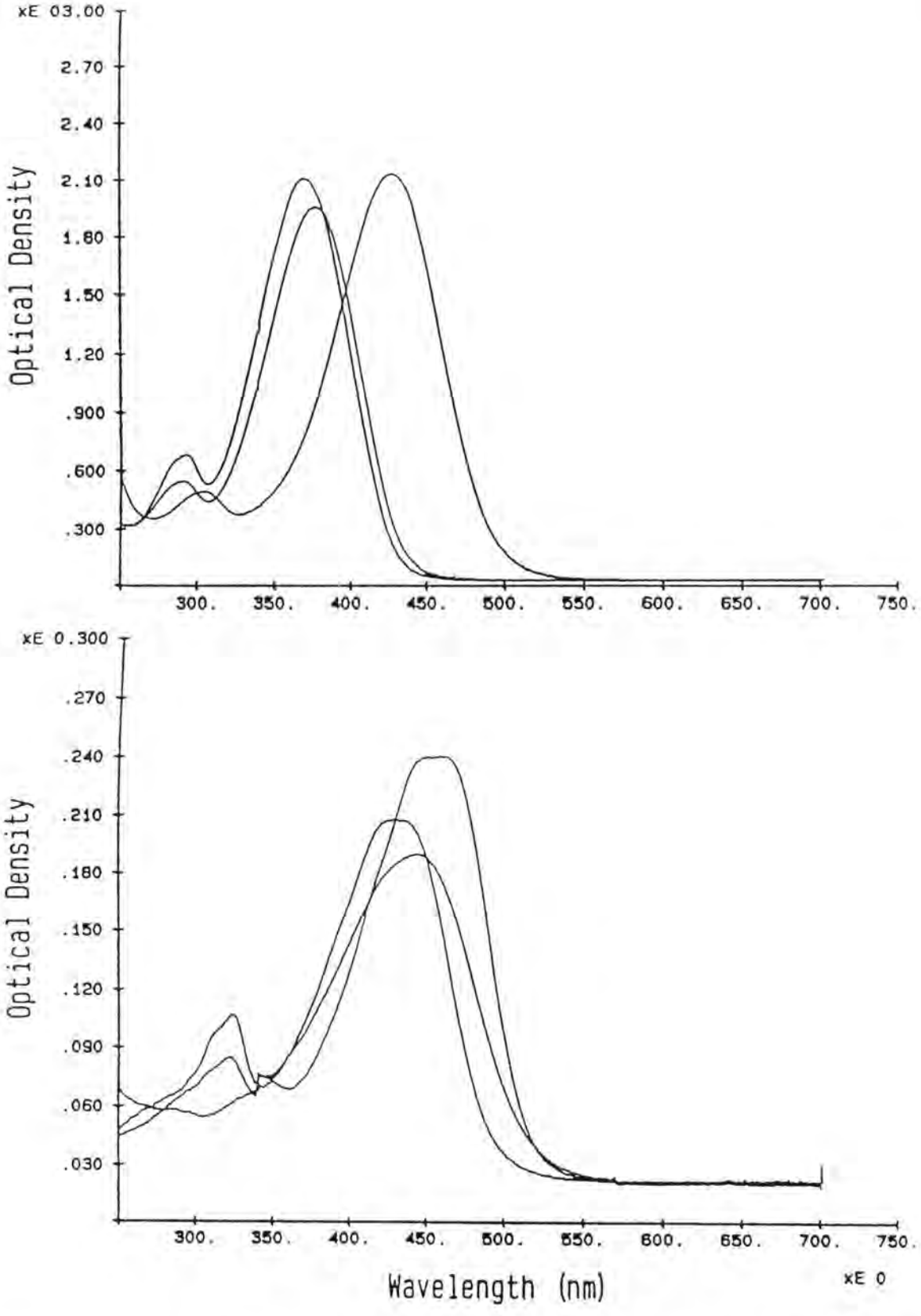

Figure A1.4 Protonated Schiff Base Formation of 6 and 7

UV-vis spectra of formation of protonated Schiff base of 2,3-dehydroretinal (top,**6**) and dioxocyclopentenylretinal (bottom, **7**). The aldehyde of each has an intermediate absorbance maximum, the Schiff base with n-butylamine is blue shifted, and the protonated Schiff base is red shifted.

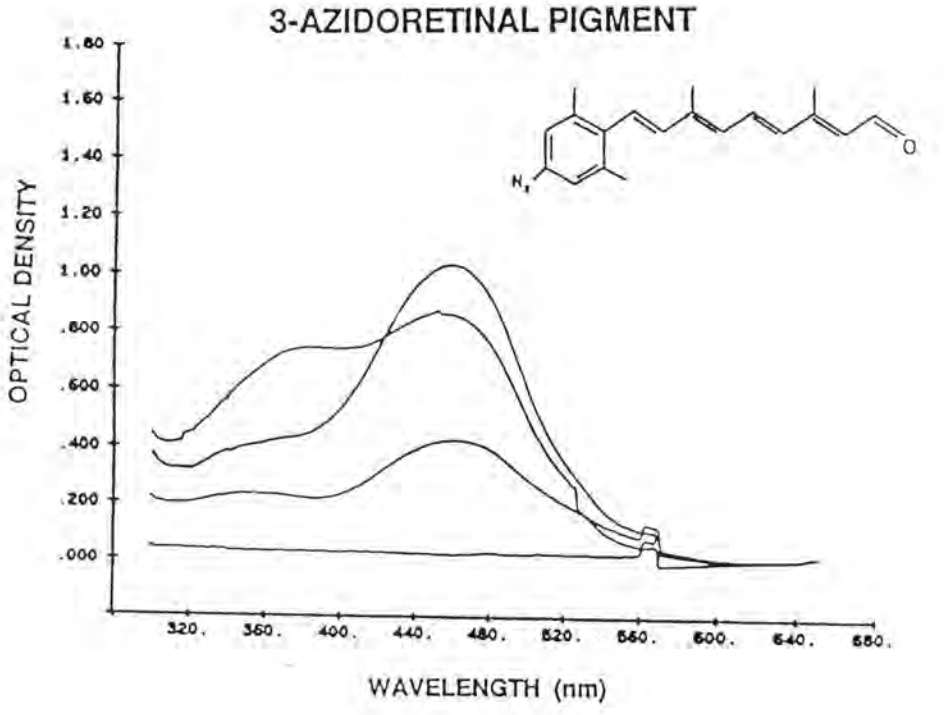

Figure A1.5 Pigment Formation with 8

UV-vis spectra of BR analog pigment formation with VBN-I **8**. The absorbance due to the pigment at ~470 nm increased with time of incubation.

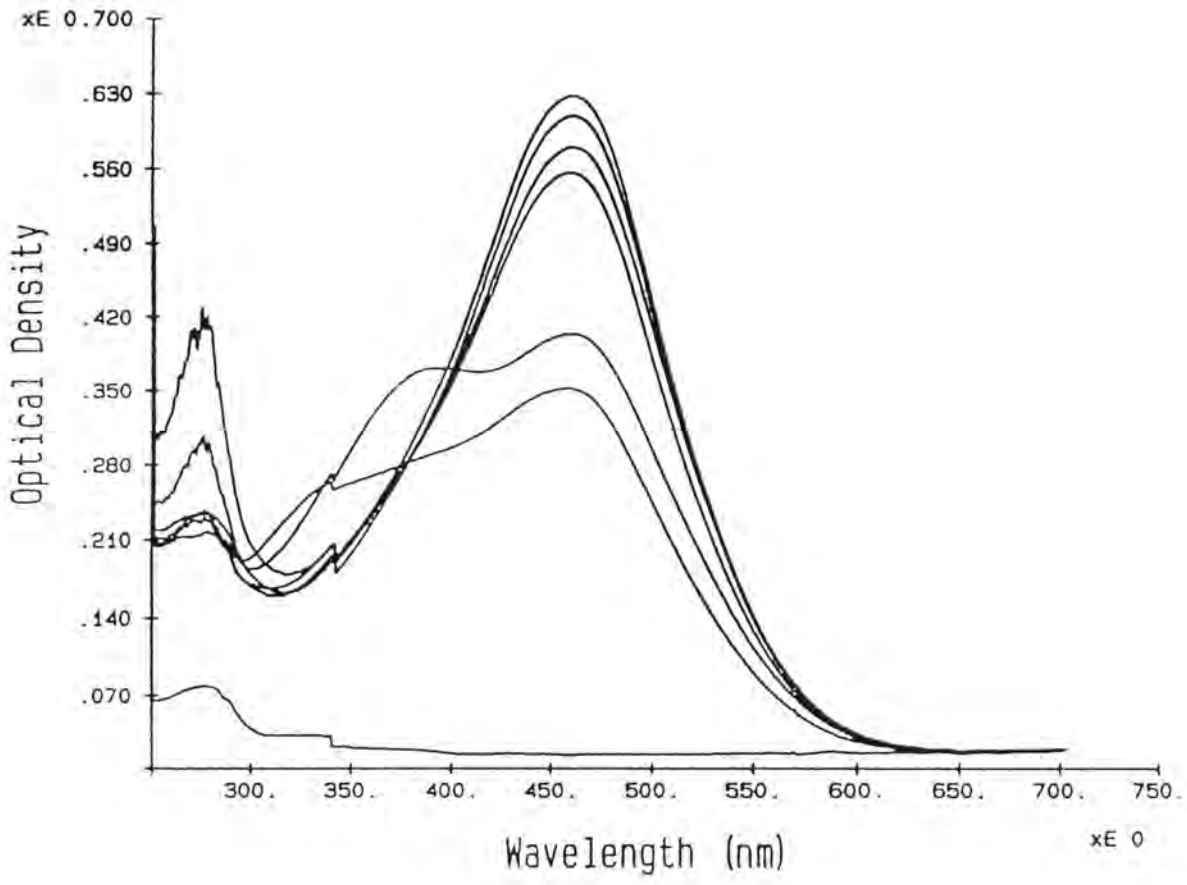

Figure A1.6 Pigment Formation with 2

UV-vis spectra of BR analog pigment formation with VBN-II **2**. The absorbance due to the pigment at ~480 nm increased with time of incubation.

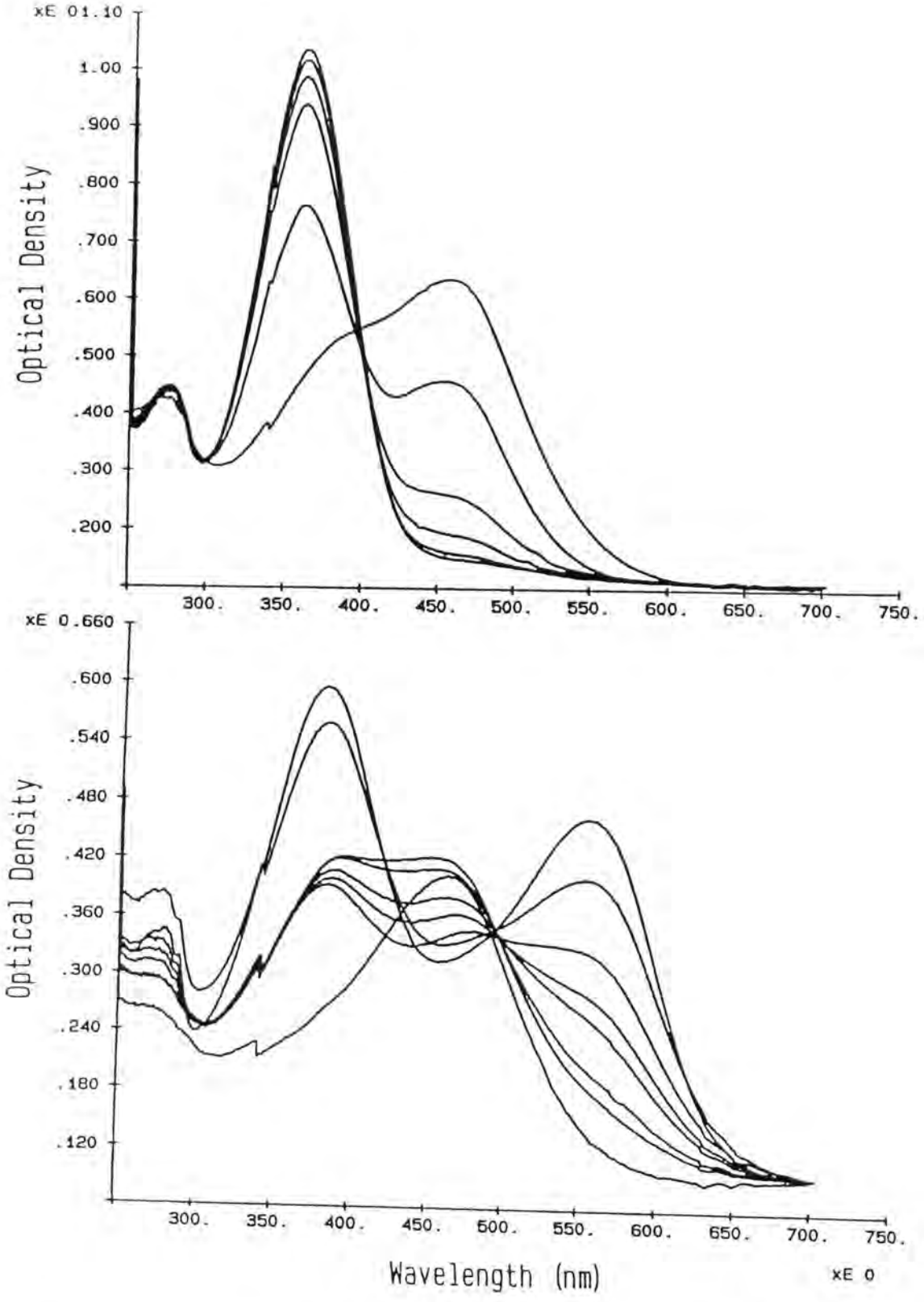

Figure A1.7 Characterization of Pigment of VBN-II 9

Top panel: Hydroxylamine Stability: the absorbance of the pigment at ~480 nm decreases as the peak due to the retinyloxime increases (~360 nm); Bottom panel: ATR Stability: the absorbance of the analog pigment (480 nm) is replaced by that of regenerated BR (570 nm) when the analog pigment is incubated with excess ATR (380 nm).

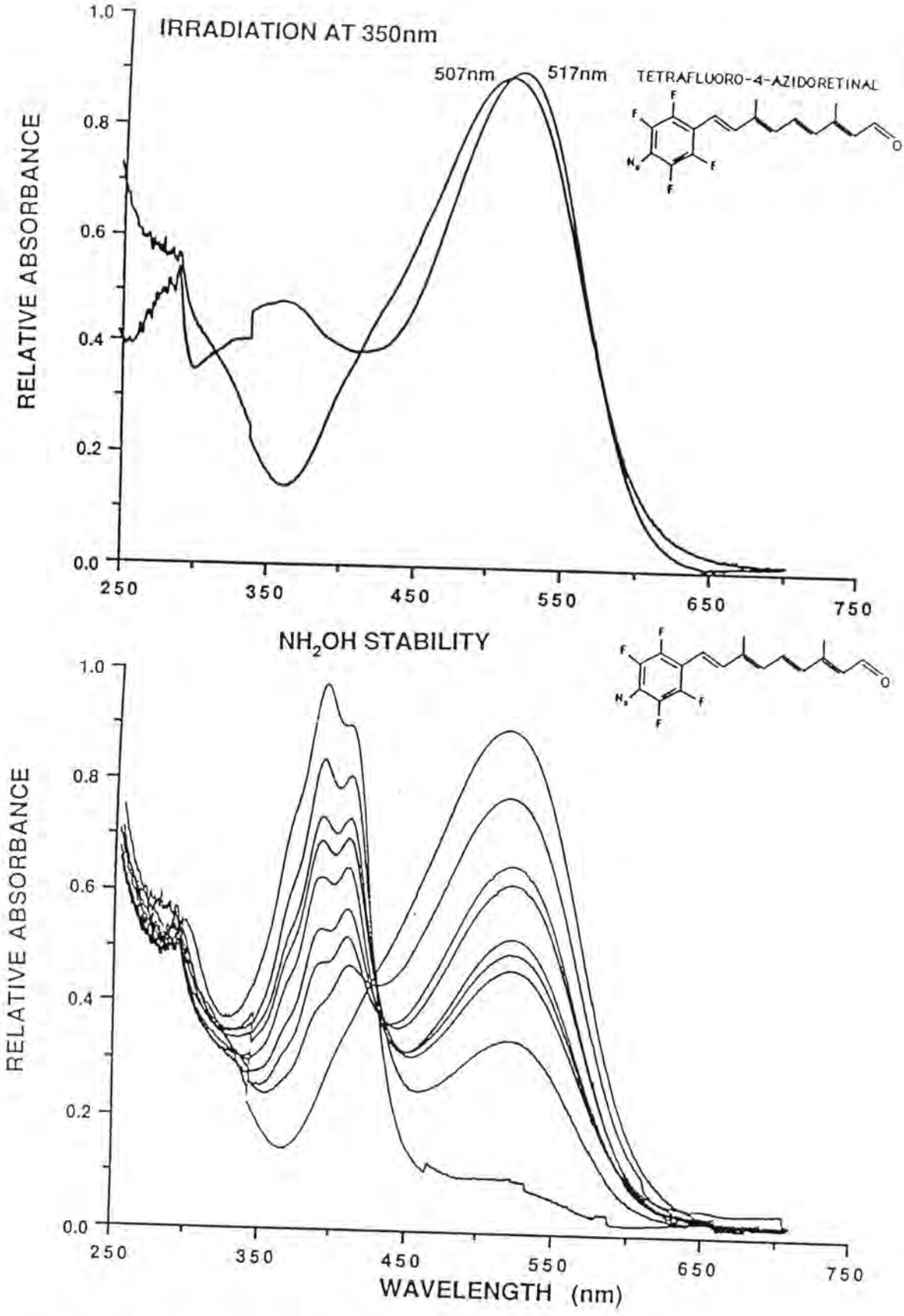

Figure A1.8 Characterization of Pigment of TF4N3 <u>11</u>

Top panel: Irradiation of Pigment at 350 nm for 10 minutes shows irreversible shift from 517 nm to 507 nm; Bottom panel: Hydroxylamine Stability of Non-irradiated Pigment: the absorbance of the pigment at ~520 nm decreases as the peak due to the retinyloxime increases (~380 nm)

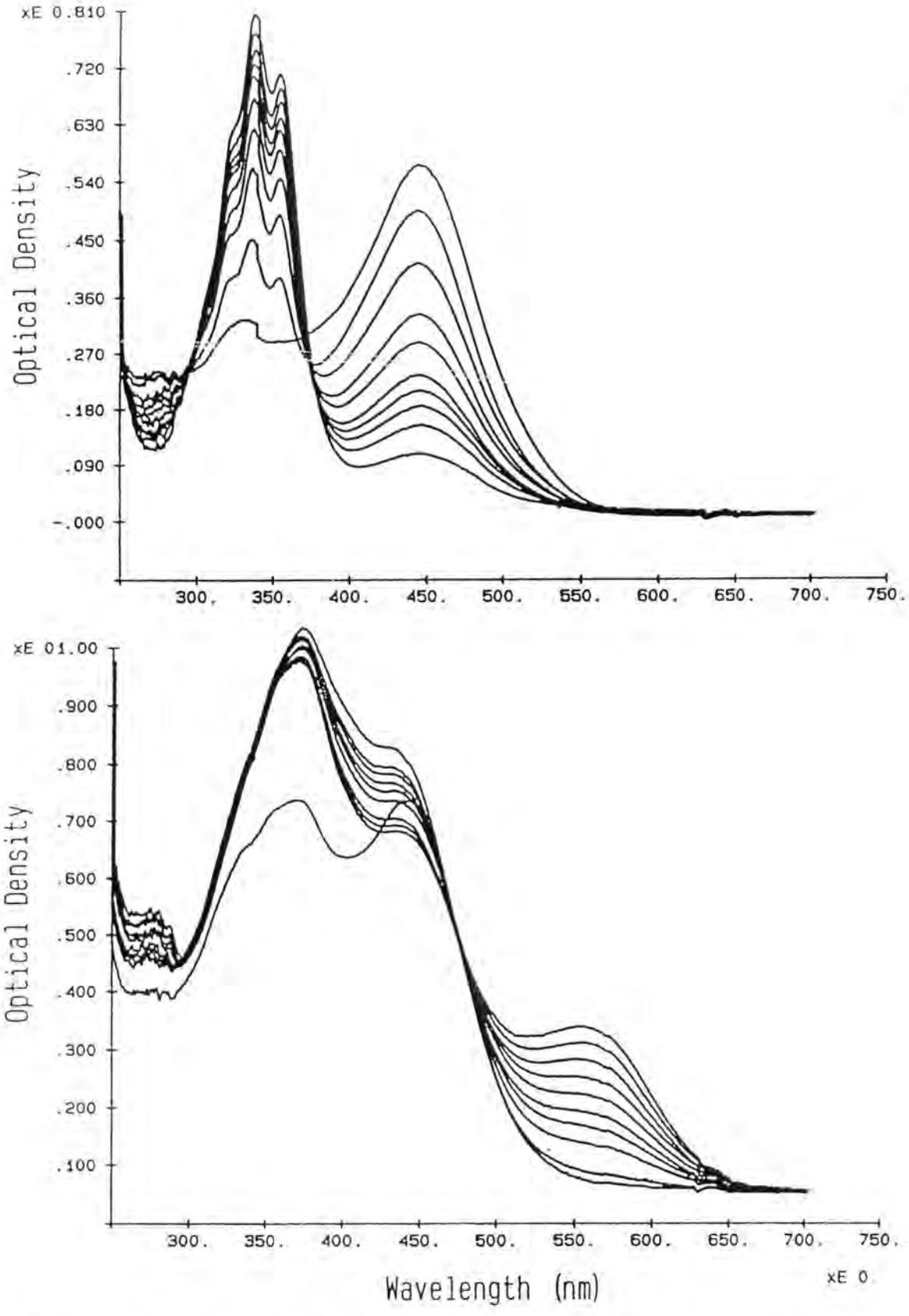

Figure A1.9 Characterization of Pigment of Acyclicretinal 12

Top panel: Hydroxylamine Stability: the absorbance of the pigment at ~460 nm decreases as the peak due to the retinyloxime increases (~340 nm); Bottom panel: ATR Stability: the absorbance of the analog pigment (460 nm) is replaced by that of regenerated BR (570 nm) when the analog pigment is incubated with excess ATR (380 nm).

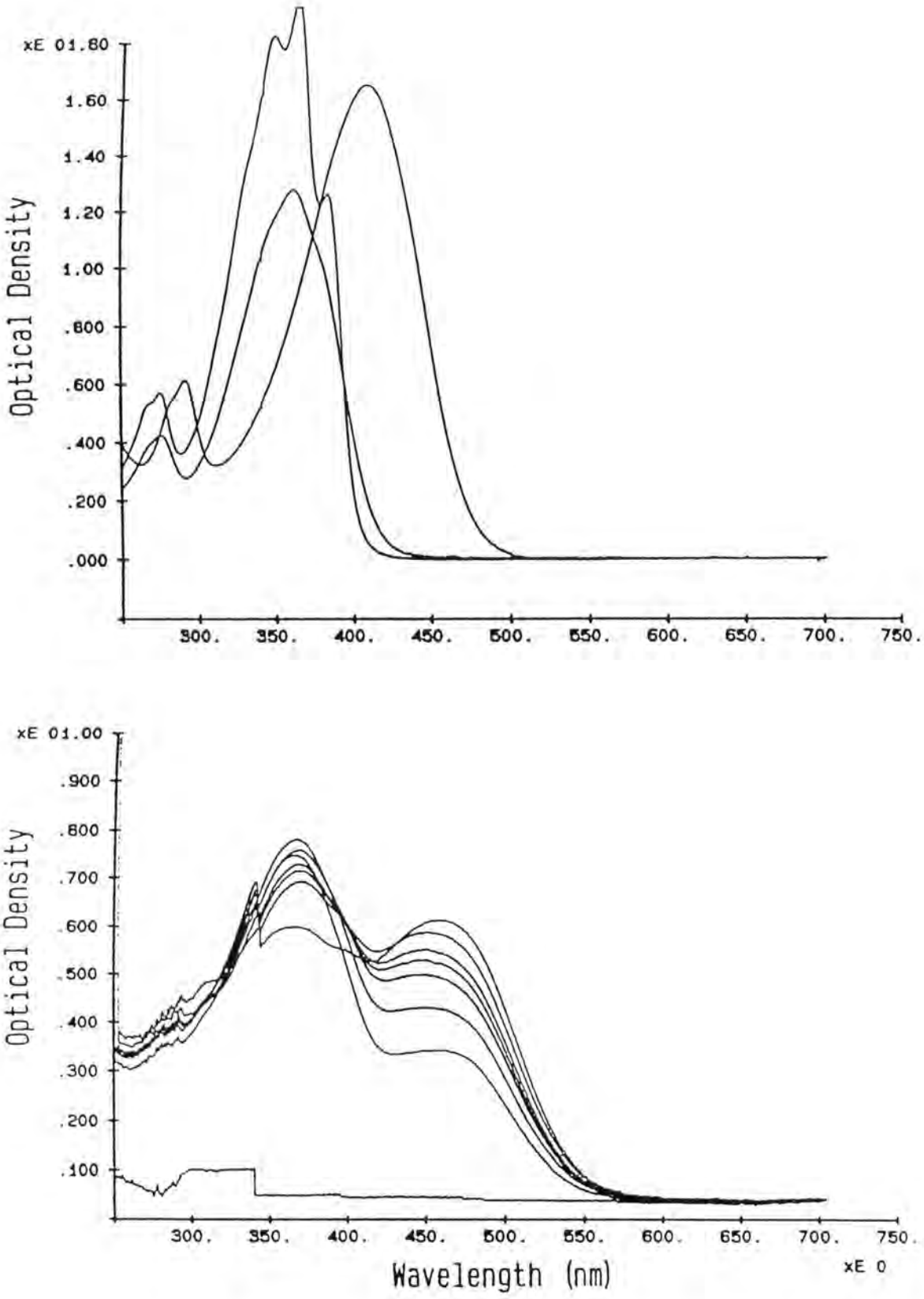

Figure A1.10 Characterization of Pentafluororetinal 13

Top panel: Formation of PSB:Aldehyde (360 nm), Schiff base: ~360 nm (fine structure and PSB: (407 nm); Bottom panel: Pigment Formation: Increase in absorbance of BR analog pigment (456 nm) with time.

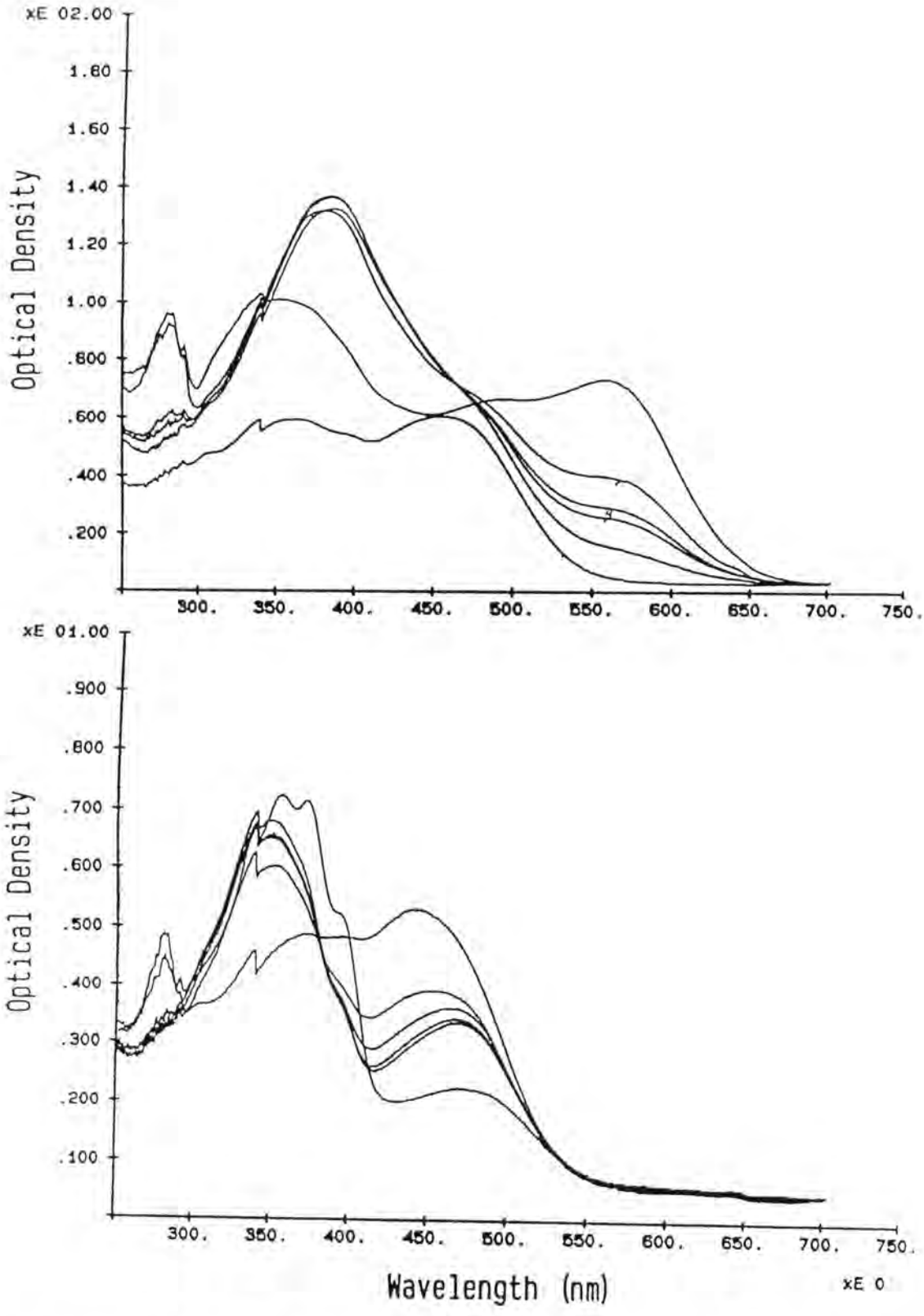

Figure A1.11 Characterization of Pigment of Pentafluororetinal 13

Bottom panel: Hydroxylamine Stability: the absorbance of the pigment at ~460 nm decreases as the peak due to the retinyloxime increases (~340 nm); Top panel: ATR Stability: the absorbance of the analog pigment (460 nm) is replaced by that of regenerated BR (570 nm) when the analog pigment is incubated with excess ATR (380 nm).

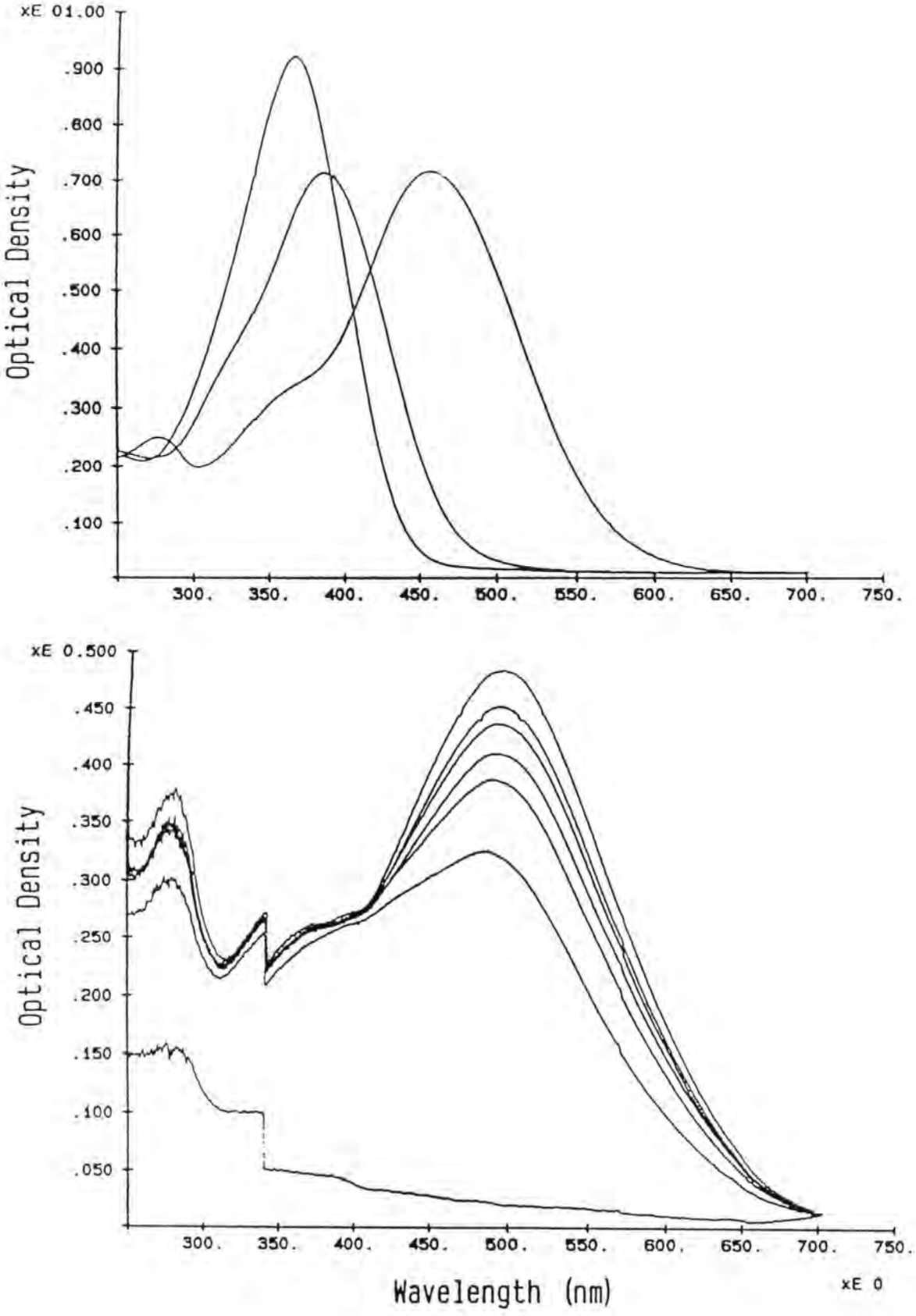

Figure A1.12 Characterization of Hydroxyretinal 14

Top panel: Formation of PSB:Aldehyde (386 nm), Schiff base: 350 nm and PSB: (456 nm); Bottom panel: Pigment Formation: Increase in absorbance of BR analog pigment (491 nm) with time.

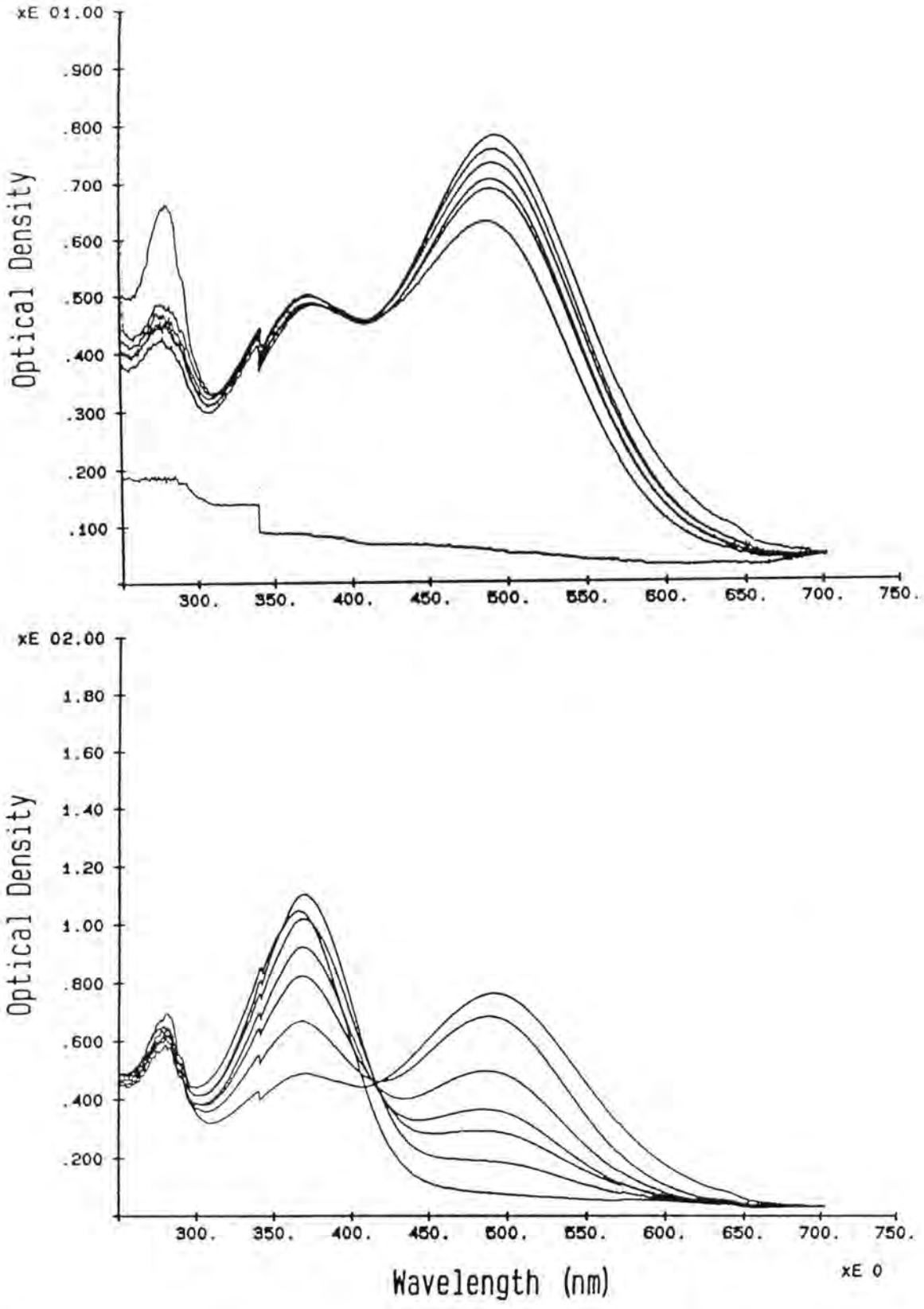

Figure A1.13 Characterization of Pigment of Methoxyretinal 15

Top panel: Pigment Formation: increas in absorbance due to BR analog pgment formation (490 nm) with time of incubation; Bottom panel: Hydroxylamine Stability:decrease in absorbance of pigment (490 nm) with increase in absorbance of retinyloxime (365 nm).

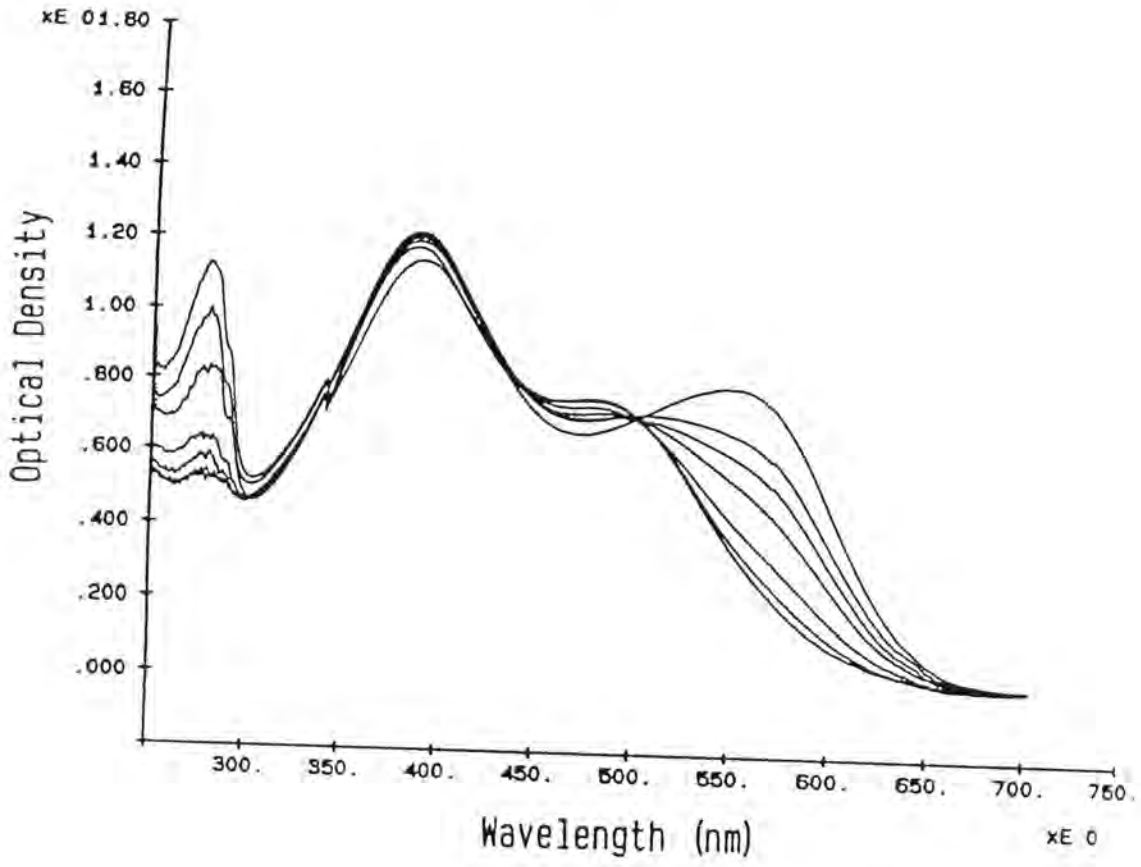

Figure A1.14 Characterization of Pigment of <u>15</u> (cont.)

ATR Stability: Replacement of absorbance of BR analog pigment with regenerated BR (570 nm) on incubation with ATR (380 nm).

Appendix 2

Sequence Analysis of Shark Immunoglobulin Light Chains using Tandem Mass Spectrometry

Portions of this appendix have been published as

Schluter, SF, CJ Beischel, SA Martin, and JJ Marchalonis.

"Sequence Analysis of Homogeneous Peptides of Shark Immunoglobulin Light Chains by Tandem Mass Spectrometry: Correlation with Gene Sequence and Homologies among Variable and Constant Region Peptides of Sharks and Mammals."

Molecular Immunology 27(1), 17-23, 1990.

Introduction. This appendix presents the application of mass spectrometry (MS) to define protein structure for immunoglobulin light chains from two different species of shark. This analysis was undertaken as a training experience in mass spectrometric analysis of proteins and peptides at the Massachusetts Institute of Technology before a mass spectrometer with the required capabilities was installed at the Medical University of South Carolina. The analysis was performed in collaboration with Jack Marchalonis, Sam Schluter and Steve Martin. The derivation of sequence information from polyclonal shark light chains is particualarly suited to analysis by MS since this method is tolerant of the peptide mixtures that inherently result from the large variability in these polyclonal proteins.

The goal of this analysis beyond training was to obtain further information on the sequence of shark immunoglobulin light chains to be used in phylogenetic studies and in the prepararion of oligonucleotide probes for the screening of genomic libraries. Peptides isolated from tryptic digests of purified tiger shark and sandbar shark polyclonal light chains [Rosenshein and Marchalonis, 1987] were sequenced. The peptides were fractionated by reversed-phase HPLC and sequenced using high-resolution tandem mass spectrometry [Biemann, 1992]. It was feasible to apply this combination of technologies to polyclonal light chain pools to obtain unique amino acid sequences corresponding to variable and constant region segments of shark light chain.

Methods. The carboxamidomethylated immunoglobulins [Rosenshein and Marchalonis, 1987] (25 nmol) were dissolved in 0.1 M ammonium carbonate, 0.1 M calcium chloride at 5 mg/mL, and digested with trypsin (1% by weight) for 1 hour at pH 8.5 and 37 C. The tryptic digest was separated by reversed-phase HPLC and prepared for mass spectrometric analysis [Martin *et al.*, 1982].

The HPLC separartion was done on a C_{18} column using a linear gradient from 100% water (containing 0.05% TFA) to 70% acetonitrile (containing 0.035% TFA) in 70 min at a flow rate of 1.0 ml/min. Individual peaks were collected manually. A small amount of glycerol (2-5 µl) was added to each sample tube and the HPLC solvents removed by evaporation using a Speed-Vac Concentrator. One microliter of 10% aqueous acetic acid was mixed with each sample (1-2 nmol) and they were analyzed by FAB MS and MS/MS [Johnson and Biemann, 1987].

Results and Discussion. The shark immunoglobulin light chains were digested with trypsin following the procedure of Allen (1981) and separated by HPLC under reversed-phase conditions. All fractions that were isolated in discrete form from both the tiger shark and sandbar shark light chain digests were characterized in terms of molecular weights, and some fragments were further analyzed for assignmemt of primary amino acid sequence by MS/MS. Ten peptides ranging from a pentamer to a 16-mer were completely sequenced and are shown in fig. A2.1. One tryptic fragment (mol. wt. 1582.1) was found in both the tiger shark digest (Tf13) and the sandbar shark digest (Sf12). The sequences of these peptides were subsequently derived from DNA sequencing. The fact that had originally been sequenced at the protein level confirms the identification of the stretch of DNA that was sequenced as a major expressed immunoglobulin gene.

The use of MS/MS to establish primary sequence of peptides is illustarted in fig. A2.2, which compares analyses of tiger shark Tf10 and sandbar shark Sf9 peptides. The primary sequence of these two peptides (tiger shark Tf10, 795.5 and sandbar shark Sf9, 781.5) differ by a single amino acid substitution in position 4 (Ile to Val; Johnson *et al.*, 1987). A comparison of their tandem mass spectra indicates the substitution and the subsequent 14 unit mass shift in all ions containing the change. This shift in mass is very similar to that outlined in fig. 1.10 that describes MS/MS of chemically modified peptides. In this case the chemical modification is addition of a methyl group at position 4 by changing a valine to a isoleucine. The use of these peptide sequences to confirm DNA sequencing from shark cDNA libraries and their use in phylogenetic studies are described in detail in Schluter *et al.*, 1990.

Tryptic Fragment	$(M+H)^{+a}$ (m/z)	Deduced Sequence
Tiger (MGC)		
Tf9	711.5	G-P-G-I-P-D-R
Tf10	795.5[b]	F-T-G-I-S-D-R
Tf13	1582.1	H-E-T-Q-A-N-P-L-Q-T-S-I-S-R
Tf17	1134.8[c]	(A,S)-E-L-Y-V-S-P-R
Sandbar (MCP)		
Sf4[d]	563.4	T-S-I-S-R
Sf4a[d]	819.5	G-N-G-V-E-T-S-R
Sf9	781.5[e]	F-T-G-V-S-D-R
Sf11	756.6[f]	X-N-L-G-S-P-R
Sf12	1582.1	H-E-T-Q-A-N-P-L-Q-T-S-I-S-R
Sf13	1570.1	D-P-V-L-T-Q-P-G-S-I-S-S-S-P-G-K

[a]Observed mass.

[b]FAB MS/MS spectrum fig. 6.6b.

[c]Assignment either A-S or S-A.

[d]Both of these components were in the same HPLC fraction. Full sequence information was obtained from both peptides in the fraction with no interference.

[e]FAB MS/MS spectrum fig. 6.6a.

[f]X indicates either I or L.

Figure A2.1 Sequence of Peptides from Shark Ig Light Chains Derived by FAB MS/MS.

Observed molecular weights and deduced primary sequences for tryptic peptides from the light chains of tiger and sandbar shark Ig obtained from FAB MS and FAB MS/MS.

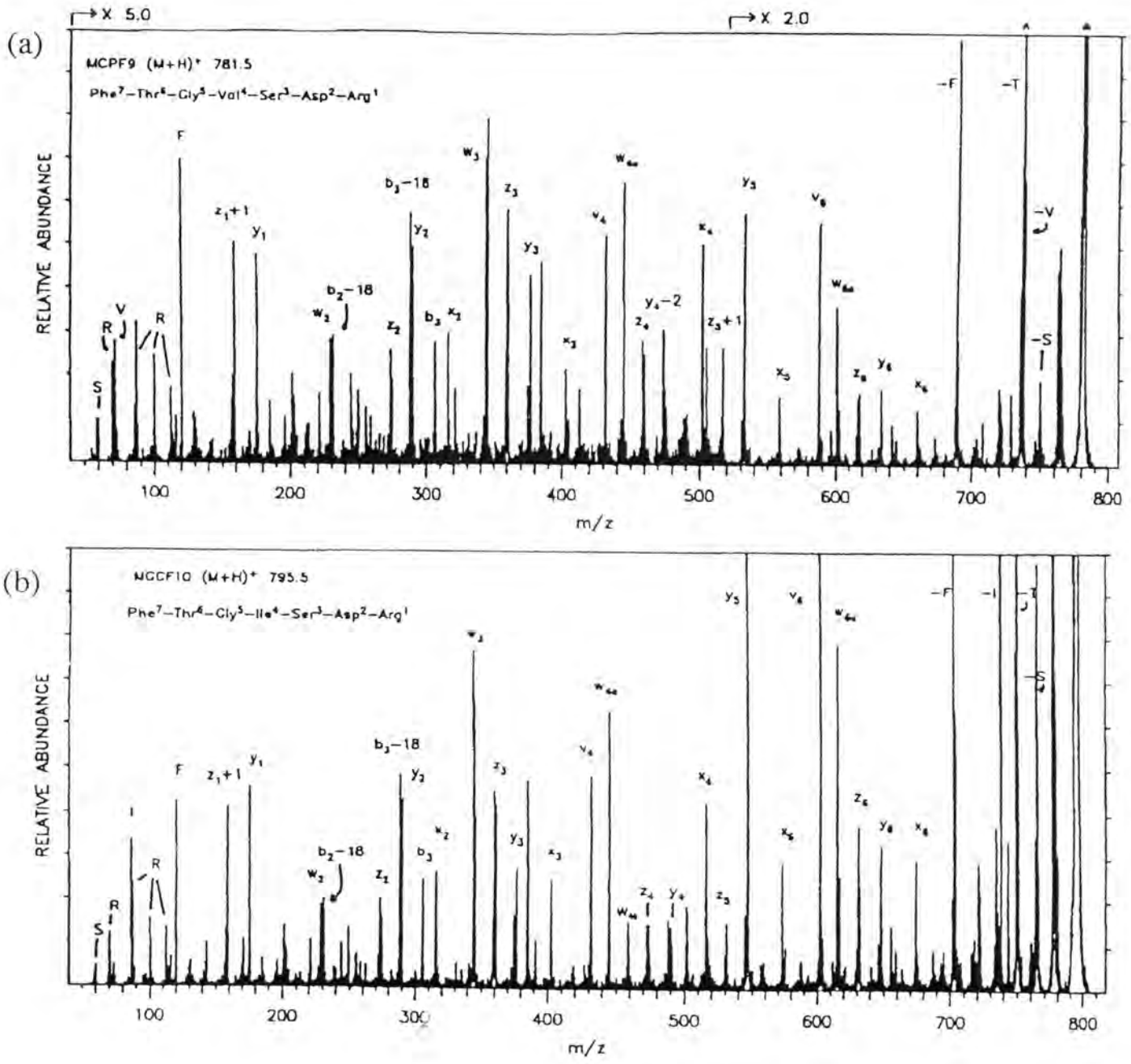

Figure A2.2 MS/MS Spectra of Tryptic Peptides From Shark Immunoglobulin Light Chains

(a) Sandbar shark $(M+H)^+$ 781.5 and (b) Tiger shark $(M+H)^+$ 795.5, highlighting the identificationof a single amino acid substitution. All C-terminal fragment ions (i.e. w_{n+1}, x_n, y_n, and z_n) from n=4,5, etc. are observed at a mass 14 higher in (b), indicating a modification in position 4. This is further supported by the abundant immonium ion (m/z 72.0) and R group loss $[(M+H)^+-43=738.1]$ for Val in (a) and the replacement of these ions by an immonium ion (m/z 86.0) and R group loss $[(M+H)^+-57=738.1]$ for xLeu in (b). The xLeu was identified as Ile, based on the characteristic w_4a and w_4b ions at m/z 445 and 459 respectively in (b). Adapted from Schluter *et al.*, 1990.